AD_____

Award Number: DAMD17-94-J-4474

TITLE: Sequence-Specific and Synergistic Binding of Drugs to DNA

PRINCIPAL INVESTIGATOR: Fu-Ming Chen, Ph.D.

CONTRACTING ORGANIZATION: Tennessee State University
Nashville, Tennessee 37209-1561

REPORT DATE: October, 1999

TYPE OF REPORT: Final

PREPARED FOR: U.S. Army Medical Research and Materiel Command
Fort Detrick, Maryland 21702-5012

REPORT DOCUMENTATION PAGE

Form Approved
OMB No. 074-0188

1. AGENCY USE ONLY (Leave blank)	2. REPORT DATE	3. REPORT TYPE AND DATES COVERED
	October, 1999	Final (23 Sep 94 – 22 Sep 99)

4. TITLE AND SUBTITLE
Sequence Specific and Synergistic Binding of Drugs to DNA

5. FUNDING NUMBERS
DAMD17-94-J-4474

6. AUTHOR(S)
Fu-Ming Chen, Ph.D.

7. PERFORMING ORGANIZATION NAME(S) AND ADDRESS(ES)
Tennessee State University
Nashville, Tennessee 37209- 1561

e-mail:
chenf@harpo.tnstate.edu

8. PERFORMING ORGANIZATION REPORT NUMBER

9. SPONSORING / MONITORING AGENCY NAME(S) AND ADDRESS(ES)
U.S. Army Medical Research and Materiel Command
Fort Detrick, Maryland 21702-5012

10. SPONSORING / MONITORING AGENCY REPORT NUMBER

11. SUPPLEMENTARY NOTES

12a. DISTRIBUTION / AVAILABILITY STATEMENT
Approved for public release
distribution unlimited

12b. DISTRIBUTION CODE

13. ABSTRACT ***(Maximum 200 Words)***

Our goals were to study the sequence specific and synergistic binding of three drugs having distinctly different binding modes: actinomycin D (ACTD), an intercalator with GpC sequence preference; chromomycin A_3 (CHR), a guanine specific minor groove binder; and distamycin A (DST), an A•T specific minor groove binder. These results formed the bases for designing suitable sequences for the synergistic binding study commenced during the later part of the grant period. It was found that ACTD binds strongly and dissociates slowly at the dGpdC site with flanking T/T mismatches. An end-stacking model for the binding of ACTD to the non-GpC-containing octamer d(CGTCGACG) was proposed. A recent observation of strong ACTD affinity for nearly complementary sequence d(CGXCGXCG) led us to speculate a possible single-strand binding mode with base-stacking on both sides of the ACTD chromophore. ACTD binding study with DNA oligomers of CXG repeats led to the finding that two ACTD molecules can bind tightly to two consecutive GpC sites separated by a single T/T mismatch, which was thought unlikely. Studies with DST led to a possible circular dichroic and kinetic differentiation of DNA binding modes of DST. Studies on the synergistic effects of drug binding, however, were less successful and may partially be the consequence of our sequence design.

14. SUBJECT TERMS
Breast Cancer, DNA

15. NUMBER OF PAGES
126

16. PRICE CODE

17. SECURITY CLASSIFICATION OF REPORT	18. SECURITY CLASSIFICATION OF THIS PAGE	19. SECURITY CLASSIFICATION OF ABSTRACT	20. LIMITATION OF ABSTRACT
Unclassified	Unclassified	Unclassified	Unlimited

NSN 7540-01-280-5500

Standard Form 298 (Rev. 2-89)
Prescribed by ANSI Std. Z39-18
298-102

FOREWORD

Opinions, interpretations, conclusions and recommendations are those of the author and are not necessarily endorsed by the U.S. Army.

_____ Where copyrighted material is quoted, permission has been obtained to use such material.

_____ Where material from documents designated for limited distribution is quoted, permission has been obtained to use the material.

_____ Citations of commercial organizations and trade names in this report do not constitute an official Department of Army endorsement or approval of the products or services of these organizations.

_____ In conducting research using animals, the investigator(s) adhered to the "Guide for the Care and Use of Laboratory Animals," prepared by the Committee on Care and use of Laboratory Animals of the Institute of Laboratory Resources, national Research Council (NIH Publication No. 86-23, Revised 1985).

_____ For the protection of human subjects, the investigator(s) adhered to policies of applicable Federal Law 45 CFR 46.

__✓__ In conducting research utilizing recombinant DNA technology, the investigator(s) adhered to current guidelines promulgated by the National Institutes of Health.

__✓__ In the conduct of research utilizing recombinant DNA, the investigator(s) adhered to the NIH Guidelines for Research Involving Recombinant DNA Molecules.

_____ In the conduct of research involving hazardous organisms, the investigator(s) adhered to the CDC-NIH Guide for Biosafety in Microbiological and Biomedical Laboratories.

PI - Signature

Date

TABLE OF CONTENTS

INTRODUCTION

Combination chemotherapy is one of the important strategies in cancer treatments. This is based on the observation that administering certain drugs together is more effective than giving individual drugs separately. Although the reason for such an effect is not understood, it may be related to the synergistic effect of their binding to bio-molecules such as proteins and DNA. Consequently, studies on the interplay among drugs capable of binding to different regions of DNA will be of considerable interest. Understanding the synergism of drugs at the molecular level may have important implication for designing more effective chemo-therapeutic strategies in breast cancer treatments. Our proposal focuses on the sequence specific binding and synergistic effects of three drugs having distinctly different sequence preferences and binding modes: actinomycin D (ACTD), a guanine specific intercalator; chromomycin A_3 (CHR), a guanine specific minor groove binder; and distamycin A (DST), an A•T specific minor groove binder. In order to investigate the possible synergistic effects of drugs on DNA binding, it is essential that binding characteristics of each individual drug be thoroughly elucidated. Sequence-specific recognition of DNA molecules by proteins and small molecules is an important component in the regulation of many biological processes. Understanding the base sequence specificity of an antibiotics is an important first step in the design of new drugs and sequence-specific probes. Elucidation of sequence specific binding of each individual drug is crucial in serving as the basis for designing suitable oligonucleotides for our subsequent synergistic studies. The approved SOW is to study the sequence-specific binding of the individual drugs the first three years and attempt the synergistic binding study during the last year.

BODY

Experimental methods.

Equilibrium Binding Titrations via Absorbance Spectral Changes. ACTD exhibits an absorption maximum near 440 nm in buffer solutions and without the presence of DNA. Progressive additions of DNA oligomeric stock result in considerable hypochromic effects of this band near 427 nm and slight bathochromic shifts to result in some hyperchromic effects around 480 nm. Absorbance differences between 427 and 480 nm were, thus, used to construct the binding isotherms and Scatchard plots. Since most of the Scatchard plots can be approximated by straight lines, the binding parameters were deduced via linear least-squares fits.

CHR exhibits an absorbance maximum at 406 nm when free in solutions. Successive additions of DNA lead to bathochromic shifts and intensity enhancements at 440 nm and a concomitant reduction at the 400-nm region. An isosbestic point is evident near 411 nm, suggesting a two-component process. Absorbance differences at 440 and 400 nm were used to obtain binding isotherms and Scatchard plots. A qualitative ranking of the relative binding affinities of CHR for different sequences can also be achieved by simply comparing the intensity enhancements of CHR absorbance around 440 nm in the presence of various oligomers of the same concentrations.

DST exhibits an absorbance maximum at 303 nm when free in solutions. Successive additions of DNA lead to slight bathochromic shift and intensity enhancements near 330 nm. Thus, absorbance changes at 350 nm (to avoid interference from the residual DNA absorbance) were used to construct binding isotherms and to obtain binding parameters.

Absorption spectra were measured with Cary 1E spectrophotometric system. Spectral titrations were carried out at 20 °C by starting with a drug solution followed by progressive additions of the oligomer stock. Ligand binding to DNA usually results in a melting temperature increase, thus the extent of the increase can give a qualitative measure of the binding affinity. Melting measurements were made with DNA alone and in the presence of various drugs. Thermal denaturation experiments of 40 μM oligomer in the absence and in the presence of appropriate concentrations of drugs were carried out with 1-cm semimicro cells by monitoring the absorbance at 275 nm. A heating rate of 0.5 °C/min was maintained by the temperature controller accessory. Melting temperatures were then deduced via differential melting profiles. Absorbance kinetic measurements were made by using a stirrer accessory with 427- and 453-nm monitoring for the ACTD association and SDS-induced dissociation, respectively. Time-dependent absorbance changes were monitored at 440 nm for the association experiments and at 340 nm for the 1% SDS-induced dissoication experiments. Kinetic rate parameters were extracted using a nonlinear least-squares fit program.

Equilibrium Binding Titrations and Spectral Characterization via Circular Dichroism. The effect of ACTD binding to a DNA duplex on the CD spectral characteristics is to induce sizable positive and negative CD intensities at the 293- and 255-nm regions, respectively. Thus, qualitative ACTD binding affinities for these oligomers can also be obtained via difference CD (ACTD/DNA – DNA) spectral comparison. Association and dissociation kinetics can also be monitored by time-dependent ellipticity changes at 293 nm.

CHR is optically active and exhibits negative and positive CD maxima at 295 and 276 nm, respectively. In the presence of DNA, however, a strong exciton-type couplet, presumably the results of dimer formation and/or aglycon-DNA base interactions, is induced which results in an inverted CD spectrum with positive and negative CD maxima appearing at 287 and 275 nm, respectively. Thus, induced CD intensities at 287 and 275 nm can also serve as gauges for the relative binding affinities of CHR for these oligomers.

DST, on the other hand, is not optically active when free in solutions. In the presence of DNA, however, a strong positive CD band with a maximum near 330 nm is induced. Thus, induced CD intensities at 330 nm can be used to construct binding isotherms via CD spectral titrations.

CD spectra were measured at room temperature by a Jasco J-500A recording spectropolarimeter using water-jacketed cylindrical cells of 2-cm pathlength. CD titrations were carried out with 80 μM DNA nucleotide followed by progressive additions of the drug stock solution. CD spectra were measured from 230 to 380 nm.

Fluorescence Experiments. Although ACTD is only slightly fluorescent, its 7-amino derivative is strongly so. The amino group substitution does not greatly alter the intercalative binding mode of this derivative. It is, thus, of interest to corroborate the ACTD results with those of this derivative via fluorescence measurements. Since both CHR and DST are fluorescent and their spectra are significantly altered upon DNA binding, fluorescence spectral measurements should also be of value.

Binding isotherms via fluorescence titrations were made by integrating emission spectral intensities from 580 to 780 nm with excitation at 560 nm for 7-amino-ACTD, from 530 to 550 nm with excitation at 410 nm for CHR, and from 400 to 500 nm with excitation at 330 nm for DST. Fluorescence kinetic measurements were made by monitoring emission

intensity changes at 650 nm with excitation at 560 nm for 7-amino-ACTD, at 540 nm with excitation at 410 nm for CHR, and 460 nm with excitation at 330 nm for DST, using a stirrer accessory. Fluorescence measurements were made with an SLM48000S system.

Stopped-flow kinetic measurements. Stopped-flow kinetic measurements were made with an Olis RSM-1000 rapid scan spectrophotometer. Association kinetic measurements were made by mixing equal volumes of 8 μM ACTD and 100 μM (nucleotide) DNA with 427-nm absorbance monitoring; the resulting solutions were then mixed with equal volumes of 2% SDS solutions for the dissociation kinetic measurements with 453-nm absorbance monitoring. For DST, time-dependent absorbance profiles were obtained with monitoring at the 341-347 nm region for the dissociation kinetic measurements. Nonlinear least-squares fits on the kinetic data and binding isotherms were carried out with the MINSQ program of Micromath.

Capillary electrophoretic experiments. Capillary electrophoretic experiments were carried out with a Beckman P/ACE 5000 instrument. Capillary electrophoresis oligonucleotide run buffer and 75 μm I.D. x 375 μm O.D. capillaries internally-coated with poly(AAEE) were purchased from Bio-Rad (Hercules, CA). Samples were loaded by pressure for 10 s and run at 15 kV and 25 °C with 254 nm absorbance detection. The sieving buffer was replenished before each run using a 5-min purge cycle at 20 p.s.i. pressure. Two water rinse cycles were used to remove residual buffer from the capillary and electrode surfaces to prevent buffer carry over into the sample vial.

Synthetic oligonucleotides were purchased from Research Genetics, Huntsville, AL, and used without further purification. Concentration of these oligomers (per nucleotide) were determined by measuring the absorbances at 260 nm after melting, with use of extinction coefficients obtained via nearest-neighbor approximation using mono- and dinucleotide values tabulated in Fasman (1975). Since DST is not very stable in aqueous solutions, stock solutions were prepared immediately before use. Drug concentrations were determined using extinction coefficients of $\varepsilon_{303} = 34{,}000$ and $\varepsilon_{440} = 24{,}500$ $cm^{-1}M^{-1}$ for DST and ACTD, respectively. All experiments were carried out in 10 mM tris/borate buffer of pH 8 containing 0.1 M NaCl and 1 mM $MgCl_2$.

Results and Discussion

Actinomycin D

ACTD is a chromopeptide antibiotic which consists of a 2-aminophenozazin-3-one chromophore and two identical pentapeptide side chains. It has been well established that this drug prefers duplex DNA and binds via intercalation of the planar chromophore, preferably at the GpC sequence, with the two pentapeptide rings resting on the minor groove. X-ray studies have clearly shown that its duplex and GpC sequence preference is the consequence of the ability of the carbonyl oxygens and the NH groups of the L-threonine residues to form hydrogen bonds with the 2-amino group and the N(3) of guanines on both sides of the intercalated drug. These essential drug-DNA hydrogen bonds are protected by the cyclic pentapeptides, which effectively shield them from solvent exposure. The size of the four-base-paired binding site suggests that the binding characteristics of ACTD to the GC site may be affected by the adjacent flanking base pairs. Consequently, ACTD binding to oligomers containing XGCY = TGCA, AGCT, CGCG, and GGCC was investigated by us via equilibrium, kinetic, and thermal denaturation studies (Chen, 1988). The results indicate that despite the presence of a GC dinucleotide

sequence, -GGCC- exhibits a much weaker binding affinity towards ACTD than the other tetranucleotide sequences. Binding constants estimated from Scatchard plots indicate that binding to the -GGCC- site is at least an order of magnitude weaker than binding to -CGCG- and -AGCT-, which in turn is only slightly weaker than binding to the -TGCA- sequence. At 18.5 °C, ACTD dissociates from a decamer containing -TGCA- roughly 4 times slower than dissociation from those containing -CGCG- and -AGCT-sequences and more than two orders of magnitude slower than that from -GGCC-. These results were also supported by the melting results in which a stronger binding and slower dissociating site exhibits a larger increase in melting temperature upon ACTD binding. During the grant period, we have further extended the sequence-specific studies to include the effect of adjacent base-pair mismatches to the GpC binding and investigated the ACTD binding to oligomers containing no GpC sequence.

Actinomycin D binds strongly and dissociates slowly at the dGpdC site with flanking T/T mismatches.

DNA base-pair mismatches can sometimes serve as initiators or intermediates in a mutagenic pathway, and they may be introduced during replication, recombination, or other chemical events. These sites can also serve as preferential targets for drugs or carcinogens. Thus, the effects of base-pair mismatches on DNA structure and their ligand interactions are of considerable interest, as they may have relevance in DNA repair, transcription, and activation of damaged genes. A logical extension of our earlier studies on the adjacent base-pair effects on the ACTD binding to a GpC site would be to investigate the effects of the flanking base mismatches on the affinity and kinetic behaviors of this preferred GpC sequence.

Comparative studies with dodecamers of the form d(ATTA-XGCX-TAAT) and their self-complementary counterparts suggest that ACTD binds strongly to a GpC site with flanking T/T mismatches and moderately to that with C/C mismatches but weakly to those with other G/G or A/A mismatches. The relative binding order is found to be T/T > C/C >G/G > A/A. The ACTD binding affinity for the GC site with T/T mismatches is comparable to the strong binding of self-complementary -XGCY- sequences. Both the ACTD association and dissociation kinetics at the GC site with flanking T/T mismatches require two-exponential fits. The slow component of the association rates is slower than those of the self-complementary sequences, whereas that of the dissociation is decidedly slower than those of -AGCT- and -CGCG- sites and is more than an order of magnitude slower than those with C/C, G/G, and A/A mismatches. These kinetics results are further corroborated by fluorescence measurements using 7-amino-ACTD, a fluorescence analog of ACTD. In addition, fluorescence and absorbance spectral characteristics indicate that the binding mode at the GC site with flanking T/T mismatches resembles those of strong-binding self-complementary -XGCY- sites which are known to be intercalative in nature. The observed slow ACTD dissociation at the T/T mismatched site suggests that the minor-groove environment near the T/T-mismatched pairs provides favorable interactions with the pentapeptide rings of the drug, whereas the others, especially those of bulkier purine/purine mismatches, result in less favorable interactions. [For details see Liu & Chen, Biochemistry 50, 16346-16353 (1996)]

Binding of actinomycin D to DNA oligomers of CXG trinucleotide repeats.

The interest in this study stems from the fact that several genetic disorders have been correlated to the dramatic amplification of trinucleotide repeats in some genes. For

example, CGG repeats have been found to be the culprit for the fragile-X syndrome, CAG repeats have been shown to be responsible for Huntington's disease and spinobulbar muscular atrophy, and CTG repeats have been associated with myotonic dystrophy. Although the mechanisms for these trinucleotide expansions are not yet clear, there have been speculations on the roles of unusual DNA conformations such as hairpin formation. Our interest in the CXG trinucleotide repeats is further heightened by the fact that heteroduplexes of such repeats contain one or more GpC sites and the formation of homoduplexes from these repeats will result in GpC sites with flanking X/X base mismatches. To understand their ACTD binding characteristics, comparative binding and kinetic studies with oligomers of CXG trinucleotide repeats were carried out using oligomers of the form d[AT$(CXG)_n$AT] and their corresponding heteroduplexes, where n varies from 2 to 4 and X = any of the four DNA bases. The choice of these oligomers was based on the desire to study the effect of base sequence, chain length, and to avoid possible complications which may arise from ACTD stacking at the terminal G•C base pairs. In particular, we set out to test the assertions by others that since ACTD cannot bind more than two drug molecules in a 3-site duplex $(XGCXGCXGCX)_2$ that the two nearest neighboring GpC sites cannot bind ACTD simultaneously in a sequence such as XGCXGCX (Lian et al., 1996).

ACTD binding propensities of DNA with CXG trinucleotide repeats were investigated using oligomers of the form d[AT$(CXG)_{n=2-4}$AT] and their corresponding heteroduplexes, where X = A, C, G, or T. These oligonucleotides contain -CXGCXG-, -CXGCXGCXG-, and -CXGCXGCXGCXG- units which can form homoduplexes containing 1, 2, and 3 GpC binding sites, respectively, with flanking X/X mismatches. The corresponding heteroduplexes contain these same sites with flanking Watson-Crick base pairs. It was found that oligomers with X = G exhibit weak ACTD affinities whereas those with $X \neq G$ and n = 3 exhibit unusually strong ACTD binding affinities with binding constants ranging from 2.3 to 3.3 x 10^7 M^{-1} and binding densities of approximately 1 drug molecule per strand (or 2 per duplex). These binding affinities are considerably higher than their shorter and longer counterparts, and are about 2- and 10-fold stronger than the corresponding CAG•CTG and CGG•CCG heteroduplexes, respectively. The CTG-containing oligomer d[AT$(CTG)_3$AT] stands out as unique in having its ACTD dissociation kinetics being dominated by a strikingly slow process with a characteristic time of 205 min at 20 °C, which is 100-fold slower than d[AT$(CAG)_3$AT], nearly 10-fold slower than the corresponding heteroduplex, and considerably slower than d[AT$(CTG)_2$AT] (63 min) and d[AT$(CTG)_4$AT] (16 min). The faster dissociation rate of the n = 4 oligomer compared to its n = 2 counterpart is in apparent contrast with the observed 10-fold stronger ACTD binding affinity of the former. It was also found that d[AT$(CCG)_3$AT] exhibits the slowest dissociation rate of the CGG/CCG series, being more than an order of magnitude slower than that of its heteroduplex (τ_{slow} of 43 vs. 2 min). The finding that a homoduplex d[AT-CXG-CXG-CXG-AT]$_2$ can bind 2 ACTD molecules tightly is significant since it was thought unlikely for two consecutive GpC sites separated by a single T/T mismatch to do so (Lian et al., 1996). [For details see Chen, Biochemistry 37, 3955-3964 (1998)]

Is the strong actinomycin D binding of d(5'CGTCGACG3') the consequence of end-stacking?

Although the GpC preference of ACTD has been well established, there have been reports to indicate that it can also bind strongly to some non-GpC sequences. In particular,

calorimetric studies by Synder et al. (1989) had led to the conclusion that ACTD binds cooperatively to the octamer d(5'CGTCGACG3') with a binding constant higher than 10^7 M^{-1} and a 2:1 drug to duplex ratio. It is important to understand the nature of such a strong binding and to delineate the origin of the high cooperativity. Since it has been suggested by Synder et al. (1989) that the mode of ACTD binding to this oligomer is distinct from its classic mode of binding to GpC sequence, it will be of value to see if this is in fact the case. We are, however, of the view that the ACTD binding of this oligomer is a consequence of the drug molecules stacking at the ends of the DNA duplex. The basis for such a speculation stems from the fact that if one is to view the classic preferred ACTD intercalative as G3'p5'C, then it follows that the drug favors to stack at the 3'-side of dG and thus stacking on the G•C base pairs at both ends of this oligomeric duplex.

To investigate this possibility, d(CGTCGACG) and several related oligomers resulting from replacing the terminal base(s) or appending with dT and/or dA are used in a comparative study employing equilibrium titration, thermal denaturation, kinetic, and various spectral measurements. Absorbance titrations at 20 °C confirm the strong and highly cooperative nature of ACTD binding to this octamer. The stoichiometric association constants for the binding of the first and second drugs were found to be 1×10^5 and 3.2×10^7 M^{-1}, respectively. The base replacements of dG and dC at the respective ends results in a much weaker ACTD binding affinity, the loss of binding cooperativity, and much faster association and dissociation kinetics. These are consistent with the inability of the drug to stack on the 3'-side of dG due to base replacements. Appending the end(s) with dA and/or dT resulted in some diminution of binding affinity and cooperativity, appearance of slower association kinetic components, and unusually strong 7-amino-ACTD fluorescence enhancement for oligomers with dA or dT attached to dG at the 3'-terminal. To further support our postulate, studies were also made with d(CGACGTCG), which is related to the parent octamer by inverting the A•T pairs. It was found that, despite the altered internal sequence, the oligomer exhibits cooperative ACTD binding and kinetic characteristics very similar to those of the parent octamer, consistent with its ability to end-stack on the 3'-side of dG. [For details see Chen & Liu, Biochemistry 35, 7283-7291 (1996)]

ACTD binds strongly to d(CGTCGTCG) and d(CGACGACG)

As described earlier, calorimetric studies had indicated that despite the absence of a GpC sequence, the self-complementary octamer d(CGTCGACG) binds strongly to actinomycin D (ACTD) with high cooperativity and a 2:1 drug to duplex ratio (Snyder et al., 1989). A subsequent optical spectral study with related oligomers led us to suggest that ACTD may likely stack at the G•C base pairs of both ends of the duplex (Chen & Liu, 1996). New findings are reported herein to indicate that despite the lack of complete self-complementarity, oligomers of d(CGXCGXCG) [X = A or T] motif exhibit unusually strong ACTD affinities with binding constants of roughly 2×10^7 M^{-1} and binding densities of 1 drug molecule per strand. The ACTD binding affinity for the corresponding heteroduplex obtained by annealing these two oligomers is, however, considerably reduced. Although spectroscopic results with related oligomers obtained by removing, replacing, or appending bases at the termini appear to be consistent with the end-stacking model, recent capillary electrophoretic (CE) evidence provides additional insights into the binding mode. CE experiments with the self-complementary oligomers d(CGAGCTCG) and d(CGTCGACG) revealed contrasting migration patterns in the presence of ACTD, with mobility retardation and acceleration exhibited by the GpC- and non-GpC-containing

octamers, respectively, whereas the X/X-mismatched d(CGXCGXCG) experienced retardation. These results along with those of related oligomers provide evidence that instead of stacking at the duplex termini, ACTD may in fact stacks at the 3'-end of dG as a single-strand which then wraps around the 2-aminophenoxazin-3-one chromophore and stacks an internal dG on the other side. The seemingly cooperative ACTD binding and the curved Scatchard plot for the self-complementary d(CGTCGACG) may, thus, be attributed to the drug-induced duplex denaturation resulting from strong binding to single strands of d(CGXCGYCG) motif. [Biochemistry, submitted]

Chromomycin A_3

CHR, mithramicin, and olivomycin are three closely related antitumor antibiotics of the aureolic class which contains an aglycon chromophore with di- and trisaccharide (2,6-dideoxyhexapyranose) side chains attached at the opposite sides of the chromophore. The antitumor activity of these drugs is believed to be the consequence of their ability to bind to duplex DNA, resulting in an inhibition of DNA-directed RNA synthesis. These drugs are known to be guanine-specific, and their DNA binding requires the presence of divalent cations such as magnesium. Footprinting studies had confirmed their guainine specificity and further indicated that the binding sites are at least three base pairs long. The presence of two contiguous G•C base pairs is necessary but not sufficient by themselves for strong DNA binding of these aureolic acids. Consequently, their affinities appear to be modulated by flanking sequences. Earlier physicochemical studies have produced contradictory conclusions on the DNA binding mode of these drugs. Recent NMR studies on the CHR-d(TTGGCCAA) (Gao & Patel, 1989; Gao et al., 1992) and CHR-d(AAGGCCTT) (Gao & Patel, 1990) complexes in Mg^{++}-containing solutions, however, have established unequivocally that CHR binds as a Mg^{++}-coordinated dimer at the minor groove of the central GGCC segment of the duplex and have revealed the structural basis for the sequence specificity at the GpC3 step. The detailed structural information available on the binding to -GGCC- and -CGCG sequences (Sastry & Patel, 1993) has provided considerable insights into the structure and dynamics of aureolic acid-DNA interactions. Hence, a systematic study on the binding specificity to other sequences via synthetic oligonucleotides is of value. To this end, systematic kinetic, equilibrium binding, melting, and electrophoretic studies were carried out with oligonucleotides to determine the sequence specificity of chromomycin A_3 (CHR) binding to DNA at the self-complementary tetranucleotide level (Liu & Chen, 1994). Results indicate that the binding preferences for CHR are in the order -GGCC- > -CGCG- > -GCGC-, -CCGG- > -AGCT- > -ACGT-, -TGCA- > -TCGA-. Detergent-induced drug dissociation studies revealed that CHR dissociates very slowly from both -GGCC- and -CGCG- sequences, with the former being measurably slower than the latter which in turn is at least an order of magnitude slower than the rest of the sequences. Thermal denaturation measurements indicate that the binding of CHR stabilizes the DNA duplex, with -GGCC- and -CGCG- exhibiting the largest effects. Results of gel electrophoretic retardation experiments support our general findings on the relative binding order. Our experimental results support earlier NMR findings by other researchers implicating the preference of aureolic acid drugs at the GpC step and further reveal significant modulations by the adjacent base pairs. During the grant period attempts were made to study the sequence-specific binding of CHR at the non-self-complementary tetranucleotide level. Binding and kinetic results were then compared with those of the self-complementary sequences.

CHR binding to non-self-complementary decamers.

To further investigate the effects of adjacent base pairs on the CHR binding behaviors, a more systematic study was carried out with decamers of the form d(GTA-XGCY-ATG) which were annealed with the corresponding complementary strands of the form d(CAT-Y'GCX'-TAC), where X, Y = G, C, A, or T and X', Y' are complementary to X, Y, respectively. Results indicate some general patterns: (1) rates of CHR association at the GC sites appear to be relatively insensitive to the adjacent base pairs; (2) binding affinities and rates of dissociation are significantly affected by the adjacent base pairs; (3) in general the -XGCY- sites with X = G and/or Y = C exhibit stronger binding and slower dissociation rates; and (4) -GGCC- exhibits the strongest CHR binding affinity and the slowest dissociation kinetics. These results are consistent with those of self-complementary decamers studied earlier.

Distamycin A

Two related antibiotics, DST and netropsin (NET), have received considerable attention as a model of sequence specific nonintercalative DNA binding molecules. They are potent antibacterial, antiviral, and antineoplastic agents whose pharmacological activity has been correlated to its ability to bind to DNA. They form non-covalent complexes with duplex DNA in the minor groove and exhibit considerable preference for the AT-rich domains such as promoter regions. These antibiotics, thus, act as template poisons and inhibit DNA-dependent polymerase activities. Its binding affinities are in some cases significantly larger than those of typical intercalating drugs. Recent years have seen the upsurge of interest in using DST as a model for the DNA minor groove binding with A•T preference. Such interests were further fueled by the recent finding of a 2:1 mode of DST binding on some base sequences which was not observed for NET. Several NMR studies of 1:1 DST-DNA complexes have provided insights into both the specificity and the forces responsible for the tight binding of this drug. The structure of the DST-d(CGCGAATTCGCG)$_2$ complex was determined by a combination of 2D NMR experiments and molecular mechanics calculations (Pelton & Wemmer, 1988). It was found that the minimal binding site consists of just four A•T base pairs and that DST fits snugly into the 5′-AATT-3′ minor-groove binding site. Most interestingly, NMR studies have further indicated that binding sites of at least five base pairs in length can accommodate two DST molecules side-by-side in an anti-parallel orientation (Pelton & Wemmer, 1989; 1990). In this 2:1 complex, each ligand preserves all the molecular recognition elements of minor groove binders. The extent of binding cooperativity (i.e., the ease of forming a complex of 2:1 vs 1:1 DST-duplex) depends strongly on the DNA sequence. During the grant period we have carried out systematic studies on the effect of sequences on these two binding modes.

Circular Dichroic and Kinetic Differentiation of DNA binding modes of distamycin.

DNA binding modes of distamycin (DST) were investigated via comparative binding studies with oligomeric duplexes of the form d(GCG-X-GCG)•d(CGC-Y-CGC), where Y is complementary to X and X = 4- or 5-base binding site. It was found that 1:1 and 2:1 drug:duplex complexes exhibit distinctly different circular dichroic (CD) spectral characteristics and can, thus, serve as diagnostic tools for binding mode differentiation. CD intensity profile at 265 or 275 nm as a function of drug to DNA ratios can reveal the extent of binding cooperativity for the 2:1 complex formation (i.e., the relative binding affinities of 2:1 vs. 1:1) at a 5-base-paired binding site. Comparison of these profiles leads to the following qualitative ranking for the binding cooperativity for the studied sites:

AAGTT, ATATA ≥ AAACT > AATAA, AAATA, AAAGT > AATAT > TAAAA ≥ AAATT ≥ AAAAA ≥ ATAAA, AAAAT. The plausibility of this ordering is strengthened by its agreement with the ranking established by earlier NMR studies on some of the sequences. The significantly slower DST dissociation kinetics of the 2:1 complexes as compared to those of 1:1 made the kinetic measurements of SDS-induced dissociation by the stopped-flow technique possible. The results indicate that the AAGTT site exhibits the slowest DST dissociation rate, with a characteristic time of 35 seconds. The rates of dissociation in general correlate reasonably well with the cooperativity order found via equilibrium CD measurements (the higher the binding cooperativity the slower the rate of dissociation). Base sequence specific binding of DST was also found for the 1:1 complex formation at the 4-base-paired sites, with AAAA, TTTT, ATTT, and AAAT sequences exhibiting the highest binding affinities. [For details see Chen & Sha, Biochemistry 37, 11143-11151 (1998)]

Based on these sequence-specific binding studies of each individual drug, oligonucleotides of appropriate lengths and sequences were designed to carry out the synergistic binding studies.

Studies on Synergistic Effects

Synergistic studies with ACTD and DST.

Oligomers of the d(ATATAXGCYTATAT) motif were employed to carry out our initial synergistic studies, where X = A, C, G, or T and Y is complementary to X. The rationale for the choice of these oligomers stems from the fact that both ACTD and CHR prefer a GpC sequence whereas DST prefers A•T base pairs. Thus, it is expected that ACTD or CHR will bind at the -XGCY- central region while DST will bind at the two AT-rich regions at both ends. ATATA sequence was chosen since the alternating AT sequence of 5 base pairs have been shown to bind DST tightly with a 2:1 drug to duplex binding stoichiometry. Studies were also made with oligomers of the form d(CGCGATATAGGCC)• d(GGCCTATATCGCG) and d(GGCCATATACGCG)•d(CGCGTATATGGCC). These oligomers will lead to ACTD binding on both ends of the duplex whereas the DST will bind at the center. It is anticipated that with ATATA at the center, DST binding will predominantly be of 2:1 drug to duplex binding mode. The rationale for studying these two distinct systems stems in part from the fact that due to the fraying motion, DST binding at duplex ends may be weaker and may exhibit binding mode somewhat different from binding at the duplex center where a 2:1 binding mode has been established.

In order to investigate the effect of DST on the ACTD binding of DNA, the DNA binding propensity of ACTD in the absence of DST must be established first. Results indicate that ACTD binding to the self-complementary 14-mer d(ATATA-GGCC-TATAT) exhibits the weakest binding affinity ($0.5 \times 10^6\ M^{-1}$), whereas that of d(ATATA-TGCA-TATAT) exhibits the strongest ($8.4 \times 10^6\ M^{-1}$). Oligomers d(ATATA-CGCG-TATAT) and d(ATATA-AGCT-TATAT) exhibit moderate binding strengths of around $2 \times 10^6\ M^{-1}$. Consistent with the presence of a single binding site, all oligomers with ATATA-XGCY-TATAT motif show binding densities of roughly 1 drug molecule per duplex. These results are consistent with our earlier studies using these same -XGCY- sequences imbedded in a different sequence context, revealing that the order of binding for ACTD to be: -TGCA- > -CGCG- > -AGCT- >> -GGCC-. These results support the notion that ACTD indeed bind at the central -XGCY- sites of these oligomers. Studies have also been made with

heteroduplexes d(GGCC-ATATA-CGCG)[d] and d(CGCG-ATATA-GGCC)[d]. Binding constants of roughly 2 x 10^6 and binding densities of roughly 2 were obtained, consistent with ACTD binding at both sites of the duplex.

Similar binding titrations in the presence of 8 μM DST were then carried out. Scatchard plots for oligomers of the form d(ATATA-XGCY-TATAT) show gross non-linearity so that the extraction of simple binding parameters from these plots was not possible. Comparison of binding isotherms in the absence and in the presence of DST clearly suggests that the presence of DST greatly hinder the ACTD binding to these oligomers. This is particularly true for d(ATATA-AGCT-TATAT) and d(ATATA-TGCA-TATAT). The observed hindrance may be rationalized by the fact that in these two oligomers the DST binding regions have been extended to 6-base duplexes, ATATAA and ATATAT, respectively, so that significant number of DST molecules will be bound to the inner 5-base region, possibly via 2:1 stoichiometries. Such binding will lead to interference with the ACTD binding at the AGCT and TGCA sites. This interpretation appears to be further supported by the binding results of heteroduplexes d(GGCC-ATATA-CGCG)[d] and d(CGCG-ATATA-GGCC)[d] where only about 2-fold reduction in binding affinities has been observed, conforming with the notion of less severe overlaps of the ACTD and DST binding sites in these two oligomers.

Equilibrium DNA binding studies of DST via CD titrations in the absence of ACTD were then made with d(ATATA-XGCY-TATAT). The estimated binding constants range from 0.8 x 10^6 to 1.5 x 10^6 M^{-1} and the binding densities are seen to be greater than 4. These results appear to be in conformity with the notion that DST binds at the two A•T track regions with 2:1 drug to duplex-region binding stoichiometries. Similar binding strengths were also obtained for the heteroduplexes d(GGCC-ATATA-CGCG)[d] and d(CGCG-ATATA-GGCC)[d] but with considerably reduced binding densities, in agreement with the notion that now DST binds at the central A•T region.

DST binding titrations with DNA oligomers were subsequently carried out in the presence of 5 μM ACTD. DST binding parameters for the d(ATATA-XGCY-TATAT) series do not appear to be greatly affected by the presence of ACTD, suggesting that a prior ACTD binding does not appear to greatly alter the subsequent DST binding at the A•T tracks. Interestingly, however, the prior binding of ACTD at the G•C regions results in the reduction of DST binding in d(GGCC-ATATA-CGCG)[d], whereas it increases the DST binding affinity in d(CGCG-ATATA-GGCC)[d].

Binding of ligand to DNA usually results in enhancing its duplex stability. Thus, the relative melting temperature increases upon ligand binding may provide qualitative indication as to their binding affinities. Comparison of melting temperatures for the d(ATATA-XGCY-TATAT) series suggests that their relative melting temperature increases upon ACTD binding are qualitatively consistent with the relative binding order established via previous binding titrations: -TGCA- > -CGCG-, -AGCT- > -GGCC-. Significant melting temperature increases were observed upon binding 8 μM DST to oligomers of the form d(ATATA-XGCY-TATAT). In particular, melting temperature increases of 12 and 14 °C have been observed for the -TGCA- and -AGCT-containing oligomers. Interestingly, the additional presence of 5 μM ACTD does not appear to further stabilize the DNA duplexes, suggesting some interference of these two drugs.

ACTD association and SDS-induced drug dissociation kinetics in the absence and in the presence of 8 μM DST have also been measured and the rate parameters extracted via

single-exponential fits. Consistent with the weakest ACTD binding for d(ATATA-GGCC-TATAT), both ACTD association kinetics in the absence and in the presence of DST are too fast to be measurable by the non-stopped-flow technique. On the other hand, the rate of ACTD association with d(ATATA-CGCG-TATAT) is only slightly reduced by the presence of DST. Interestingly, however, nearly 3- and 8-fold reductions on the ACTD association rate are observed for d(ATATA-TGCA-TATAT) and d(ATATA-AGCT-TATAT), respectively. These results are consistent with the notion that A•T base pairs at the central sites -TGCA- and -AGCT- are partially occupied by DST so as to interfere with the ACTD binding at these sites. The kinetic results are consistent with the considerably larger melting temperature increases observed upon DST binding for these two oligomers, with the AGCT-containing oligomer exhibiting a larger melting temperature increase.

CD spectral alterations during a DST titration can reveal the mode of its DNA binding. For example, our earlier studies have indicated that, in addition to a larger presence of the positive 330 nm CD band, a 2:1 DST binding mode is characterized by the appearance of a negative CD band near 290 nm and a positive CD intensity enhancement near 275 nm. CD difference spectra during DST titrations in the absence and in the presence of 5 μM ACTD for d(ATATA-TGCA-TATAT) and d(ATATA-AGCT-TATAT) indicate that in the presence of ACTD, stronger negative CD bands near 290 nm were observed. This is consistent with the notion that a prior ACTD binding at the central site has resulted in blocking off the innermost A•T base pairs for DST binding. In addition, the resulting stabilization of the 5-base-paired A•T regions led to a more favorable 2:1 mode of DST binding.

Other research during the grant period

Fragile X syndrome is the most common cause of inherited mental retardation. Individuals affected by this disorder have an X chromosome in which the tip of its long arm is attached by only a slender thread of DNA. A gene designated as FMR-1 contains about 60 or fewer tandem repeats of CGG trinucleotide sequence in normal individuals. In sick individuals, however, the tandem repeat region is dramatically larger. As mentioned earlier that, recently, amplification of trinucleotide repeats have also been shown to be associated with several other disorders, including Kennedy and Huntington diseases. Although the mechanism of this unusual trinucleotide amplification is still unknown, it would not be surprising if there were structural bases for such remarkable amplifications.

Guanine is unique among the four DNA bases by virtue of its four hydrogen bonding sites being strategically distributed in such a way that four G bases can readily form 8 hydrogen bonds to result in a cyclic base-quartet. Thus, a DNA sequence with a stretch of G bases can form a four-stranded helical structure called G-quadruplex, which is of current intense interest. This interest has been further stimulated by the possible relevance of such structures in recombinational events at the immunoglobulin switching regions as well as in telomeric functions. Effects of monovalent cations on the G-quadruplex structural formation of telomeric DNA sequences have been extensively studied in recent years. Evidence suggests that due to its optimal size, K^+ is much more effective in stabilizing G-quadruplex formation. The ion is found to be sandwiched between two G-tetrads to form an octa-coordination complex with the carbonyl groups of guanines. We have recently uncovered an interesting phenomenon of K^+-induced CD intensity enhancement and aggregate formation on oligomers with CGG repeats. The finding was later extended to

include XGG repeats and the observation on synergistic effects of K^+ and Mg^{2+} on the aggregation formation.

Acid-facilitated supramolecular assembly of G-quadruplexes in d(CGG)$_4$.

Molar [K^+] induces aggregate formation in d(CGG)$_4$, as evidenced by absorbance, circular dichroic (CD), and gel measurements. The kinetics of this transformation are extremely slow at pH8 but are found to be greatly facilitated in acidic conditions. Kinetic profiles via absorbance or CD monitoring at a single wavelength resemble those of autocatalytic reacting systems with characteristic induction periods. More than 0.8 M KCl is needed to observe the onset of aggregation at 20 °C and pH 5.4 within the time span of 1 day. Time-dependent CD spectral characteristics indicate the formation of parallel G-tetraplexes prior to the onset of aggregation. Despite the evidence of K^+-induced parallel G-quadruplex and higher molecular weight complex formation, both d(TGG)$_4$ and d(CGG)$_4$T fail to exhibit the observed phenomenon, thus strongly implicating the crucial roles played by the terminal G and base protonation of cytosines. A plausible mechanism for the formation of a novel self-assembled structure is speculated. Aided by the C^+•C base pair formation, parallel quadruplexes are initially formed and subsequently converted to quadruplexes with contiguous G-tetrads and looped-out cytosines due to high [K^+]. These quadruplexes then vertically stack as well as horizontally expand via inter-quadruplex C^+•C base pairing to result in dendrimer-type self-assembled super structures. [Fos details see Chen, J. Biol. Chem. 270, 23090-23096 (1995)]

Supramolecular self-assembly of d(TGG)$_4$, synergistic effects of K^+ and Mg^{2+}.

Spectral evidence indicates that molar concentration of K^+ induce aggregate formation in d(TGG)$_4$. The 320-nm turbidity monitoring indicates that more than 1 M KCl is needed for the onset of aggregation to occur at 20°C within the time span of 24 h. The kinetic profile is reminiscent of autocatalytic reactions that consist of a lag period followed by accelerative and leveling phases. Progressive shortening of lag periods and more rapid accelerative phases accompany further increases in [K^+]. Interestingly, the presence of Mg^{2+} greatly facilitates the aggregate formation and results in the prominent appearance of an intense Ψ-type CD. For example, whereas 1 M K^+ fails to induce aggregate formation of d(TGG)$_4$ within 24 h, the addition of 1 mM Mg^{2+} to a 1 M K^+ solution is sufficient to induce the onset of aggregation in approximately 12 h. Furthermore, adjustment of the buffer to 16 mM Mg^{2+}/1M KCl reduces the lag time to less than 10 min and aggregation is nearly complete in 2 h. The requirement of [K^+] for aggregation is reduced to 2 mM in the presence of 16 mM Mg^{2+}. The effects of K^+ and Mg^{2+} ions are synergistic, because the presence of 16 mM Mg^{2+} alone does not induce aggregate formation in this oligomer. Thermal stabilities of the aggregates are strongly dependent on the concentrations of these two ions. Although aggregates formed in the presence of 2 M KCl alone melt around 55°C, those formed with added 16 mM Mg^{2+} melt at ~90°C, with some aggregates remaining unmelted even at 95°C. The slow kinetics of aggregate formation led to the appearance of gross hystereses in the cooling profiles. The interplay of these two ions appears to be specific, because the replacement of K^+ by Na^+ or the replacement of Mg^{2+} by other divalent cations does not lead to the observed self-assembly phenomenon, although Sr^{2+} can substitute for K^+. A possible mechanism for the formation of self-assembled structure is suggested. [For details see Chen, Biophysical J. 73, 348-356 (1997)]

Self-aggregation of DNA oligomers with XGG trinucleotide repeats: kinetic and atomic force microscopy measurements.

Turbidity measurements via absorbance monitoring at 320 nm were employed to obtain autocatalytic-like kinetic profiles of K^+-induced aggregate formation of $d(XGG)_4$ and some related oligomers, where X = A, C, G, and T. At least 1M KCl is needed to observe the turbidity-measurable aggregation at pH 8 and the relative propensity for aggregate formation is shown to follow the order: $d(GGG)_4 > d(AGG)_4 \approx d(TGG)_4 >> d(CGG)_4$. The presence of Mg^{++} greatly facilitates and dramatically reduces the amount of K^+ required to initiate aggregation and significantly enhances the thermal stabilities of the aggregates. Replacement of K^+ by Na^+ fails to induce a similar phenomenon. The Ψ-type CD characteristics of aggregates are strongly dependent on the sequence and ionic conditions. Despite their ease in aggregate formation, oligomers with AGG trinucleotide repeats fail to exhibit Ψ-CD formation. The propensity for aggregation is greatly affected by the chain length, with oligomers of 4 repeats being most facile. Appending X base at the 3′-end of d(GGXGGXGGXGG) appears to provide a greater hindrance on aggregation than at the 5′-end. Atomic force microscopic images support some of these findings and reveal the morphologies of these aggregates. The presence of $MgCl_2$ in solutions appears to considerably elongate the K^+-induced aggregates. [For details see Sha et al., Biophysical J. 77, 410-423 (1999)]

KEY RESEARCH ACCOMPLISHMENTS

- ACTD is found to bind strongly and dissociates slowly at the dGpdC site with flanking T/T mismatches.
- ACTD binding studies with oligonucleotides of CXG trinucleotide repeats revealed that the binding order is: $(CTG)_n > (CAG)_n$, $(CCG)_n >> (CAG)_n$ and two ACTD molecules can bind tightly to two consecutive GpC sites separated by a single T/T mismatch, which was initially thought to be unlikely.
- An end-stacking model was proposed to rationalize the strong ACTD binding to d(5'CGTCGACG3') which does not contain a GpC sequence.
- The demonstration that the DNA binding modes of DST can be differentiated via circular dichroic and kinetic means.
- The observation that oligomers of CGG trinucleotide repeat can be induced to form G-quadruplex aggregates by the presence of molar $[K^+]$ and facilitated by moderate acidity.
- K^+ and Mg^{2+} are found to act synergistically in the induction of aggregate formation of oligomers with TGG trinucleotide repeats.
- Atomic force microscopic imaging of aggregates formed by oligomers with XGG trinucleotide repeats.

REPORTABLE OUTCOMES

Publications and manuscripts submitted during the funding period:

Sha, F. and Chen, F.-M. *Biochemistry* (submitted) Actinomycin D Binds Strongly to d(CGACGACG) and d(CGTCGTCG).

Sha, F., Mu, R., Henderson, D. and Chen, F.-M. (1999) *Biophysical Journal 77*, 410-423. Self-Aggregation of DNA Oligomers with XGG Trinucleotide Repeats: Kinetic and Atomic Force Microscopy Measurements.

Chen, F.-M. & Sha, F. (1998) *Biochemistry 37*, 11143-11151. Circular Dichroic and Kinetic Differentiation of DNA Binding Modes of Distamycin.

Chen, F.-M. (1998) *Biochemistry 37*, 3955-3964. Binding of Actinomycin D to DNA Oligomers of CXG Trinucleotide Repeats.
Chen, F.-M. (1997) *Methods in Molecular Biology, Vol. 90: Drug-DNA Interaction Protocols*. Edited by: K. R. Fox. Humana Press Inc., Totowa, NJ. Methods for the Studies of Drug Dissociation from DNA.
Chen, F.-M. (1997) *Biophysical Journal 73*, 348-356. Supramolecular Self-Assembly of $d(TGG)_4$, Synergistic Effects of K^+ and Mg^{2+}.
Liu, C. & Chen, F.-M. (1996) *Biochemistry 35*, 16346-16353. Actinomycin D Binds Strongly and dissociates Slowly at the dGpdC Stie with Flanking T/T Mismatches.
Chen, F.-M. & Liu, C. (1996) *Biochemistry 35*, 7283-7291. Is the Strong Actinomycin D Binding of d(5'CGTCGACG) the Consequence of End-Stacking?
Chen, F.-M. (1995) *J. Biol. Chem. 270*, 23090-23096. Acid-facilitated Supramolecular Assembly of G-quadruplexes in $d(CGG)_4$.

Presentations at Scientific Meetings:

Sha, F. and Chen, F.-M. Eleventh Conversation in Biomolecular Stereodynamics, June 15-19, 1999, Albany, New York. Actinomycin D Binds Strongly to d(CGACGACG) and d(CGTCGTCG).
Sha, F., Mu, R., Henderson, D. and Chen, F.-M*. 43rd Annual Biophysical Society Meeting, 13-17 February 1999, Baltimore, Maryland. Self-Aggregation of DNA Oligomers with XGG Trinucleotide Repeats, Kinetic and AFM Measurements.
Chen, F.-M. & Sha, F. 54th American Chemical Society Southwest Regional Meeting, Nov. 1 - 3, 1998, Baton Rouge, LA. Circular Dichroic and Kinetic Differentiation of DNA Binding Modes of Distamycin.
Chen, F.-M. 42nd Annual Biophysical Society Meeting, 22-26 February 1998, Kansas City, Missouri. Binding of Actinomycin D to DNA Oligomers of CXG Trinucleotide Repeats.
Chen, F.-M. 41st Annual Physical Society Meeting, 2-6 March 1997, New Orleans, Louisiana. Supramolecular Self-Assembly of $d(TGG)_4$, Synergistic Effects of K^+ and Mg^{2+}.
Chen, F.-M. 40th Annual Biophysical Society Meeting, 17-21 February, Baltimore, Maryland. Observation of K^+-induced Supramolecular Chiral Self-Assembly in $d(TGG)_4$ with a Single T $\rightarrow$ C Replacement.
Chen, F.-M. DNA Symposium, Joint Southeast-Southwest Regional Meeting of the American Chemical Society, November 29 – December 1, 1995, Memphis, Tennessee. Is the Strong Actinomycin D Binding of d(5'CGTCGACG) the Consequence of End-Stacking?
Chen, F.-M. 39th Annual Biophysical Society Meeting, February 12-16, 1995, San Francisco, California. K^+induced Supramolecular Assembly of G-quadruplexes in d(CGG).

Personnel
Chen, Fu-Ming: PI.
Sha, Feng: Research Assistant.

CONCLUSION

Some interesting findings were made during our studies on individual drugs. For example, it was found that ACTD binds strongly and dissociates slower at the dGpdC site with flanking T/T mismatches. Studies with related oligomers led us to propose an end-stacking model for ACTD binding to the non-GpC-containing octamer d(CGTCGACG). A more recent finding of ours is the observation that ACTD also binds strongly to the nearly self-complementary sequence d(CGXCGXCG) which led to a speculation of a possible single-strand binding mode with base-stacking on both sides of the ACTD chromophore. ACTD binding study with DNA oligomers of CXG repeats led to the conclusion that two ACTD molecules can bind tightly to two consecutive GpC sites separated by a single T/T mismatch, which was initially thought to be unlikely. Studies with DST led to a possible circular dichroic and kinetic differentiation of DNA binding modes of DST. Our studies on the synergistic effects of drug binding was, however, not as successful. Instead of finding enhancement in bindings, interference was found. This possibly resulted from the fault in our oligonucleotide design.

REFERENCES

Chen, F.-M. (1995) *J. Biol. Chem. 270*, 23090-23096.
Chen, F.-M. (1988) *Biochemstry 27*, 6393-6397.
Chen, F.-M. (1997) *Biophysical J. 73*, 348-356.
Chen, F.-M. (1998) *Biochemstry 37*, 3955-3964.
Chen, F.-M. & Liu, C. (1996) *Biochemstry 35*, 7283-7291.
Chen, F.-M. & Sha, F. (1998) *biochemistry 37*, 11143-11151.
Fasman, G. D.,Ed. (1975) *CRC Handbook of Biochemistry andMolecular Biology*, 3rd ed., Vol. I. P 589, Chemical Rubber Publishing Co., Cleveland, OH.
Gao, X. & Patel, D. J. (1989) *Biochemistry 28*, 751-762.
Gao, X. & Patel, D. J. (1990) *Biochemistry 29*, 10940-10956.
Gao, X., Mirau, P., & Patel, D. J. (1992) *J. Mol. Biol. 223*, 259-279.
Lian, C., Robinson, H., and Wang, A. H.-J. (1996) *J. Am. Chem. Soc. 118*, 8791-8801.
Liu, C & Chen, F.-M. (1994) *Biochemistry 33*, 1419-1424.
Liu, C. & Chen, F.-M. (1996) *Biochemstry 35*, 16346-16353.
Pelton, J. G. & Wemmer, D. E. (1988) *Biochemistry 27*, 8088-8096.
Pelton, J. G. & Wemmer, D. E. (1989) *Proc. Natl. Acad. Sci. U.S.A. 86*, 5723-5727.
Pelton, J. G. & Wemmer, D. E. (1990) *J. Am. Chem. Soc. 112*, 1393-1399.
Sastry, M. & Patel, D. J. (1993) *Biochemistry 32*, 6588-6604.
Sha, F., Mu, R., Henderson, D., Chen, F.-M. (1999) *Biophysical J. 77*, 410-423.
Snyder, J. G., Hartman, N. G., D'Estantoit, B. L., Kennard, O., Remeta, D. P., & Breslauer, K. J. (1989) *Proc. Natl. Acad. Sci. U.S.A. 85*, 3968-3972.

APPENDICES

Reprints and manuscript attached:

Sha, F. and Chen, F.-M. (manuscript) Actinomycin D Binds Strongly to d(CGACGACG) and d(CGTCGTCG).

Sha, F., Mu, R., Henderson, D. and Chen, F.-M. (1999) *Biophysical Journal 77*, 410-423. Self-Aggregation of DNA Oligomers with XGG Trinucleotide Repeats: Kinetic and Atomic Force Microscopy Measurements.

Chen, F.-M. & Sha, F. (1998) *Biochemistry 37*, 11143-11151. Circular Dichroic and Kinetic Differentiation of DNA Binding Modes of Distamycin.

Chen, F.-M. (1998) *Biochemistry 37*, 3955-3964. Binding of Actinomycin D to DNA Oligomers of CXG Trinucleotide Repeats.

Chen, F.-M. (1997) *Methods in Molecular Biology, Vol. 90: Drug-DNA Interaction Protocols*. Edited by: K. R. Fox. Humana Press Inc., Totowa, NJ. Methods for the Studies of Drug Dissociation from DNA.

Chen, F.-M. (1997) *Biophysical Journal 73*, 348-356. Supramolecular Self-Assembly of $d(TGG)_4$, Synergistic Effects of K^+ and Mg^{2+}.

Liu, C. & Chen, F.-M. (1996) *Biochemistry 35*, 16346-16353. Actinomycin D Binds Strongly and dissociates Slowly at the dGpdC Stie with Flanking T/T Mismatches.

Chen, F.-M. & Liu, C. (1996) *Biochemistry 35*, 7283-7291. Is the Strong Actinomycin D Binding of d(5'CGTCGACG) the Consequence of End-Stacking?

Chen, F.-M. (1995) *J. Biol. Chem. 270*, 23090-23096. Acid-facilitated Supramolecular Assembly of G-quadruplexes in $d(CGG)_4$.

Actinomycin D Binds Strongly to d(CGACGACG) and d(CGTCGTCG)†

Feng Sha and Fu-Ming Chen*

Department of Chemistry, Tennessee State University, Nashville, TN 37209-1561

†Research Supported by Army Medical Research Grant DAMD17-94-J-4474 and a subproject of Minority Biomedical Research Support Grant S06GM0892.

*Corresponding Author:

Dr. Fu-Ming Chen

Tel: (615)963-5325

FAX: (615)963-5434

E-Mail: chenf@harpo.tnstate.edu

ABSTRACT

Earlier calorimetric studies had indicated that despite the absence of a GpC sequence, the self-complementary octamer d(CGTCGACG) binds strongly to actinomycin D (ACTD) with high cooperativity and a 2:1 drug to duplex ratio. A subsequent optical spectral study with related oligomers led us to suggest that ACTD may likely stack at the G•C base pairs of both ends of the duplex. New findings are reported herein to indicate that despite the lack of complete self-complementarity, oligomers of d(CGXCGXCG) [X = A or T] motif exhibit unusually strong ACTD affinities with binding constants of roughly 2 x 10^7 M^{-1} and binding densities of 1 drug molecule per strand. The ACTD binding affinity for the corresponding heteroduplex obtained by annealing these two oligomers is, however, considerably reduced. Although spectroscopic results with related oligomers obtained by removing, replacing, or appending bases at the termini appear to be consistent with the end-stacking model, capillary electrophoretic (CE) evidence provides additional insights into the binding mode. CE experiments with the self-complementary oligomers d(CGAGCTCG) and d(CGTCGACG) revealed contrasting migration patterns in the presence of ACTD, with mobility retardation and acceleration exhibited by the GpC- and non-GpC-containing octamers, respectively, whereas the X/X-mismatched d(CGXCGXCG) experienced retardation. These results along with those of related oligomers provide evidence that instead of stacking at the duplex termini, ACTD may in fact stacks at the 3`-end of dG as a single-strand which then wraps around the 2-aminophenoxazin-3-one chromophore and stacks an internal dG on the other side. The seemingly cooperative ACTD binding and the curved Scatchard plot for the self-complementary d(CGTCGACG) may, thus, be attributed to the drug-induced duplex denaturation resulting from strong binding to single strands of d(CGXCGYCG) motif.

Actinomycin D (ACTD) is an antitumor antibiotic which contains a 2-aminophenoxazin-3-one chromophore and two cyclic pentapeptide lactones. This drug has been employed clinically for the treatment of highly malignant tumors, such as Wilms tumor (Farber, S. J. 1966) and gestational choriocarcinoma (Lewis, J. L. 1972; Schink et al. 1992), and has also been used in combinations with other antitumor agents to treat high-risk tumors (Newlands et al. 1991; Marina et al. 1992; Nashamura et al. 1992).

A wealth of information has been compiled regarding the interaction of ACTD with DNA. It is well known that ACTD prefers duplex DNA and binds via intercalation of the planar chromophore, preferably at the GpC sequence, with the two pentapeptide rings resting on the minor groove (see the schematic drawing of Figure 1A). A model of DNA-ACTD complex has been generally accepted in which the phenoxazone ring is intercalated between the G•C and C•G base pairs (where guanine residues are on opposite strands), forming strong hydrogen bonds in the minor groove between the guanine 2-amino groups and the carbonyl oxygen atoms of the L-threonine residues of the cyclic peptapeptides (Sobell et al. 1971; 1972). Additional stabilizations are derived from hydrophobic interactions between groups on the pentapeptides and sugar residues as well as from other specific weaker hydrogen bonds (Kamitori & Takusagawa, 1992; 1994). Since the pentapeptide rings of this drug span about 4-5 base pairs, the binding affinity of ACTD is expected and indeed was found to be affected by adjacent and neighboring bases (Scramrov & Beabealashivilli 1983; Goodisman et al. 1992; Chen 1988; 1992).

However, there have been recent reports to indicate that ACTD may also bind strongly via some non-classic modes, such as to single-stranded DNA (Wadkin & Jovin, 1991;

Hsieh et al., 1994; Wadkins et al., 1998) and to some DNA sequences containing no GpC site (Rill et al. 1989; Snyder et al. 1989; Bailey et al. 1994). In particular, calorimetric studies by Synder et al. (1989) have indicated that despite the absence of GpC sequence ACTD can bind cooperatively to the octamer d(5'CGTCGACG3') with a binding constant on the order of 10^7 M^{-1} and a 2:1 drug to duplex stoichiometry. Further optical evidence from this laboratory led us (Chen and Liu, 1996) to postulate that ACTD may in fact stack on the G•C base pairs at both ends of this oligomeric duplex (see schematic drawing of Figure 1B). This was based on the rationale that the classic intercalative preference of ACTD for 5'G3'p5'C3' implies that the drug favors the 3'-side of dG.

Further studies in this laboratory have led to new findings that despite the lack of complete self-complementarity and the absence of GpC sequence, octamers d(5'CGTCGTCG3') and d(5'CGACGACG3') also bind tightly to ACTD. In an attempt to understand the nature and to delineate the origin of such a strong binding, studies were made with these and related oligomers using capillary electrophoretic and various spectroscopic techniques. The results of these experiments and their significance are presented and discussed in this report.

MATERIALS AND METHODS

Oligonucleotides were purchased from Integrated DNA Technologies, Coralville, Iowa and used without further purification. ACTD and 7-amino-ACTD were purchased from Serva. Stock solutions for oligonucleotides and drugs were prepared by dissolving in 10 mM N'-2-hydoxyethylpiperazine-N'-propanesulfonic acid (HEPPS) buffer solution of pH 8 containing 0.1 M NaCl and 1 mM $MgCl_2$. Concentrations of the DNA solutions were determined by measuring the absorbances at 260 nm after melting and calculating the concentrations by Beer's law. The extinction coefficients of DNA were obtained via

nearest-neighbor approximation using mono- and dinucleotide values tabulated in Fasman (1975). Heteroduplex formation was accomplished by mixing equal molar amounts of the two complementary oligomers, heating the mixture to 95 °C for 5 minutes, and slowly cooling it back to room temperature. Concentrations of the drug solutions were determined by measuring the absorbances at 440 nm (for ACTD) and 528 nm (for 7-amino-ACTD), using extinction coefficients of 24,500 and 23,600 cm^{-1} M^{-1}, respectively. Absorption spectra were measured with a Cary 1E spectrophotometric system. Data were collected from 600 nm to 350 nm. Absorption spectral titrations were carried out by starting with a 5 μM ACTD solution of 2 mL followed by progressive additions of the oligomer stock at equal time intervals. Absorbance differences between 427 and 480 nm during absorption spectral titrations were used to obtain the binding isotherms and Scatchard plots. The binding parameters were deduced via linear least-squares fits on the Scatchard plots. The bound extinction coefficients were estimated through extrapolations to high DNA concentrations. Circular dichroic (CD) spectra were measured at room temperature with a Jasco J-500A recording spectropolarimeter using water-jacketed cylindrical cells of 2-cm pathlength. The data were collected from 350 nm to 230 nm with a scan speed of 50 nm/min. The CD difference spectra were obtained by subtracting out the spectra of 40 μM oligomers (per nucleotide) from those in the presence of 7 μM ACTD. Fluorescence spectra were obtained at 20 °C with a SLM 48000S system. Emission spectra were measured in the region of 580-780 nm with 560 nm excitation, whereas excitation spectra were taken in the region of 420-600 nm with 650 nm emission monitoring.

Stopped-flow kinetic measurements were made with an Olis RSM-1000 rapid scan spectrophotometer. Association kinetic measurements were achieved by injecting equal

volumes of 200 μM oligomeric stock and 20 μM ACTD to result in a mixture of 10 μM ACTD and 100 μM nucleotide. Time dependent absorbance changes at 427 nm were monitored. Dissociation kinetics were measured by mixing a 2 % sodium dodecyl sulfate (SDS) solution with an equal volume of ACTD-DNA mixture and time dependent absorbance changes at 427 nm were also used to obtain kinetic parameters. Nonlinear least-squares fits of the kinetic data were carried out with Graphpad Prism program .

Capillary electrophoretic experiments were carried out in a Beckman P/ACE 5000 instrument. Capillary electrophoresis oligonucleotide run buffer and 75 μm I.D. x 375 μm O.D. capillaries internally-coated with poly(AAEE) were purchased from Bio-Rad (Hercules, CA). Samples were loaded by pressure for 10 s and run at 15 kV and 25 °C with 254 nm absorbance detection. The sieving buffer was replenished before each run using a 5-min purge cycle at 20 p.s.i. pressure. Two water rinse cycles were used to remove residual buffer from the capillary and electrode surfaces to prevent buffer carry over into the sample vial.

RESULTS

Unusually Strong ACTD Binding of d(CGACGACG) and d(CGTCGTCG).

Representative absorption spectral alterations during a typical titration are illustrated with the ACTD+d(CGACGACG) system and are shown in Figure 2A. ACTD exhibits an absorption maximum near 440 nm in buffer solutions and without the presence of DNA. Progressive additions of DNA oligomeric stock result in considerable hypochromic effects of this band and slight bathochromic shifts to result in small hyperchromic effects around 480 nm. The observed hyperchromic effects near 480 nm, however, are significantly less than those observed in ACTD titrations with GpC-containing oligomers (Chen, 1988; 1992). Absorbance differences between 427 and 480 nm were used to

construct the binding isotherms and some representative Scatchard plots are shown in Figures 2B-D. Most of the plots appear to be approximately linear and the extracted binding parameters via linear least-squares fits along with some melting results are summarized in Table 1-3. It is apparent that despite the absence of a GpC sequence and complete self-complementarity, both d(5'CGTCGTCG3') and d(5'CGACGACG3') bind strongly to ACTD with binding constants of 2.5×10^7 and 1.7×10^7 M^{-1}, respectively, and with binding densities of roughly 1 drug molecule per strand. The strong ACTD binding affinities are also evidenced by huge melting temperature increases upon ACTD binding. In the absence of ACTD, these two octamers do not exhibit cooperative melting above 20 °C at 40 μM nucleotide concentrations and 0.1 M NaCl. However, dramatic ACTD-induced duplex stabilization resulted in melting temperatures of 65 and 66 °C for the drug complexes of d(CGTCGTCG) and d(CGACGACG), respectively, exhibiting increases of more than 45 °C (see Table 2).

Replacement or Removal of End Bases Results in Considerably Weaker ACTD Binding Affinity. The ACTD binding parameters for the parent octamers and oligomers derived from replacing the end bases of d(5'CGTCGTCG3') and d(5'CGACGACG3') are compared in Table 1 and some representative Scatchard plots are shown in Figure 2B. More than an order of magnitude reduction in the binding affinities are seen for these end-base-replaced oligomers. For example, d(5'GGTCGTCC3') and d(5'GGACGACC3') exhibit binding constants of 1.5×10^6 and 0.6×10^6 M^{-1} as compared to 2.5×10^7 and 1.7×10^7 M^{-1} for the parent octamers d(5'CGTCGTCG3') and d(5'CGACGACG3'), respectively. A similar reduction in the ACTD binding affinity is seen with the removal of terminal bases from both ends to result in hexamers of the form d(5'GXCGXC3') or with the removal of an XCG unit to result in pentamers of the form d(5'CGXCG3')

having the same terminal bases as those of parent octamers. Binding constants of approximately 7 x 10^5 M^{-1} were obtained for these oligomers which are more than an order of magnitude weaker than those of the parent octamers.

Appending Bases at Sequence Termini Results in Somewhat Reduced Binding Affinities. Binding parameters for oligomers obtained by appending dA and/or dT to the 5' and/or 3' end(s) are compared in Table 2 and the representative Scatchard plots are shown in Figure 2C. Although the binding affinities of the single-base-appended oligomers are somewhat diminished from the parent oligomers, their binding strengths are still quite substantial. Addition of a dT at the 5' or 3' end of d(5'CGTCGTCG3') resulted in a binding constant of 1.3 x 10^7 or 1.5 x 10^7 M^{-1}, respectively, a slight decrease from that of 2.5 x 10^7 M^{-1} of the parent octamer. Similarly, addition of dA at the 5' or 3' end of d(5'CGACGACG3') resulted in a binding constant of 0.4 or 1.1 x 10^7 M^{-1}, respectively, which is to be compared with 1.7 x 10^7 M^{-1} of the parent octamer. Oligomers with bases appended at both ends exhibit further moderate reduction in binding affinities from the corresponding single-base-appended oligomers, with binding constants now ranging from 1.7 to 5 x 10^6 M^{-1}.

ACTD Also Binds Strongly to d(5'CGTCGTCGTCG3') and d(5'CGACGACGACG3') with 1:1 Drug to Strand Ratios. Binding studies with 11-mers d(5'CGTCGTCGTCG3') and d(5'CGCACGACGACG3') and some related oligomers were also made and the results are compared in Table 3 while the representative Scatchard plots are shown in Figure 2D. These two 11-mers are obtained by adding one additional XCG unit to the corresponding parent octamers. It is apparent that both of these 11-mers exhibit strong ACTD binding with roughly 2 x 10^7 M^{-1} in binding constant, comparable to those of the corresponding parent octamers. Most interestingly, the extracted binding densities are

also approximately 1 drug molecule per strand, same as those of the parent octamers. Again, appending the oligomers with dA and/or dT reduces the binding affinities somewhat. The strong ACTD affinities are further supported by dramatic melting temperature increases of roughly 44 °C upon ACTD binding (see Table 3).

Binding Affinities for the Corresponding Hetero-duplexes are Considerably Reduced. The parent octamers d(5'CGTCGTCG3') and d(5'CGACGACG3') are in fact complementary to each other. Thus, mixing equal molar amounts of the two oligomers will result in a predominantly hetero-duplex formation at 20 °C. Interestingly, the ACTD binding ability of the heteroduplex is considerably diminished. The binding constant obtained via Scatchard plot yielded a value of $3.1 \times 10^6\ M^{-1}$ for the heteroduplex, contrasting those of roughly $2 \times 10^7\ M^{-1}$ for the component strands. Similar reductions in the binding affinity of nearly an order of magnitude for the heteroduplexes are also observed for the base-appended oligomers (see Table 2). The diminished ACTD binding ability of the heterduplex as compared to the constituent oligomers is even more dramatically illustrated by the 11-mers in which the corresponding hetero-duplex exhibits a binding affinity of $3 \times 10^5\ M^{-1}$ as compared to those of $2 \times 10^7\ M^{-1}$ for the component oligomers, a nearly two orders of magnitude reduction (see Table 3). The importance of proximal base-pair mismatches on ACTD binding is further investigated by replacing those mismatches with base pairs and leaving only a single T/T mismatch at the center. The ACTD binding affinities for the resulting 11-mers d(5'CGTCGTCGACG3') and d(5'CGACGTCGTCG3') are seen to be smaller and larger than the corresponding 3 X/X-mismatched d(5'CGXCGXCGXCG3') and fully base-paired d(5'CGXCGXCGXCG3')[d], respectively (see Table 3 and Figure 2D).

CD Measurements Support the Results of Equilibrium Binding Titrations. Binding of ACTD to DNA can induce a characteristics CD spectrum consisting of positive and negative maxima near 293 and 270 nm, respectively. Thus, it is possible to obtain relative ACTD binding affinities qualitatively by comparing the induced CD intensities at 293 nm. CD difference spectral comparison (ACTD/DNA - DNA) of d(5'CGTCGTCGTCG3') and its heteroduplex along with those of d(CGTCGTCGACG) and d(CGACGTCGTCG) are illustrated in Figure 3. The last two oligomers are essentially self-complementary except for the dT at the center. In agreement with the results of absorbance binding titrations, d(5'CGTCGTCGTCG3') exhibits a considerably larger CD intensity at 293 nm than its heteroduplex while the two nearly self-complementary 11-mers are intermediate of these two extremes.

CD measurements were also extended to cover the 460-nm spectral region. In contrast to the GpC containing oligomers, ACTD binding to both d(CGACGACG) and d(CGTCGTCG) induces positive rather than negative CD in this region.

Comparison with the Fluorescence Results of 7-Amino-ACTD. Unlike ACTD, the fluorescence of its 7-amino derivative (7-amino-ACTD) is quite substantial. It is, thus, of interest to corroborate the ACTD results with those of this derivative via fluorescence measurements since its 7-amino group substitution has been shown not to greatly alter the intercalative binding nature of this derivative (Muller, 1962). The binding of 7-amino-ACTD with DNA usually results in an enhanced fluorescence emission spectrum exhibiting a maximum near 650 nm and a fluorescence intensity enhancement near 540 nm in the excitation spectrum with 650-nm emission monitoring. Difference fluorescence excitation spectra as typified by d(CGTCGTCG) and related oligomers are compared in Figure 4. Consistent with the weaker ACTD binding affinities, the double-base-appended

oligomers exhibit somewhat lower fluorescence intensities than those of the single-base-appended ones whereas all the base-appended oligomers induce significantly stronger fluorescence than the parent octamers.

Capillary Electorphoretic Profiles. Capillary electropherograms of d(CGTCGTCG) (upper panel), d(CGTCGACG) (middle panel), and d(CGAGCTCG) (lower panel) in the absence (lower trace of each panel) and in the presence of ACTD (upper trace of each panel) are compared in Figure 5. Consistent with a single-stranded conformation at room temperatures, the octamer with T/T mismatches exhibits a considerably shorter migration time than those of the two self-complementary octamers which exist mainly in the duplex form at room temperature (compare lower traces of the three panels). It is interesting that binding of ACTD resulted in distinctly different migration patterns for these oligomers. The self-complementary octamer d(CGAGCTCG) contains a central GpC site and thus an ACTD molecule is expected to be intercalated at that location. Indeed, in the presence of ACTD in the running buffer, the electrophoretic mobility of the oligomer is retarded to result in a slower migration time (see the lower panel). In contrast, the binding of ACTD to the non-GpC-containing octamer d(CGTCGACG) resulted in a considerably faster migration time. Interestingly, a moderate retardation of electrophoretic mobility was observed for the T/T-containing d(CGTCGTCG) upon ACTD binding. CE results of these three oligomers are summarized in Table 4.

DISCUSSION

Despite the absence of a strong binding sequence GpC and the lack of complete self-complementarity, both d(CGACGACG) and d(CGTCGTCG) exhibit unusually strong ACTD binding affinities of roughly 2×10^7 M^{-1} in binding constant and about 1 drug molecule per DNA strand in binding density. In contrast to the previously studied self-

complementary counterparts (Snyder et al., 1989; Chen & Liu, 1996), the Scatchard plots for ACTD binding to d(CGXCGXCG) do not exhibit unusual curvatures. Melting experiments indicate that the melting temperatures of the X/X-mismatched octamers are below 20°C whereas the ACTD-bound complexes melt around 65°C, same as those of self-complementary counterparts. Interestingly, the ACTD binding propensity of the heteroduplex formed by annealing these two oligomers together is considerably diminished. Removing as well as replacing the end bases resulted in a diminution of the ACTD binding strength by more than an order of magnitude. A slight reduction in the binding affinity for oligomers with a single-base terminal addition and a further reduction in the binding affinity upon a terminal A•T base pair addition were also observed. These results are similar to those found for the self-complementary octamer d(CGTCGACG) and appear to be consistent with our earlier speculation that drug molecules stack at the terminal G•C base pairs of the duplex. Furthermore, addition of an XCG unit to the parent octamers resulted in no apparent reduction in binding affinities and the binding densities remained approximately 1 drug molecule per strand. Similar to their parent octamers, more than an order of magnitude reduction in the binding strength is seen for the annealed heteroduplex of these 11-mers. The finding that the binding densities of 1 drug molecule per strand is maintained for the ACTD binding to the d(CGXCGXCGXCG) oligomers, despite a 3-base addition to the parent octamers, is consistent with such a model since if the binding were to be at the internal sequences, the binding densities for the 11-mers would have been significantly increased.

The results of CD as well as fluorescence spectral measurements also appear to conform with the notion of end-stacking binding mode. Appending base(s) at one or two end(s) results in the reduced CD intensities at 293 nm and the resulting order are

consistent with the relative binding affinities obtained via absorption spectral titrations. Despite the fact that the extents of fluorescence enhancement of 7-amino-ACTD do not exactly correlate well with the binding order for the oligomers studied, it is apparent that changing the end bases of a sequence greatly affects the fluorescence intensities induced. The fluorescence results, however, appear to provide a more convincing evidence that the binding of ACTD to d(CGXCGXCG) occurs at the termini rather than at the internal sequences. If the binding were to occur at the internal sequences, changes at the sequence ends would not be expected to make a significant influence on the fluorescence spectral characteristics of the bound drug. Yet, the fluorescence results clearly indicate that when dangling bases were added at one or two sequence ends, strong fluorescence enhancements were observed. It is likely that the dangling base folds back to rest on the stacked drug molecule.

The interpretation of ACTD stacking at the terminal G•C base pairs, however, begs the question as to why the hetero-duplex formed by annealing d(CGTCGTCG) and d(CGACGACG) exhibits a dramatic reduction in ACTD binding affinity. One could argue that this may be the consequence of the fact that an optimal ACTD binding via stacking on a terminal G•C base pair requires not only strong hydrogen-bondings of the drug with the base pair but also a snug fit for one of the pentapeptide rings in the minor groove. Because of its somewhat more rigid structure, it would be more difficult for a fully base-paired duplex to achieve an optimal fit than a duplex with a proximal base pair mismatch since the former would be less accomodating to the drug's side chains. Such a rationale appears to be in line with the significant reduction in ACTD binding affinities of d(CGTCGTCGACG) and d(CGACGTCGTCG), where the two outer T/T mismatches have been replaced by A•T pairs. from 2.1×10^7 M^{-1} of the parent 11-mer

d(CGTCGTCGTCG) to 4.2 and 1.4 x 10^6 M^{-1}, respectively. The fully base-paired hetero-duplex d(CGTCGTCGTCG)[d] showed further reduction, with a binding constant of merely 3 x 10^5 M^{-1}.

Additional insights into the binding mode, however, are provided by the intriguing and contrasting capillary electrophoretic migration patterns of d(CGAGCTCG) and d(CGTCGACG) in the absence and in the presence of ACTD. Although the distinct electrophoretic behaviors are consistent with their differing binding modes, it is somewhat puzzling that an ACTD intercalation at the central GpC site resulted in a mobility retardation for d(CGAGCTCG) whereas binding at d(CGTCGACG), presumably stacking at duplex termini, resulted in an faster migration. The CE migration patterns of the T/T-mismatched octamer d(CGTCGTCG) provide a possible resolution. The considerably faster mobility of d(CGTCGTCG) in the absence of ACTD as compared to the two self-complementary octamers suggests that it exists predominantly in the hairpin or single-stranded form and its mobility retardation in the presence of ACTD is consistent with its drug binding to form a complex of a larger molecular weight. Thus, the unusual accelerated mobility upon ACTD binding to the self-complementary d(CGTCGACG) may be interpreted as the result of drug-induced denaturation for ACTD binding to the higher-affinity single strands and forming faster migrating complexes than its duplex form. This will also explain the significant reduction of ACTD binding affinity of the heteroduplex when compared to its constituent oligomers, since the stronger binding single strands have been mainly tied up in the duplex formation. Consequently, the the duplex stability adversely affects its ACTD binding.

In view of the proposed single strand binding, the absence of curvatures in the Scatchard plots for octamers d(CGXCGXCG) and the apparent presence of strong

cooperativity for the previously studied self-complementary octamer d(CGTCGACG) may be worthy of comment. The presence of X/X mismatches in d(CGXCGXCG) dictates that the oligomers exist predominantly in the single-stranded form which binds strongly to ACTD, thus the absence of unusual Scatchard plots. On the other hand the self-complementary octamer d(CGTCGACG) should exist predominantly in the duplex form at room temperature and an ACTD-induced denaturation would be needed to provide single strands for binding and, thus, result in a curvature in the Scatchard plot and apparent binding cooperativity. The near identical melting temperatures of the ACTD complexes regardless of whether they are formed by self-complementary or mismatched octamers also appear pausible under the single-strand binding model.

To further delineate the binding contributions of hairpin vs single-stranded forms, studies were also made with d(TGXCGXCG) and d(CGXCGXCA). The replacement of one of the terminal bases of the parent octamers d(CGXCGXCG) with a non-complementary base should result in a reduction of hairpin-forming tendency of the oligomers. Our binding as well as capillary electrophoretic results indicate that ACTD binds strongly to d(TGXCGXCG) while its affinities for d(CGXCGXCA) is reduced by several folds. This seems to illustrate the importance of the dG presence at the 3'-end and the non-essential role of hairpin in the the ACTD binding of d(CGXCGXCG). Although the hairpin formation is not essential for the ACTD binding of these oligomers, it is likely that the oligomer wraps around the ACTD chromophore so as to have an internal dG (possibly the one near the other end) stacking on the other side of the drug chromophore. This may explain the observed huge melting temperature increases upon drug binding to d(CGXCGXCG).

The positive induced CD of ACTD in the 460-nm region (results not shown) upon binding to d(CGACGACG) and d(CGTCGTCG) strongly implicates drug stacking at the terminal dG. In contrast to binding of ACTD to GpC-containing oligomers which results in negative CD intensity at this wavelength, a positive CD intensity results when binding to the mononucleotide pdG (Homer, 1969).

REFERENCES

Bailey, S. A., Graves, D. E., and Rill, R. (1994) *Biochemstry 33*, 11493-11500.

Chen, F.-M and Liu, C. D. (1996) *Biochemistry 35*, 7283-7291.

Chen, F.-M. (1988) *Biochemstry 27*, 6393-6397.

Chen, F.-M. (1992) *Biochemstry 31*, 6223-6228.

Farber, S. J. (1966) *J. Am. Med. Assoc. 198*, 826-836.

Fasman, G. D.,Ed. (1975) *CRC Handbook of Biochemistry andMolecular Biology*, 3rd ed., Vol. I. P 589, Chemical Rubber Publishing Co.,Cleveland, OH.

Hommer, R. B. (1969) *Arch. Biochem. Biophys. 129*, 405-407.

Hsieh, Y. L., Li, Y. T., and Henion, J. D. (1994) *Biol. Mass Spectrom 116*, 272-276.

Goodisman, J., Rehfuss, R., Ward, B., and Dabrowiak, J. C. (1992) *Biochemistry 31*, 1046-1058.

Kamitori, S., and Takusagawa, F. (1992) *J. Mol. Biol. 225*, 445-456.

Kamitori, S., and Takusagawa, F. (1992) *J. Am. Cem. Soc. 116*, 4154-4165.

Lewis, J. L. (1972) *Cancer 30*, 1517-1521.

Marina, N., Fontanesi, J., Kun, L., Rao, B., Jenkins, J. J., Thompson, E. I., and Etcubanas, E. (1992) *Cancer 70*, 2568-2575.

Nakamura, E., Kaneko, Y., Takenawa, J., and Sasaki, M. (1992) *Acta Urol. Jpn. 38*, 913-918.

Newlands, E. S., Bagshawe, K. D., Begent, R. H. J., Rustin, G. J. S., and Holden, L. B. (1991) *J. Obstet. Gynaecol. 98*, 550-557.

Rill, R. L. and Hecker, K. H. (1996) *Biochemistry 35*, 3525-3533.

Rill, R. L., Marsch, G. A., and Graves, D. E. (1989) *J. Biomol. Struct. Dynam. 7*, 591-605.

Schink, J. C., Singh, D. K., Rademaker, A. W., Miller, D. S., and Lurain, J. R. (1992) *Obstet. Gynecol. 80*, 817-820.

Scramrov, A. V. and Beabealashivilli, R. Sh. (1983) *FEBS Lett. 164*, 97-101.

Snyder, J. G., Hartman, N. G., D'Estantoit, B. L., Kennard, O., Remeta, D. P., and Breslauer, K. J. (1989) *Proc. Natl. Acad. Sci. U. S. A. 86*, 3968-3972.

Sobell, H. M., Jain, S. C., Sakore,T. D., and Nordman, C. E. (1971) *Nature (New Biol.) 231*, 200-200.

Sobell, H. M. (1972) *J. Mol. Biol. 68*, 21-34.

Wadkins, R. M., Jares-Erijman, E. A., Klement, R., Rudiger, A., and Jovin, T. M. (1996) *J. Mol. Biol. 262*, 53-68.

Wadkins, R. M., Jovin, T. M. (1991) *Biochemstry 30*, 9469-9478.

Wadkins, R. M., Vladu, B., and Tung, C.-S. (1998) *Biochemistry 37*, 11915-11923.

Table 1. Comparison of ACTD Binding Parameters at 20°C for d(CGXCGXCG) and Some Related Oligomers via Replacement or Removal of End Base(s).

Oligomer	$K(\mu M^{-1})$	n/strand
CGTCG	0.8	
GTCGTC	0.7	
CGTCGTCG	25	1.0
GGTCGTCC	1.5	
TGTCGTCA	1.7	
AGTCGTCT	1.8	
CGACG	0.7	
GACGAC	0.7	
CGACGACG	17	0.9
GGACGACC	0.6	
TGACGACA	0.9	
AGACGACT	0.5	

Table 2. Comparison of ACTD Binding Parameters at 20 °C for d(5'CGXCGXCG3') and Related Oligomers via Appending Base(s) at the Terminal(s).

Oligomer	K (μM^{-1})	n/strand	$T_m°$(°C)	T_m(°C)
CGTCGTCG	25	1.0	< 20	65
CGACGACG	17	0.9	< 20	66
CGTCGTCG[d]	3.1	1.1	41	66
CGTCGTCG-T	15	0.9	< 20	68
A-CGACGACG	4.1	1.1	~ 20	62
CGTCGTCGT[d]	0.7			
T-CGTCGTCG	13	0.7	~ 20	65
CGACGACG-A	11	1.1	< 20	68
T-CGTCGTCG[d]	0.5			
A-CGTCGTCG-T	4.5	1.0		
A-CGACGACG-T	1.7			
A-CGTCGTCG-T[d]	0.9			
T-CGTCGTCG-A	5.0	1.1		
T-CGACGACG-A	3.8	1.0		
T-CGTCGTCG-A[d]	0.4			

$T_m°$ and T_m designate the estimated melting temperatures of 40 μM DNA (nucleotide) in the absence and in the presence of 7 μM ACTD, respectively. Absorbance changes on melting were monitored at 275 nm. Heteroduplex is designated by [d].

Table 3. Comparison of ACTD Binding Parameters for d(5'CGXCGXCGXCG3') and Related Oligomers at 20 °C.

Oligomer	K(μM^{-1})	n/strand	$T_m°$(°C)	T_m(°C)
CGTCGTCGTCG	21	1.1	32	76
CGACGACGACG	20	1.1	28	78
CGTCGTCGTCG[d]	0.3		56	75
CGTCGTCGACG	4.2	1.1	40	78
CGACGTCGTCG	1.4		52	77
CGTCGTCGTCG-T	14	1.0		
A-CGACGACGACG	2.0			
A-CGACGACGACG[d]	1.5			
T-CGTCGTCGTCG	13	1.2		
CGACGACGACG-A	12	1.0		
T-CGTCGTCGTCG[d]	<0.2			

$T_m°$ and T_m designate the estimated melting temperatures of 40 μM DNA (nucleotide) in the absence and in the presence of 7 μM ACTD. Absorbance changes on melting were monitored at 275 nm. Heteroduplex is designated by [d].

Table 4. Comparison of Capillary Electrophoretic Profiles at 25 °C for d(5'CGTCGTCG3') and Related Oligomers in the Presence and in the Absence of ACTD.

Oligomer	[ACTD] in DNA	[ACTD] in buffer	Δt (min)[a]
d(CGAGCTCG)	0.00 μM	0.00 μM	3.935
	0.0	40	4.027
	0.25	40	3.843, 4.529
	0.50	40	4.484
	0.75	40	4.530
d(CGTCGACG)	0.00	0.00	3.981
	0.0	40	3.889
	0.25	40	3.385
	0.50	40	3.157
	0.75	40	3.020
d(CGTCGTCG)	0.00	0.00	2.517
	0.0	40	2.517
	0.25	40	2.653
	0.50	40	2.743
	0.75	40	2.745

[a]Δt is the migration time relative to that of dT as an internal reference.

FIGURE LEGENDS

Figure 1. Schematic drawings of intercalative mode (panel A) and the proposed end-stacking mode (panel B) of ACTD binding to DNA.

Figure 2. (A): Typical spectral alterations during absorption spectral titrations as illustrated by the ACTD + d(CGACGACG) system. [nucleotide] / [drug] ratio is designated by P/D. (B): Comparison of Scatchard plots for d(CGXCGXCG) with oligomers derived via end-base replacement, as typified by X = T series. (C): Comparison of Scatchard plots for d(CGXCGXCG) with oligomers derived via appending base(s) at the terminal(s), as typified by X = A series. (D): Comparison of Scatchard plots for d(CGXCGXCGXCG) and some related oligomers, as typified by X = T series. Spectral titrations were carried out at 20 °C and the absorbance differences between 427 and 480 nm have been used to obtain the binding isotherms. [Bound drug] / [DNA, nucleotide] is designated by **r**, and **m** represents the free drug concentration in μM.

Figure 3. Comparison of ACTD-induced CD spectral characteristics at room temperature for d(CGTCGTCGTCG), its heteroduplex, and some related oligomers. Spectra were measured at room temperature using a cylindrical cell of 2-cm pathlength for 40 μM (base) of oligonucleotide in the absence and in the presence of 5 μM ACTD. Difference CD spectra were obtained by subtracting out the contribution due to DNA.

Figure 4. Comparison of difference fluorescence excitation spectra of 7-am-ACTD as induced by d(CGTCGTCG) and related oligomers as derived via appending base(s) at the terminal(s). Spectra were measured with 2 μM 7am-ACTD in the presence of 40 μM nucleotide at 20 °C with 650-nm monitoring of fluorescence emission.

Figure 5. Comparison of capillary electropherograms at 25 °C in the absence (lower trace) and in the presence (upper trace) of 0.8 μM ACTD in the running buffer for d(CGAGCTCG) (lower panel), d(CGTCGACG) (middle panel), and d(CGTCGTCG) (upper panel). DNA concentrations are roughly 0.8 mM in nucleotide.

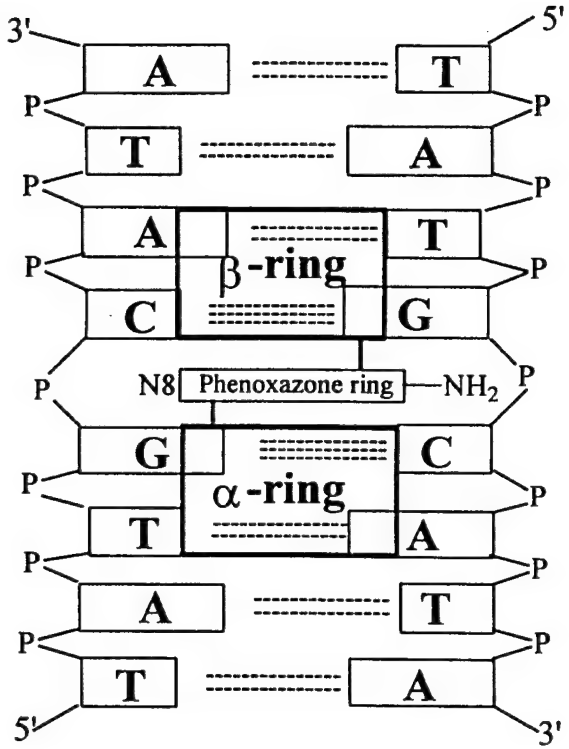

Strand-2 Strand-1

(A)

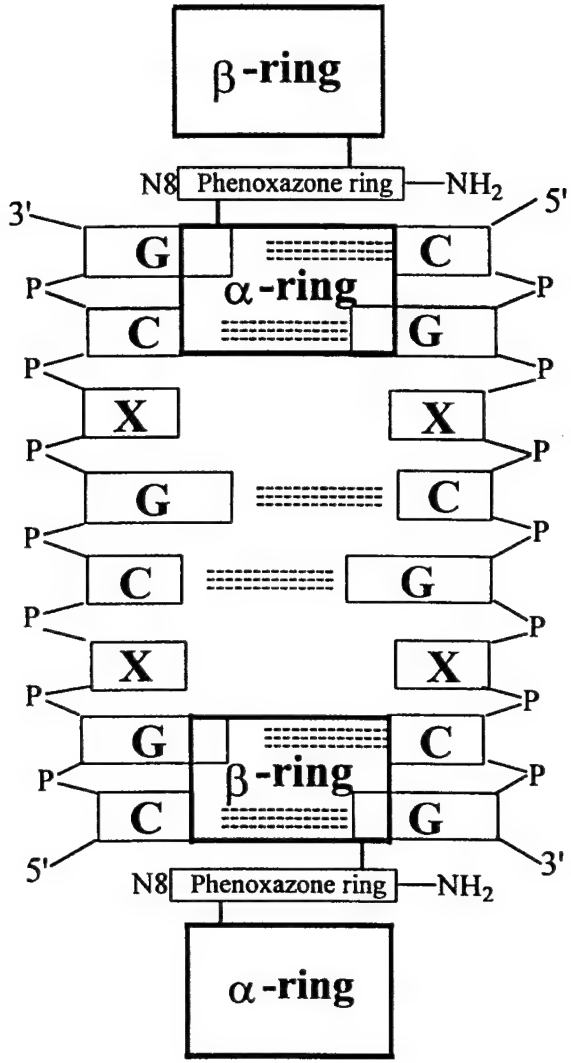

Strand-2 Strand-1

(B)

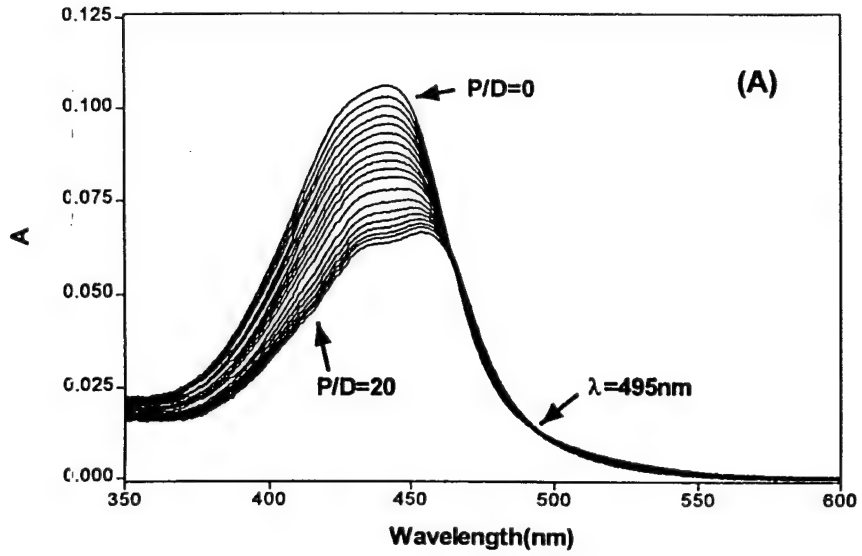
(A)
P/D=0
P/D=20
λ=495nm
A
Wavelength(nm)
0.125
0.100
0.075
0.050
0.025
0.000
350
400
450
500
550
600

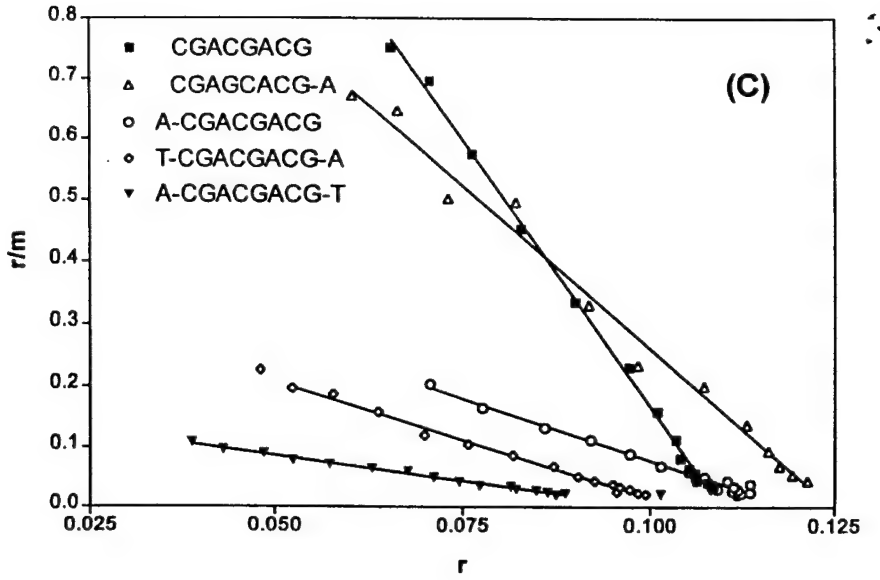
(C)
CGACGACG
CGAGCACG-A
A-CGACGACG
T-CGACGACG-A
A-CGACGACG-T
r/m
r
0.8
0.7
0.6
0.5
0.4
0.3
0.2
0.1
0.0
0.025
0.050
0.075
0.100
0.125

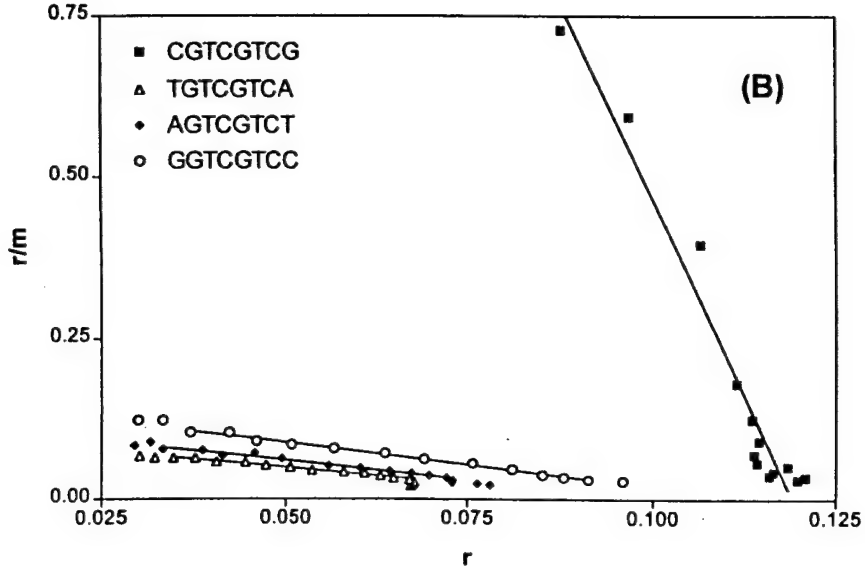
(B)
CGTCGTCG
TGTCGTCA
AGTCGTCT
GGTCGTCC
r/m
r
0.75
0.50
0.25
0.00
0.025
0.050
0.075
0.100
0.125

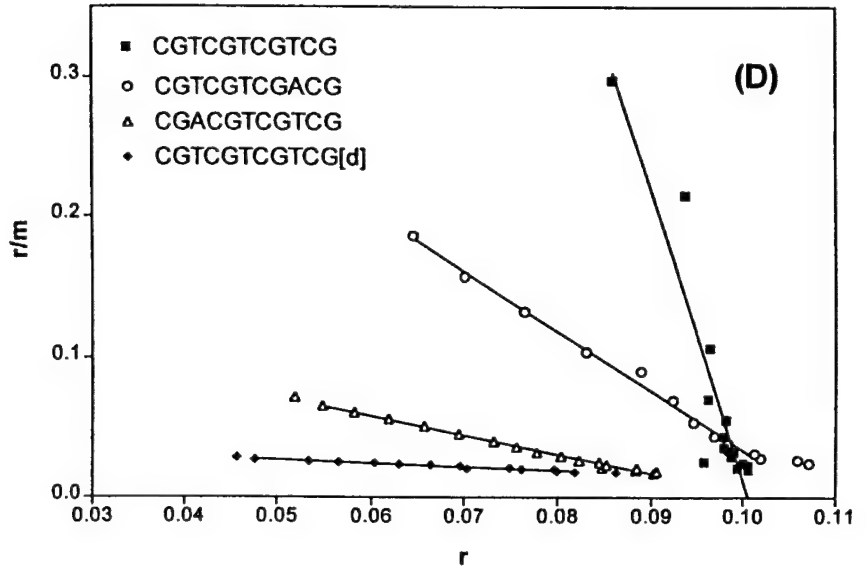
(D)
CGTCGTCGTCG
CGTCGTCGACG
CGACGTCGTCG
CGTCGTCGTCG[d]
r/m
r
0.3
0.2
0.1
0.0
0.03
0.04
0.05
0.06
0.07
0.08
0.09
0.10
0.11

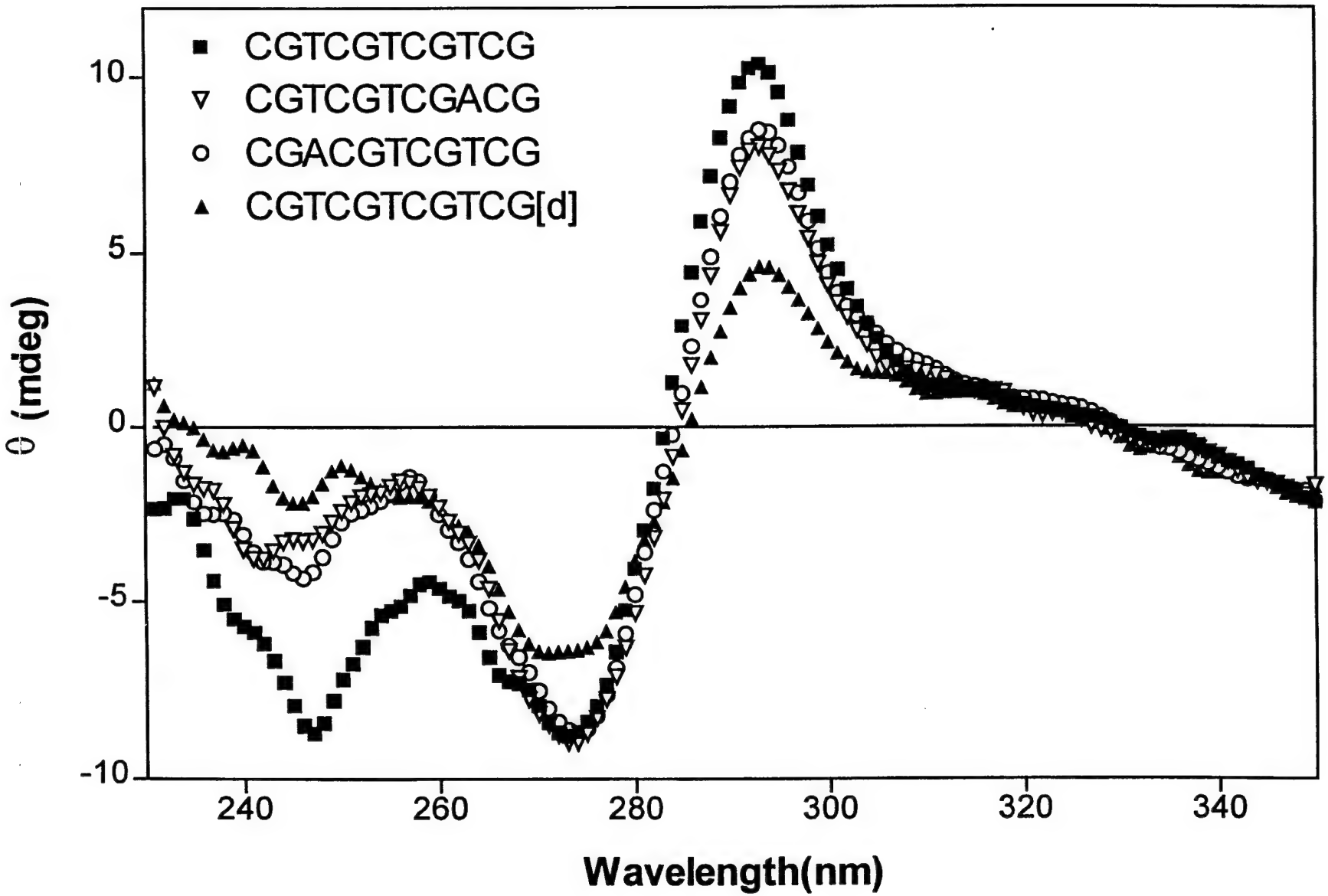
CGTCGTCGTCG
CGTCGTCGACG
CGACGTCGTCG
CGTCGTCGTCG[d]
10
5
0
-5
-10
θ (mdeg)
240
260
280
300
320
340
Wavelength(nm)

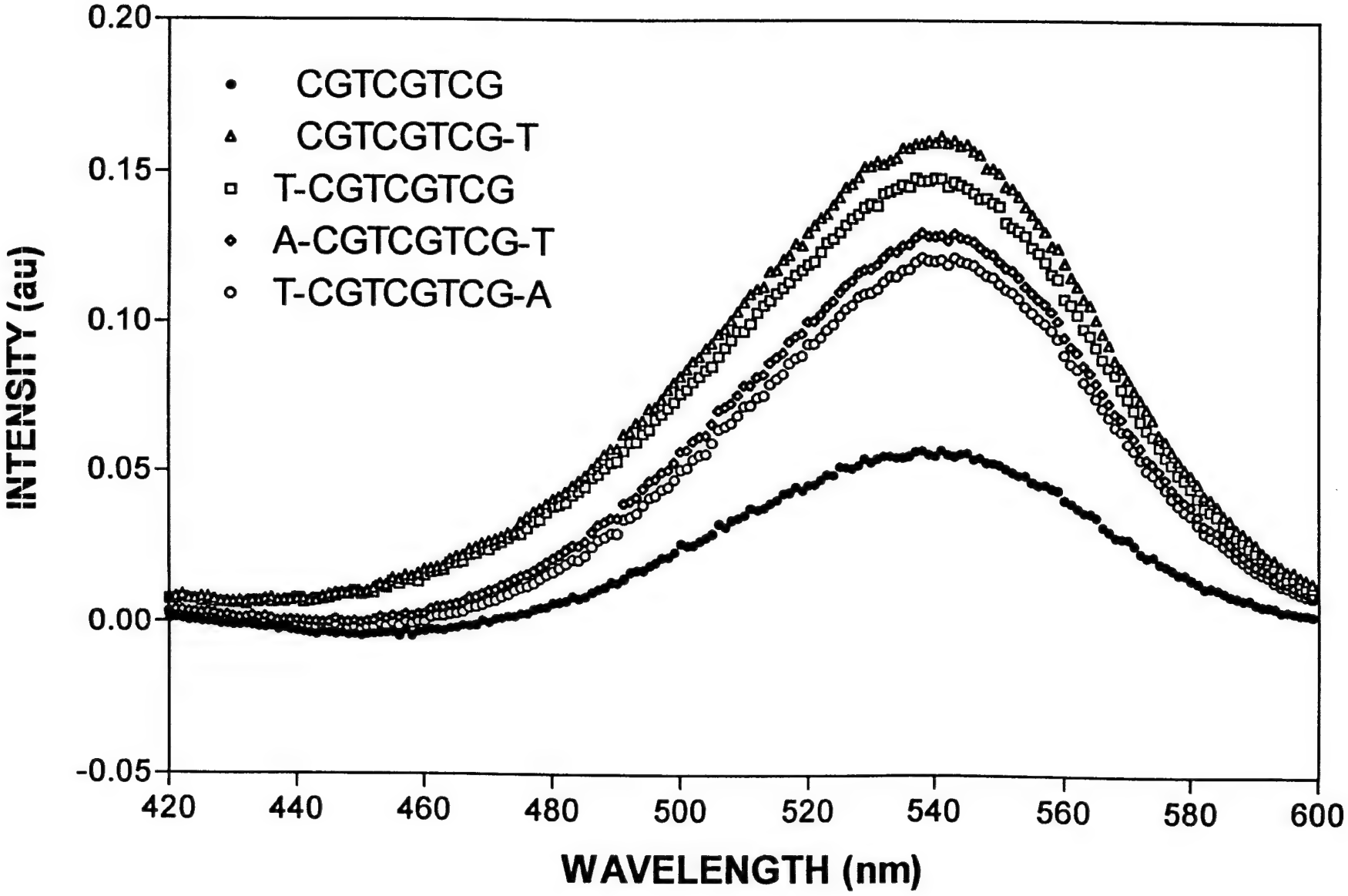
CGTCGTCG
CGTCGTCG-T
T-CGTCGTCG
A-CGTCGTCG-T
T-CGTCGTCG-A
INTENSITY (au)
0.20
0.15
0.10
0.05
0.00
-0.05
420
440
460
480
500
520
540
560
580
600
WAVELENGTH (nm)

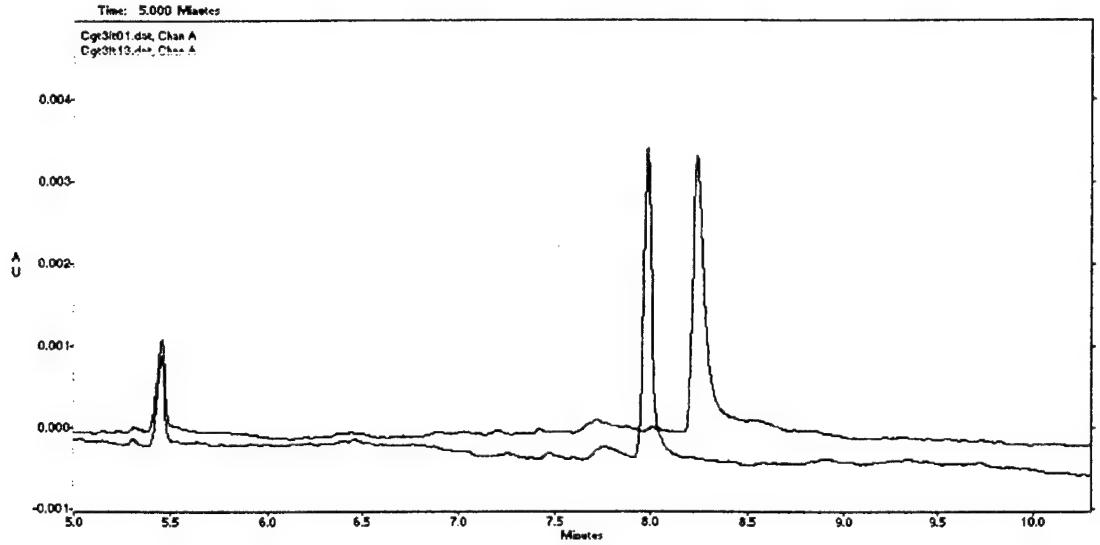
Time: 5.000 Minutes
Cgt3lt01.dat, Chan A
0.004
0.003
0.002
0.001
0.000
-0.001
A U
5.0
5.5
6.0
6.5
7.0
7.5
8.0
8.5
9.0
9.5
10.0
Minutes

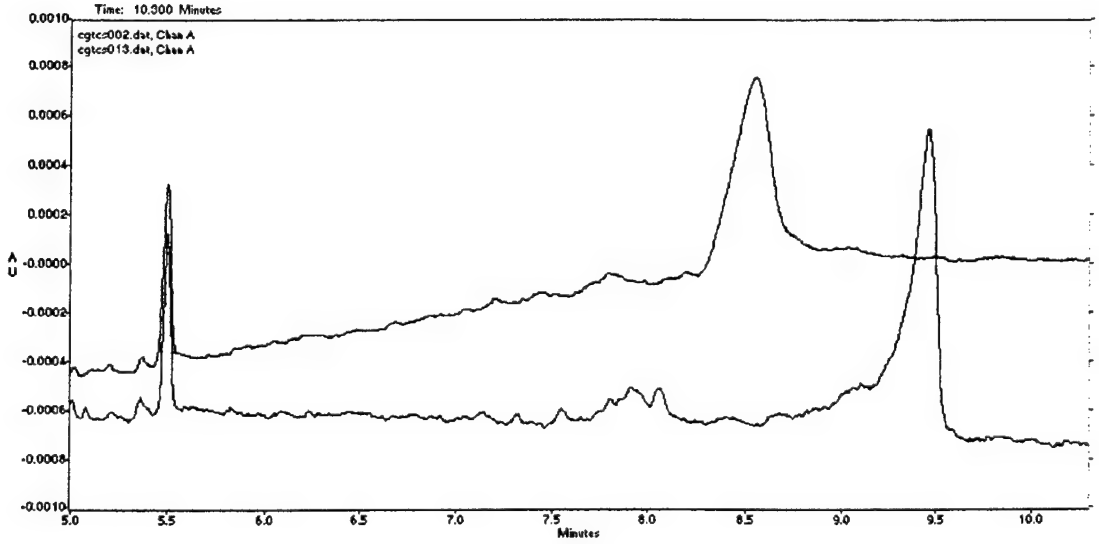
Time: 10.300 Minutes
cgtcs002.dat, Chan A
cgtcs013.dat, Chan A
0.0010
0.0008
0.0006
0.0004
0.0002
-0.0000
-0.0002
-0.0004
-0.0006
-0.0008
-0.0010
A U
5.0
5.5
6.0
6.5
7.0
7.5
8.0
8.5
9.0
9.5
10.0
Minutes

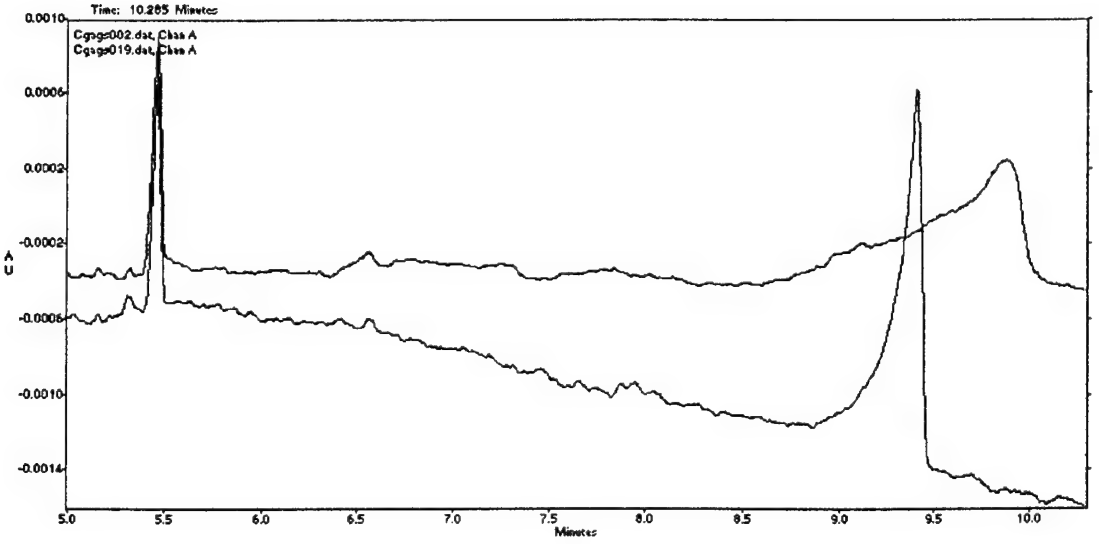
Time: 10.265 Minutes
Cgagc002.dat, Chan A
Cgagc019.dat, Chan A
0.0010
0.0006
0.0002
-0.0002
-0.0006
-0.0010
-0.0014
A U
5.0
5.5
6.0
6.5
7.0
7.5
8.0
8.5
9.0
9.5
10.0
Minutes

Biophysical Journal Volume 77 July 1999 410–423

Self-Aggregation of DNA Oligomers with XGG Trinucleotide Repeats: Kinetic and Atomic Force Microscopy Measurements

Feng Sha,* Rixiang Mu,# Don Henderson,# and Fu-Ming Chen*
*Department of Chemistry, Tennessee State University, Nashville, and #Chemical Physics Laboratory, Department of Physics, Fisk University, Nashville, Tennessee 37209-1561 USA

ABSTRACT Turbidity measurements via absorbance monitoring at 320 nm were employed to obtain autocatalytic-like kinetic profiles of K^+-induced aggregate formation of $d(XGG)_4$ and some related oligomers, where X = A, C, G, and T. At least 1 M KCl is needed to observe the turbidity-measurable aggregation at pH 8, and the relative propensity for aggregate formation is shown to follow the order $d(GGG)_4 > d(AGG)_4 \approx d(TGG)_4 \gg d(CGG)_4$. The presence of Mg^{2+} greatly facilitates and dramatically reduces the amount of K^+ required to initiate aggregation and significantly enhances the thermal stabilities of the aggregates. Replacement of K^+ by Na^+ fails to induce a similar phenomenon. The Ψ-type CD characteristics of aggregates are strongly dependent on the sequence and ionic conditions. Despite their ease of aggregate formation, oligomers with AGG trinucleotide repeats fail to exhibit Ψ-CD formation. The propensity for aggregation is greatly affected by the chain length, with oligomers of four repeats being most facile. Appending X base at the 3′ end of d(GGXGGXGGXGG) appears to provide a greater hindrance to aggregation than at the 5′ end. Atomic force microscopic images support some of these findings and reveal the morphologies of these aggregates. The presence of $MgCl_2$ in solutions appears to considerably elongate the K^+-induced aggregates.

INTRODUCTION

Structural properties of G-rich DNA are of current intense interest, as they may be intimately related to the telomeric functions. Telomeres are specialized DNA-protein structures at the termini of chromosomes that have been shown to be important for their stability and accurate replication (Lumdblad and Szostak, 1989; Sandell and Zakian, 1993; Blackburn, 1994). Telomeric DNAs consist of simple repetitive guanine-rich sequences, with the most common units consisting of three or four guanine nucleotides. It has been shown that these G-rich oligomers can form intermolecular or intramolecular G-quadruplexes, depending on the chain length and intervening non-G nucleotides, with strong dependence on the monovalent cations such as K^+ and Na^+ (Williamson, 1994). These tetraplexes are cyclic arrays of four hydrogen-bonded guanine bases in which each base acts as both donor and acceptor of two hydrogen bonds with other guanines, and the pairing between bases is of the Hoogsteen type. The interest in these structures has been further stimulated by their possible relevance to the recombinational events at the immunoglobulin switching regions (Sen and Gilbert, 1988). Effects of monovalent cations on the G-quadruplex structural formation of telomeric DNA sequences have been extensively studied in recent years. Evidence suggests that K^+ is much more effective in stabilizing G-quadruplex formation, possibly because of its optimal size. The ion is found to be sandwiched between two G-tetrads to form an octacoordinated complex with the carbonyl groups of guanines. It was also found that for contiguous guanine oligomers, the parallel strand orientation is thermodynamically more favorable than the antiparallel orientation in the G-quadruplex formation (Sen and Gilbert, 1988; Lu et al., 1993).

A rather interesting phenomenon, likely related to quadruplex structures, was uncovered earlier in our laboratory, in which molar K^+ induces chiral aggregate formation in $d(CGG)_4$ (Chen, 1995). The kinetics of this transformation are very slow at pH 8 but are greatly facilitated in acidic conditions. The kinetic profiles resemble those of autocatalytic reacting systems, with characteristic induction periods followed by accelerative and leveling phases. Time-dependent CD spectral characteristics indicate the formation of parallel G-tetraplexes before the onset of aggregation. A mechanism for the formation of a novel self-assembled super quadruplex structure of dendrimer-type via interquadruplex $C{\cdot}C^+$ base pairing was speculated on. Recently, however, it was further found that $d(TGG)_4$ can also be induced to form aggregates by molar concentrations of K^+, despite the absence of Ψ-CD formation (Chen, 1997). In fact, it was found that $d(TGG)_4$ is kinetically more facile in forming aggregates than $d(CGG)_4$ at pH 8, suggesting that the presence of cytosine is not essential and is in fact detrimental to aggregation. It was further found that the presence of Mg^{2+} greatly facilitates the aggregate formation and results in the prominent appearance of an intense Ψ-type CD. In an effort to further elucidate the mechanism for the observed self-assembly processes, systematic studies are herein made with oligomers containing XGG trinucleotide repeats, where X = A, C, G, or T, under various chain lengths and ionic conditions.

Received for publication 30 November 1998 and in final form 22 April 1999.

Address reprint requests to Dr. Fu-Ming Chen, Department of Chemistry, Tennessee State University, Nashville, TN 37209-1561. Tel: 615-963-5325; Fax: 615-963-5434; E-mail: chenf@harpo.tnstate.edu.

0006-3495/99/07/410/14 $2.00

Atomic force microscopy (AFM) has been used to characterize structures of various biological macromolecules and their interactions (Hansma and Hoh, 1994). In particular, AFM has recently been used to give direct evidence on the formation of a novel DNA nanostructure termed the *G-wire* (Marsh et al., 1995). Because the proposed mechanisms and structures of the $d(XGG)_4$ aggregates are closely related to those of the G-wire, AFM images of these aggregates will be of considerable interest. This paper reports some of our findings on the kinetic and AFM measurements of these systems. Results indicate that the propensity and morphology of the K^+-induced aggregation of $d(XGG)_n$ depend strongly on the base sequence, the number of repeating units, the nature of terminal bases, and the ionic conditions.

MATERIALS AND METHODS

Synthetic oligonucleotides were purchased from Research Genetics (Huntsville, AL) and used without further purification. These oligomers were purified by the vendor via reverse-phase oligonucleotide purification cartridges and exhibited single-band electrophoretic mobilities in denaturing polyacrylamide gel electrophoresis, with a stated purity of ≥95%. Concentrations of oligomers (per nucleotide) were determined by measuring absorbances at 260 nm after melting, with the use of extinction coefficients obtained via nearest-neighbor approximation, using mono- and dinucleotide values tabulated by Fasman (1975). Aggregation kinetic profiles were obtained by monitoring the time-dependent absorbance changes at 320 nm and maintaining the temperature at 25°C. The reaction was initiated by addition of the appropriate amount of oligomer stock to a buffer solution containing the desired salt concentrations. Thermal denaturation experiments were carried out with 1-cm semimicro cells by monitoring absorbances at appropriate wavelengths. A heating (or cooling) rate of 0.5°C/min was maintained by the temperature controller accessory of a Cary 1E spectrophotometric system. Circular dichroic (CD) spectra were measured with a Jasco J-500A recording spectropolarimeter, using water-jacketed cylindrical cells of 1 cm path length. All experiments were carried out in 10 mM HEPPS (*N*-(2-hydroxyethyl)-piperazine-*N'*-propanesulfonic acid) buffer solutions of pH 8 (adjusted by droplet additions of 1 M NaOH).

DNA solutions (40 μM in nucleotide) used in AFM imaging were those saved from the turbidity kinetic measurements. A volume of 5 μl was deposited on a freshly cleaved mica substrate. The aggregates were allowed to be adsorbed on the surface for ~30 s before being washed with 200 ml of distilled water in a container via rigorous hand agitation for ~20 s and dried overnight in a hood. Imaging was performed in tapping mode with an oxide-sharpened Si_3N_4 tip at room temperature, using a nanoscope III scanning probe microscope with an E-scanner (Digital Instruments). Images were captured under the following conditions: scan rate of 2.6 Hz; drive frequency around 300 kHz; set point ~3 V; an integral-to-proportional gain ratio of 1:10; and 256 scan lines per image.

RESULTS

The nature of the X base strongly affects the propensity of the K^+-induced aggregate formation of oligomers with XGG repeats

The kinetic profiles of aggregate formation via turbidity monitoring at 320 nm for $d(XGG)_4$ in the presence of 2 M KCl are compared in Fig. 1 *A*. It is apparent that $d(GGG)_4$ forms aggregates most readily, whereas $d(CGG)_4$ fails to do so in a time span of 15 h (900 min) at pH 8 and 25°C. The kinetic profiles for $d(AGG)_4$ and $d(TGG)_4$ exhibit autocatalytic-like behaviors, consisting of lag periods or induction times (t_i) of 48 and 45 min, which are followed by accelerative and leveling phases exhibiting characteristic half-times ($t_{1/2}$) of 99 and 118 min, respectively. No apparent lag period ($t_i < 1$ min) appears to be evident for the aggregate formation of $d(GGG)_4$. The 320-nm absorbance decreases at the long-time regions for $d(GGG)_4$ and $d(TGG)_4$ are likely the consequence of slow sedimentation of larger aggregated particulates. These results suggest that the kinetic propensities for the K^+-induced aggregation are strongly sequence dependent and, at pH 8, appear to have the order $d(GGG)_4 > d(TGG)_4 \approx d(AGG)_4 \gg d(CGG)_4$, with $d(TGG)_4$ exhibiting the highest turbidity. It should be noted in passing that 2 M Na^+ failed to induce the observed aggregation phenomenon, and the K^+-induced aggregation of $d(CGG)_4$ is greatly facilitated by a moderate solution acidity (Chen, 1995).

Mg^{2+} greatly facilitates the aggregate formation and acts synergistically with K^+.

Salt concentration-dependent studies led to the finding that the K^+-induced aggregation of $d(XGG)_4$ requires more than 1 M KCl (not shown). Indeed, 1 M KCl failed to induce aggregation of $d(AGG)_4$ and $d(TGG)_4$ in a time span of 15 h. It was found, however, that the presence of Mg^{2+} in the K^+-containing solution can greatly facilitate the aggregation processes. Aggregation kinetic profiles of $d(XGG)_4$ in the presence of 1 M KCl and 16 mM $MgCl_2$ are compared in Fig. 1 *B*. The rates of aggregation are seen to be much faster than those of 2 M KCl and result in much higher turbidity (note the more than twofold scale change in Fig. 1 *B*). Indeed, in the Mg^{2+}-containing solution, a t_i of ~1 min with $t_{1/2}$ of 92 and 31 min were found for $d(AGG)_4$ and $d(TGG)_4$, respectively, and the former exhibits a higher turbidity than the latter, in contrast to their behavior in 2 M KCl. Even $d(CGG)_4$, which exhibits no evidence of aggregation in 2 M KCl, now shows a slow rise in turbidity in the solution containing 1 M KCl and 16 mM $MgCl_2$ with $t_i \approx$ 100 min. The ease of aggregate formation for $d(GGG)_4$ is further manifested by both t_i and $t_{1/2}$ being less than 1 min in the Mg^{2+}-containing solution.

The presence of Mg^{2+} dramatically enhances the thermal stabilities of the aggregates

Fig. 2 *A* compares the thermal melting profiles of aggregates formed with 2 M KCl. The melting temperatures are seen to be ~55°C and do not appear to be strongly sequence dependent. As can be seen in Fig. 2 *B*, the presence of Mg^{2+} greatly enhances the thermal stabilities of the aggregates. The melting temperatures for aggregates of $d(AGG)_4$ and $d(TGG)_4$ in the presence of 1 M KCl and 16 mM $MgCl_2$ are now ~85°C. Interestingly, the turbidity of $d(GGG)_4$ in-

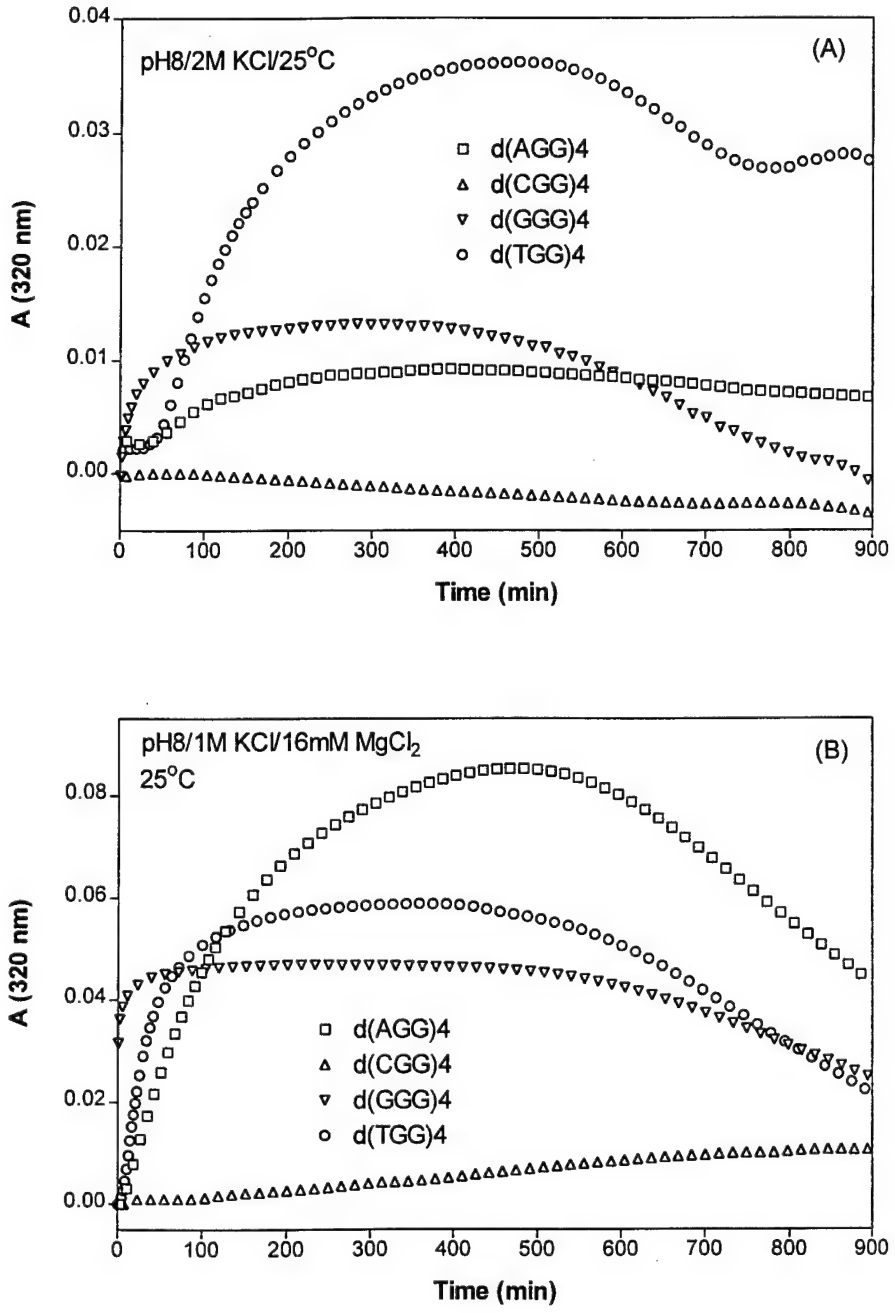

FIGURE 1 Comparison of turbidity-monitored aggregation kinetic profiles at 25°C for 40 μM (in nucleotides) of dodecamers of the form $d(XGG)_4$ in solutions of pH 8 at two different ionic conditions. (*A*) In the presence of 2.0 M KCl. (*B*) In the presence of 1.0 M KCl and 16 mM $MgCl_2$. The solution was first heated to 95°C for 1 min, and the kinetic run started as soon as the solution was cooled back to 25°C. The data have not been corrected for baseline drift or lamp instability because separate experiments with buffer alone at different salt concentrations have indicated a drift of no more than $\pm$0.001 absorbance units at 320 nm in a time span of 900 min.

creases rather than decreases near this same temperature, indicating additional aggregation, and with the disruption of aggregates occurring at temperatures higher than 95°C. Results of the kinetic and melting experiments for $d(XGG)_4$ in the two ionic conditions studied are summarized in Table 1.

Chiroptical properties of the aggregates are strongly sequence dependent, and $d(AGG)_4$ fails to exhibit Ψ-CD characteristics, despite its ease of aggregation

CD spectra of $d(XGG)_4$ in two different solution conditions are compared in Fig. 3. In 2 M KCl solutions (Fig. 3 *A*), only $d(GGG)_4$ exhibits an intense CD spectrum of Ψ-type, with a positive maximum at 260 nm, a shoulder near 285 nm, and a negative tail at longer wavelengths. Despite the significant aggregate formation in 2 M KCl, as indicated by turbidity measurements (see Fig. 1 *A*), $d(TGG)_4$ fails to exhibit Ψ-CD spectral characteristics. In contrast, a huge CD spectrum is induced for $d(TGG)_4$ in the 1 M KCl/16 mM $MgCl_2$ solution, resulting in positive double-hump maxima near 270 and 295 nm and a positive long-wavelength tail (see Fig. 3 *B*). A sizable Ψ-CD was also observed for $d(CGG)_4$ with a maximum at 300 nm, a shoulder near 270 nm, and a positive long-wavelength tail. On the other hand, the CD spectral characteristics of $d(GGG)_4$ are very

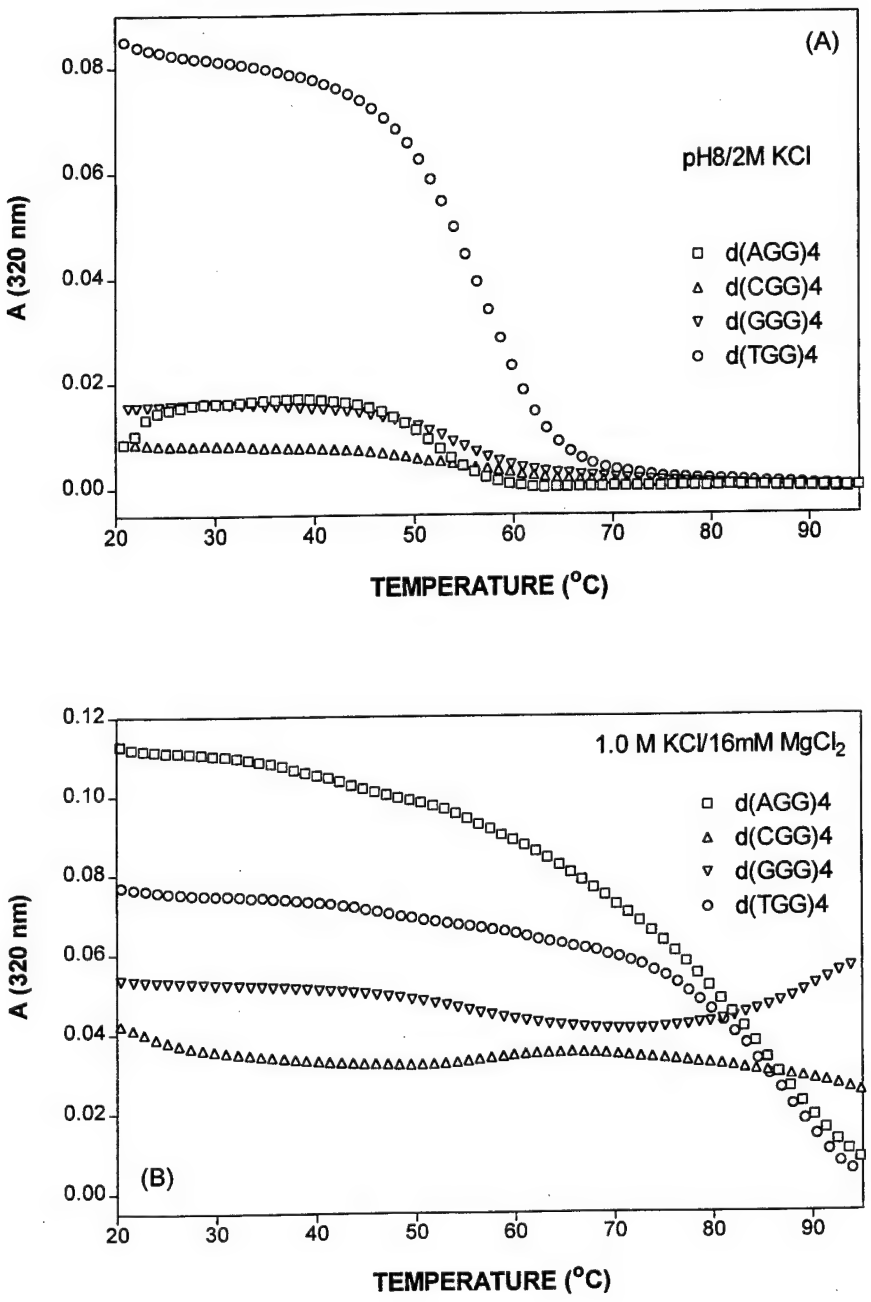

FIGURE 2 Comparison of turbidity-monitored thermal melting profiles of aggregates formed by 40 μM (in nucleotides) of dodecamers of the form $d(XGG)_4$ in solutions of pH 8 at two different ionic conditions. (*A*) In the presence of 2.0 M KCl. (*B*) In the presence of 1.0 M KCl and 16 mM $MgCl_2$. Solutions were allowed to stand for more than 2 days and shaken before the melting run. A heating rate of 0.5°C/min was maintained during the experiment.

similar in the two solutions. It is also of interest to note that $d(AGG)_4$ fails to exhibit Ψ-CD characteristics, despite its considerable aggregate formation in the solution of 1 M KCl/16 mM $MgCl_2$.

The propensity for aggregation is greatly affected by the chain length, with oligomers of four repeating units being most facile

Aggregation kinetic profiles at 20°C for oligomers with three, four, and five trinucleotide repeats are compared in Fig. 4 for oligomers of AGG (*A* and *B*) and TGG (*C* and *D*) repeats at two different solution conditions. In 2 M KCl solutions, the ease of aggregation is seen to follow the order $d(AGG)_4 > d(AGG)_3 \gg d(AGG)_5$ (Fig. 4 *A*). No evidence of aggregate formation is apparent for $d(AGG)_5$ in a time span of 15 h, whereas t_i of 180 and 25 min with $t_{1/2}$ of ~500 and 95 min are found for the three and four repeats, respectively. Again, the facilitation due to the presence of Mg^{2+} is clearly seen in the much faster aggregation kinetics observed in solutions containing 1 M KCl/16 mM $MgCl_2$ (Fig. 4 *B*). Aside from $t_i < 1$ min and $t_{1/2} = 83$ min observed for $d(AGG)_4$, it is interesting to note that in contrast to the absence of aggregation in 2 M KCl solution, $d(AGG)_5$ now exhibits a faster aggregation rate ($t_i = 48$ min, $t_{1/2} = 220$ min) than that of $d(AGG)_3$ ($t_i = 80$ min, $t_{1/2} \approx 500$ min). In contrast, no evidence of aggregation is apparent for both $d(TGG)_3$ and $d(TGG)_5$, whereas $d(TGG)_4$ exhibits aggrega-

TABLE 1 Comparison of kinetic and melting parameters for d(XGG)$_4$ in two different ionic conditions

Oligomer	$[K^+]$ (M)	$[Mg^{2+}]$ (mM)	t_i (min)	ΔA_{max} ($t_{1/2}$, min)	t_m (°C)
d(AGG)$_4$	2		48	0.0093 (99)	53
d(TGG)$_4$	2		45	0.0361 (118)	57
d(GGG)$_4$	2		<1	0.0132 (13)	53
d(CGG)$_4$	2		*		53
d(AGG)$_4$	1	16	1	0.0847 (92)	85
d(TGG)$_4$	1	16	1	0.0589 (31)	87
d(GGG)$_4$	1	16	<1	0.0467 (<1)	>95
d(CGG)$_4$	1	16	~100	[0.0112]	—

Kinetic measurements were made at 25°C, and t_i is the lag time or the induction period before the onset of aggregation. ΔA_{max} is the maximum absorbance change at 320 nm when the kinetic profile becomes asymptotic, and $t_{1/2}$ is the time required for reaching half of this maximum value. Kinetic profiles for which asymptotes were not reached in a time span of 15 h are indicated by brackets, with the absorbance values at 900 min enclosed. The kinetic trace for which no discernible aggregation occurs in a time span of 15 h is designated by *. Thermal denaturation was monitored at 320 nm.

tion in both solution conditions, but with greater facility in the presence of Mg^{2+} (compare Fig. 4, *C* and *D*), having t_i of < 5 versus 60 min and $t_{1/2}$ of 33 versus 209 min, respectively. Results on the effects of chain lengths on the aggregation kinetics are summarized in Table 2.

The nature and the location of the terminal bases strongly affect the aggregation processes

The aggregation kinetic profiles for d(GGXGGXGGXGG) and the related oligomers having X = A or T base attached to one or both end(s) are compared in Fig. 5. It is apparent that in the X = A series (*left panels*), d(GGAGGAGGAGG) is the most facile in forming aggregates in 2 M KCl (t_i < 1 min, $t_{1/2}$ = 17 min), which is followed by d(AGGAGGAGGAGG) (t_i = 20 min, $t_{1/2}$ = 95 min), an oligomer with dA added at the 5′ end. Appending dA at the 3′ end or at both terminals results in the absence of turbidity-measurable aggregate formation in 2 M KCl solutions and time spans of 15 h (Fig. 5 *A*). These last two oligomers can, however, readily form aggregates in solutions containing 1 M KCl/16 mM $MgCl_2$, with the oligomer having both ends appended by dA to be most resistant (see Fig. 5 *B*). The ease in aggregation in this ionic condition is shown to follow the order d(GGAGGAGGAGG) (t_i < 5 min, $t_{1/2}$ = 21 min) > d(AGGAGGAGGAGG) (t_i < 5 min, $t_{1/2}$ = 83 min) ≈ d(GGAGGAGGAGGA) (t_i = 10 min, $t_{1/2}$ = 55 min) > d(AGGAGGAGAGGA) (t_i = 74 min, $t_{1/2}$ = 257 min). For the X = T series, d(GGTGGTGGTGG) and d(TGGTGGTGGTGG) are shown to readily form aggregates, with the former being more facile in 2 M KCl (t_i of <5 versus 60 min and $t_{1/2}$ of 95 versus 209 min), whereas the order appears to be reversed in solutions containing 1 M KCl/16 mM $MgCl_2$ (t_i of 8 versus < 5 min and $t_{1/2}$ of 90 versus 33 min). Neither d(GGTGGTGGTGGT) nor d(TGGTGGTGGTGGT) exhibits aggregation phenomena in a time span of 15 h under both ionic conditions. It thus appears that appending X base at the 3′ end of d(GGXGGXGGXGG) provides a greater hindrance to aggregation than appending X base at the 5′ end. Results on the effects of terminal bases on the aggregation kinetics are summarized in Table 3.

Scanning probe images of aggregates

AFM images of d(XGG)$_4$ aggregates formed in two different solution conditions are compared in Fig. 6. It is immediately apparent that the images of turbidity-measurable aggregates are of sufficient size and can easily be captured by AFM. In the presence of 2 M KCl (*left panels*), d(GGG)$_4$ (Fig. 6 *D*) exhibits the highest density of aggregates formed, which is followed by d(AGG)$_4$ (Fig. 6 *B*) and d(TGG)$_4$ (Fig. 6 *C*), where d(CGG)$_4$ (Fig. 6 *A*) is the lowest. Despite the absence of turbidity at 320 nm (see Fig. 1 *A*), some formation of aggregates is clearly visible for d(CGG)$_4$, albeit smaller in both number and particle size. The particulate size for the d(TGG)$_4$ (Fig. 6 *C*) aggregates appears to be somewhat larger than those of d(AGG)$_4$ (Fig. 6 *B*), despite their similar aggregation densities. This observation is consistent with the significantly higher turbidity exhibited by d(TGG)$_4$ in 2 M KCl (see Fig. 1 *A*). In the presence of $MgCl_2$, the aggregates appear to be considerably elongated (see Fig. 6 *E–H*), in agreement with the much higher turbidities observed (compare Fig. 1, *A* and *B*). The significantly higher aggregate density exhibited by d(AGG)$_4$ than d(TGG)$_4$ (compare Fig. 6, *F* and *G*) appears to be consistent with the higher turbidity observed for the former in this solution (see Fig. 1 *B*). The considerably larger aggregates formed in the presence of $MgCl_2$, in terms of both widths and lengths, are also quite striking for d(CGG)$_4$ (compare Fig. 6, *A* and *E*).

Chain-length-dependent morphologies of aggregates formed in 1 M KCl/16 mM $MgCl_2$ for d(XGG)$_{n\,=\,3–5}$, with X = A (*left panels*) or T (*right panels*), are shown in Fig. 7. As is apparent, the oligomers with four repeats (Fig. 7, *B* and *E*) exhibit the highest aggregation densities, whereas aggregates formed by oligomers with three (Fig. 7, *A* and *D*) and five (Fig. 7, *C* and *F*) repeats are much less numerous. These results are in conformity with those of turbidity measurements indicating the very facile aggregate formation for oligomers with four repeating units (see Fig. 4, *A* and *D*). It should also be noted in passing that the aggregates of d(TGG)$_4$ (Fig. 7 *E*) appear to be significantly elongated when compared with those of d(AGG)$_4$ (Fig. 7 *B*).

AFM images on aggregates formed by oligomers with varying capping bases and in the presence of 1 M KCl/16 mM $MgCl_2$ are shown in Fig. 8. Consistent with the propensities for facile aggregate formation of oligomers with dG at both ends (Fig. 8, *A* and *E*) and dG at the 3′ terminal (Fig. 8, *B* and *F*), high aggregation densities are observed for these oligomers. Except for the somewhat more elongated features for the T-containing oligomers, no great

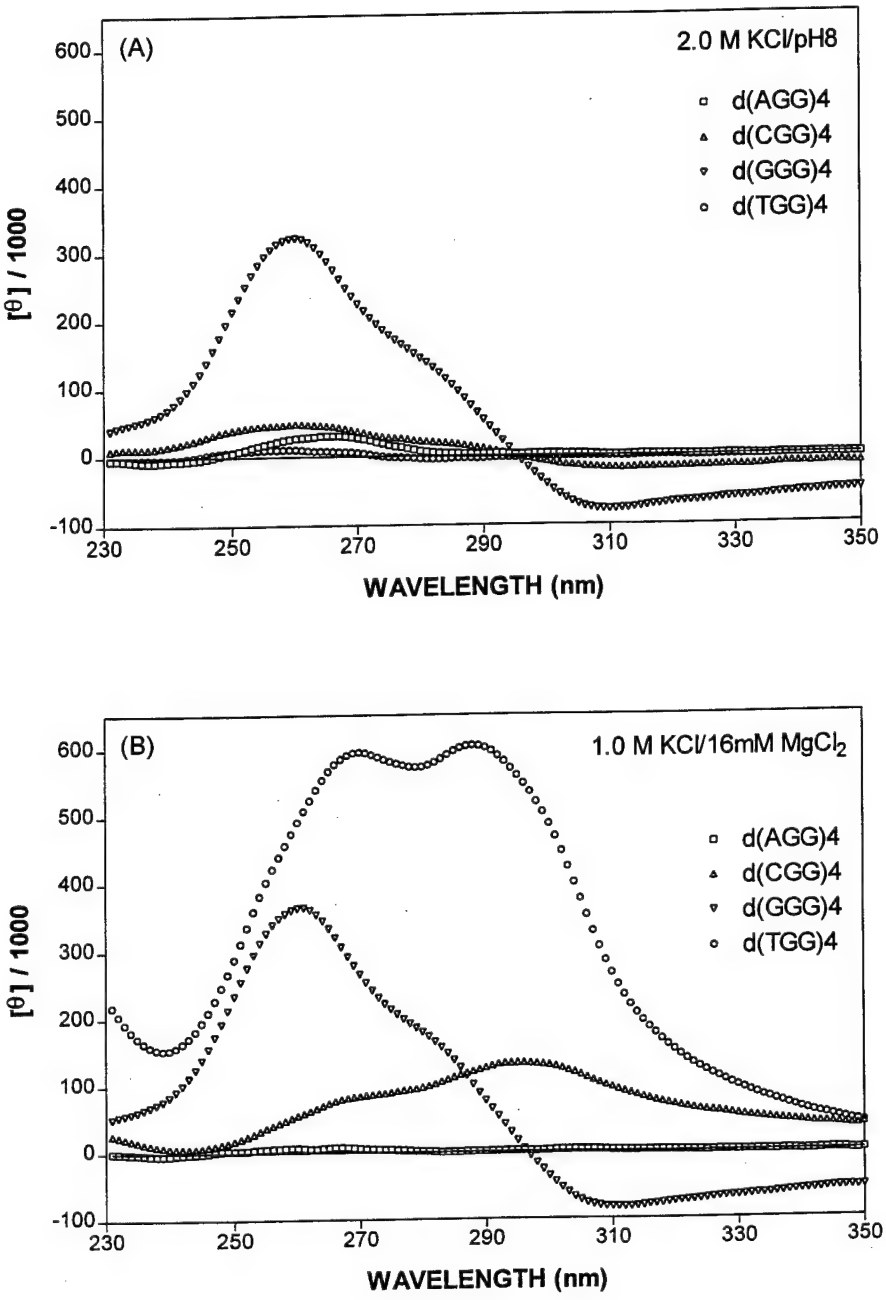

FIGURE 3 Comparison of CD spectral characteristics at room temperature for 40 μM of dodecamers of the form $d(XGG)_4$ in solutions of pH 8 at two different ionic conditions. (*A*) In the presence of 2.0 M KCl. (*B*) In the presence of 1.0 M KCl and 16 mM $MgCl_2$. Solutions were heated to 95°C and cooled back to room temperature (with a 10-day wait) before the CD measurements.

difference in aggregation density is found among them. On the other hand, oligomers capped with dA or dT at the 3′ end (Fig. 8, *C* and *G*) exhibit shorter aggregates and much lower aggregation density, whereas those with both ends capped exhibit sparsely formed aggregates (Fig. 8, *D* and *H*). The much greater hindrance of aggregate formation with a dA or dT capped at the 3′ end than with a dA or dT capped at the 5′ end is dramatically illustrated via comparison of Fig. 8, *B* or *F*, versus Fig. 8, *C* or *G*, respectively.

Kinetics of aggregate formation were also investigated by AFM, by taking images of the d(GGAGGAGGAGG) aggregating solution at various times. Progressive increase in the density of aggregates is clearly visible for images taken 1, 2, 4, and 8 h after the 2 M KCl addition (results not shown).

DISCUSSION

Systematic aggregation studies with various oligomers of XGG trinucleotide repeats under different ionic conditions led to the following findings: 1) More than 1 M KCl is needed to observe the turbidity-measurable aggregation for these oligomers (40 μM in nucleotide and at 25°C), and NaCl fails to induce a similar phenomenon. 2) Acting synergistically with K^+, the presence of Mg^{2+} greatly facilitates the aggregate formation and dramatically enhances the

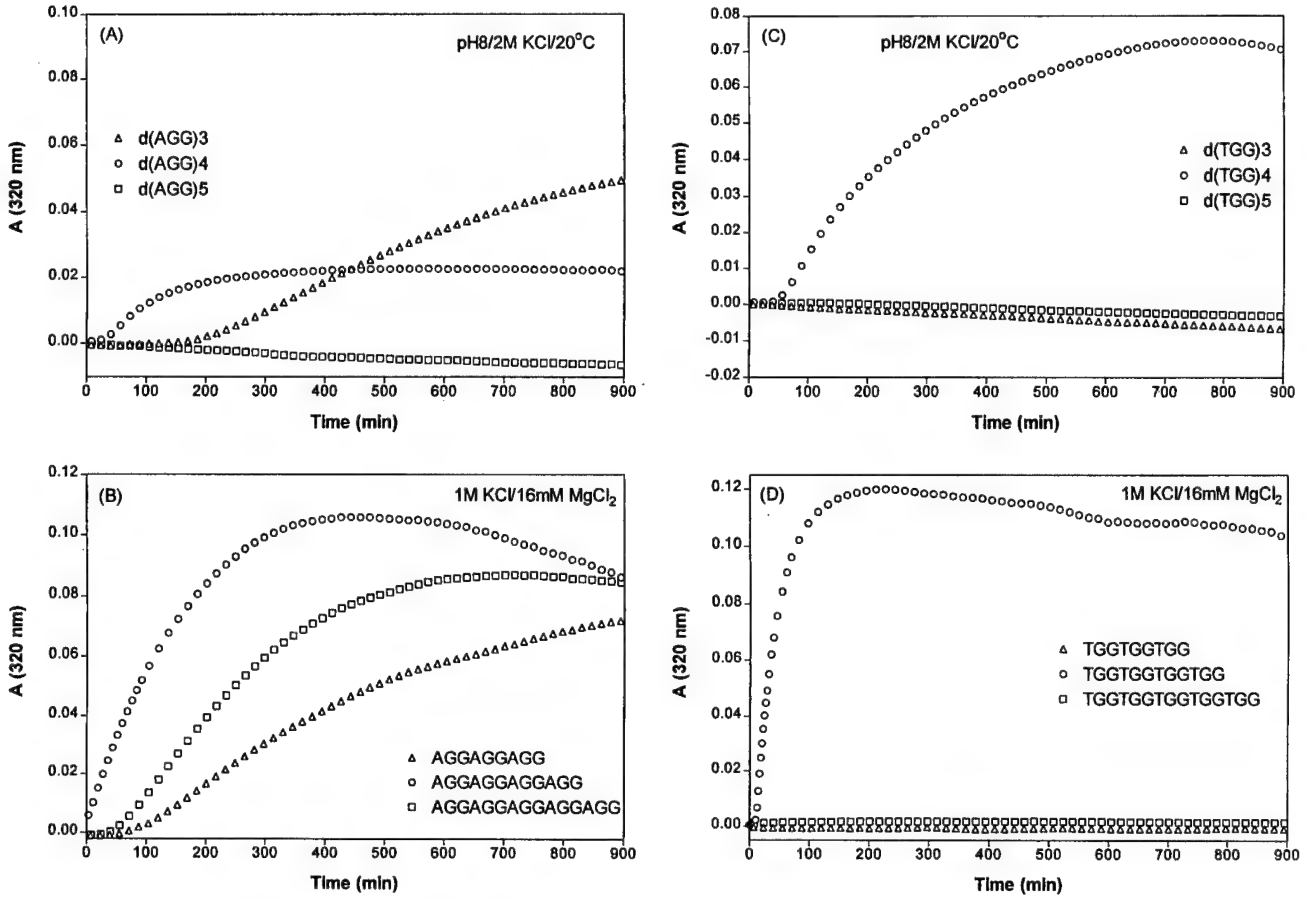

FIGURE 4 Comparison of aggregation kinetic profiles at 20°C of 40 μM $d(AGG)_n$ and $d(TGG)_n$ in solutions of pH 8 at two different ionic conditions. (*A*) $d(AGG)_n$ in the presence of 2.0 M KCl. (*B*) $d(AGG)_n$ in the presence of 1.0 M KCl and 16 mM $MgCl_2$. (*C*) $d(TGG)_n$ in the presence of 2.0 M KCl. (*D*) $d(TGG)_n$ in the presence of 1.0 M KCl and 16 mM $MgCl_2$.

thermal stabilities of the aggregates formed. 3) The nature of the X base strongly affects the propensity of the K^+-induced aggregate formation, and at pH 8 the observed order appears to be $d(GGG)_4 > d(AGG)_4 \approx d(TGG)_4 \gg$ $d(CGG)_4$, with CGG repeats greatly facilitated by moderate acidities. 4) Chiroptical properties of the aggregates depend strongly on the base sequence and ionic conditions of the solution, e.g., $d(TGG)_4$ exhibits intense Ψ-CD characteristics, distinct from those of $d(GGG)_4$, in the presence but not in the absence of Mg^{2+}, whereas despite its relative ease of aggregate formation, $d(AGG)_4$ fails to exhibit Ψ-CD characteristics, even in the presence of Mg^{2+}. 5) The propensity for aggregation is greatly affected by the chain length, with oligomers of four repeats being most facile. 6) The nature and location of the terminal bases also strongly affect the aggregation processes; appending with X = A or T base at the 3′ end of d(GGXGGXGGXGG) appears to provide a greater hindrance to aggregation than appending an X base at the 5′ end. 7) Both $d(AAGG)_4$ and $d(TTGG)_4$ failed to exhibit the K^+-induced aggregation phenomena, even in the presence of Mg^{2+} (results not shown).

TABLE 2 Effects of chain lengths on the aggregation kinetics at 20°C

Oligomer	$[K^+]$ (M)	$[Mg^{2+}]$ (mM)	t_i (min)	ΔA_{max} ($t_{1/2}$, min)
AGGAGGAGG	2		180	[0.0494] (~500)
AGGAGGAGGAGG	2		25	0.0225 (95)
AGGAGGAGGAGGAGG	2		*	
TGGTGGTGG	2		*	
TGGTGGTGGTGG	2		60	0.0729 (209)
TGGTGGTGGTGGTGG	2		*	
AGGAGGAGG	1	16	80	[0.0761]
AGGAGGAGGAGG	1	16	<1	0.1053 (83)
AGGAGGAGGAGGAGG	1	16	48	0.0870 (220)
TGGTGGTGG	1	16	*	
TGGTGGTGGTGG	1	16	<5	0.1196 (33)
TGGTGGTGGTGGTGG	1	16	*	

*See Table 1 footnote.

A speculative model was earlier proposed by us (Chen, 1997) to rationalize the self-assembly phenomenon of $d(TGG)_4$. This same mechanism may also be operative in oligomers with XGG trinucleotide repeats in general. The oligomer likely first forms parallel-stranded homoduplexes in the K^+-containing solutions, which in turn form in-

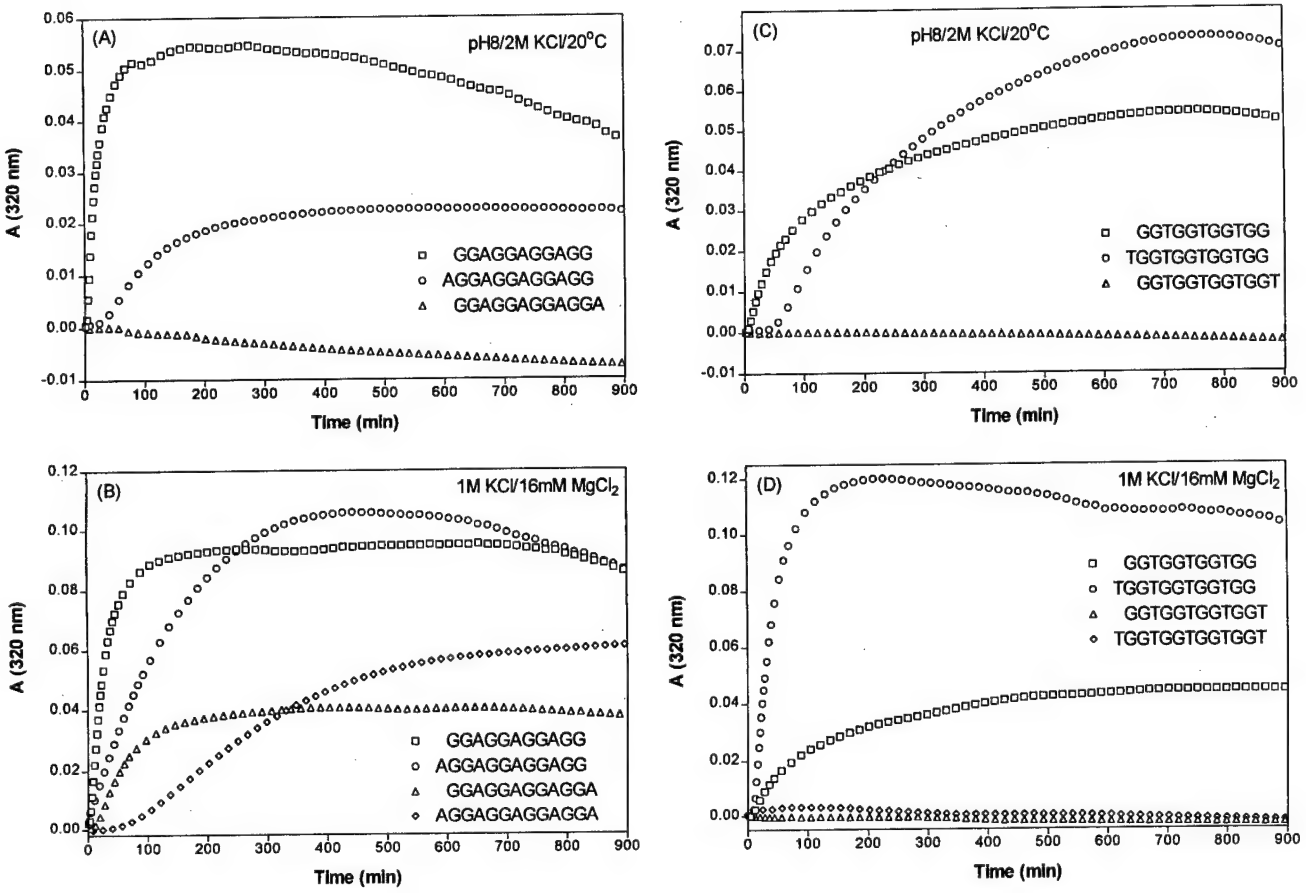

FIGURE 5 Comparison of aggregation kinetic profiles at 20°C of 40 μM d(GGXGGXGGXGG) and related oligomers in solutions of pH 8 at two different ionic conditions. (*A*) X = A in the presence of 2.0 M KCl. (*B*) X = A in the presence of 1.0 M KCl and 16 mM $MgCl_2$. (*C*) X = T in the presence of 2.0 M KCl. (*D*) X = T in the presence of 1.0 M KCl and 16 mM $MgCl_2$. Kinetic profiles for d(XGGXGGXGGXGGX) are nearly identical to those of d(GGXGGXGGXGGX) in *A* and *C* and are not shown.

and/or out-of-registered quadruplexes (presumably aided by the optimal size of K^+ that fits into quadruplex cages). Axial extension of the out-of-register quadruplexes could result if repeated quadruplex formation occurred with sticky ends to form G-wires (Marsh and Henderson, 1994), whereas those of in-register quadruplexes could result from head-to-tail stacking. In addition, lateral expansion could be achieved by interquadruplex association via phosphate-Mg^{2+} bond formation.

The need for molar concentration of KCl to form turbidity-measurable aggregation and the inability of Na^+ to do likewise may be a consequence of their differential effectiveness in inducing parallel quadruplex formation. Raman studies by Miura et al. (1995) on the quadruplex formation of $d(TTTTGGGG)_4$ led to the finding that both Na^+ and K^+ facilitate an antiparallel foldback quadruplex at low salt concentrations but a parallel quadruplex at higher concentrations, with K^+ being more effective in inducing the parallel association. It has long been suggested that the greater thermal stability of DNA quadruplex structures in the presence of K^+ is primarily a result of the optimal fit of this ion in the coordination sites formed by G quartets. However, Hud et al. (1996) have recently argued that such a preference is actually driven by the greater energetic cost of Na^+ dehydration with respect to K^+ dehydration.

The observed synergistic effects of K^+ and Mg^{2+} may be the consequence of complementary roles played by these two cations—the ability to facilitate the parallel quadruplex formation of the former and binding to phosphates by the latter. The inability of Mg^{2+} to induce aggregation in the absence of K^+ supports the important role of parallel quadruplex formation in the supramolecular self-assembly in $d(XGG)_4$. In view of its strong affinity for phosphates, the role of Mg^{2+} in the self-assembly process may be twofold: 1) facilitation of the initial homoduplex and subsequent tetraplex formation for axial extension via phosphate charge neutralization and 2) bridging interquadruplex phosphate groups for lateral expansion.

The speculated mechanism appears to be consistent with the finding that $d(GGG)_4$ is more facile than $d(AGG)_4$ and $d(TGG)_4$ in aggregate formation, which in turn aggregate more readily than $d(CGG)_4$ at pH 8, with the aggregation of C-containing oligomer being facilitated by acidic conditions. The ability to form out-of-register quadruplexes with-

TABLE 3 Effects of terminal bases on the aggregation kinetics at 20°C

Oligomer	$[K^+]$ (M)	$[Mg^{2+}]$ (mM)	t_i (min)	ΔA_{max} ($t_{1/2}$, min)
GGAGGAGGAGG	2		<1	0.0576 (17)
AGGAGGAGGAGG	2		20	0.0225 (95)
GGAGGAGGAGGA	2	*		
GGTGGTGGTGG	2		<5	0.0542 (95)
TGGTGGTGGTGG	2		60	0.0729 (209)
GGTGGTGGTGGT	2		*	
GGAGGAGGAGG	1	16	<5	0.0928 (21)
AGGAGGAGGAGG	1	16	<5	0.1033 (83)
GGAGGAGGAGGA	1	16	10	0.0405 (55)
AGGAGGAGGAGGA	1	16	74	0.0520 (257)
GGTGGTGGTGG	1	16	8	0.0443 (90)
TGGTGGTGGTGG	1	16	<5	0.1196 (33)
GGTGGTGGTGGT	1	16	*	
TGGTGGTGGTGGT	1	16	*	

*See Table 1 footnote.

out the constraints of the intervening non-G bases likely accounts for its ease of aggregation for $d(GGG)_4$. On the other hand, the presence of cytosines in $d(CGG)_4$ may have trapped this oligomer in conformations that utilize G·C base pairings at pH 8, such as dimeric duplexes or monomeric hairpins, so as to hinder quadruplex formation. Thus the acid-facilitated aggregation of $d(CGG)_4$ may partly be the consequence of the destabilization of these trapped conformers resulting from weakened G·C base pairs due to base protonation of the cytidine, and partly the consequence of the facilitation of parallel duplex and/or quadruplex formation via $C{\cdot}C^+$ base pairing (Chen, 1995).

The inability of $d(AAGG)_4$ and $d(TTGG)_4$ to form aggregates is most likely the consequence of constraints and steric hindrance introduced by intervening and two terminal non-G bases in forming appropriate G-quadruplexes for axial extension. Similarly, the effect of capping oligomers with non-G bases on aggregation may be attributed to the steric hindrance of quadruplex formation due to the presence of these bases. Thus it is understandable that capping both ends will provide a greater resistance to aggregate formation than a single cap at either end of the oligomer. It is less clear, however, why capping at the 3′ end will render a considerably greater hindrance of aggregation than capping at the 5′ end. The chain length dependence may partly be rationalized in terms of hairpin formation. The oligomer with five repeats may be long enough to be easily trapped into hairpin conformations to become less efficient in parallel quadruplex formation than the ones with three or four repeating units, where the latter are more facile because of the larger numbers of G-quartet formed.

It is noteworthy that the appearance of Ψ-CD spectral characteristics is related to the chirality and other characteristics of the formed superstructure. It is well known that the CD spectrum of an optically active molecule can sometimes change drastically when the molecule becomes part of a larger aggregate particle (Tinoco et al., 1980). When this aggregate reaches a size comparable to the wavelength of the light used in the CD experiment, anomalous spectral changes occur. A long tail often apppears in the CD at wavelengths outside the absorption bands of the constituent molecules, and as the aggregate particles grow in size, the magnitudes and band shapes of the CD inside the absorption bands also change. The origin of the tail anomalies has been attributed to the ability of large chiral particles to preferentially scatter right or left circularly polarized light away from the transmitted beam (Bustamante et al., 1983). On the other hand, the physical origin of the nonscattering Ψ-type CD anomalies is that when the dimensions of a chiral object are similar to the wavelength of the incident light, the large-scale handedness of the object will have a much greater effect in enhancing or suppressing the absorption of circularly polarized light than when the chiral object is small compared to wavelength. In large, dense chiral molecular aggregates, the eigenmodes of excitation are greatly delocalized throughout the entire aggregate particle, which necessitates the inclusion of intermediate and radiation coupling mechanisms in addition to the static dipole coupling (Keller and Bustamante, 1986). It was found that long-range coupling is possible when the aggregate is three-dimensional and large (~1/4 λ) and has a high density of chromophores. Deficiency in one or more of these factors likely accounts for the absence of Ψ-CD in some of our sequences and other G-rich polymers observed in other laboratories under lower salt concentrations.

Superstructures formed by G-rich DNAs have been observed previously in the presence of K^+ by others, although in ionic strengths of no more than 1 M. Sen and Gilbert (1992) reported that oligomers with a single multiguanine (more than 3 Gs) motif at their 3′ or 5′ end can form higher order products, consisting of 8, 12, and 16 strands. Based on their methylation protection experiments, a nested head-to-tail superstructure containing two or more tetraplexes bonded front to back via G quartet formation of out-of-registered guanines was suggested. It was noted that superstructural formation was achieved in a buffer containing KCl but not in a buffer containing NaCl. It was further shown by Lu et al. (1992) that in the presence of K^+, but not Na^+, higher order complexes are formed in dT_4G_4. The presence of a T at the 3′ end inhibits such association in dT_4G_4T. Formation of these superstructures usually requires high salt as well as high oligonucleotide concentrations, and the limited number of superstructures formed may have resulted from steric hindrance caused by the protruding T-tails.

Marsh and Henderson (1994) later found that the telomeric DNA oligonucleotide 5′-GGGGTTGGGG-3′ spontaneously assembles into large superstructures (*termed G-wires*) that can be resolved by gel electrophoresis as a ladder pattern, most efficiently in Na^+, but a greater degree of stability was acquired by the addition of K^+. Its self-association is noncovalent and exhibits characterstics of

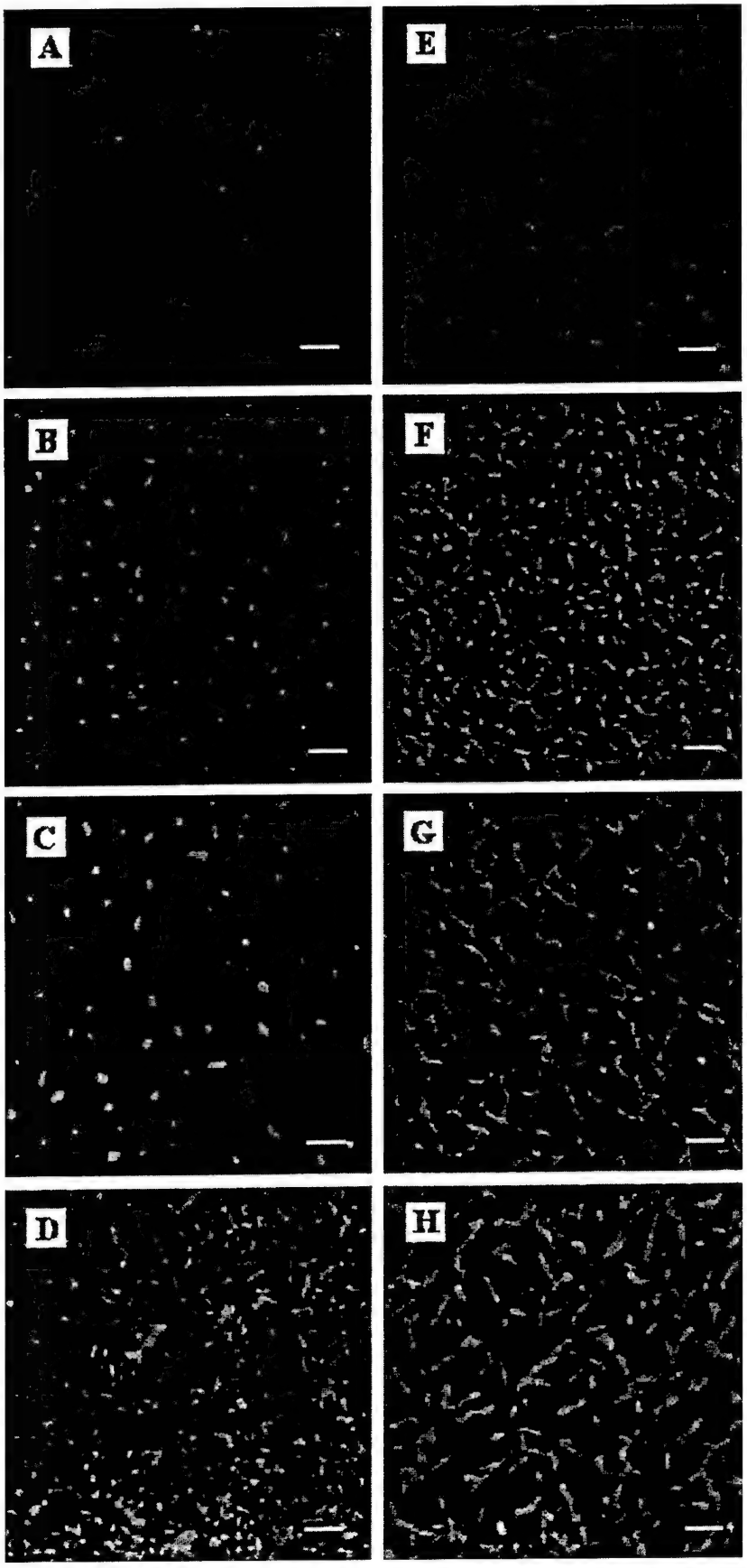

FIGURE 6 Comparison of AFM images of aggregates formed by $d(XGG)_4$ in two different ionic conditions: 2 M KCl (*left panels*) and 1 M KCl/16 mM $MgCl_2$ (*right panels*). (*A* and *E*) $d(CGG)_4$; (*B* and *F*) $d(AGG)_4$; (*C* and *G*) $d(TGG)_4$; (*D* and *H*) $d(GGG)_4$. All scale bars are 150 nm.

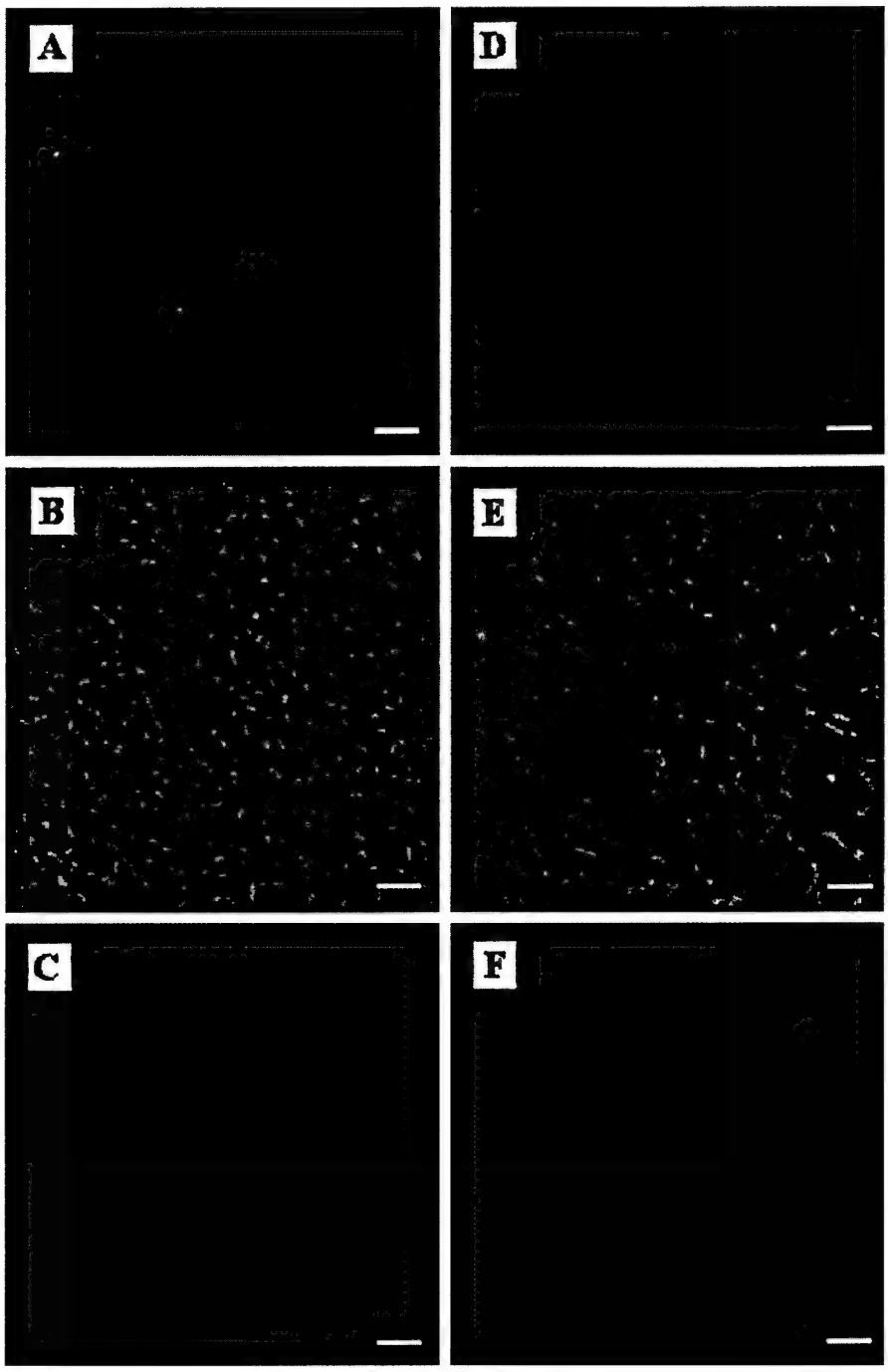

FIGURE 7 Effects of chain length on the AFM images of aggregates formed in solutions containing 1 M KCl/16 mM $MgCl_2$. (*A*) $d(AGG)_3$; (*B*) $d(AGG)_4$; (*C*) $d(AGG)_5$; (*D*) $d(TGG)_3$; (*E*) $d(TGG)_4$; (*F*) $d(TGG)_5$. All scale bars are 150 nm.

G4-DNA, a parallel four-stranded structure stabilized by guanine tetrads. The spontaneous self-assembly into large polymers is likely facilitated by the presence of blocks of guanines at both the 5′ and 3′ ends. It was proposed that the G-wire consists of G4-DNA domains punctuated by T nodes. The initial starting structure consists of a G4 domain containing four quartets formed by the association of the 5′ half of a duplex with the 3′ half of another duplex, forming a slipped tetraplex structure with G-duplex "sticky ends." The strands run parallel to each other and can accept an additional duplex at either end, reminescent of the slipped architecture proposed by Sen and Gilbert (1992) for their observed superstructures.

Subsequently, the morphology of G-wires was investigated by AFM (Marsh et al., 1995). The length of G-wires was found to range from 10 to >1000 nm, and the height and width of G-wires appeared to be uniform, with few bends, kinks, or branches. This indicated that G-wires were ordered, relatively rigid polymers. Magnesium induced synergy of G-wire self-assembly. The height of G-wires was found to be two to three times greater than the height of plasmid DNA in the AFM, ranging from 12.7 to 23.9 Å,

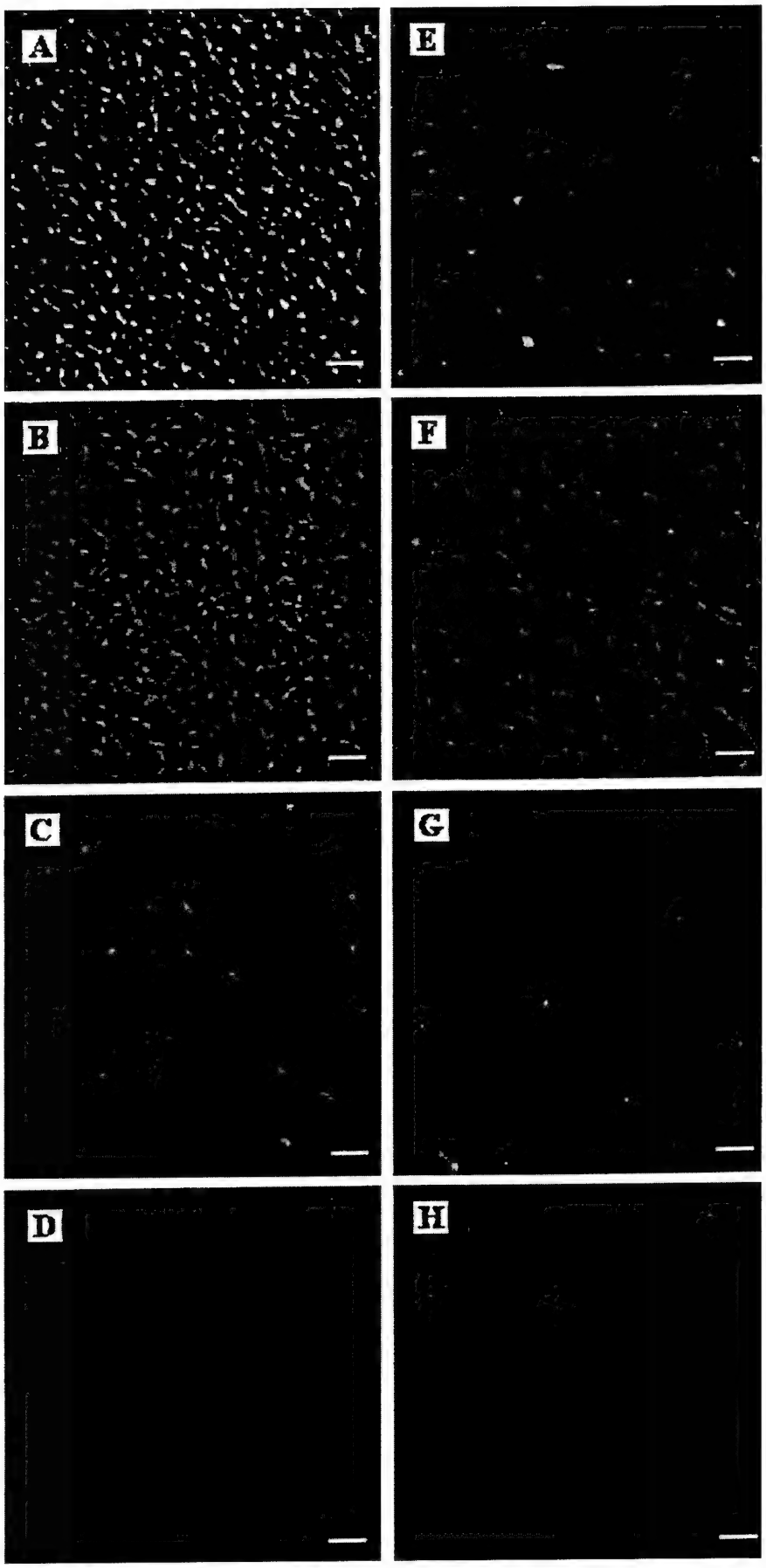

FIGURE 8 Comparison of AFM images of aggregates formed by oligomers with differing terminal base in solutions containing 1 M KCl/16 mM $MgCl_2$. (*A*) d(GGAGGAGGAGG); (*B*) d(AGGAGGAGGAGG); (*C*) d(GGAGGAGGAGGA); (*D*) d(AGGAGGAGGAGGA); (*E*) d(GGTGGTGGTGG); (*F*) d(TGGTGGTGGTGG); (*G*) d(GGTGGTGGTGGT); (*H*) d(TGGTGGTGGTGGT). All scale bars are 150 nm.

depending on the ionic conditions. The height of G-wires measured in the AFM under some conditions was close to the diameter of G-quartets determined by x-ray crystallography (~28 Å) (Kang et al., 1992; Laughlan et al., 1994). Interestingly, assembly of G-wires occurred most efficiently in Na^+, yet a greater degree of stability was acquired by the addition of K^+. This is at odds with our observation that Na^+ is ineffective in inducing the aggregation phenomenon in the XGG trinucleotide repeats.

A related structure was later reported by Dai et al. (1995) for the $C_4T_4G_4T_{1-4}G_4$ series of oligomers, which self-assemble into multistranded species of high molecular weight in the presence of 100 mM K^+ plus 20 mM Mg^{2+}. Data suggest that these higher order species arise from successive additions of parent oligomer to an initially formed quadruplex. Because the self-assembly is not observed with K^+ or Mg^{2+} alone, these cations behave in a synergistic manner in the formation and/or stability of the supermolecular self-assemblies. Subsequently, Marotta et al. (1996) studied DNA oligomers possessing $G_xT_2G_y$ segments. Electrophoresis of these oligomers in the presence of both 100 mM K^+ and 20 mM Mg^{2+} gives a ladder of multiple bands of high molecular weight, indicative of multistranded DNA formation. The results indicate that self-assembly into high-molecular-weight species is favored by the presence of Mg^{2+} as well as the presence of four or more bases in the terminal G_y segment.

In addition to the duplex and quadruplex formation in d(GGGGCCCC), Deng and Braunlin (1995) noted the broadening of proton resonances and the appearance of a series of slower moving faint gel electrophoretic bands in their titration studies with KCl, indicating the formation of some higher order structures in the presence of added KCl. Furthermore, Protozanova and Macgregor (1996) found that in aqeous solutions containing mono- and divalent cations, the oligomer $d(A_{15}G_{15})$ readily self-assembles into high-molecular-weight species that resolve as discrete bands on native and denaturing electrophoresis gels. In the proposed model for the oligomers and polymers of $d(A_{15}G_{15})$, several molecules of the monomers interact via a stem of tetraplex structure formed by the guanine residues. The 5′ end adenine forms single-stranded arms that are displaced from the guanine-containing stem. In deference to the G-wires introduced by Marsh and Henderson (1994), these structures were called *frayed wires*. Divalent cations at millimolar concentrations lead to the formation of the polymers, whereas the presence of the monovalent cations stabilizes lower-molecular-weight complexes consisting of two to six strands of $d(A_{15}G_{15})$. The data showed that stable frayed wires form only when there are between four and eight guanosine residues at the 3′ end of the oligomer.

All of these observations are likely related to the self-aggregation phenomena observed in our XGG trinucleotide repeating systems. As for the possible biological significance of these observations, it is interesting to note that the single-stranded termini of all chromosomal telomeres sequenced to date have a guanine motif at their 3′ termini, with guanine as the terminal base. Given a sufficient local density of telomeres in the potassium-rich environment of the cell with some presence of Mg^{2+}, these higher order superstructures may arise. This suggests that the structure of telomeric DNA may be quite unusual. Although the salt concentrations of 2 M KCl and 1 M KCl/16 mM KCl employed in this report are far from being physiological conditions, it should be noted that the onsets of aggregation in a time frame of less than 15 h have been observed in solutions containing only mM concentrations of K^+ and Mg^{2+}. Examples are $d(TGG)_4$ in the presence of 2 mM KCl/16 mM $MgCl_2$ (Chen, 1997), $d(AGG)_4$ in the presence of 40 mM KCl/16 mM $MgCl_2$, and d(GGAGGAGGAGG) and d(GGTGGTGGTGG) in the presence of 16 mM KCl/16 mM $MgCl_2$ (not shown).

We thank Dr. Yei-ShinTung for his help during the course of AFM measurements.

This work was supported by Army Medical Research grant DAMD17-94-J-4474 and a subproject of Minority Biomedical Research Support (MBRS) grant S06GM0892.

REFERENCES

Blackburn, E. H. 1994. Telomeres: no end in sight. *Cell.* 77:621–623.

Bustamante, C., I. Tinoco, Jr., and M. F. Maestre. 1983. Circular differential scattering can be an important part of the circular dichroism of macromolecules. *Proc. Natl. Acad. Sci. USA.* 80:3568–3572.

Chen, F.-M. 1995. Acid-facilitated supramolecular assembly of G-quadruplexes in $d(CGG)_4$. *J. Biol. Chem.* 270:23090–23096.

Chen, F.-M. 1997. Supramolecular self-assembly of $d(TGG)_4$, synergistic effects of K^+ and Mg^{2+}. *Biophys. J.* 73:348–356.

Dai, T.-Y., S. P. Marotta, and R. D. Sheardy. 1995. Self-assembly of DNA oligomers into high molecular weight species. *Biochemistry.* 34: 3655–3662.

Deng, H., and W. H. Braunlin. 1995. Duplex to quadruplex equilibrium of the self-complementary oligonucleotide d(GGGGCCCC). *Biopolymers.* 35:677–681.

Fasman, G. D., editor. 1975. CRC Handbook of Biochemistry and Molecular Biology: Nucleic Acids, Vol. 1, 3rd Ed. CRC Press, Cleveland, OH. 589.

Hansma, H. G., and H. Hoh. 1994. Biomolecular imaging with the atomic force microscope. *Annu. Rev. Biophys. Biomol. Struct.* 23:115–139.

Hud, N. V., F. W. Smith, F. A. L. Anet, and J. Feigon. 1996. The selectivity for K^+ versus Na^+ in DNA quadruplexes is dominated by relative free energies of hydration: a thermodynamic analysis by ^1H NMR. *Biochemistry.* 35:15383–15390.

Kang, C. H., X. Zhang, R. Ratliff, R. Moyzis, and A. Rich. 1992. Crystal structure of four-stranded Oxytricha telomeric DNA. *Nature.* 356: 126–131.

Keller, D., and C. Bustamante. 1986. Theory of the interaction of light with large inhomogeneous molecular aggregates. II. Psi-type circular dichroism. *J. Chem. Phys.* 84:2972–2980.

Laughlan, G., A. I. H. Murchie, D. G. Norman, M. H. Moore, P. C. E. Moody, D. M. Lilley, and B. Luisi. 1994. The high resolultion crystal structure of a parallel-stranded guanine tetraplex. *Science.* 265:520–524.

Lu, M., Q. Guo, and N. R. Kallenbach. 1992. Structure and stability of sodium and potassium complexes of dT_4G_4T. *Biochemistry.* 31: 2455–2459.

Lu, M., Q. Guo, and N. R. Kallenbach. 1993. Thermodynamics of G-tetraplex formation by telomeric DNAs. *Biochemistry.* 32:598–601.

Lumdblad, L. L., and J. W. Szostak. 1989. A mutant with a defect in telomere elongation leads to senescence in yeast. *Cell.* 57:633–643.

Marotta, S. P., P. A. Tamburri, and R. D. Sheardy. 1996. Sequence and environmental effects on the self-assembly of DNA oligomers possessing $G_xT_2G_y$ segments. *Biochemistry.* 35:10484–10492.

Marsh, T. C., and E. Henderson. 1994. G-wires: self-assembly of a telomeric oligonucleotide, d(GGGGTTGGGG), into large superstructures. *Biochemistry.* 33:10718–10724.

Marsh, T. C., J. Vesenka, and E. Henderson. 1995. A new DNA nanostructure, the G-wire, imaged by scanning probe microscopy. *Nucleic Acids Res.* 23:696–700.

Miura, T., J. M. Benevides, and G. J. Thomas, Jr. 1995. A phase diagram for sodium and potassium ion control of polymorphism in telomeric DNA. *J. Mol. Biol.* 248:233–238.

Protozanova, E., and R. B. Macgregor, Jr. 1996. Frayed wires: a thermally stable form of DNA with two distinct structural domains. *Biochemistry.* 35:16638–16645.

Sandell, L. L., and V. A. Zakian. 1993. Loss of a yeast telomere: arrest, recovery, and chromosome loss. *Cell.* 75:729–739.

Sen, D., and W. Gilbert. 1988. Formation of parallel four-stranded complexes by guanine-rich motifs in DNA and its implications for meiosis. *Nature.* 334:364–366.

Sen, D., and W. Gilbert. 1992. Novel DNA superstructures formed by telomere-like oligomers. *Biochemistry.* 31:65–70.

Tinoco, I., C. Bustamante, and M. F. Maestre. 1980. The optical activity of nucleic acids and their aggregates. *Annu. Rev. Biophys. Bioeng.* 9:107–141.

Williamson, J. R. 1994. G-quartet structures in telomeric DNA. *Annu. Rev. Biophys. Biomol. Struct.* 23:703–730.

Circular Dichroic and Kinetic Differentiation of DNA Binding Modes of Distamycin

Fu-Ming Chen and Feng Sha

Department of Chemistry, Tennessee State University, Nashville, Tennessee 37209-1561

Biochemistry®

Reprinted from
Volume 37, Number 32, Pages 11143–11151

Biochemistry

 Volume 37, Number 32 August 11, 1998

Articles

Circular Dichroic and Kinetic Differentiation of DNA Binding Modes of Distamycin†

Fu-Ming Chen* and Feng Sha

Department of Chemistry, Tennessee State University, Nashville, Tennessee 37209-1561

Received April 27, 1998; Revised Manuscript Received June 12, 1998

ABSTRACT: DNA binding modes of distamycin (DST) were investigated via comparative binding studies with oligomeric duplexes of the form d(GCG-X-GCG)·d(CGC-Y-CGC), where Y is complementary to X and X = 4- or 5-base binding site. It was found that 1:1 and 2:1 drug−duplex complexes exhibit distinctly different circular dichroic (CD) spectral characteristics and can, thus, serve as diagnostic tools for binding mode differentiation. CD intensity profiles at 265 or 275 nm as a function of drug to DNA ratios can reveal the extent of binding cooperativity for 2:1 complex formation (i.e., the relative binding affinities of 2:1 vs 1:1) at a 5-base-paired binding site. Comparison of these profiles leads to the following qualitative ranking for the binding cooperativity for the studied sites: AAGTT, ATATA ≥ AAACT > AATAA, AAATA, AAAGT > AATAT > TAAAA ≥ AAATT ≥ AAAAA ≥ ATAAA, AAAAT. The plausibility of this ordering is strengthened by its agreement with the ranking established by earlier NMR studies on some of the sequences. The significantly slower DST dissociation kinetics of the 2:1 complexes as compared to those of 1:1 made the kinetic measurements of SDS-induced dissociation by the stopped-flow technique possible. The results indicate that the AAGTT site exhibits the slowest DST dissociation rate, with a characteristic time of 35 s. The rates of dissociation in general correlate reasonably well with the cooperativity order found via equilibrium CD measurements (the higher the binding cooperativity, the slower the rate of dissociation). Base sequence specific binding of DST was also found for the 1:1 complex formation at the 4-base-paired sites, with AAAA, TTTT, ATTT, and AAAT sequences exhibiting the highest binding affinities.

Sequence-specific recognition of DNA by proteins and small molecules is a central element in the regulation of many biological processes. Understanding the structure, sequence specificity, and forces responsible for the binding of antibiotics to DNA is an important first step in the design of new drugs and sequence-specific probes. Two closely related antibiotics, netropsin (NET) and distamycin A (DST), have received considerable attention as models of sequence-specific nonintercalative DNA binding molecules. These two oligopeptides are potent antibacterial, antiviral, and antineoplastic agents whose pharmacological activity has been correlated to their abilities to bind to DNA (*1*). They form noncovalent complexes with duplex DNA in the minor groove and exhibit considerable preference for AT-rich domains such as the promoter regions. These antibiotics, thus, act as template poisons and inhibit DNA-dependent polymerase activities. Both DST and NET show a DNA

† Research supported by Army Medical Research Grant DAMD17-94-J-4474 and a subproject of Minority Biomedical Research Support Grant S06GM0892.

* Corresponding author. Telephone: (615)963-5325. FAX: (615)963-5434. E-Mail: chenf@harpo.tnstate.edu.

S0006-2960(98)00950-7 CCC: $15.00
Published on Web 07/21/1998

binding affinity which is in some cases significantly larger than that of typical intercalating drugs (*2*). Until recently, physical studies have focused mainly on the smaller NET molecule, and the results from such studies were then extended by analogy to the larger DST molecules. Recent years, however, have seen the upsurge of interest in using DST as a model for the DNA minor groove binding with A·T preference.

There have been numerous structural studies characterizing the DNA complexes of these antibiotics. In most of the crystallographic complexes studied thus far, a single ligand is bound per binding site of several successive A·T base pairs. The ligand is bound deep in the minor groove, making van der Waals contacts with both sides of the groove and forming hydrogen bonds between amides of the ligand and the acceptor groups of the bases (*3*). The positively charged end groups of the ligands are positioned to favorably interact with the electrostatic potential of the DNA. All of these factors contribute to the high affinity of these molecules for DNA. The preference of NET and DST binding to A·T sequences was further rationalized in terms of the protrusion of the amino group of guanosine into the minor groove which interferes sterically with binding at sites containing G·C pairs (*4*). This assertion, however, was being challenged by a study with poly(d2NH_2A-dT) indicating that despite the presence of the 2-amino group this polynucleotide exhibits significant binding to NET and DST (*5*).

Several NMR studies of 1:1 DST−DNA complexes have provided further insights into both the specificity and the forces responsible for the tight binding of this drug. The structure of the DST−d(CGCGAATTCGCG)$_2$ complex was determined by a combination of 2D NMR experiments and molecular mechanics calculations (*6*). It was found that the minimal binding site consists of just four A·T base pairs and that DST fits snugly into the 5′-AATT-3′ minor-groove binding site. This complex is characterized by van der Waals contacts between adenine C2H and drug H3 protons, potential three-center hydrogen bonds between drug amide and adenine N3 and thymine O2 atoms that protrude from the minor groove, and stacking of DNA O1′ atoms over each of the three pyrrole rings. The first two rings of the drugs are approximately parallel, while the third ring is turned to conform to the rotation of the helix. No large structural changes were observed for the DNA. It was suggested that the dipole-induced dipole interactions of the sugar O1′ atoms and the three *N*-methylpyrrole rings contribute to the stability of the complex and provide a molecular basis for the fact that binding is enhanced by the addition of *N*-methylpyrrole rings.

Calorimetric studies (*7*) have shown that DST binds tightly to the same four-base-paired site within the sequence d(GCGAATTCGC)$_2$, with a binding constant of 2.7×10^8 M^{-1}. This is in striking contrast to the binding constant of 2×10^5 M^{-1} reported for the 5′-TATA-3′ site within the sequence d(GGTATACC)$_2$, obtained by quantitative analysis of footprinting data (*8*). Although the discrepancies may largely be attributed to the sequence length and experimental techniques, sequence specificity of this drug may also be the culprit. The possible sequence specificity of this drug is further underscored by a recent crystallographic study of DST with d(CGCAAATTTGCG)$_2$ (*9*) revealing that the drug binds to the 5′-ATTT-3′ sequence, although other sites with four A·T base pairs were available in this oligomer.

Most interestingly, NMR studies have further indicated that binding sites of at least five base pairs in length can accommodate two DST molecules side-by-side in an antiparallel orientation (*10, 11*). In this 2:1 complex, each ligand preserves all the molecular recognition elements of minor groove binders. The extent of binding cooperativity (i.e., the ease of forming a complex of 2:1 vs 1:1 DST−duplex) depends strongly on the DNA sequence. Recently, Geierstanger et al. (*12*) have observed that DST can also bind to 5-base-paired sequences which contain G·C as well as A·T base pairs. When DST is titrated into a sample containing the binding site AAGTT·AACTT, a single set of new resonances is observed, saturating at a final stoichiometry of two DST molecules per DNA duplex. In addition, a crystal structure of the side-by-side complex of DST with [d(IC)$_4$]$_2$ has been reported (*13*). While DST binds exclusively 2:1 to AAGTT·AACTT and ATATA·TATAT even at low [ligand]/[duplex] ratios, only 1:1 DST complexes are observed with AAAAA·TTTTT at [ligand]/[duplex] ratios of up to 1. At higher ratios, DST also forms 2:1 complexes with AAAAA·TTTTT (*14*). The AAATT site was found to be intermediate in its cooperativity for 2:1 DST binding (*10*). These results indicate that the DST binding modes are strongly dependent on the base sequence of the binding site. In contrast to DST, the dication NET binds only as a single molecule per binding site, suggesting that charge interactions inhibit the side-by-side arrangement of two NET molecules in the minor groove.

These studies reinforce the importance of base sequence on the formation of both 1:1 and 2:1 complexes. Understanding the factors which govern the formation of these two types of complexes will be of value in discovering new ligands, which can be optimized for binding in specific modes to specific sequence targets. Therefore, a systematic sequence−specific binding study of DST was carried out, utilizing oligonucleotides containing binding sites of 4 and 5 base pairs. Spectral titrations and comparisons of spectral characteristics using these two types of oligomers were made to provide binding parameters and to find a possible means of differentiating these two modes of binding. CD spectral measurements were found to be most promising since a dimer formation devoid of plane or center of symmetry can lead to the formation of an exciton-type of CD couplet. This spectral feature is very distinct from that of monomer binding. The results of this study were then compared with those of NMR works already carried out on some of the sequences. This report describes our efforts and findings.

MATERIALS AND METHODS

Synthetic oligonucleotides were purchased from Research Genetics, Inc., Huntsville, AL, and used without further purification. These oligomers were purified by the vendor via reverse-phase oligonucleotide purification cartridges and exhibited single-band electrophoretic mobilities in denaturing polyacrylamide gel electrophoresis with stated purities of ≥95%. Concentrations of these oligomers (per nucleotide) were determined by measuring the absorbances at 260 nm after melting, with the use of extinction coefficients obtained via nearest-neighbor approximation using mono- and di-

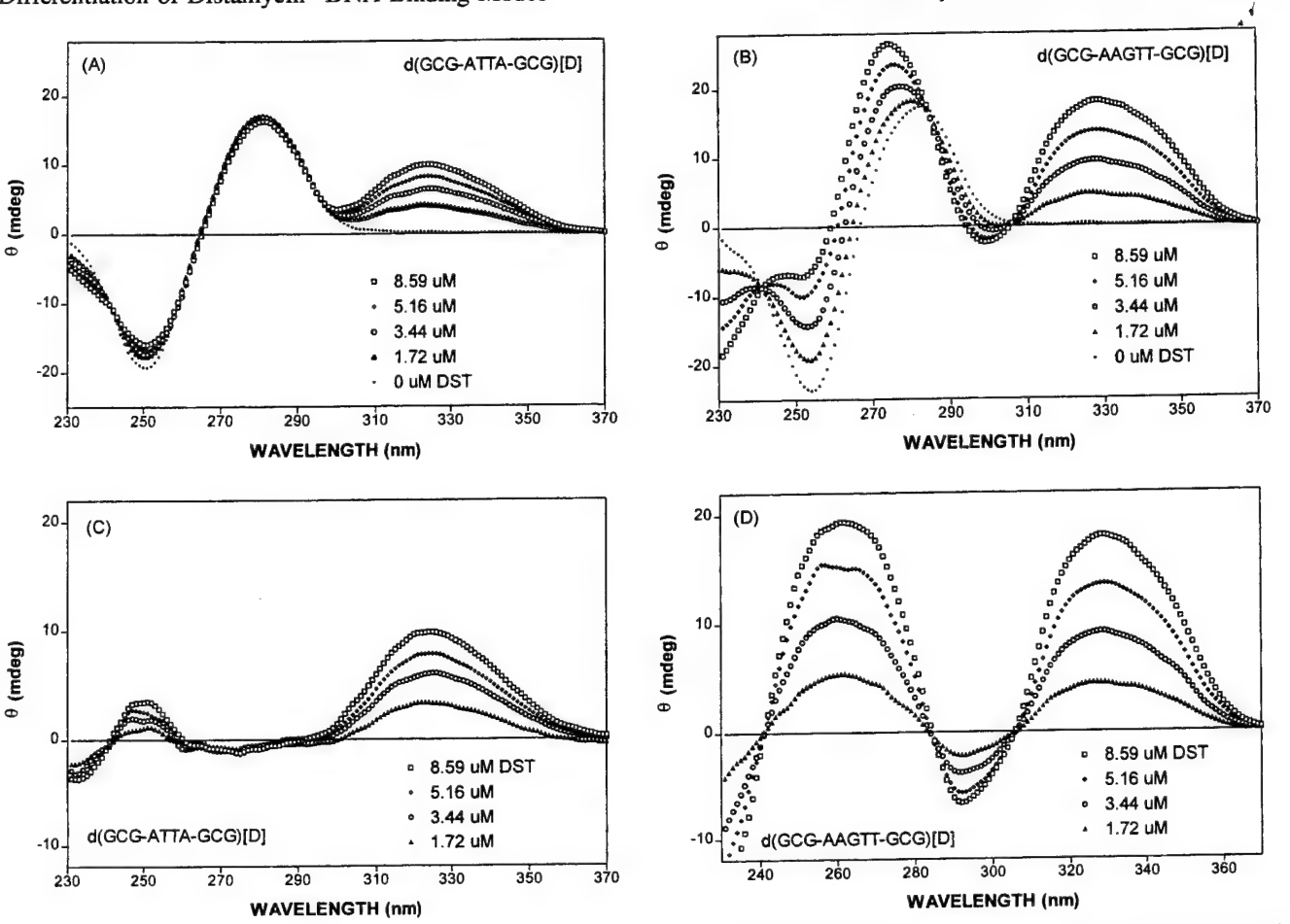

FIGURE 1: CD spectral comparison at room temperature for 4 μM (in duplex) d(GCG-ATTA-GCG)·d(CGC-TAAT-CGC) (panel A) and d(GCG-AAGTT-GCG)·d(CGC-AACTT-CGC) (panel B) in the presence of varying amounts of DST. The corresponding difference spectra, having the DNA spectral contributions subtracted off, are shown in panels C and D, respectively.

nucleotide values tabulated in Fasman (*15*). DNA heteroduplexes were formed by annealing complementary oligomers via heating equal molar mixtures to 95 °C for 5 min and slowly cooling back to ambient temperature. DST was purchased from Sigma and used without further purification. The extinction coefficient of 34 000 M^{-1} cm^{-1} at 303 nm was used for the DST concentration determination. Absorption spectral measurements were made with a Cary 1E spectrophotometric system. Thermal denaturation experiments were carried out with 1 cm semimicro cells by monitoring absorbances at 275 nm and maintaining a heating rate of 0.5 °C/min by the temperature controller accessory. Absorption spectral titrations of Job-type were carried out at 25 °C by making spectral measurements of two separate cells originally containing 5 μM DST and DNA (in duplex), respectively. Simultaneous transfer of a given volume from one cell to the other is then made, and the spectra were again taken. The process continued with progressive volume increases at strategic points. Absorbance changes at 350 nm were used to obtain equilibrium binding isotherms. Since DST is not very stable in aqueous solutions, the drug solution was prepared the same day the measurements were made. All experiments were carried out in 10 mM HEPPS [*N*-(2-hydroxyethyl)piperazine-*N*′-propanesulfonic acid] buffer solution of pH 8 containing 0.1 M NaCl and 1 mM $MgCl_2$.

Circular dichroic (CD) spectra were measured at room temperature with a Jasco J-500A recording spectropolarimeter using water-jacketed cylindrical cells of 2 cm path length. CD spectral titrations were made by starting with an oligomer of 80 μM (in nucleotide) which is followed by subsequent progressive additions of aliquots of DST stock. Ellipticities at 330 nm were used to construct equilibrium binding isotherms. Stopped-flow kinetic measurements were made with an Olis RSM-1000 system.

RESULTS

CD Spectral Characterization of 1:1 and 2:1 DST−Duplex Complexes. As mentioned earlier, a 4-base-pair site can only bind one DST molecule whereas the AAGTT site can bind two molecules to form an exclusively 2:1 complex. Oligomers containing ATTA and AAGTT were selected as prototypes for the 1:1 and 2:1 binding modes to investigate their possible spectral differences and to obtain binding parameters. DST is not optically active when free in solutions. In the presence of DNA, however, a sizable CD spectrum can be induced upon complex formation. CD spectral characteristics are compared in Figure 1 for d(GCG-ATTA-GCG)[d] (panel A) and d(GCG-AAGTT-GCG)[d] (panel B) in the absence and in the presence of increasing amounts of DST, where [d] designates the DNA heteroduplex. It is apparent that the two modes of binding induce distinctly different CD spectral characteristics. DST binding to the ATTA-containing decameric duplex results in a CD intensity enhancement of a band centering around 325 nm, with surprisingly little spectral alterations below 300 nm, except for some changes near 250 and 230 nm (panel A).

The maintenance of an isoelliptic point near 240 nm suggests a two-component process, with the complex being of 1:1 drug:duplex ratio. In contrast, binding of DST to -AAGTT- results in a more dramatic spectral change. In addition to the maintenance of the isoelliptic point at 241 nm and a somewhat larger intensity enhancement with a slight red shift of the 325 nm band, gross spectral alterations were seen in the spectral region below 300 nm. The appearance of a negative indentation near 291 nm and the presence of additional isoelliptic points around 284 and 306 nm are quite noteworthy (see panel B). The presence of these isoelliptic points again signifies a two-component binding process, with the bound species now being the 2:1 complexes as determined by an earlier NMR experiment (*12*). The general CD spectral features appear to be similar to those observed for the DST−d(CGC-AAATT-GGC)·d(GCC-AATTT-GCG) system (*16*).

The CD spectral alterations of these two binding modes can be more clearly seen if presented as difference spectra, where the DNA spectral contributions have been subtracted out. The results are shown in panels C and D for the -ATTA- and -AAGTT-containing oligomers, respectively. In addition to a stronger 330 nm band, a large positive CD band is induced near 265 nm upon DST binding to the -AAGTT- site with a magnitude slightly larger than that of the 330 nm band. The presence of three isoelliptic points (at 306, 284, and 241 nm) and the induction of a negative CD maximum near 291 nm are much more transparent in the difference CD spectra (panel D).

The observation of distinctly different CD spectral characteristics induced by the binding of DST at the -AAGTT- site when compared to the -ATTA- site is consistent with 2:1 complex formation at this 5-base binding site. An exciton-type CD couplet is to be expected for some absorbance bands if the drug dimer bound to the DNA minor groove is devoid of a plane or center of symmetry. Indeed, the dramatic positive and negative CD intensity enhancements near 265 and 230 nm, respectively, and the appearance of a negative maximum near 291 nm are consistent with the presence of exciton couplets centering near 240 and 285 nm, respectively.

CD Spectral Characteristics and Sequence-Specific Binding of DST at the 4-Base-Paired Binding Sites. To further investigate the feasibility of using CD spectral features to characterize the DST binding mode and to elucidate its possible sequence specificity, a series of oligomers were studied. As a first step in elucidating the tetranucleotide sequence specificity of DST, binding studies were carried out on decameric duplexes of the form d(GCG-X-GCG)·d(CGC-Y-CGC), where Y is complementary to X and X = AAAA, AAAT, AATA, ATAA, TAAA, ATTT, TATT, TTAT, TTTA, and TTTT. Representative CD difference spectral characteristics are shown in Figure 2. The general [DST]-dependent spectral features (especially those of TAAA, see panel D) are similar to those observed for the -ATTA-containing oligomer presented earlier (see Figure 1C). These are a sizable positive CD intensity enhancement near 325 nm and the presence of an isoelliptic point near 240 nm flanked by weak positive and negative intensity enhancements at 250 and 230 nm, respectively. Some sequence-dependent spectral differences, however, are also evident. For example, the progressive induction of a negative band near 275 nm resulted in the appearance of an additional isoelliptic point at 265 nm for the -AAAT-, -AAAA-, and -TTTT-containing decameric duplexes (see panels A, E, and F, respectively). Notice also the significantly smaller induced CD intensities of the 325 nm band for the -AATA- and -ATAA- sites (panels B and C, respectively), evidence of less favorable DST binding preference at these sequences. Similar studies were also made with oligomers containing the sequence isomers ATTT, TATT, TTAT, and TTTA. Again some sequence-dependent spectral features were observed (results not shown).

Ellipticities at 330 nm were used to construct Scatchard plots, and the binding parameters extracted via linear least-squares fits are shown in Table 1. Binding constants ranging from 1.5×10^7 to less than 2×10^5 M^{-1} were obtained, underscoring some sequence specificity of this drug. Consistent with the 1:1 complex formation, the extracted binding densities at strong binding sites are found to be slightly larger than 1 drug molecule bound per duplex. Comparison of the extracted binding constants led to a qualitative ranking on the DST binding affinities to the 4-base-paired sites studied. The results are (in descending binding affinity) as follows: TTTT, AAAA, ATTT ≥ AAAT >TAAA, TTTA, TTAT ≥ TATT > ATAA > AATA.

DST binding also enhances DNA duplex stability. Melting temperature increases upon DST binding for the oligomers studied are included in Table 1 for comparison. Although the extent of melting temperature increase does not correspond exactly to the established binding order, the general trend of larger and smaller melting temperature increases for higher and lower DST binding affinities appears to be in order.

Sequence Specificity and Binding Mode Characterization of 5-Base-Paired Sites via CD Titration. Sequence-specific binding and CD spectral characterization of DST at the 5-base-paired sites were investigated by comparative studies with undecameric duplexes of the form d(GCG-X-GCG)-[d], where X = AAAAA, AAAAT, AAATA, AATAA, ATAAA, TAAAA, AAATT, AATAT, ATATA, AAACT, and AAAGT. Difference CD spectra of some representative titrations are shown in Figure 3. The gross spectral features of DST binding at these 5-base-paired binding sites are quite distinct from those of the 4-base-paired counterparts. The appearance of a negative difference CD spectral maximum near 291 nm and somewhat larger positive CD intensity enhancements around 330 and 265 nm are the outstanding features of DST binding at the 5-base-paired binding sites.

For the -AAAAA- and -AAAAT-containing oligomers (panels A and B, respectively), the initial progressive intensity increase of the weak negative CD band around 275 nm and the maintenance of an isoelliptic point near 265 nm are clearly evident for [DST]/[duplex] ≤ 1. These spectral features are very similar to those observed for the 4-base-paired sites -AAAA- and -AAAT- (see Figures 2E and 2A, respectively.) For [DST]/[duplex] ratios greater than 1, however, the 265 nm isoelliptic point is no longer maintained. Instead, CD intensities near this wavelength become progressively more positive to result in the appearance of a new isoelliptic point in the 285−290 nm region. These spectral alterations differ significantly from those of -AAGTT-, where the maintenance of the 285-nm isoellptic point is evident throughout the titration (see Figure 1D). These results

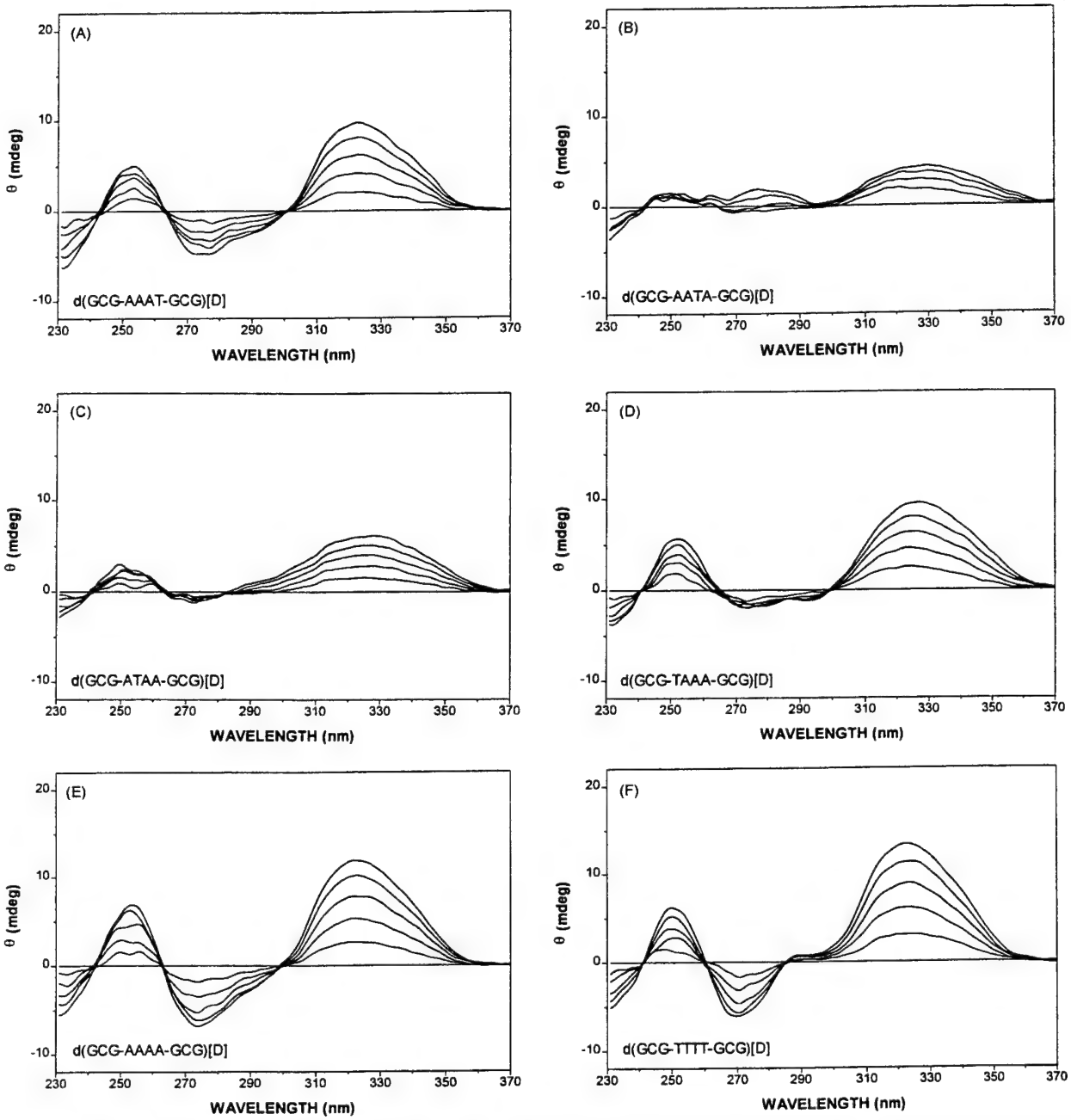

FIGURE 2: Comparison of induced CD difference spectra of DST at representative 4-base-paired binding sites. The spectra shown correspond to 4 μM DNA duplex in the presence of 0.86, 1.72, 2.58, 3.44, and 4.30 μM DST. Oligomers shown are d(GCG-AAAT-GCG)·d(CGC-ATTT-CGC) (panel A), d(GCG-AATA-GCG)·d(CGC-TATT-CGC) (panel B), d(GCG-ATAA-GCG)·d(CGC-TTAT-CGC) (panel C), d(GCG-TAAA-GCG)·d(CGC-TTTA-CGC) (panel D), d(GCG-AAAA-GCG)·d(CGC-TTTT-CGC) (panel E), and d(GCG-TTTT-GCG)·d(CGC-AAAA-CGC) (panel F).

suggest the formation of a 1:1 complex when [DST]/[duplex] is ≤ 1 and is subsequently followed by 2:1 complex formation when the ratios are greater than 1. This interpretation is consistent with earlier NMR titrations of the AAAAA·TTTTT site showing that 1:1 complexes are formed up to a [DST]/[duplex] ratio of 1 with subsequent 2:1 complex formation only after saturation of the 1:1 binding mode.

Although no clear-cut presence of an isoelliptic point near 265 nm is evident during the [DST]/[duplex] ≤ 1 phase of titration for the -AAATT-containing oligomeric duplex (panel C), the induction of a significantly larger CD intensity near 265 nm during the [DST]/[duplex] ≥ 1 phase of titration is clearly apparent. These results suggest the presence of a 2-step binding process with a higher cooperativity for 2:1 binding than those of AAAAA- and AAAAT-containing oligomers, a result consistent with the earlier NMR finding (*14*). As for the titrations of the AAACT-containing oligomeric duplex (panel D), the spectral changes are characterized by an immediate progressive positive intensity enhancement near 265 nm (instead of the presence of an initial isoelliptic point) and the maintenance of an approximate isoelliptic point near 285 nm. These spectral features are reminiscent of those of the AAGTT site, suggesting nearly exclusive 2:1 complex formation at the AAACT site, bypassing the 1:1 complexation stage.

Single-Wavelength CD Intensity Profiles and Cooperativity of 2:1 Complex Formation. As noted earlier, 1:1 complex formation at most sequences is accompanied by little or no

Table 1: Comparison of Distamycin A Binding Parameters and Melting Temperatures

oligomer	K (μM^{-1})	n (/duplex)	t^0_m (°C)[a]	t_m (°C)[a]	Δt_m (°C)
d(GCG-AAAA-GCG)·d(CGC-TTTT-CGC)	14.9	1.1	38.0	53.1	15.1
d(GCG-AAAT-GCG)·d(CGC-ATTT-CGC)	10.9	1.4	45.0	53.5	8.5
d(GCG-AATA-GCG)·d(CGC-TATT-CGC)	<0.2		43.5	47.5	4.0
d(GCG-ATAA-GCG)·d(CGC-TTAT-CGC)	0.33		39.8	45.0	5.2
d(GCG-TAAA-GCG)·d(CGC-TTTA-CGC)	1.5		37.5	45.0	8.5
d(GCG-ATTT-GCG)·d(CGC-AAAT-CGC)	14.4	1.1	46.0	55.5	9.5
d(GCG-TATT-GCG)·d(CGC-AATA-CGC)	1.0	1.1	43.7	52.0	8.3
d(GCG-TTAT-GCG)·d(CGC-ATAA-CGC)	1.2		41.3	48.1	6.8
d(GCG-TTTA-GCG)·d(CGC-TAAA-CGC)	1.3	1.2	43.5	47.5	4.0
d(GCG-TTTT-GCG)·d(CGC-AAAA-CGC)	15.5	1.1	45.4	53.3	7.9

[a] t^0_m and t_m are melting temperatures of 40 μM (base) oligomeric duplexes in pH 8 buffer containing 0.1 M NaCl and in the absence and in the presence of 7 μM DST, respectively.

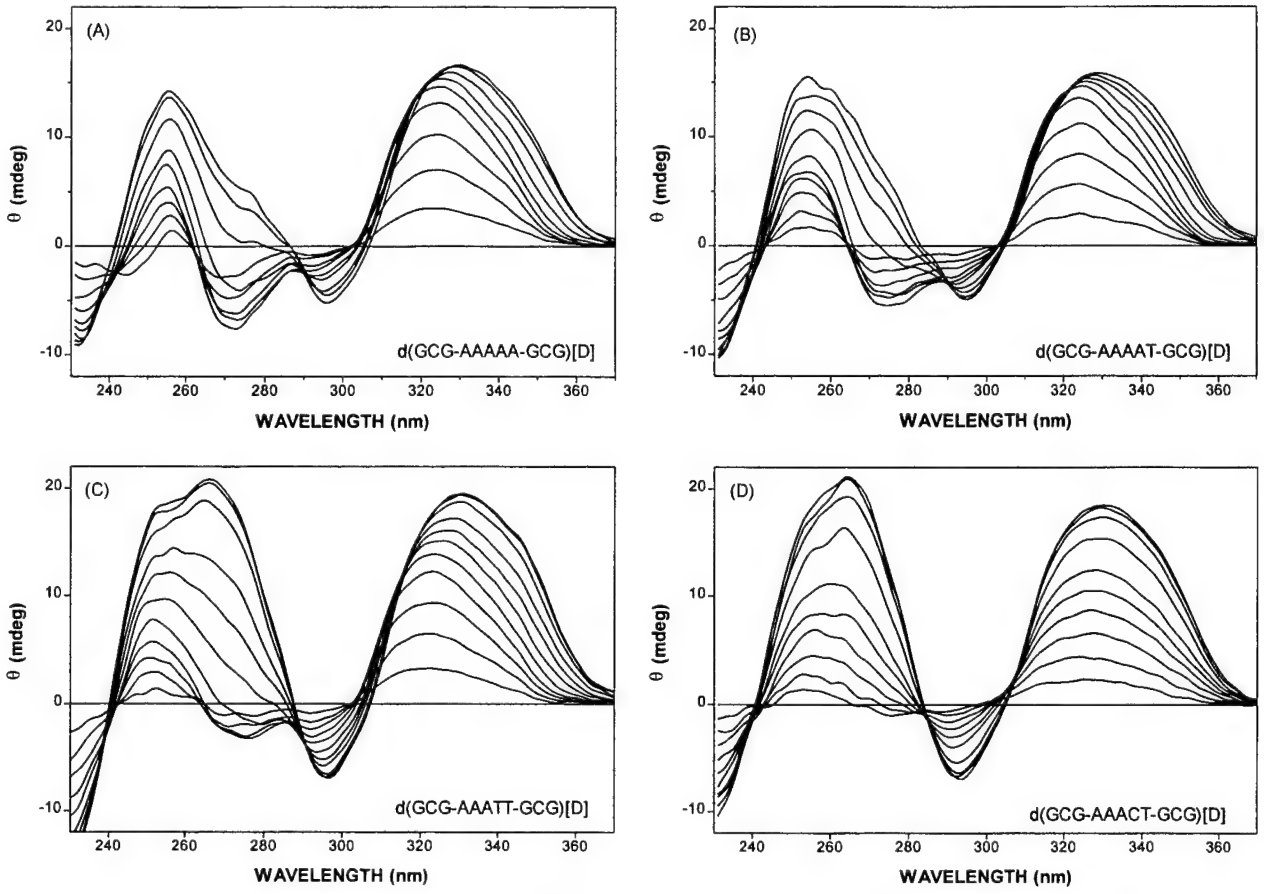

FIGURE 3: Comparison of induced CD difference spectra of DST at representative 5-base-paired binding sites. The spectra shown correspond to 4 μM DNA duplex in the presence of 0.86, 1.72, 2.58, 3.44, 4.30, 5.16, 6.88, 8.60, 10.3, 12.1, and 13.8 μM DST. Oligonucleotides represented are d(GCG-AAAAA-GCG)·d(CGC-TTTTT-CGC) (panel A), d(GCG-AAAAT-GCG)·d(CGC-ATTTT-CGC) (panel B), d(GCG-AAATT-GCG)·d(CGC-AATTT-CGC) (panel C), d(GCG-AAACT-GCG)·d(CGC-AGTTT-CGC) (panel D).

change in the CD intensity near 265 nm whereas a dramatic intensity enhancement is induced at this same wavelength upon formation of 2:1 complexes. This suggests that monitoring of the CD intensity at this wavelength may provide useful information in differentiating binding modes at different sites. CD intensities at 265 nm were plotted against [DST]/[duplex], and the results for some representative oligomers are shown in Figure 4. For the oligomer containing the -AAAAT- site, the intensity remains near zero until the [DST]/[duplex] ratios surpass 1, wherein the 265 nm intensity becomes more enhanced. These results are consistent with the formation of 1:1 complexes when the [DST]/[duplex] ratios are below 1 and 2:1 complex formation when they exceed 1. The [DST]/[duplex] ratio at which the intensity starts to take off becomes progressively smaller for the AAATT, AATAT, and AAATA sites at approximate values of 0.8, 0.6, and 0.4, respectively. These results suggest that the 2:1 complex formation becomes more cooperative and begins at a lower and lower drug/duplex ratio. For the ATATA and AAACT sites, the intensity enhancement begins immediately at the start of the titration. The intensity profile for the prototypical AAGTT sequence (not shown) is very similar to those exhibited by these two sites. These results are consistent with their nearly exclusive formation of the 2:1 complexes even at low drug/duplex ratios. Intensity monitoring at 275 nm may in fact be more informative since its intensity becomes slightly more negative during 1:1 complex formation for some sites whereas its

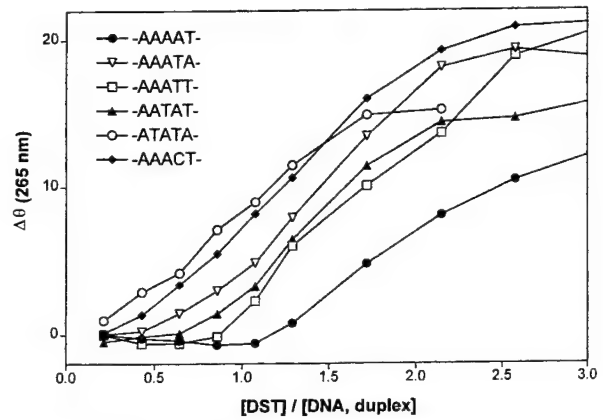

FIGURE 4: CD intensity profiles for representative oligomers as a function of [DST]/[duplex] at 265 nm for representative 5-base-paired binding sites.

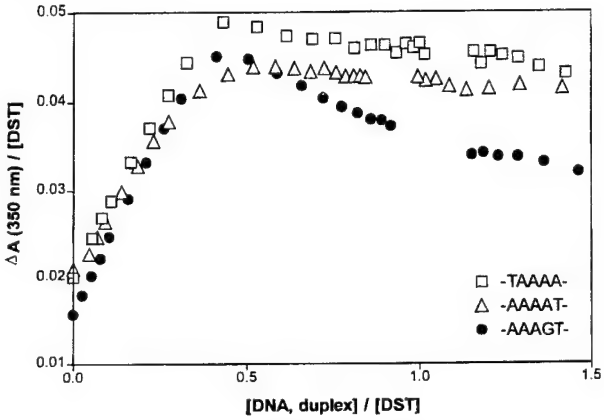

FIGURE 5: Representative equilibrium binding isotherms plotted as apparent extinction coefficients at 350 nm vs [duplex]/[DST]. Absorption titrations were carried out at 25 °C. The discontinuities exhibited in the binding isotherms are the consequence of not being able to reach equal drug concentrations in our two-cell Job-type titrations.

intensity turns more positive with subsequent 2:1 complex formation. Therefore, the distinction of these two modes of binding can more readily be made with the intensity monitoring at this wavelength by noting the slope change from negative to positive (results not shown). Based on the comparison of [drug]/[duplex] ratios at the intensity takeoff of these profiles, the extent of binding cooperativity for the formation of 2:1 complexes can be ranked approximately as follows: AAGTT, ATATA ≥ AAACT > AATAA, AAATA, AAAGT > AATAT > TAAAA ≥ AAATT ≥ AAAAA ≥ ATAAA, AAAAT.

Evidence of 2:1 Complex Formation via Absorption Spectral Titrations for the 5-Base-Paired Sites. DST exhibits an absorbance maximum at 303 nm when free in solutions. Successive additions of DNA lead to slight bathochromic shifts and intensity enhancements near 330 nm. Absorbance changes at 350 nm (to avoid interference from the residual DNA absorbance) were used to construct binding isotherms and to obtain binding parameters. Binding isotherms via absorbance monitoring were constructed to provide evidence for the formation of 2:1 complexes for oligomers containing 5-base-paired binding sites. Representative plots of ϵ (apparent) vs [duplex]/[DST] are shown in Figure 5. It is apparent that these binding isotherms (and indeed for all the sequences studied) show breaks near [duplex]/[DST] = 0.5,

Table 2: Comparison of SDS-Induced DST Dissociation Kinetic Parameters at 20 °C for the 5-Base-Paired Sites[a]

oligomer	K (s^{-1})	τ (s)
d(GCG-AAAAA-GCG)·d(CGC-TTTTT-CGC)	2.46 ± 0.04	0.41
d(GCG-AAAAT-GCG)·d(CGC-ATTTT-CGC)	2.53 ± 0.01	0.40
d(GCG-AAATA-GCG)·d(CGC-TATTT-CGC)	0.28 ± 0.003	3.57
d(GCG-AATAA-GCG)·d(CGC-TTATT-CGC)	0.61 ± 0.01	1.63
d(GCG-ATAAA-GCG)·d(CGC-TTTAT-CGC)	2.16 ± 0.04	0.46
d(GCG-TAAAA-GCG)·d(CGC-TTTTA-CGC)	1.04 ± 0.02	0.96
d(GCG-AAATT-GCG)·d(CGC-AATTT-CGC)	0.69 ± 0.004	1.45
d(GCG-AATAT-GCG)·d(CGC-ATATT-CGC)	2.23 ± 0.05	0.45
d(GCG-ATATA-GCG)·d(CGC-TATAT-CGC)	0.144 ± 0.001	6.94
d(GCG-AAGTT-GCG)·d(CGC-AACTT-CGC)	0.0284 ± 0.0003	35.2
d(GCG-AAAGT-GCG)·d(CGC-ACTTT-CGC)	1.98 ± 0.05	0.51
d(GCG-AAACT-GCG)·d(CGC-AGTTT-CGC)	2.02 ± 0.07	0.50

[a] Measurements were made by mixing a solution containing 7.5 μM DST/75 μM DNA (in nucleotide) with an equal volume of 2% SDS solution. The time-dependent absorbance profile at the 341−347 nm region was used for curve-fit.

suggesting the formation of complexes having 2 drug molecules bound per duplex.

Binding Mode Differentiation via Kinetic Measurements. Due to the ability of the DST dimer to make extensive hydrogen bonding and van der Waal contacts with both walls of the minor groove, it is anticipated that both their association and their dissociation kinetics will be considerably slower than the corresponding 1:1 complexes. Thus, stopped-flow kinetic measurements were made. The rates of association kinetics appear to be too fast to give meaningful rate information, although there are indications that the rates of DST binding at the 5-base-pair sites are indeed slower than at the 4-base-pair sites. Although the rates of dissociation from the 4-base-paired sites are too fast to be measured by the stopped-flow technique, those of 5-base sites are amenable for such measurements. The extracted SDS-induced DST dissociation rate parameters via single-exponential fits are summarized in Table 2. It is apparent that the measurable rates of DST dissociation vary greatly among these 5-base-paired sites, ranging from a characteristic time of 35.2 s for the AAGTT site to 0.4 s for the AAAAT site. The ranking of the dissociation rates is (slowest at the left): AAGTT > ATATA > AAATA > AATAA ≥ AAATT > TAAAA > AAAGT, AAACT, ATAAA, AATAT, AAAAA, AAAAT. Except for AAACT and AAAGT, the ordering appears to conform in general to that of 2:1 binding cooperativity as suggested via equilibrium CD titrations. Our observed SDS-induced DST dissociation rates of the 2:1 complexes appear reasonable since NMR studies of DST binding with $d(CGCAAATTTGCG)_2$ revealed that the off-rate for the drug from the 2:1 mode was found to be slow on the NMR time scales, with a characteristic time of 5 s at 30 °C (*11*).

DISCUSSION

Of all A·T specific minor groove binders studied thus far, DST and its analogues appear to be the only molecules found to form both 1:1 and 2:1 complexes. Based on X-ray (*17*) and NMR (*6*) data, this drug spans 4 base pairs in forming a 1:1 complex. However, a 5-base-paired site can be occupied simultaneously by two DST molecules side-by-side with the positively charged end groups pointing in opposite directions (*10, 11*). The degree of cooperativity,

i.e., the relative binding affinities of the 2:1 vs 1:1 modes, depends strongly on the DNA sequence. Our results indicate that these two binding modes exhibit distinctly different CD spectral characteristics. Thus, CD measurements can be employed to identify and differentiate the DNA binding modes and to obtain meaningful binding parameters for this drug.

Sequence specificity of DST for the formation of the 1:1 complex is observed, and binding parameters extracted via Scatchard plots suggest equilibrium binding constants ranging from 1.5×10^7 to less than 2×10^5 M^{-1}. Sequences containing a 3 or 4 homo-base stretch appear to provide stronger 1:1 bindings whereas the presence of alternating sequences at the binding sites seems to significantly reduce their DST binding affinities. Our finding of strong DST binding at the -ATTT- site appears to be consistent with the recent crystallographic study of DST+d(CGCAAATTTGCG)$_2$ revealing that the drug bound to only one site, namely, 5′-ATTT-3′, although other 4-base sites were also available (*9*). In addition, it was shown by NOESY experiments that DST binds to the AAATT site as a 1:1 complex at low [DST]/[duplex] ratios and the AAAT/ATTT site is preferred by 2.2 to 1 over the AATT/AATT site (*10, 11*).

Sequence-dependent spectral variations were also observed for the 5-base-paired binding sites studied. CD intensity profiles at 275 and 265 nm vs [DST]/[duplex] provide indications on the cooperativity of the 2:1 binding mode at these sites to result in a qualitative ranking. In contrast to 1:1 complex formation, sequences containing 3 or more homo-base stretches appear to provide a less favorable environment while sequences with alternating bases provide a more favorable environment for 2:1 complex formation.

Binding isotherms via absorbance titration further confirm the formation of 2:1 complexes at these 5-base-paired binding sites. In addition, SDS-induced drug dissociation experiments indicate considerable variation in their rates of drug dissociation, with AAGTT and AAAAT sites exhibiting the slowest and the fastest dissociation rates, respectively. Except for some G·C-containing sequences, the ranking via dissociation rates appears to generally conform to that of binding cooperativity of the 2:1 complexes, with the highest cooperative binding exhibiting the slowest DST dissociation rate.

The validity of our cooperativity ordering on 2:1 complex formation appears to be supported by earlier NMR studies on oligomers containing some of the same sequences (*14*). NMR titrations of the AAAAA·TTTTT site have shown that 1:1 complexes are formed up to a [DST]/[duplex] ratio of 1, which is then followed by 2:1 complex formation. On the other hand, the opposite behavior is seen with the alternating site ATATA·TATAT. Only a 2:1 complex is observed for all [DST]/[duplex] ratios, even as low as 0.25 equiv of DST per DNA duplex. An intermediate case is found for the sequence AAATT·AATTT in which NMR results (*11*) indicate that at a [DST]/[duplex] ratio of 0.75:1 about 10% of the population of the bound DNA is already in the 2:1 complex form. These results, thus, suggest that the 2:1 binding cooperativity follows the order ATATA > AAATT > AAAAA (*14*), in agreement with our ranking. Furthermore, their studies also suggested that in oligomers containing a AAGTT, AAACT, or AAAGT site, only 2:1 complexes were observed. Indeed, all three of these sites are high on our ranking order.

Based on their NMR results, Wemmer et al. (*14*) had speculated that the binding behavior of DST reflects the local variations in DNA groove geometry and flexibility, especially the groove width. DST forms tight complexes with DNA only if it can provide close van der Waals contacts with the walls of the minor groove, and the DNA minor groove must expand to accommodate two DST molecules. A comparison of crystal structures suggests that the minor groove is narrowest in poly(dA)-type sequences (*18*−*21*) and such sequences are also particularly stable against base-pair opening (*22*). The AAAAA·TTTTT and sites containing 3 or 4 homo-base, therefore, represent preferred 1:1 DST binding sites because of the narrowness of their grooves. The slight extra width and greater flexibility may have contributed to the observed weaker DST affinities for 1:1 complex formation at sites containing ATA or TAT and enhanced cooperativity of 2:1 binding at ATATA·TATAT. NMR studies have further indicated that 2:1 complexes of DST and its analogues are able to form close contacts and tight complexes with the minor groove of mixed G·C/A·T sequences. This seems somewhat puzzling in view of the fact that the A·T specificity of NET and DST has been attributed to the steric interference with binding at sites containing G·C pairs (*4*), a consequence of the protruding amino group of guanosine at the minor groove. However, it has been seen in the crystal structure of B-form DNA that the minor groove in regions containing G·C pairs is decidedly wider (*20, 23, 24*). It was thus suggested that the loss of shape complementarity and contact surface between ligand and groove is more important than the depth of the groove (*14*). A wider groove easily accommodates a 2:1 complex, making AAGTT the most cooperative 2:1 binding site. This same binding mode is observed for the sequences AAAGT·ACTTT and AAACT·AGTTT as well, indicating that the G·C pair need not be in the center of the site. It should be pointed out, however, that our results indicate they exhibit distinctly different dissociation kinetic behaviors. The two sites with off-centered G·C exhibit 7-fold faster dissociation rates than that with a central G·C base pair.

The notion that the introduction of a G·C base pair into an A·T stretch of DNA widens the minor groove locally and results in DST binding exclusively in the 2:1 mode appears plausible. This may also explain why the IIICC·IICCC site only exhibits one type of complex with a 2:1 stoichiometry (*25*). It was shown that this complex is a 2:1 side-by-side complex exactly as that observed with AAATT·AATTT. As base pairs in the AAATT·AATTT site are successively replaced with I·C base pairs, DST binding becomes progressively more cooperative in proportion to the number of substituted base pairs, apparently without any preference for location in the sequence. Since I·C base pairs contain the same minor groove functional groups as A·T base pairs, their binding differences most likely are the consequence of different groove geometry due to differences in base pair stacking, propeller twist, and other structural parameters. It would be reasonabe to suspect that the structural attributes of I·C are quite similar to those of G·C.

Rentzeperis and Marky (*16*) had carried out thermodynamic characterization of NET and DST binding to an AAATT-containing oligomer and found that binding of NET

to this sequence occurs with favorable enthalpy and small but also favorable entropy. The first DST binding yielded similar affinities ($\sim 10^7$ M^{-1}) and more favorable enthalpy contribution to that of NET binding. However, the binding of the second molecule gives a much more favorable enthalpy, which was interpreted as arising from increased van der Waals interactions, a heat capacity effect, and much less favorable entropy, arising from a combination of ion and water interactions. These contributions lead to a favorable free energy of binding slightly less than that for the first DST molecule.

It should be noted in passing that DST complexation with a nucleic acid triple helix has also been investigated recently (*26*). CD spectral analysis indicates that DST can bind to the triple-stranded form but its binding affinity is weaker than the corresponding duplex form. The bound DST appears to exhibit a conformation and an environment slightly different from those bound to the corresponding double-stranded form. Thermal denaturation experiments demonstrate that DST binding destabilizes the triplex whereas it stabilizes the duplex. Furthermore, the 2:1 complex formation is not observed with the triple-stranded host. The inability of the triplex to form 2:1 complex was rationalized in terms of its failure to expand the minor groove to bind two DST molecules due to the presence of the third strand bound at the major groove of DNA.

These results suggest that there are subtle differences in the minor groove width for different DNA sequences, and that DST is a sensitive probe for these differences in the DNA structure. Information obtained from such studies should aid in the design of new drugs and should also provide insight into both DNA conformational flexibility and protein−DNA interactions.

REFERENCES

1. Hahn, F. E. (1977) *Pharmacol. Ther., Part A 1*, 475−485.
2. Luck, G., Zimmer, C., Reinert, K., and Arcamone, F. (1977) *Nucleic Acids Res. 4*, 2655−2670.
3. Zimmer, C., and Wahnert, U. (1986) *Prog. Biophys. Mol. Biol. 47*, 31−112.
4. Kopka, M. L., Yoon, C., Goodsell, D., Pjura, P., and Dickerson, R. E. (1985) *Proc. Natl. Acad. Sci. U.S.A. 82*, 1376−1380.
5. Dasgupta, D., Howard, F. B., Sasisekharan, V., and Miles, T. (1990) *Biopolymers 30*, 223−227.
6. Pelton, J. G., and Wemmer, D. E. (1988) *Biochemistry 27*, 8088−8096.
7. Breslauer, K. J., Remeta, D. P., Chou, W.-Y., Ferrante, R., Curry, J., Zaunczkowski, D., Synder, J. G., and Marky, L. A. (1987) *Proc. Natl. Acad. Sci. U.S.A. 84*, 8922−8926.
8. Fish, E. L., Lane, M. J., and Vournakis, J. N. (1988) *Biochemistry 27*, 6026−6032.
9. Coll, M., Frederick, C. A., Wang, A. H.-J., and Rich, A. (1987) *Proc. Natl. Acad. Sci. U.S.A. 84*, 8385−8389.
10. Pelton, J. G., and Wemmer, D. E. (1989) *Proc. Natl. Acad. Sci. U.S.A. 86*, 5723−5727.
11. Pelton, J. G., and Wemmer, D. E. (1990) *J. Am. Chem. Soc. 112*, 1393−1399.
12. Geierstanger, B. H., Dwyer, T. J., Bathini, Y., Lown, J. W., and Wemmer, D. E. (1993) *J. Am. Chem. Soc. 115*, 4474−4482.
13. Chen, X., Ramakrishnan, B., Rao, S. T., and Sundaralingan, M. (1994) *Nat. Struct. Biol. 1*, 169−174.
14. Wemmer, D. E., Geierstanger, B. H., Fagan, P. A., Dwyer, T. J., Jacobsen, J. P., Pelton, J. G., Ball, G. E., Leheny, A. R., Chang, W.-H., Bathini, Y., Lown, J. W., Rentzeperis, D., Marky, L. A., Singh, S., and Kollman, P. (1994) in *Structural Biology: The State of the Art. Vol 2. Proceedings of the 8th Conversation in the Discipline Biomolecular Stereodynamics* (Sarma, H., and Sarma, M. H., Eds.) pp 301−323, Adenine Press, New York.
15. Fasman, G. D., Ed. (1975) *CRC Handbook of Biochemistry and Molecular Biology*, 3rd ed., Vol. I, p 589, Chemical Rubber Company Publishing, Cleveland, OH.
16. Rentzeperis, D., and Marky, L. A. (1995) *Biochemistry 34*, 2937−2945.
17. Coll, M., Aymami, J., van der Marel, G. A., van Boom, J. H., Rich, A., and Wang, A. H.-J. (1989) *Biochemistry 28*, 310−320.
18. Wing, R., Drew, H., Takano, T., Broka, C., Tanaka, S., Itakura, K., and Dickerson, R. E. (1980) *Nature 287*, 755−758.
19. Nelson, H. C. M., Finch, J. T., Bonaventura, L. F., and Klug, A. (1987) *Nature (London) 330*, 221−226.
20. Yoon, C., Prive, G. G., Goodsell, D. S., and Dickerson, R. E. (1988) *Proc. Natl. Acad. Sci. U.S.A. 85*, 6332−6336.
21. DiGabriele, A. D., Sanderson, M. R., and Steiz, T. A. (1989) *Proc. Natl. Acad. Sci. U.S.A. 86*, 1816−1820.
22. LeRoy, J. L., Charretier, E., Kochoyan, M., and Gueron (1988) *Biochemistry 27*, 8894−8898.
23. Heinemann, U., and Alings, C. (1989) *J. Mol. Biol. 210*, 369−381.
24. Goodsell, D. S., Kopka, M. L., Cascio, D., and Dickerson, R. E. (1993) *Proc. Natl. Acad. Sci. U.S.A. 90*, 2930−2934.
25. Fagan, P., and Wemmer, D. E. (1992) *J. Am. Chem. Soc.114*, 1080−1081.
26. Durand, M., and Maurizot, J. C. (1996) *Biochemistry 35*, 9133−9139.

BI980950L

Binding of Actinomycin D to DNA Oligomers of CXG Trinucleotide Repeats

Fu-Ming Chen

Department of Chemistry, Tennessee State University, Nashville, Tennessee 37209-1561

Biochemistry®

Reprinted from
Volume 37, Number 11, Pages 3955–3964

Binding of Actinomycin D to DNA Oligomers of CXG Trinucleotide Repeats†

Fu-Ming Chen*

Department of Chemistry, Tennessee State University, Nashville, Tennessee 37209-1561

Received August 25, 1997; Revised Manuscript Received December 18, 1997

ABSTRACT: Actinomycin D (ACTD) binding propensities of DNA with CXG trinucleotide repeats were investigated using oligomers of the form d[AT(CXG)$_{n=2-4}$AT] and their corresponding heteroduplexes, where X = A, C, G, or T. These oligonucleotides contain -CXGCXG-, -CXGCXGCXG-, and -CXGCXGCXGCXG- units that can form homoduplexes containing one, two, and three GpC binding sites, respectively, with flanking X/X mismatches. The corresponding heteroduplexes contain these same sites with flanking Watson−Crick base pairs. It was found that oligomers with X = G exhibit weak ACTD affinities whereas those with X ≠ G and $n = 3$ exhibit unusually strong ACTD binding affinities with binding constants ranging from 2.3×10^7 to 3.3×10^7 M^{-1} and binding densities of approximately 1 drug molecule/strand (or 2/duplex). These binding affinities are considerably higher than those of their shorter and longer counterparts and are about 2- and 10-fold stronger than the corresponding CAG·CTG and CGG·CCG heteroduplexes, respectively. The CTG-containing oligomer d[AT(CTG)$_3$AT] stands out as unique in having its ACTD dissociation kinetics being dominated by a strikingly slow process with a characteristic time of 205 min at 20 °C, which is 100-fold slower than d[AT(CAG)$_3$AT], nearly 10-fold slower than the corresponding heteroduplex, and considerably slower than d[AT(CTG)$_2$AT] (63 min) and d[AT(CTG)$_4$AT] (16 min). The faster dissociation rate of the $n = 4$ oligomer compared to its $n = 2$ counterpart is in apparent contrast with the observed 10-fold stronger ACTD binding affinity of the former. It was also found that d[AT(CCG)$_3$AT] exhibits the slowest dissociation rate of the CGG/CCG series, being more than an order of magnitude slower than that of its heteroduplex (τ_{slow} of 43 vs 2 min). The finding that a homoduplex d[AT-CXG-CXG-CXG-AT]$_2$ can bind two ACTD molecules tightly is significant since it was thought unlikely for two consecutive GpC sites separated by a single T/T mismatch to do so.

Actinomycin D (ACTD) is an antitumor antibiotic that contains a 2-aminophenoxazin-3-one chromophore and two cyclic pentapeptide lactones. The biological activity of this drug is believed to be the consequence of its ability to bind to duplex DNA so as to inhibit the DNA-dependent RNA polymerase activities. The DNA binding mode and base sequence specificity of ACTD have been well characterized by X-ray crystallography (*1*−*4*), footprinting (*5*−*13*), and hydrodynamic (*14*) and spectroscopic (*15*−*22*) measurements. The ACTD−DNA complex is formed by the phenoxazinone chromophore of ACTD intercalating into the 5′GpC3′ sequence from the minor groove, with the two cyclic pentapeptide rings anchoring on both sides of the minor groove and covering four base pairs of DNA. The formation of four threonine−guanine hydrogen bonds accounts for the preference of this drug for the 5′GpC3′ step. These essential drug−DNA hydrogen bonds are protected by the cyclic pentapeptides, which effectively shield them from solvent exposure (*4*). The size of the four-base-paired binding site suggests that the binding characteristics of ACTD to the GpC site may be affected by the adjacent flanking base pairs. Indeed, studies with self- as well as non-self-complementary -XGCY-containing decameric duplexes (*23, 24*) have revealed that the binding affinity and dissociation kinetics of this drug are greatly affected by the nature of X and Y bases. For example, ACTD binds strongly to and dissociates very slowly from the -TGCA- site, whereas it binds weakly and dissociates very rapidly from the -GGCC- sequence. Similar adjacent base-pair effects had also been observed by others (*25, 26*). In addition to the observed GpC sequence preference, there have been other reports to indicate that this drug can also bind to some non-GpC sites (*27*−*29*). Of some interests are the observations of ACTD binding to some single-stranded DNA (*30, 31*) and of strong ACTD binding and slow dissociation from the -TGGGT- duplex site (*26, 32*).

Our studies on the effects of adjacent base pairs on the ACTD binding to a GpC site have recently been extended to include flanking base-pair mismatches (*33*). The results indicate that ACTD binds strongly to a GpC site with flanking T/T mismatches and moderately to that with C/C mismatches but weakly to those with G/G or A/A mismatches. The slow component of the ACTD association kinetics at the T/T-mismatched GpC site is slower than those of the self-complementary sequences, whereas that of dissociation is only slightly faster than that of -TGCA- sequence but is decidedly slower than those of -AGCT- and -CGCG- sites and is more than an order of magnitude slower than those with C/C, G/G, and A/A mismatches. These results suggest that the minor-groove environment near the T/T-

† Research supported by Army Medical Research Grant DAMD17-94-J-4474 and a subproject of Minority Biomedical Research Support Grant S06GM0892.

* Telephone (615) 963-5325; Fax (615) 963-5434; E-mail chenf@harpo.tnstate.edu.

S0006-2960(97)02110-7 CCC: $15.00
Published on Web 02/18/1998

mismatched pairs provides favorable interactions with the pentapeptide rings of the drug, whereas the others, especially those of bulkier purine/purine mismatches, result in less favorable interactions.

Lian et al. (*34*) have recently investigated the structural details of the complexes of ACTD with d(GAAGCTTC)$_2$, d(GATGCATC)$_2$, d(GATGCTTC)$_2$, and d(GAAGCATC)$_2$ by nuclear Overhauser effect- (NOE) restrained refinement. It was found that the binding of ACTD to the -(AGCT)$_2$- sequence causes the *N*-methyl group of MeVal of the pentapeptide ring to wedge between the bases at the ApG step, resulting in kinks on both sides of the intercalator site. The van der Waals clashes between adenine base and MeVal-MeN found in -AGCT-, however, become diminished in -TGCA-, making it energetically more favorable. These results provide the structural rationalization for our earlier observed stronger ACTD affinity and slower dissociation kinetics of -TGCA- than those of -AGCT- (*23*). Most interestingly, ACTD was also found to form a very stable complex with d(GA-TGCT-TC)$_2$ in which the same methyl group now fits snugly in a cavity at the TpG step created by the T·T mismatched base pair. Such a tight fit apparently provides an increased stability for the binding of ACTD to the -TGCT- sequence. In contrast, ACTD does not stabilize the unstable A·A-mismatched d(GA-AGCA-TC)$_2$ duplex to a significant extent. These results have yielded considerable insights and formed the structural basis for our observation that a GpC flanked by T/T mismatches is a tighter and slower-dissociating binding site than the one flanked by A/A (*33*).

In their NMR studies, Lian et al. (*34*) also investigated the ACTD binding with d(GCTGCTGC)$_2$, an octameric duplex containing three consecutive GpC sites separated by single T/T mismatches. The results indicated that this duplex can only bind a maximum of two ACTD molecules with the bound drugs located at the two outer GpC steps. Similar results of two drug molecules binding at the two outer GpC sites, albeit with weaker affinity, were also observed for d(GCAGCAGC)$_2$. The inability of ACTD to bind more than two drug molecules in these three-site systems led them to conclude that the two nearest neighboring GpC sites cannot bind ACTD simultaneously in a sequence such as TGCT-GCT. It was argued that since the outer edges of the peptide rings (i.e., the SarMeVal dipeptide part) of ACTD reach the minor-groove side of the T·T base pairs, there would be severe van der Waals clashes between pentapeptide rings of the two neighboring bound ACTDs. One of the objectives of this report is to investigate the validity of such an assertion.

Effects of base pair mismatches on DNA structures and their ligand interactions are of considerable interest, as they may have relevance in DNA repair, transcription, replication, and activation of damaged genes. In addition, there has recently been intense interests in the study of DNA trinucleotide repeats. This interest stems from the fact that several genetic disorders have been correlated to the dramatic amplification of such repeats in some genes. For example, CGG repeats have been found to be the culprit for the fragile-X syndrome (see ref *35* and references therein), CAG repeats have been shown to be responsible for Huntington's disease and spinobulbar muscular atrophy (*36, 37*), and CTG repeats have been associated with myotonic dystrophy (*38, 39*). Although the mechanisms for these trinucleotide expansions are not yet clear, there have been speculations on the roles of unusual DNA conformations such as hairpin formation (*40*−*46*). Our interest in the CXG trinucleotide repeats is further heightened by the fact that heteroduplexes of such repeats contain one or more GpC sites and the formation of homoduplexes from these repeats will result in GpC sites with flanking X/X base mismatches. To understand their ACTD binding characteristics, comparative binding and kinetic studies with oligomers of CXG trinucleotide repeats were carried out via spectroscopic techniques using oligomers of the form d[AT(CXG)$_n$AT] and their corresponding heteroduplexes, where n varies from 2 to 4 and X = any of the four DNA bases. The choice of these oligomers was based on the desire to study the effect of base sequence, chain length, and to avoid possible complications that may arise from ACTD stacking at the terminal G·C base pairs. In particular, we set out to test the assertions that ACTD cannot bind more than two drug molecules in a three-site duplex (XGCXGCXGCX)$_2$ and that the two nearest neighboring GpC sites cannot bind ACTD simultaneously in a sequence such as XGCXGCX (*34*). This report describes our findings and discuss their possible biological implications.

MATERIALS AND METHODS

Synthetic oligonucleotides were purchased from Integrated DNA Technologies, Inc., and used without further purification. All experiments were carried out in 10 mM HEPPS [*N*-(2-hydroxyethyl)piperazine-*N*′-propanesulfonic acid) buffer solutions of pH 8 containing 0.1 M NaCl and 1 mM $MgCl_2$. Concentrations of these oligomers (per nucleotide) were determined by measuring the absorbances at 260 nm after melting, with use of extinction coefficients obtained via nearest-neighbor approximation using mono- and dinucleotide values tabulated in Fasman (*47*). Heteroduplexes were formed by annealing complementary oligomers via heating the equal molar mixtures to 95 °C for 5 min and slowly cooled back to ambient temperature. The extinction coefficients used for drug concentration determination are 24 500 M^{-1} cm^{-1} at 440 nm for ACTD and 23 600 M^{-1} cm^{-1} at 528 nm for 7-amino-ACTD. Absorption spectral measurements were made with a Cary 1E spectrophotometric system. Thermal denaturation experiments were carried out with 1-cm semimicro cells by monitoring absorbances at 275 nm. A heating rate of 0.5 °C/min was maintained by the temperature controller accessory. Spectral titrations were carried out at 20 °C by adding aliquots of DNA stock to the drug solution. Differences of absorbance changes at 427 and 480 nm were used to obtain binding isotherms. Linear least-squares fits of the linear portion of the Scatchard plots with the simple equation $r/m = K_a(n - r)$ were made to estimate the binding parameters, where r is the ratio of bound drug to DNA concentrations, n is the saturation binding density, K_a is the apparent association constant, and m is the free drug concentration. Equations used to calculate the relevant quantities are $C_b = C(\epsilon_f - \epsilon)/(\epsilon_f - \epsilon_b)$, $m = C - C_b$, and $r = C_b/C_{DNA}$, where ϵ_f, ϵ_b, and ϵ are the free, bound, and apparent extinction coefficients of the drug, respectively, whereas C, C_b, and C_{DNA} are total drug, bound drug, and DNA concentrations, respectively. The bound extinction coefficient was obtained via a plot of $1/\epsilon$ vs $1/C_{DNA}$ and an extrapolation to $1/C_{DNA} = 0$. Absorbance kinetic measure-

Table 1: Comparison of Equilibrium Binding and Melting Parameters

oligomer	K_a (μM^{-1})	n (per strand)	t_m^o (°C)	t_m (°C)
d[AT-CAGCAG-AT]	1.1		<20 (b)	34[b], 60(b)
d[AT-CTGCTG-AT]	1.1		<20[b]	43
d[AT-(CAG)$_2$-AT]·d[AT-(CTG)$_2$-AT]	1.8	0.7	40	50
d[AT-CGGCGG-AT]	0.8		<20[b]	30[b], 65[b]
d[AT-CCGCCG-AT]	1.1		<20[b]	33[b], 65[b]
d[AT-(CGG)$_2$-AT]·d[AT-(CCG)$_2$-AT]	0.9		48	55
d[AT-CAGCAGCAG-AT]	32.8	1.2	<20[b]	43[b], 65[b]
d[AT-CTGCTGCTG-AT]	22.6	1.2	27	61
d[AT-(CAG)$_3$-AT]·d[AT-(CTG)$_3$-AT]	11.7	1.2	52	68
d[AT-CGGCGGCGG-AT]	1.3		38[b]	43[b], 65[b]
d[AT-CCGCCGCCG-AT]	26.0	1.2	28[b]	35[b], 68[b]
d[AT-(CGG)$_3$-AT]·d[AT-(CCG)$_3$-AT]	0.8		64	68
d[AT-CAGCAGCAGCAG-AT]	6.2	1.4	46[b]	35[b], 70[b]
d[AT-CTGCTGCTGCTG-AT]	11.8	1.3	51	75
d[AT-(CAG)$_4$-AT]·d[AT-(CTG)$_4$-AT]	8.0	1.8	61	77
d[AT-CGGCGGCGGCGG-AT]	1.4		34[b], 62[b]	38[b], 76[b]
d[AT-CCGCCGCCGCCG-AT]	2.2	1.6	43	35[b], 88[b]
d[AT-(CGG)$_4$-AT]·d[AT-(CCG)$_4$-AT]	1.4		72	76

[a] t_m^o and t_m are the estimated melting temperatures of 40 μM DNA (in nucleotides) solutions containing 0.1 M NaCl in the absence and in the presence of 6 μM ACTD, respectively. [b] The melting profile is too broad to yield accurate melting temperature estimates.

ments were made by using a stirrer accessory with 427 and 453 nm monitorings for the ACTD association and SDS-induced dissociation, respectively. Kinetic rate parameters were extracted using the nonlinear least-squares fit program of GraphPad Prism, whereas binding constants for the multisite binding model were made with the Scientist program of Micromath.

Electrophoretic measurements were made on a Pharmacia Phast system using 20% polyacrylamide gels at 200 V with appropriate pre- and postloading run times at different temperatures. PhastGel native buffer strips containing 0.88 M L-alanine and 0.25 M Tris of pH 8.8 were used, and the gels were developed by silver staining.

RESULTS

ACTD Binds Strongly to d[AT(CXG)$_3$AT], X ≠ G, with a Binding Density of Approximately 1 Drug Molecule/Strand (or 2/Duplex). Comparative ACTD binding studies with oligomers of CXG trinucleotide repeats were carried out via absorbance spectral titrations with oligomers of the form d[AT(CXG)$_{n=2-4}$AT] and their corresponding hetero-duplexes. The results are shown as Scatchard plots in Figure 1 and as extracted binding parameters in Table 1. It is immediately apparent from Figure 1 that d[AT(CGG)$_n$AT] (panel E) and their corresponding heteroduplexes (panel D) exhibit weak ACTD binding affinities irrespective of the chain length. In contrast, oligomers with X ≠ G are strongly chain-length dependent, with $n = 3$ exhibiting unusually high ACTD binding affinities that are significantly stronger than that of their $n = 4$ counterparts, and these in turn are considerably higher than those of their corresponding $n = 2$ oligomers (see panels B, C, and F). The extracted binding constants for d[AT(CXG)$_3$AT] with X ≠ G range from 2.3 × 10^7 to 3.3 × 10^7 M^{-1} and the binding densities are roughly 1 drug molecule/strand (or 2/duplex) (see Table 1). Interestingly, these binding affinities are about 2-fold stronger than that of the fully hydrogen-bonded d[AT(CAG)$_3$AT]·d[AT-(CTG)$_3$AT] and more than an order of magnitude higher than that of d[AT(CGG)$_3$AT]·d[AT(CCG)$_3$AT]. It should also be noted that the ACTD binding affinities of heteroduplexes containing two, three, and four CAG·CTG repeats (having one, two, and three AGCA·TGCT sites) are about 2 × 10^6, 12 × 10^6, and 8 × 10^6 M^{-1} with binding densities somewhat higher than 1, 2, and 3 drug molecules/duplex, respectively. These binding strengths are approximately 2-, 15-, and 5-fold stronger than their counterparts with CGG·CCG repeats (see Table 1). It is also worthy of note that despite the presence of an additional GpC site and a strong ACTD affinity (K_a = 1.2 × 10^7 M^{-1}), d[AT(CTG)$_4$AT] exhibits a binding density of slightly greater than 2 drug molecules/duplex, which is not greatly different from that of d[AT(CTG)$_3$AT].

Fitting of Binding Isotherms to Multisite Binding Model. In the absence of a linear Scatchard plot, as evident in some plots of Figure 1, the extraction and interpretation of binding parameters from such a plot are not straightforward (see, e.g., ref *48*). Thus, binding isotherms are replotted as r ([bound drugs]/[duplex]) vs m ([free drug]), which are then fitted with a binding model consisting of four consecutive stoichiometric binding constants for the possibility of binding up to 4 drugs per duplex. The relevant equation for this model is (*48*):

$$r = \frac{K_1 m + 2K_1K_2m^2 + 3K_1K_2K_3m^3 + 4K_1K_2K_3K_4m^4}{1 + K_1 m + K_1K_2m^2 + K_1K_2K_3m^3 + K_1K_2K_3K_4m^4}$$

Reasonably good fits are obtained and the extracted binding parameters are summarized in Table 2. Although a good fit does not guarantee the correctness of the extracted parameters, the plausibility of the results is reflected by the exhibited consistent patterns obtained, which are in agreement with those of Scatchard plots.

For the d[AT(CXG)$_2$AT] oligomers, the fits yielded K_3, $K_4 = 0$ and $K_1 \gg K_2$. Except for the considerably weaker binding of d[AT(CGG)$_2$AT], K_1 values are roughly 2.1 × 10^6 M^{-1}, which is at least an order of magnitude higher than K_2. This is consistent with the presence of one strong binding site -XGCX- in each of these oligomers. Similar binding patterns are found for the heteroduplexes, with the value of K_1 for d[AT(CAG)$_2$AT]·d[AT(CTG)$_2$AT] (K_1 = 3.9 × 10^6 M^{-1}) being somewhat higher than those of its constituent

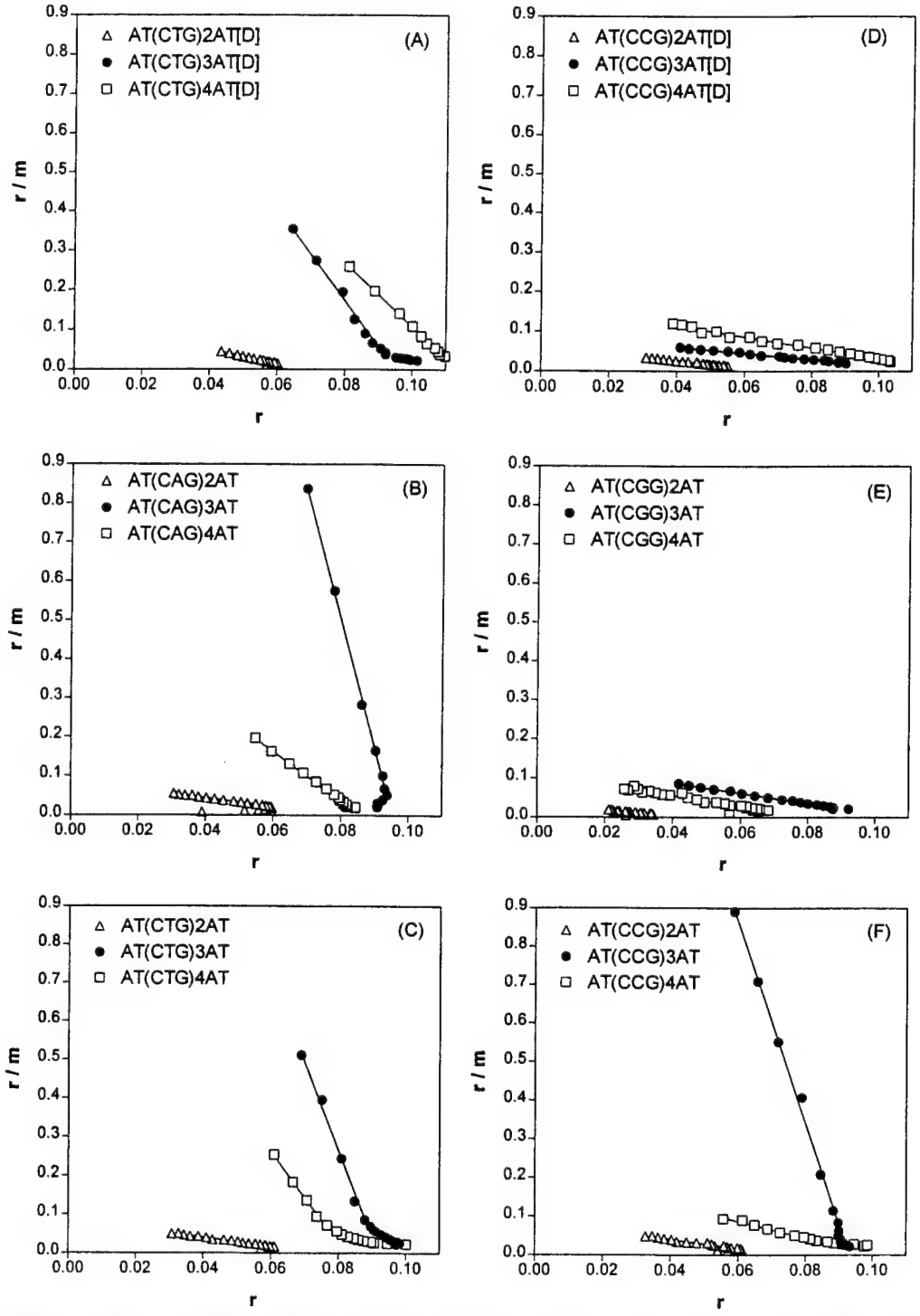

FIGURE 1: Comparison of ACTD equilibrium binding isotherms presented as Scatchard plots for oligomers of CXG trinucleotide repeats at 20 °C. The duplex form is designated as [D] in the figure: d[AT(CAG)$_{n=2-4}$AT]·d[AT(CTG)$_{n=2-4}$AT] (A), d[AT(CAG)$_{n=2-4}$AT] (B), d[AT(CTG)$_{n=2-4}$AT] (C), d[AT(CGG)$_{n=2-4}$AT]·d[AT(CCG)$_{n=2-4}$AT] (D), d[AT(CGG)$_{n=2-4}$AT] (E), and d[AT(CCG)$_{n=2-4}$AT] (F). The absorbance difference between 427 and 480 nm has been used to obtain the binding isotherms. [Bound drug]/[DNA, nucleotide] is designated by r, and m represents the free drug concentration (micromolar).

oligomers, whereas that of d[AT(CGG)$_2$AT]·d[AT(CCG)$_2$AT] ($K_1 = 1.5 \times 10^6$ M^{-1}) being lower than that of its CCG oligomer. The ordering found for the values of K_1 is consistent with that of binding constants estimated from the Scatchard plots.

Except for the CGG-containing oligomers, which exhibit much weaker binding, the extracted values for the binding constants for the d[AT(CXG)$_3$AT] series exhibit the pattern of $K_4 = 0$ and $K_1 \ll K_2 \gg K_3$, with K_3 being less than 8×10^5 M^{-1} for all oligomers. These results are consistent with the presence of two strong binding sites in these oligomers and the notion of positive cooperative binding for the second drug in these oligomers. In fact, the value of K_1K_2 reflects the overall binding affinity of binding 2 drug molecules to a duplex and ranges from 2.9×10^{14} to 7.8×10^{14} M^{-2} for d[AT(CXG)$_3$AT] with X $\neq$ G. The $(K_1K_2)^{1/2}$ values and their ordering are in agreement with those of ACTD affinities obtained via Scatchard plots. Interestingly, despite the

Table 2: Comparison of Extracted Multisite Stoichiometric Binding Constants[a]

oligomer	K_1 (μM^{-1})	K_2 (μM^{-1})	K_3 (μM^{-1})	K_4 (μM^{-1})
d[AT-CAGCAG-AT]	2.1	0.21	0.00	0.00
d[AT-CTGCTG-AT]	2.1	0.16	0.00	0.00
d[AT-$(CAG)_2$-AT]·d[AT-$(CTG)_2$-AT]	3.9	0.10	0.00	0.00
d[AT-CGGCGG-AT]	<0.4	0.00	0.00	0.00
d[AT-CCGCCG-AT]	2.2	0.14	0.00	0.00
d[AT-$(CGG)_2$-AT]·d[AT-$(CCG)_2$-AT]	1.5	0.08	0.00	0.00
d[AT-CAGCAGCAG-AT]	0.18	4310	0.73	0.00
d[AT-CTGCTGCTG-AT]	0.036	8040	0.37	0.00
d[AT-$(CAG)_3$-AT]·d[AT-$(CTG)_3$-AT]	0.19	840	0.33	0.00
d[AT-CGGCGGCGG-AT]	2.8	1.6	0.23	0.00
d[AT-CCGCCGCCG-AT]	0.21	1830	0.57	0.00
d[AT-$(CGG)_3$-AT]·d[AT-$(CCG)_3$-AT]	2.4	0.80	0.29	0.00
d[AT-CAGCAGCAGCAG-AT]	0.34	160	0.63	0.00
d[AT-CTGCTGCTGCTG-AT]	1.0	55	0.65	0.00
d[AT-$(CAG)_4$-AT]·d[AT-$(CTG)_4$-AT]	0.97	7.1	27	0.36
d[AT-CGGCGGCGGCGG-AT]	3.1	1.3	0.16	0.00
d[AT-CCGCCGCCGCCG-AT]	2.4×10^{-4}	1.4×10^{4}	0.70	0.12
d[AT-$(CGG)_4$-AT]·d[AT-$(CCG)_4$-AT]	28	0.54	2.6	0.19

[a] The equation used for the fits is given in the text.

Table 3: Comparison of 1% SDS-Induced ACTD Dissociation Kinetic Parameters at 20 °C

oligomer	k (%),[a] min^{-1}	k_f (%),[b] min^{-1}	k_s (%),[b] min^{-1}
d[AT-CGG-CGG-AT]	0.6 ± 0.1 (23)	5.7 ± 0.8 (39)	0.33 ± 0.03 (61)
d[AT-CCG-CCG-AT]	2.4 ± 0.2 (56)	3.4 ± 0.1 (78)	0.24 ± 0.04 (22)
d[AT$(CGG)_2$AT]·d[AT$(CCG)_2$AT]	1.16 ± 0.05 (71)	2.3 ± 0.1 (57)	0.49 ± 0.03 (43)
d[AT-CAG-CAG-AT]	1.2 ± 0.1 (73)	1.9 ± 0.1 (73)	0.29 ± 0.04 (27)
d[AT-CTG-CTG-AT]	0.0185 ± 0.0005 (79)	0.29 ± 0.02 (17)	0.0159 ± 0.0002 (83)
d[AT$(CAG)_2$AT]·d[AT$(CTG)_2$AT]	0.0435 ± 0.0004 (98)		
d[AT-CGG-CGG-CGG-AT]	3.6 ± 0.2 (39)	5.5 ± 0.2 (75)	0.7 ± 0.1 (25)
d[AT-CCG-CCG-CCG-AT]	0.037 ± 0.02 (43)	2.7 ± 0.2 (28)	0.023 ± 0.001 (72)
d[AT$(CGG)_3$AT]·d[AT$(CCG)_3$AT]	0.94 ± 0.04 (84)	2.1 ± 0.1 (39)	0.54 ± 0.02 (61)
d[AT-CAG-CAG-CAG-AT]	0.52 ± 0.02 (40)	067 ± 0.05 (73)	0.07 ± 0.11 (27)
d[AT-CTG-CTG-CTG-AT]	0.0071 ± 0.0002 (100)	0.189 ± 0.006 (8)	0.00487 ± 0.00006 (92)
d[AT$(CAG)_3$AT]·d[AT$(CTG)_3$AT]	0.0491 ± 0.0009 (90)	0.41 ± 0.02 (13)	0.0418 ± 0.0004 (87)
d[AT-CGG-CGG-CGG-CGG-AT]	0.95 ± 0.09 (31)	2.3 ± 0.2 (60)	0.20 ± 0.03 (40)
d[AT-CCG-CCG-CCG-CCG-AT]	0.435 ± 0.006 (100)		
d[AT$(CGG)_4$AT]·d[AT$(CCG)_4$AT]	0.78 ± 0.02 (73)	1.14 ± 0.07 (71)	0.25 ± 0.04 (29)
d[AT-CAG-CAG-CAG-CAG-AT]	0.59 ± 0.03 (44)	2.9 ± 0.2 (36)	0.32 ± 0.02 (64)
d[AT-CTG-CTG-CTG-CTG-AT]	0.096 ± 0.007 (62)	0.90 ± 0.05 (34)	0.064 ± 0.001 (66)
d[AT$(CAG)_4$AT]·d[AT$(CTG)_4$AT]	0.0553 ± 0.0006 (90)		

[a] The percentage in this column represents the measurable absorbance change compared to that of the total change. [b] Kinetic parameters extracted via two-exponential fits. The percentages in these columns represent the contributions of the fast (f) and slow (s) kinetic components of the measurable absorbance.

presence of four CXG units, d[AT$(CAG)_4$AT] and d[AT-$(CTG)_4$AT] exhibit binding patterns very similar to those with three CXG units (i.e., $K_4 = 0$ and $K_1 \ll K_2 \gg K_3$). Although four binding constants are needed to achieve good fits for d[AT$(CCG)_4$AT], K_3 and K_4 are considerably smaller than K_2, which in turn is much larger than K_1. These results suggest that only two drug molecules are bound strongly to each of these oligomeric duplexes despite the presence of four CXG (or three XGCX) units. In contrast, the values of the binding constants are in the order of $K_1 < K_2 < K_3 \gg K_4$ for d[AT$(CAG)_4$AT]·d[AT$(CTG)_4$AT], a pattern that is consistent with three drug molecules binding at the three strong binding AGCA·TGCT sites in this duplex exhibiting an overall association binding constant of approximately $K_1K_2K_3 = 1.9 \times 10^{20}\ M^{-3}$.

ACTD Dissociates Very Slowly from d[AT(CTG)$_3$AT] with a Rate Nearly an Order of Magnitude Slower Than That of the Corresponding Heteroduplex. SDS-induced dissociation kinetic profiles of ACTD from d[AT$(CXG)_n$AT] and their corresponding heteroduplexes are shown in Figure 2 and the extracted kinetic parameters via one- and two-exponential fits are presented in Table 3. It is immediately apparent from Figure 2 that ACTD dissociates considerably faster from the CGG/CCG series (right panels) than from their CAG/CTG counterparts (left panels; note the 50-fold difference in the time scale). For the latter series, the ACTD dissociation kinetic profiles of d[AT$(CAG)_n$AT] decay significantly faster than those of d[AT$(CTG)_n$AT] and the corresponding heteroduplexes d[AT$(CAG)_n$AT]·d[AT$(CTG)_n$AT]. Most interestingly, the ACTD dissociation kinetics of d[AT-$(CTG)_3$AT], and to a lesser extent those of d[AT$(CTG)_2$AT], are decidedly slower than those of their corresponding heteroduplexes. In fact, the slow dissociation rate of ACTD from d[AT$(CTG)_3$AT] is found to be 0.00487 min^{-1} (or a characteristic time of 205 min), which is 2 orders of magnitude slower than that of the corresponding one with CAG repeats (0.52 min^{-1} or 1.9 min) and nearly an order of magnitude slower than that of the corresponding heteroduplex (0.0418 min^{-1} or 23.9 min). Although the dissociation rates do not vary greatly with chain length for the heteroduplexes,

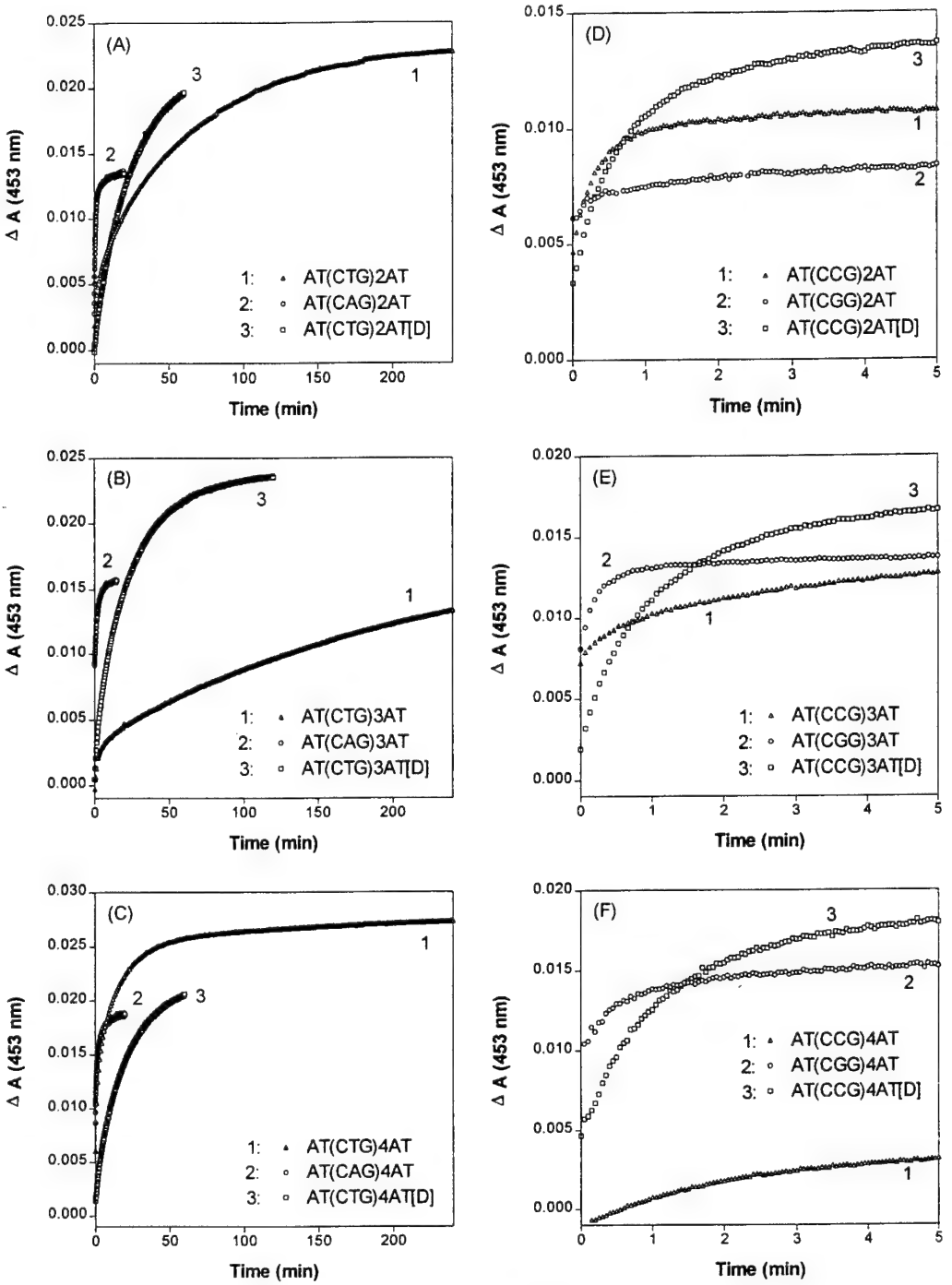

FIGURE 2: Comparison of representative 1% SDS-induced ACTD dissociation kinetic profiles via absorbance monitoring at 20 °C for various oligomers of CXG trinucleotide repeats: d[AT(CAG)$_2$AT]·d[AT(CTG)$_2$AT] and the constituent oligomers (A), d[AT(CAG)$_3$AT]·d[AT(CTG)$_3$AT] and the constituent oligomers (B), d[AT(CAG)$_4$AT]·d[AT(CTG)$_4$AT] and the constituent oligomers (C), d[AT(CGG)$_2$AT]·d[AT(CCG)$_2$AT] and the constituent oligomers (D), d[AT(CGG)$_3$AT]·d[AT(CCG)$_3$AT] and the constituent oligomers (E), d[AT(CGG)$_4$AT]·d[AT(CCG)$_4$AT] and the constituent oligomers (F). The drug dissociation was initiated by adding an appropriate amount of 20% SDS to a solution mixture containing 4 μM ACTD and 80 μM DNA in nucleotide.

they do so strongly for the CTG-containing oligomers. For example, whereas the slowest dissociation component for d[AT(CTG)$_3$AT] exhibits a characteristic time of 205 min, those for d[AT(CTG)$_2$AT] and d[AT(CTG)$_4$AT] are 63 and 15.6 min, respectively. It should be noted that these last two rates cited are in apparent contrast to a 10-fold higher binding affinity ($K_a = 1.2 \times 10^7$ vs 1.1×10^6 M^{-1}) of the four repeats than that of two repeats. Interestingly, d[AT(CCG)$_3$AT] also exhibits the slowest dissociation kinetics in the CGG/CCG series and its slow component is more than an order of magnitude slower than the corresponding heteroduplex (43 vs 1.9 min).

Association kinetic profiles of ACTD binding to d[AT-(CXG)$_n$AT] and their corresponding heteroduplexes have also been measured. The results (not shown) indicate that whereas the heteroduplexes exhibit the largest non-stopped-flow measurable components (ranging from 14% to 43% of the total absorbance changes) and their kinetic profiles can be approximated by single-exponential decays with characteristic lifetimes of 0.3−0.6 min, the constituent oligomers

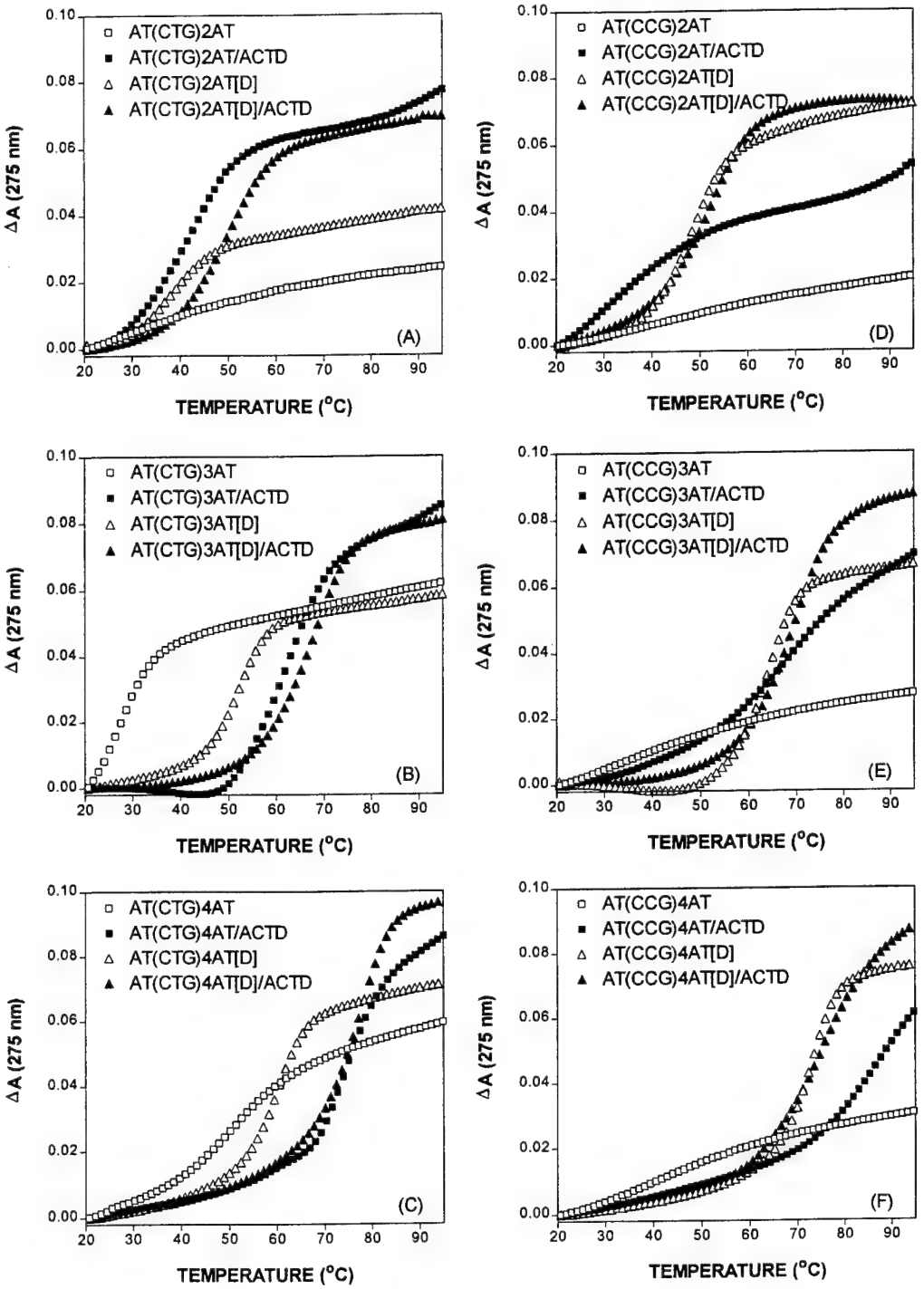

FIGURE 3: Representative thermal melting profiles of various oligomers (40 μM in nucleotide) of CXG trinucleotide repeats in the absence and in the presence of ACTD (6 μM) at pH 8 and 0.1 M NaCl: d[AT(CTG)$_2$AT] and its corresponding heteroduplex (A), d[AT(CTG)$_3$AT] and its corresponding heteroduplex (B), d[AT(CTG)$_4$AT] and its corresponding heteroduplex (C), d[AT(CCG)$_2$AT] and its corresponding heteroduplex (D), d[AT(CCG)$_3$AT] and its corresponding heteroduplex (E), and d[AT(CCG)$_4$AT] and its corresponding heteroduplex(F).

exhibit smaller measurable absorbance changes that require two-exponential fits. Oligomers d[AT(CXG)$_3$AT], X = T and C, are unusual in exhibiting significant contributions from slow association components having characteristic times of about 8 and 5 min, respectively, which are considerably slower than those of their respective longer and shorter counterparts.

Thermal Stabilities of Oligomers with CXG Repeats Are Greatly Enhanced by ACTD Binding. Melting profiles of d[AT(CTG)$_n$AT] (panels A−C) and d[AT(CCG)$_n$AT] (panels D−F) in the absence and in the presence of ACTD are compared with their respective heteroduplexes in Figure 3 and the estimated melting temperatures are included in Table 1. In the absence of ACTD, 40 μM (in nucleotide) d[AT-(CAG)$_2$AT]·d[AT(CTG)$_2$AT] at pH 8 with 0.1 M NaCl melts near 40 °C, whereas the melting temperature increases to around 50 °C in the presence of 6 μM ACTD (panel A). In contrast, d[AT(CXG)$_2$AT] alone does not exhibit cooperative melting above 20 °C, suggesting melting temperatures of <20 °C for the homodimeric duplexes. However, a characteristic cooperative melting profile is apparent in the presence of ACTD for d[AT(CTG)$_2$AT], exhibiting a melting

temperature of around 43 °C (panel A). For decamers of X ≠ T, the presence of ACTD results in very diffuse biphasic melting profiles with barely discernible melting temperatures. The dramatic melting temperature increases upon ACTD binding to oligomers with CTG repeats can more clearly be seen with the oligomer of three CTG repeats (see panel B). A cooperative melting near 27 °C is seen for d[AT-$(CTG)_3$AT] but is shifted to 61 °C in the presence of ACTD, a dramatic 34 °C melting temperature increase. In contrast, the melting temperature of d[$AT(CAG)_3$AT]·d[$AT(CTG)_3$AT] only changes from 53 to 68 °C upon ACTD binding. For n = 4, both d[$AT(CAG)_4$AT]·d[$AT(CTG)_4$AT] and d[AT-$(CTG)_3$AT] exhibit melting temperatures of approximately 76 °C in the presence of ACTD, whereas 61 and 51 °C, respectively, are noted in the drug's absence (panel C). Significant ACTD-induced melting temperature increases were also observed for d[$AT(CXG)_n$AT], X ≠ T, but the melting profiles are much broader and biphasic in nature. The much weaker ACTD binding affinities of d[AT-$(CGG)_n$AT]·d[$AT(CCG)_n$AT] are also evidenced by the considerably smaller melting temperature increases upon ACTD binding (see panels D−F).

Our ability to detect a melting temperature above 20 °C for d[$AT(CTG)_3$AT] but not for d[$AT(CAG)_3$AT] is in agreement with the finding of Smith et al. (*43*) indicating that the order in melting temperatures is $[d(CAG)_3]_2$ < $[d(CTG)_3]_2$ ≪ $d(CAG)_3$·$d(CTG)_3$, suggesting that the presence of A·A mismatches in such sequence context has a more profound destabilizing effect than that of T·T mismatches.

DISCUSSION

In summary, ACTD binding studies with oligomers of the form d[$AT(CXG)_{n=2-4}$AT] and their corresponding heteroduplexes, where X = any of the four DNA bases, indicate that the heteroduplexes containing CAG·CTG repeats exhibit higher ACTD binding affinities and more than an order of magnitude slower dissociation kinetics than the CGG·CCG counterparts. Of the constituent oligomers, d[$AT(CGG)_n$AT] oligomers exhibit the weakest ACTD binding affinities and are relatively insensitive to chain length, whereas oligomers with X ≠ G are strongly chain-length-dependent and those with n = 3 exhibit unusually high ACTD binding affinities. The extracted binding constants for d[$AT(CXG)_3$AT] with X = A, C, and T range from 2.3×10^7 to 3.3×10^7 M^{-1} and the binding densities are approximately 1 drug molecule/strand (or 2/duplex). These binding affinities are considerably higher than those of their corresponding longer and shorter counterparts, about 2-fold stronger than that of the fully hydrogen-bonded d[$AT(CAG)_3$AT]·d[$AT(CTG)_3$AT], and more than an order of magnitude higher than that of d[$AT(CGG)_3$AT]·d[$AT(CCG)_3$AT]. Despite the comparable ACTD binding affinities for these X ≠ G oligomers of three repeats, the CTG-containing oligomer d[$AT(CTG)_3$AT] stands out as unique in having its ACTD association kinetic profile exhibiting a significant contribution from a slow component (approximately 8-min lifetime) and its ACTD dissociation kinetics being dominated by a strikingly slow process with a characteristic time of 205 min at 20 °C, which is 100-fold slower than that of d[$AT(CAG)_3$AT] and nearly 10-fold slower than that of the corresponding heteroduplex. In contrast to the heteroduplexes, the dissociation rates of d[$AT(CTG)_n$AT] are found to be strongly chain-length-dependent, as evidenced by the two remaining oligomers in the CTG-repeating series, d[$AT(CTG)_2$AT] and d[AT-$(CTG)_4$AT], exhibiting slow dissociation times of 63 and 15.6 min, respectively. The faster dissociation rate of the n = 4 oligomer appears to be at variance with the observed 10-fold stronger ACTD binding affinity of this oligomer when compared to its n = 2 counterpart. It was also found that d[$AT(CCG)_3$AT] exhibits the slowest dissociation kinetics of the CGG/CCG series and its slow component is more than an order of magnitude slower than that of its heteroduplex (τ_s of 43 vs 1.9 min).

Oligomers of the form d[$AT(CXG)_{n=2-4}$AT] contain -CXGCXG-, -CXGCXGCXG-, and -CXGCXGCXGCXG- units, respectively, which can form homoduplexes consisting of one, two, and three GpC binding sites with flanking X/X mismatches. The finding of unusually strong ACTD binding affinities of d[$AT(CXG)_3$AT], X ≠ G, with two drug molecules bound to a duplex is of particular significance since its homoduplex d[AT-CXG-CXG-CXG-AT]$_2$ is seen to contain two consecutive GpC sites that are separated by an X/X mismatch. Thus, our results suggest that two ACTD molecules can bind tightly to two consecutive GpC sites that are separated by an X/X mismatch, in direct conflict with the assertion of Lian et al. (*34*). It is likely that a duplex with an X/X mismatch is flexible enough to alter the conformation of DNA to accommodate two clashing pentapeptide rings and turn them into van der Waals attractions for snug fit. An outstanding example of two drug molecules binding to two consecutive GpC sites is the formation of a unique 2:1 complex of ACTD to d[ATGCGCAT]$_2$, as studied by NMR (*19, 20*). It was found that two 1:1 unsymmetric complexes form in unequal proportions at the ratio of 1 ACTD:duplex. At the ratio of 2 ACTD:duplex, however, both COSY and NOESY spectra confirm the formation of a unique 2:1 species with C_2 symmetry. The oligomer remains in a right-handed duplex but undergoes extreme conformational changes both at and adjacent to the binding site. This conformational change widens the minor groove and help alleviate the steric crowding of the ACTD peptides. It is, thus, reasonable to expect that two consecutive GpC sites separated by an X/X mismatch can do likewise with more facility because of the additional spacing introduced by the mismatched base pair.

Formation of a homoduplex by four CXG repeats will result in a duplex, -(CXGCXGCXGCXG)$_2$- consisting of one central and two off-center GpC sites separated by single X/X mismatches. Consequently, results from our d[$AT(CXG)_4$AT] series will in fact be akin to the underlined three-site system investigated by Lian et al. (*34*). Our binding titrations indicate that these oligomers exhibit somewhat smaller ACTD binding affinities than the corresponding oligomers of three repeats but the binding densities remain essentially 1 drug molecule/strand (2/duplex), in agreement with their finding of two drug molecules bound at the two outer sites. The rationale for two instead of three ACTD molecules binding to the three-site systems, $d(GCXGCXGC)_2$, may be that when one of the off-center GpC sites is occupied, a second molecule will prefer the other off-center site instead of the central site to avoid steric hindrance. Once both off-center sites are occupied, the DNA conformational rigidity will be such that an additional binding at the central site will be much more difficult.

It is, however, somewhat puzzling that a nearly 2-fold reduction in the binding affinity and an approximately 10-fold faster ACTD dissociation rate are accompanied by an increase of the CTG repeats from three to four. Similarly, a significant binding reduction is coupled with greater than 10-fold faster dissociation kinetics when the number of CCG repeats is increased from three to four. These results may possibly be rationalized in terms of the absence of close contacts of the intermolecular peptide rings when the two ACTD molecules are bound to the outer GpC sites to result in weaker binding and more facile dissociation processes. The predominance of hairpin conformation in solutions of d[AT(CXG)$_4$AT], especially under the low concentrations used in our optical studies, may have partially contributed to the observed weaker ACTD binding affinities and faster dissociation rates than their $n = 3$ counterparts. A hairpin formation of the $n = 4$ oligomer will result in an X/X-mismatched GpC site on the duplex stem with the central GpC as part of the single-stranded loop, thus, accounting for the observed 1 drug/strand binding densities. Furthermore, the proximity of the duplex binding site to the loop region will likely result in a poorer pentapeptide rings−minor-groove interactions with the consequent more rapid dissociation of ACTD. Our observations of very broad melting profiles in the absence of ACTD and the seemingly biphasic melting curves in the presence of ACTD appear to suggest some contributions from the hairpins. ACTD binding to the hairpin form will be less important for the $n = 3$ oligomers, since the hairpin formation of such oligomers will result in the absence of GpC sites in the duplex stem. Attempts to delineate the relative ACTD binding contributions to dimeric duplex vs hairpin forms were made with electrophoretic experiments using the heteroduplexes as benchmarks (results not shown). The dominance of hairpin species for the $n = 4$ oligomers in the absence of ACTD is readily apparent in the electrophoretic patterns. However, in the presence of the drug, the mobility patterns are characterized by the prominent presence of the ACTD−intermolecular duplex bands and a conspicuous absence of the ACTD−hairpin bands. These results are consistent with the stronger ACTD affinity and/or slower dissociation for the dimeric duplex than for the monomeric hairpin.

Our finding that some of the constituent oligomers, especially those with X = pyrimidine, exhibit stronger ACTD affinities and slower dissociation kinetics than their corresponding heteroduplexes are of significance. One would have anticipated that the dimeric duplex destabilized by the presence of mismatched bases should have resulted in a weaker drug complex that would dissociate very rapidly in the presence of SDS. The anticipated conformational rearrangements and close fits likely account for the observed slow association and dissociation behaviors for d[AT-CXG-CXG-CXG-AT]$_2$. The fact that the X = T and C oligomers provide much slower ACTD dissociation kinetics in their respective series suggests that T/T and C/C mismatches can provide more favorable minor-groove environments for snug fits, likely the consequence of smaller sizes of the pyrimidines. The weaker ACTD binding and faster dissociation kinetics of the corresponding fully hydrogen-bonded heteroduplexes may be the consequence of their diminished conformational flexibility for snugly fitting these pentapeptide rings into the minor groove. The very weak ACTD affinities exhibited by oligomers and their heteroduplexes of CGG repeats most likely are the consequence of the protruding 2-amino groups at the minor groove of the G/G mismatches to result in poor minor-groove interactions with the pentapeptide rings.

The finding that the ACTD binding affinities, the rates of ACTD dissociation, and the melting temperature increases of d[AT(CAG)$_{n=2-4}$AT]·d[AT(CTG)$_{n=2-4}$AT] are respectively higher, slower, and larger than those of d[AT-(CGG)$_{n=2-4}$AT]·d[AT(CCG)$_{n=2-4}$AT] is to be expected. These heteroduplexes consist of one, two, or three units, respectively, of tetranucleotide binding site AGCA·TGCT or GGCG·CGCC. Our earlier studies on the binding specificity of ACTD to duplex tetranucleotide sequences of the form -XGCY- have revealed that the binding affinity and dissociation kinetics of this drug are greatly affected by the nature of X and Y bases (*23, 24*). In particular, when X = G and/or Y = C, the oligomers exhibit significantly weaker ACTD binding affinities, faster SDS-induced ACTD dissociation rates, and smaller melting temperature increases upon drug binding than the other sequences.

A closer examination of the binding characteristics of oligomers containing a single GpC site with flanking X/X mismatches is of interest. Except for a somewhat smaller value for the X = G oligomer, ACTD binding affinities of d[AT(CXG)$_2$AT] are nearly identical ($K_a = 1.1 \times 10^6$ M^{-1}) which are slightly larger than that of d[AT(CGG)$_2$AT]·d[AT(CCG)$_2$AT] and somewhat smaller than that of d[AT-(CAG)$_2$AT]·d[AT(CTG)$_2$AT] ($K_a = 1.8 \times 10^6$ M^{-1}). Depite their comparable binding affinities, the decamer with X = T exhibits the slowest ACTD association kinetics, more than an order of magnitude slower dissociation kinetics than the other decamers studied, and severalfold slower ACTD dissociation rate than its heteroduplex. Except for the binding order, these results are in general agreement with our earlier studies (*33*) using dodecamers of the form d[ATTA-XGCX-TAAT] and their self-complementary counterparts. The apparent absence of binding preference in the decameric system is at variance with our earlier dodecameric studies, which indicated a binding order of T/T > C/C > G/G, A/A for the mismatched duplexes. These parities may likely be the consequence of differences in chain lengths and flanking sequences. In this connection, it should also be pointed out that despite the earlier finding of weaker ACTD affinity for a GC site with flanking A/A mismatches (*33, 34*), d[AT(CAG)$_{3-4}$AT] studied here exhibit strong ACTD binding affinities (albeit with rapid dissociation rates) that are comparable to their CTG counterparts. The presence of multiple X/X base-pair mismatches for more facile conformational alterations may have played the key role.

Finally, our finding that the ACTD binding affinities of some constituent oligomers of trinucleotide repeats are stronger than those of their heteroduplexes is consistent with the observation of Lian et al. (*34*) that the annealing propensities of two long DNA oligos, G(CAG)$_{10}$C and G(CTG)$_{10}$, are significantly reduced in the presence of ACTD. Such a phenomenon may have biological relevance since the DNA triplet expansion associated with genetic diseases usually involves a large number of such repeats. It is conceivable that a (CXG)$_n$·(CYG)$_n$ sequence may be in dynamic equilibria with cruciform structures consisting of extended arms composed of (CXG)$_n$ and (CYG)$_n$ homo-

duplexes. The presence of ACTD may, thus, trap these cruciform structures of the $(CXG)_n/(CYG)_n$ sequence by preferentially binding to their stems. Such an interference of equilibrium between a duplex and cruciform structures by a drug or protein can possibly result in serious consequences on the subsequent functions associated with the normal $(CXG)_n{\cdot}(CYG)_n$ heteroduplexes (*34*).

ACKNOWLEDGMENT

I thank C. Edwards for some technical assistance.

REFERENCES

1. Sobell, H. M., and Jain, S. C. (1972) *J. Mol. Biol. 68,* 21−34.
2. Takusagawa, F., Dabrow, M., Neidle, S., and Berman, H. M. (1982) *Nature 296,* 466−469.
3. Kamitori, S., and Takusagawa, F. (1992) *J. Mol. Biol. 225,* 445−456.
4. Kamitori, S., and Takusagawa, F. (1994) *J. Am. Chem. Soc. 116,* 4154−4165.
5. Lane, M. J., Dabrowiak, J. C., and Vouurrnakis, J. N. (1983) *Proc. Natl. Acad. Sci. U.S.A. 80,* 3260−3264.
6. Scamrov, A. V., and Beabealashvilli, R. Sh. (1983) *FEBS Lett. 164,* 97−101.
7. Van Dyke, M. W., and Dervan, P. B. (1983) *Nucleic Acids Res. 11,* 5555−5567.
8. Van Dyke, M. W., Hertzberg, R. P., and Dervan, P. B. (1983) *Proc. Natl. Acad. Sci. U.S.A. 79,* 5470−5474.
9. Fox, K. R., and Waring, M. J. (1984) *Nucleic Acids Res. 12,* 9271−9285.
10. White, R. J., and Phillips, D. R. (1989) *Biochemistry 28,* 6259−6269.
11. Rehfuss, R., Goodisman, J., and Dabrowiak, J. C. (1990) *Biochemistry 29,* 777−781.
12. Goodisman, J., Rehfuss, R., Ward, B., and Dabrowiak, J. C. (1992) *Biochemistry 31,* 1046−1058.
13. Goodisman, J., and Dabrowiak, J. C. (1992) *Biochemistry 31,* 1058−1064.
14. Muller, W., and Crothers, D. M. (1968) *J. Mol. Biol. 35,* 251−290.
15. Krugh, T. R. (1972) *Proc. Natl. Acad. Sci. U.S.A. 69,* 1911−1914.
16. Patel, D. J. (1974) *Biochemistry 13,* 2396−2402.
17. Krugh, T. R., Mooberry, E. S., and Chiao, Y.-C. C. (1977) *Biochemistry 16,* 740−755.
18. Brown, S. C., Mullis, K., Levenson, C., and Shafer, R. H. (1984) *Biochemistry 23,* 403−408.
19. Scott, E. V., Jones, R. L., Banville, D. L., Zon, G., Marzilli, L. G., and Wilson, W. D. (1988) *Biochemistry 27,* 915−923.
20. Scott, E. V., Zon, G., Marzilli, L. G., and Wilson, W. D. (1988) *Biochemistry 27,* 7940−7951.
21. Zhou, N., James, T. L., and Shafer, R. H. (1989) *Biochemistry 28,* 5231−5239.
22. Brown, D. R., Kurz, M., Kearns, D. R., and Hsu, V. L. (1994) *Biochemistry 33,* 651−664.
23. Chen, F.-M. (1988) *Biochemistry 27,* 6393−6397.
24. Chen, F.-M. (1992) *Biochemistry 31,* 6223−6228.
25. Aivasashvilli, V. A, and Beabealashvilli, R. S. (1983) *FEBS Lett. 160,* 124−128.
26. Rill, R. L., Marsch, G. A., and Graves, D. E. (1989) *J. Biomol. Struct. Dyn. 7,* 591−605.
27. Snyder, J. G., Hartman, N. G., D'Estantoit, B. L., Kennard, O., Remeta, D. P., and Breslauer, K. J. (1989) *Proc. Natl. Acad. Sci. U.S.A. 86,* 3968−3972.
28. Waterloh, K., and Fox, K. R. (1992) *Biochim. Biophys. Acta 1131,* 300−306.
29. Bailey, S. A., Graves, D. E., Rill, R., and Marsch, G. (1993) *Biochemistry 32,* 5881−5887.
30. Wadkins, R. M., and Jovin, T. M. (1991) *Biochemistry 30,* 9469−9478.
31. Wadkins, R. M., Jares-Erijman, E. A., Klement, R., Rudiger, A., and Jovin, T. M. (1996) *J. Mol. Biol. 262,* 53−68.
32. Bailey, S. A., Graves, D. E., and Rill, R. (1994) *Biochemistry 33,* 11493−11500.
33. Liu, C., and Chen, F.-M. (1996) *Biochemistry 35,* 16346−16353.
34. Lian, C., Robinson, H., and Wang, A. H.-J. (1996) *J. Am. Chem. Soc. 118,* 8791−8801.
35. Sutherland, R. G., and Richards, R. I. (1994) *Am. Sci. 82,* 157−163.
36. The Huntington's Disease Collaborative Research Group (1993) *Cell 72,* 971−983.
37. LaSpada, A. R., Wilson, E. M., Lubahn, D. B., Harding, A. E., and Fischbeck, K. H. (1991) *Nature 352,* 77−99.
38. Brook, J. D., McCurrash, A. E., Harley, H. G., Buckler, A. J., Church, D., Aburatani, H., Hunter, K., Stanton, V. P., Thirion, J.-P, Hudson, T., Sohn, R., Zemelman, B., Snell, R. G., Rundle, S. A., Crow, S., Davies, J., Shelbourne, P., Buxton, J., Jones, C., Juvonen, V., Johnson, K., Harper, P. S., Shaw, D. J., and Housman, D. E. (1992) *Cell 68,* 799−808.
39. Mahadevan, M., Tsilfidis, C., Sabourin, L., Shutler, G., Amemiya, C., Jansen, G., Neville, C., Narang, M., Barcelo, J., O'Hoy, K., Leblond, S., Earle-Macdonald, J., de Jong, P. J., Wieringa, B., and Korneluk, R. G. (1992) *Science 255,* 1253−1255.
40. Chen, X., Mariappan, S. V. S., Catasti, P., Ratliff, R., Moyzis, R. K., Laayoun, A., Smith, S. S., Bradbury, E. M., and Gupta, G. (1995) *Proc. Natl. Acad. Sci. U.S.A. 92,* 5199−5203.
41. Mita, M., Yu, A., Dill, J., Kamp, T. J., Chambers, E. J., and Haworth, I. S. (1995) *Nucleic Acids Res. 23,* 1050−1059.
42. Zhu, L. M., Chou, S. H., Xu, J. D., and Reid, B. R. (1995) *Nat. Struct. Biol. 2,* 1012−1017.
43. Smith, G. K., Jie, J., Fox, G. E., and Gao, X. L. (1995) *Nucleic Acids Res. 23,* 4303−4311.
44. Mariappan, S. V. S., Garcia, A. E., and Gupta, G. (1996) *Nucleic Acids Res. 24,* 775−783.
45. Mariappan, S. V. S., Catasti, P., Chen, X., Ratliff, R., Moyzis, R. K., Bradbury, E. M., and Gupta, G. (1996) *Nucleic Acids Res. 24,* 784−792.
46. Gacy, A. M., Goellner, G., Juranic, N., Macura, S., and McMurray, C. T. (1995) *Cell 81,* 533−540.
47. Fasman, G. D., Ed. (1975) *CRC Handbook of Biochemistry and Molecular Biology,* 3rd ed., Vol. I, p 589, Chemical Rubber Company Publishing, Cleveland, OH.
48. Klotz, I. M. (1997) *Ligand−Receptor Energetics,* Wiley, New York.

BI972110X

18

Methods for the Studies of Drug Dissociation from DNA

Fu-Ming Chen

1. Introduction

In addition to binding affinity, the on and off rates of drug–DNA interactions are important in determining the biological activities of a drug. For example, the rate of dissociation of a drug from DNA has been shown to be related to its pharmacological activities *(1)*. Various techniques have been employed to study the dissociation kinetics of drugs from DNA. These include detergent sequestration technique pioneered by Muller and Crothers *(1)*, a modification of the footprinting technique for examining the dissociation of ligands from individual binding sites *(2)*, relaxation methods such as T-jump for measuring fast kinetics *(3)*, and a procedure that can yield drug–DNA dissociation kinetics under conditions of active transcription of the DNA *(4)*. The simplest and most widely used method is detergent-induced dissociation rate measurement incorporating the detergent sodium dodecyl sulfate (SDS). This chapter will thus focus on the SDS-sequestration technique and include only conventional spectrophotometric and stopped-flow methods. An example of an actinomycin D dissociation measurement from the author's laboratory will be used to illustrate the methodology.

2. Materials

1. Appropriate buffer for the system of interest. For example, a buffer of pH ≥8.0 that contains (1–10 m*M*) Mg^{2+} will be required for the studies of chromomycin A_3 and mithramycin.
2. A 20% SDS solution can be prepared by dissolving 20 g SDS in 80 mL of buffer solution (*see* **Note 7**).

From: *Methods in Molecular Biology, Vol. 90: Drug–DNA Interaction Protocols*
Edited by: K. R. Fox Humana Press Inc., Totowa, NJ

3. Method

3.1. Non–Stopped-Flow Technique

1. A drug–DNA solution mixture is either obtained as an end product of the association kinetic measurement or prepared by mixing together appropriate amounts of drug and DNA solutions.
2. The solution mixture is usually allowed to reach equilibrium. The waiting time depends on the rate of association. A time period of $\geq 5 \times \tau_a$ (the characteristic association time) should be sufficient (*see* **Note 4**).
3. Record the initial value A_i, where A represents any measurable physical properties such as absorbance, fluorescence, or ellipticity at the wavelength of interest (*see* **Note 3**).
4. The dissociation of the drug is initiated by the addition of an appropriate volume of 20% SDS to the DNA–drug mixture to result in a 1% final SDS concentration (*see* **Note 5**).
5. The solution is then thoroughly mixed by either rigorous manual shaking or mechanical stirring (*see* **Notes 1** and **2**).
6. Data collection should commence as soon as it is feasible, via computer or chart recorder.
7. The run is terminated when reasonable A_∞ can be estimated, usually with $t > 2$–$3\ \tau_d$ (characteristic dissociation time).

3.2. Stopped-Flow Technique

1. Prepare a 2% SDS solution via a 10-fold dilution from the 20% stock.
2. Fill the two reservoir syringes with the drug–DNA and 2% SDS solutions, respectively.
3. Carefully fill the driving syringes (*see* **Note 8**) and wait until the temperature reaches equilibrium (*see* **Note 6**).
4. Actuate the plungers via pressured gas and commence the data collection.
5. The run is terminated when the decay curve shows sign of leveling.

3.3. Data Analysis

3.3.1. Manual Graphical Method (see **Fig. 1**)

1. A_∞ at the monitoring wavelength is first estimated or obtained experimentally by waiting until there is no longer any change in the value of A.
2. Values of $\Delta A \equiv |A_t - A_\infty|$ are then calculated and plotted vs time on a semilogrithmic graph paper, where A_t is the value of A at time t.
3. A reasonable value of A_∞ will yield a straight line plot for a single-exponential rate process and the rate constant is then obtained by $-2.303 \times$ (slope). Extrapolation to $t = 0$ will yield ΔA_o, the total measurable change of A as a result of this process.
4. The percentage contribution of this process can then be obtained by the following formula: $100 \times \Delta A_o / |A_\infty - A_i$(dilution corrected)$|$
5. For a multiexponential process, a curved plot with a straight line portion at the longtime data region will result. The slowest rate constant $k(1)$ and the measur-

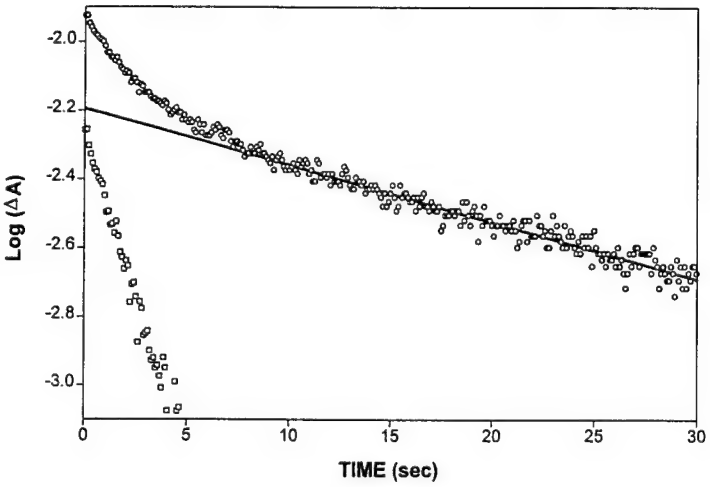

Fig. 1. An example illustrating how kinetic parameters can be extracted via graphical method for a multiexponential kinetic profile.

1. Estimate a reasonable A_∞.
2. Calculate $\Delta A \equiv |A - A_\infty|$.
3. Plot ΔA vs t on a semilogrithmic graph paper. (**Note:** The vertical scale is a linear scale of log ΔA and not the logrithmic scale of a semilog graph paper.)
4. Repeat **steps 1–3** until a linear plot is obtained for the long-time region (s).
5. A best straight line is drawn through these long-time data points and extended to $t = 0$ (connected line) to obtain k and ΔA_0 for this process.
6. ΔA value corresponding to each experimental time point is read directly from the straight line and subtracted from the experimental value to obtain new ΔA.
7. These new ΔA values are replotted on the semilog paper (open squares).
8. Repeat **steps 5–7** with this new data set.
9. The process is continued until the new plot is a straight line without the presence of a curvature at the short-time region.

able total change associated with this process ΔA_{01} are then obtained from the slope of the straight line and its intercept at zero time, respectively. The values of the straight line at each time-point are read directly from the graph and then subtracted point-by-point from the original ΔA. These new values are then replotted to obtain $k(2)$ and ΔA_{02} and the process continues until the last straight line plot is obtained.

3.3.2. Nonlinear Least-Squares Curve Fit (see ***Figs. 2*** *and* ***3***)

1. The kinetic data can be fitted directly with any commercially available nonlinear least-squares program. The equations to be used are $\Delta A = \Delta A_0 e^{-kt} + B$ for a single-exponential and $\Delta A = \Delta A_{01} e^{-k(1)t} + \Delta A_{02} e^{-k(2)t} + B$ for a double-exponential process, and so forth.

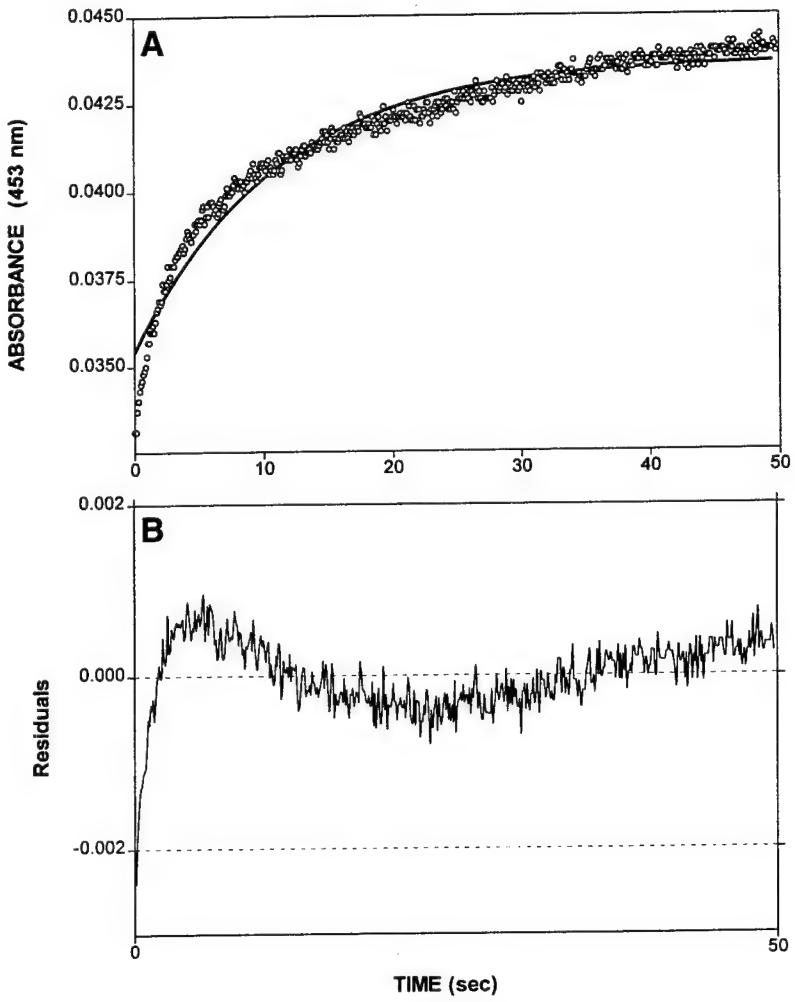

Fig. 2. **(A)** Comparison of experimental data and a single-exponential fit. **(B)** The corresponding residual plot. It is apparent that the kinetics cannot be adequately described by a single exponential process.

2. The kinetic parameters k's and ΔA_0's are obtained directly from the fit.
3. The goodness of the fit can be appraised by visual comparison of the experimental data with the fitted curve, the value of sum of square deviation, or the residual plot.
4. Since a higher order exponential model will in general result in a better fit because of the larger number of parameters, use of a higher order model may not be warranted unless significant improvement, such as several-fold reduction in the sum of square deviation, is obtained.

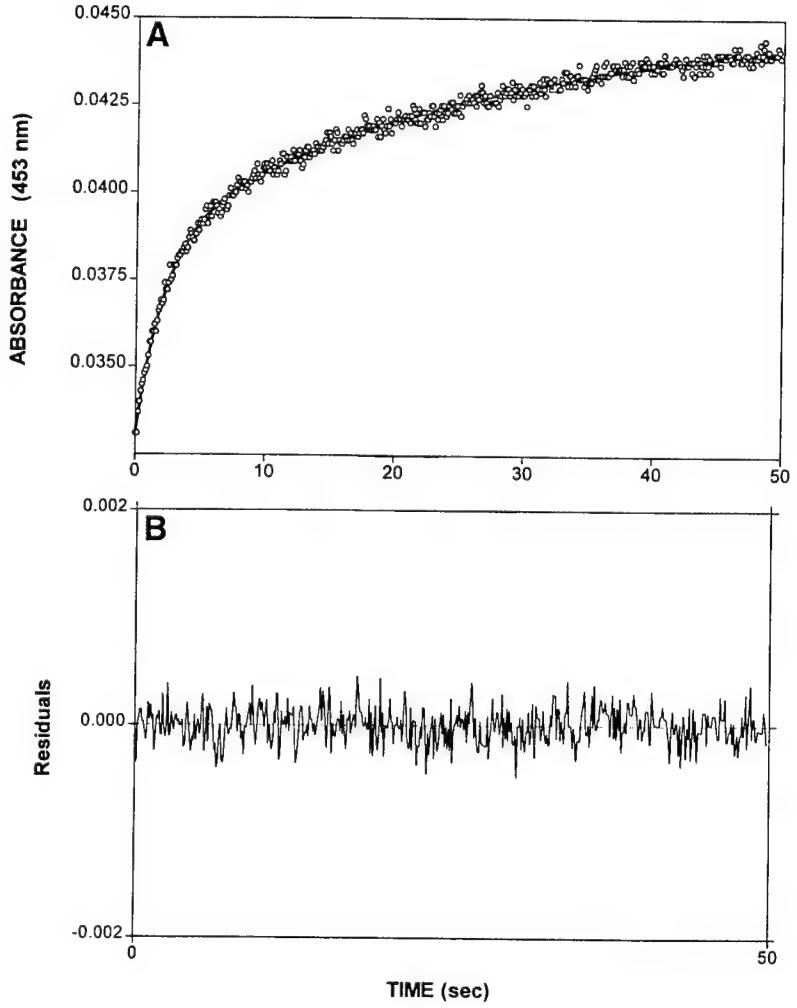

Fig. 3. **(A)** Comparison of experimental data and a two-exponential nonlinear least-squares fit. The extracted parameters are $k(1) = 0.0381 \pm 0.0016\ s^{-1}$, $\Delta A_{o1} = 0.00641 \pm 0.00005$; $k(2) = 0.444 \pm 0.015\ s^{-1}$, $\Delta A_{o2} = 0.00548 \pm 0.00009$. **(B)** The corresponding residual plot.

5. Judging the goodness of fit is best done by residual plot, since the visual comparison of the experimental data and the fitted curve can sometimes give an erroneous impression of a good fit.

3.3.3. Global Analysis

If a series of spectra can be measured during a kinetic run, kinetic profiles at different wavelengths can be obtained and analyzed after the experiment.

Furthermore, global analysis using the data at every wavelength can be performed which can sometimes help eliminate or suggest certain mechanistic models.

4. Notes

1. A gentle inversion of the cuvet after rigorous manual shaking may help minimize the numbers of tiny air bubbles sticking on the cell walls.
2. The use of a mechanical stirrer is preferable as it shortens the dead time, minimizes the bubble generation, and assures continuous uniform mixing during the course of a kinetic run.
3. Absorbance monitoring should preferably be at the wavelength that corresponds to the isosbestic point of free and SDS-sequestered drug spectra so that the measured intensity changes reflect the drug dissociation from DNA more accurately. This can be determined via spectral titrations of drug-vs-stock SDS solutions.
4. Since reaction kinetics are temperature sensitive, maintaining a constant temperature during the run is essential.
5. Although the 1% SDS strength is usually sufficient for most purposes, it may be a good idea to experimentally confirm it for a particular system of interest.
6. Measurements should not be made below 15°C, as SDS forms precipitates near or below this temperature.
7. SDS powders are extremely fine and can easily get into the nasal passages to cause irritation. Thus, SDS should be handled very gently during weighing and the use of a nose-mask is strongly recommended.
8. Careful and slow filling of the driving syringes can help minimize the bubble formation in the stopped-flow experiment.

References

1. Muller, W. and Crothers, D. M. (1968) Studies of the Binding of Actinomycin and Related Compounds to DNA. *J. Mol. Biol.* **35,** 251–290.
2. Fletcher, M. C. and Fox, K. R. (1993) Visualising the Kinetics of Dissociation of Actinomycin from Individual Sites in Mixed Sequence DNA by Dnase I Footprinting. *Nucleic Acids Res.* **21,** 1339–1344.
3. Chaires, J. B., Dattagupta, N., and Crothers, D. M. (1985) Kinetics of the Daunomycin-DNA Interaction. *Biochemistry* **24,** 260–267.
4. Phillips, D. R. and Crothers, D. M. (1986) Kinetics and Sequence Specificity of Drug-DNA Interactions: An in Vitro Transcription Assay. *Biochemistry* **25,** 7355–7362.

Biophysical Journal Volume 73 July 1997 348–356

Supramolecular Self-Assembly of $d(TGG)_4$, Synergistic Effects of K^+ and Mg^{2+}

Fu-Ming Chen
Department of Chemistry, Tennessee State University, Nashville, Tennessee 37209-1561 USA

ABSTRACT Spectral evidence indicates that molar concentrations of K^+ can induce aggregate formation in $d(TGG)_4$. The 320-nm turbidity monitoring indicates that more than 1 M KCl is needed for the onset of aggregation to occur at 20°C within the time span of 24 h. The kinetic profile is reminiscent of autocatalytic reactions that consist of a lag period followed by accelerative and leveling phases. Progressive shortening of lag periods and more rapid accelerative phases accompany further increases in $[K^+]$. Interestingly, the presence of Mg^{2+} greatly facilitates the aggregate formation and results in the prominent appearance of an intense ψ-type CD. For example, whereas 1 M K^+ fails to induce aggregate formation of $d(TGG)_4$ within 24 h, the addition of 1 mM Mg^{2+} to a 1 M K^+ solution is sufficient to induce the onset of aggregation in approximately 12 h. Furthermore, adjustment of the buffer to 16 mM Mg^{2+}/1 M KCl reduces the lag time to less than 10 min and aggregation is nearly complete in 2 h. The requirement of $[K^+]$ for aggregation is reduced to 2 mM in the presence of 16 mM Mg^{2+}, a reduction of nearly three orders of magnitude when compared to solutions without Mg^{2+}. The effects of K^+ and Mg^{2+} ions are synergistic, because the presence of 16 mM Mg^{2+} alone does not induce aggregate formation in this oligomer. Thermal stabilities of the aggregates are strongly dependent on the concentrations of these two ions. Although aggregates formed in the presence of 2 M KCl alone melt around 55°C, those formed with added 16 mM Mg^{2+} melt at ~90°C, with some aggregates remaining unmelted even at 95°C. The slow kinetics of aggregate formation led to the appearance of gross hystereses in the cooling profiles. The interplay of these two ions appears to be specific, because the replacement of K^+ by Na^+ or the replacement of Mg^{2+} by other divalent cations does not lead to the observed self-assembly phenomeon, although Sr^{2+} can substitute for K^+. A possible mechanism for the formation of self-assembled structures is suggested.

INTRODUCTION

Our laboratory has recently uncovered a rather interesting phenomenon in which molar $[K^+]$ induces aggregate formation of $d(CGG)_4$, as indicated by 1) intense ψ-type circular dichroic (CD) spectra (a huge CD band with long-wavelength tail), 2) the presence of absorbance tails at wavelengths well above 310 nm, and 3) the appearance of high-molecular-weight species on electrophoretic gels (Chen, 1995). The rates of aggregation are extremely slow at pH 8 but are greatly enhanced in acidic conditions. The kinetic profiles resemble those of autocatalytic reacting systems, showing characteristic lag periods followed by accelerative phases. Time-dependent CD spectral characteristics indicate an initial positive intensity enhancement near 265 nm, suggesting the formation of parallel G-tetraplexes before the onset of aggregation. Both $d(TGG)_4$ and $d(CGG)_4T$ fail to exhibit the induction of ψ-CD spectra under similar conditions, suggesting that the terminal G and the base protonation of cytosine play crucial roles in the observed phenomenon. Finally, the aggregations are not induced by molar concentrations of NaCl. To explain these observations, we proposed that parallel quadruplexes may form initially and be converted to quadruplexes with contiguous G-tetrads and looped-out cytosines in the presence of high $[K^+]$. These quadruplexes could stack vertically and expand horizontally via interquadruplex C^+·C base pairing to result in dendrimer-type self-assembled superstructures.

We report here the results of a more detailed study with $d(TGG)_4$ that reveals this oligomer can also be induced to form aggregates under appropriate conditions. Absorbance (turbidity) data indicate that this oligomer forms aggregates in the presence of molar K^+. The presence of Mg^{2+} greatly facilitates aggregation and leads to the formation of large Ψ-CD spectra. The effects of K^+ and Mg^{2+} on the aggregation of this oligomer appear to be synergistic.

MATERIALS AND METHODS

Synthetic oligonucleotides were purchased from Research Genetics (Huntsville, AL) and used without further purification. These oligomers were purified by the vendor via reverse-phase oligonucleotide purification cartridges and exhibited single-band electrophoretic mobilities in denaturing polyacrylamide gel electrophoresis with stated purities of ≥95%. Concentrations of oligomers (per nucleotide) were determined by measuring absorbances at 260 nm after melting, with the use of extinction coefficients obtained via nearest-neighbor approximation using mono- and dinucleotide values tabulated in Fasman (1975). Aggregation kinetic profiles were obtained by maintaining the temperature at 20°C and monitoring the time-dependent absorbance changes at 320 nm. The reaction was initiated by addition of the appropriate amount of oligomeric stock to a buffer solution containing the desired salt concentrations. Thermal denaturation experiments were carried out with 1-cm semimicro cells by monitoring absorbances at appropriate wavelengths. A heating (or cooling) rate of 0.5°C/min was maintained by the temperature controller accessory. CD spectra were measured with a Jasco J-500A recording spectropolarimeter using water-jacketed cylindrical cells of 1 cm path length. All experiments

Received for publication 21 January 1997 and in final form 24 March 1997.

Address reprint requests to Dr. Fu-Ming Chen, Department of Chemistry, Tennessee State University, Nashville, TN 37209-1561. Tel.: 615-963-5325; Fax: 615-963-5434; E-mail: chenf@harpo.tnstate.edu.

0006-3495/97/07/348/09 $2.00

were carried out in 10 mM HEPPS (*N*-(2-hydroxyethyl)-piperazine-*N'*-propanesulfonic acid) buffer solutions of pH 8 (adjusted by droplet additions of 1 M NaOH). In contrast to our work on $d(CGG)_4$, no 0.1 M NaCl was added to the buffer.

RESULTS

Absorbance monitoring of K^+-induced aggregate formation in $d(TGG)_4$

Ordinary DNA exhibits an absorbance maximum near 260 nm and is transparent to light beyond 310 nm. Absorbance at the long wavelengths, however, can be induced by the solution turbidity due to the presence of aggregated particulates. The absorbance evidence on the K^+-induced aggregation of $d(TGG)_4$ is shown in Fig. 1 *A*, where the kinetic profiles via 320-nm monitoring are presented for solutions containing molar amounts of KCl. It is apparent that the kinetics of aggregation are autocatalytic-like, with a characteristic lag period being followed by an accelerative phase of absorbance increase and an eventual leveling. Only a hint of absorbance increase is evident near 650 min in the presence of 1.2 M KCl, and equilibrium was not reached until several days later. In contrast, the onset of aggregation can more clearly be discerned near 300 min in the 1.4 M KCl solution. The progressive shortening of the lag periods, along with the appearance of more rapid accelerative phases, is apparent with further increases in $[K^+]$. In a 2.6 M KCl solution, for example, a lag period of less than 10 min is seen, and the aggregation is nearly complete in about 2 h. The decreases in absorbance, evident at longer times for solutions containing higher $[K^+]$, most likely are the consequence of slow sedimentations of larger aggregated particles, inasmuch as rigorous shaking of the cuvettes after the run results in significantly higher absorbance readings.

Mg^{2+} greatly facilitates the K^+-induced aggregate formation

The presence of Mg^{2+} in solutions greatly facilitates the K^+-induced aggregate formation of $d(TGG)_4$. The intricate interplay of these two cations is illustrated by the effects of Mg^{2+} on the kinetic profiles of the 1 M KCl-induced aggregate formation of 40 μM $d(TGG)_4$ (Fig. 1 *B*). Although no sign of aggregate formation is detected in a time span of 24 h (1440 min) for a 1.0 M KCl solution (not shown), the mere presence of 1 mM Mg^{2+} leads to the appearance of an absorbance increase starting around 750 min. A dramatic reduction in the lag period and the concomitant appearance of a more rapid accelerative phase are evident as the $[Mg^{2+}]$ is progressively increased. For example, the presence of 8 mM Mg^{2+} reduces the lag period to ~1 h, similar to that of 2.0 M KCl solution without divalent cation (see Fig. 1 *A*), but with a much steeper accelerative phase. Furthermore, the presence of 16 mM Mg^{2+} reduces the lag time to less than 10 min, and the reaction appears to be nearly complete in ~2 h.

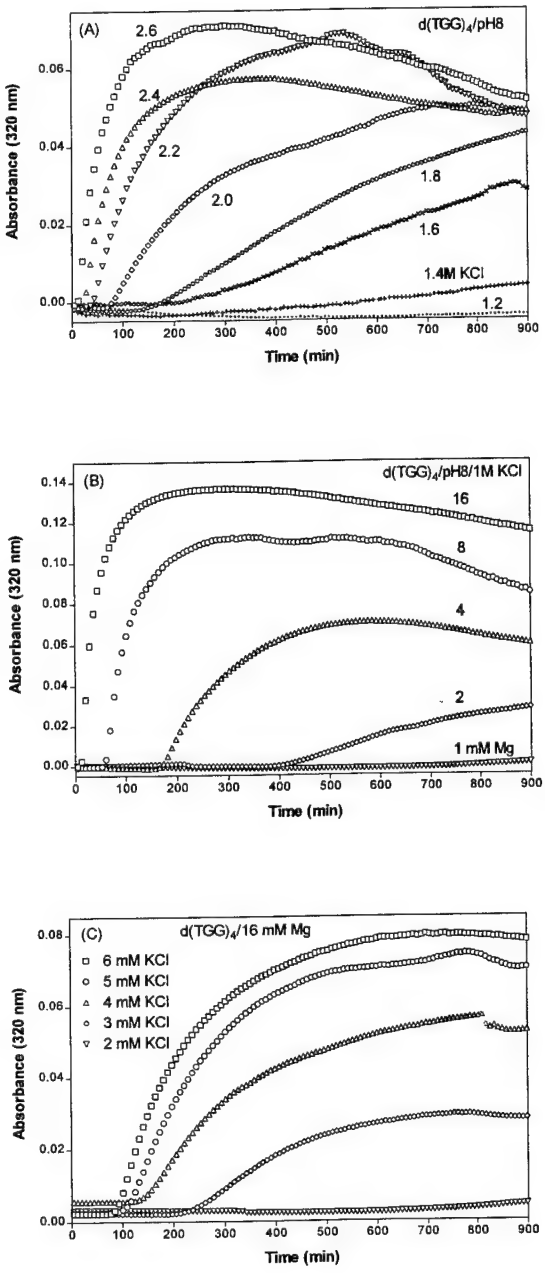

FIGURE 1 Aggregation kinetic profiles of 40 μM (in nucleotide) $d(TGG)_4$ at pH 8 via 320-nm absorbance monitoring at 20°C. (*A*) Comparison of solutions in the presence of different $[K^+]$ with no Mg^{2+}. (*B*) Comparison of solutions in the presence of 1 M KCl and differing $[Mg^{2+}]$. (*C*) Comparison of solutions containing 16 mM Mg^{2+} and differing $[K^+]$. Reactions were initiated by adding the appropriate amounts of DNA stocks with the use of a stirrer accessory into pH 8 solutions containing the desired cation concentrations.

Synergistic effects of K^+ and Mg^{2+} in aggregate formation

The effect of Mg^{2+} in lowering the requirement of KCl for aggregation of oligomers can be seen by comparing the kinetic profiles of 40 μM $d(TGG)_4$ in the presence of 16 mM Mg^{2+} and differing amounts of KCl (Fig. 1 *C*). It is apparent that 2 mM KCl is sufficient to induce the aggregate

formation of $d(TGG)_4$ in a 16 mM Mg^{2+} solution (as indicated by the onset of absorbance enhancement near 700 min), whereas 1.2 M KCl is needed to produce this effect in the absence of Mg^{2+} (see Fig. 1 *A*), reflecting a reduction of nearly three orders of magnitude in the K^+ requirement. Additional 1.5- and 2-fold increases in $[K^+]$ (from 2 mM to 3 and 4 mM, respectively) lead to decreases in the lag times to 240 and 120 min, respectively. Furthermore, even though the onset of aggregation for 40 μM $d(TGG)_4$ in the presence of 16 mM Mg^{2+} and 6 mM K^+ occurs at roughly the same time (70–80 min) as that of 2 M KCl alone, a more rapid accelerative phase is clearly evident. The further shortening of lag periods and more rapid accelerative phases for aggregate formation are seen with further increases in KCl concentrations (not shown). The synergistic effect of these two cations is shown by the inability of 16 mM Mg^{2+} to cause aggregate formation in the absence of K^+.

Melting profiles of the aggregates and the gross cooling hystereses

Thermal stabilities of aggregates can be revealed by the melting profiles obtained from monitoring the absorbance decrease at 320 nm as complexes are denatured. Melting profiles of aggregates formed in the presence of differing amounts of KCl alone are shown in Fig. 2 *A*. As expected, the melting temperature increases as the $[K^+]$ is increased and the melting profiles become progressively more cooperative. In contrast to most regular duplex DNA melting, the cooling profiles of these solutions are seen to exhibit gross hystereses, as exemplified in solutions containing 2.8 and 2.4 M KCl. Although the melting temperatures for the 2.8 and 2.4 M KCl-induced aggregates are close to 65°C and 61°C, respectively (see Fig. 1 *A*), their cooling profiles provide no sign of reaggregation (as indicated by the 320-nm absorbance increase) until around 55°C and 40°C, respectively, with only ~15% and <10% recoveries by the time they reach 20°C. It may be of interest to note that, although the melting temperature of the aggregates is progressively increased as $[K^+]$ is inceased, the 320-nm absorbance exhibits an unexpected progressive decrease as the $[K^+]$ exceeds 2.6 M (compare the 2.6 and 2.8 M KCl profiles). This may be a consequence of changes in the nature of aggregates formed at higher ionic strengths, such as the formation of smaller particles.

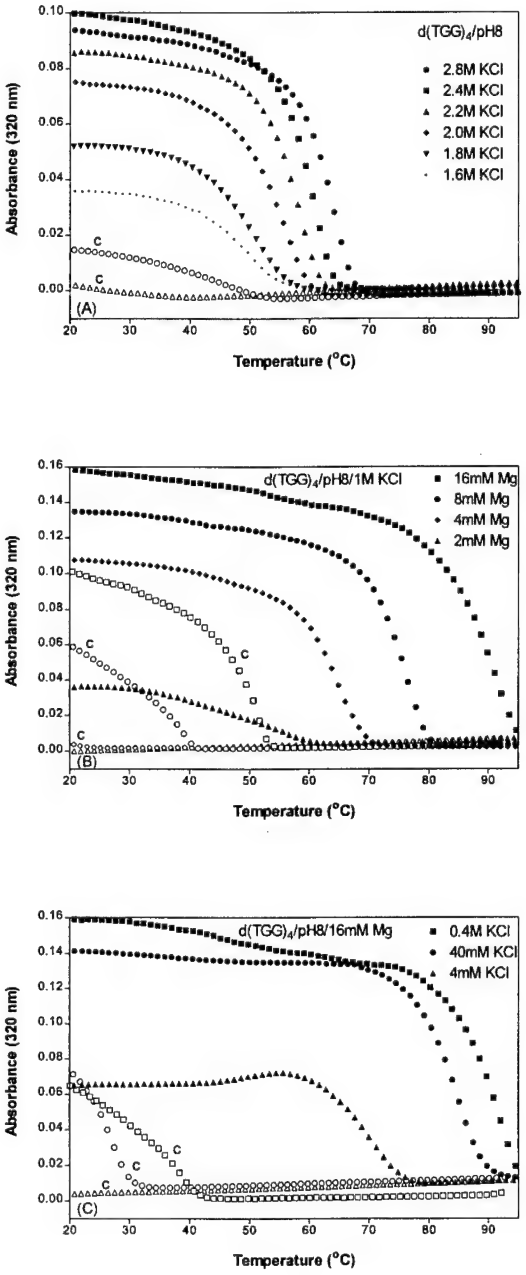

FIGURE 2 Melting profiles of $d(TGG)_4$ aggregates formed by 40 μM nucleotide at pH 8 under various ionic conditions. Corresponding open symbols are those of cooling profiles (with c designations). (*A*) Comparison of melting profiles of aggregates formed by molar KCl in the absence of Mg^{2+}. (*B*) Comparison of melting profiles of aggregates formed by 1.0 M KCl in the presence of differing $[Mg^{2+}]$. (*C*) Representative melting profiles of aggregates formed by differing $[K^+]$ in the presence of 16 mM Mg^{2+}.

Thermal stabilities of aggregates are greatly enhanced by the presence of Mg^{2+}

The effects of Mg^{2+} on the thermal stabilities of the aggregates can be seen by a comparison of melting profiles of aggregates formed by 1 M KCl and in the presence of differing $[Mg^{2+}]$, as shown in Fig. 2 *B*. It is apparent that the presence of Mg^{2+} dramatically enhances the thermal stabilities of the aggregates. For example, the 1 M KCl-induced aggregates melt around 50°C in the presence of 2 mM Mg^{2+}; further two-, four-, and eightfold increases in $[Mg^{2+}]$ result in melting temperatures of 65°C, 75°C, and 89°C, respectively. In fact, a small fraction of aggregates in the latter solution were not completely melted at 95°C, as evidenced by the residual 320-nm absorbance retained at this temperature. Representative cooling profiles are included to highlight the gross hysteretic effects. For example,

there is no hint of reaggregation of oligomer in solutions containing 2 mM Mg^{2+}, even when returning to 20°C. The onset of reaggregation for solutions containing 4, 8, and 16 mM Mg^{2+} is evident near 25°C, 41°C, and 53°C, respectively.

The effect of K^+ on the thermal stability of aggregates formed by d(TGG)$_4$ in solutions containing 16 mM Mg^{2+} is shown in Fig. 2 *C*. As can be seen, a 10-fold increase in [K^+] from 4 to 40 mM increases the melting temperature from 68°C to 84°C, and an additional 10-fold increase from 40 to 400 mM increases it to ~90°C. The cooling profiles again exhibit gross hystereses, with the onset of reaggregation occurring near 43°C and 34°C, respectively, in solutions containing 400 and 40 mM K^+, and showing no sign of reaggregation upon returning to 20°C in solutions containing 4 mM K^+.

ψ-CD spectral characteristics

A highly condensed form of DNA is sometimes characterized by a CD spectrum an order of magnitude higher in intensity than that of unaggregated DNA (Shin and Eichhorn, 1984). This so-called ψ-type CD is presumably a manifestation of differential light scattering and superorganization of the DNA in the aggregates (Maestre and Reich, 1980). Consequently, ψ-CD spectral characterization of the aggregates formed will be of interest.

Time-dependent CD spectral characteristics under various solution conditions are compared in Fig. 3. Spectral alterations in a solution containing 2.0 M KCl are shown in Fig. 3 *A*. The oligomer initially exhibits a spectrum with a weak positive CD maximum near 265 nm. The onset of spectral intensity enhancement commences after a latent lag period of ~50 min to eventually develop into a spectrum consisting of a positive maximum at 265 nm with a shoulder near 290 nm and a negative long-wavelength tail. Except for a much shorter lag period of less than 10 min and a more dramatic intensity enhancement, the spectral features of the 2.8 M KCl solution (Fig. 3 *B*; note the fourfold vertical scale increase) are not very different. Spectral features in solutions containing 16 mM Mg^{2+} and two different [K^+] are shown in Fig. 3, *C* and *D*, respectively. The presence of Mg^{2+} enhanced the absorbance near 290 nm relative to that near 265 nm, producing a positive maximum at 290 nm, a shoulder near 265 nm, and a positive (0.01 M KCl, Fig. 3 *C*) or a weak negative (1.0 M KCl, Fig. 3 *D*) long-wavelength tail.

CD spectral measurements were also made after melting the aggregates and cooling the solutions back to room temperature and waiting for a few days. Interestingly, the postmelt spectra were strongly dependent on solution conditions. For example, a further intensity enhancement with a slight red-shift as compared to the premelt spectrum is seen for the solution containing 16 mM Mg^{2+} and 1.0 M KCl (note the 1.5-fold reduction in intensity for the solid curve to fit into the scale of Fig. 3 *D*). In contrast, a much weaker bisignate CD with negative and positive maxima near 300 and 265 nm, respectively, developed in the 2.8 M KCl solution (see the *solid curve* of Fig. 3 *B*).

The kinetics of spectral alterations can be seen more clearly by monitoring ellipticity changes at individual wavelengths, as shown in Fig. 4. Consistent with those of absorbance monitoring, the kinetics are autocatalytic-like, exhibiting a lag period and an accelerative phase. A dramatic reduction in the lag period from ~50 to less than 10 min and a more rapid accelerative phase are seen when [K^+] increases from 2.0 to 2.8 M (compare Fig. 4, *A* and *B*). The facilitation of ψ-CD by Mg^{2+} is illustrated by the less than 10 min lag time needed for aggregate formation in the presence of 16 mM Mg^{2+}/1.0 M KCl (see Fig. 4 *D*). No onset of aggregation is evident in the time span of 1440 min (24 h) in the absence of the divalent cation. Furthermore, 16 mM Mg^{2+} alone does not induce spectral alterations, but the presence of 10 mM KCl leads to aggregate formation with a lag time of slightly over 1 h (see Fig. 4 *C*). The development of a large positive CD tail is indicated by the sizable positive-going kinetic profile of the 310-nm ellipticity monitoring of this solution.

Other divalent cations failed to exhibit similar effects

To determine whether divalent cations other than Mg^{2+} affect the aggregation of d(TGG)$_4$, rudimentary studies were made with Sr^{2+}, Ba^{2+}, Zn^{2+}, and Ni^{2+}. The results indicate these ions are not effective in promoting aggregate formation by the oligomer in solutions with K^+. Interestingly, however, our preliminary results suggest some synergistic effect between Sr^{2+} and Mg^{2+}, similar to that exhibited by K^+ and Mg^{2+}.

DISCUSSION

Our results indicate that molar K^+ induces aggregate formation by d(TGG)$_4$. In fact, the onset of aggregation occurs near 1 h at 20°C at pH 8 in the presence of 2 M KCl. This is considerably faster than that of d(CGG)$_4$ under similar conditions (Chen, 1995). The features of the kinetic profiles are like those of autocatalytic reactions, consisting of a lag period followed by accelerative and leveling phases. Interestingly, the presence of Mg^{2+} greatly enhances aggregate formation and results in the prominent appearance of an intense ψ-type CD spectrum. In contrast to the absence of aggregate formation in a time span of 24 h (1440 min) in a 1 M K^+ solution at 20°C, the presence of 1 mM Mg^{2+} induces aggregate formation in ~700 min, and 16 mM Mg^{2+} induces aggregation in less than 10 min. Furthermore, the presence of 16 mM Mg^{2+} reduces the requirement for K^+ on aggregation to merely 2 mM. The effects of K^+ and Mg^{2+} ions appear to be synergistic, inasmuch as the presence of 16 mM Mg^{2+} alone does not induce aggregate formation in this oligomer. In addition, thermal stabilities of the aggregates are strongly dependent on the concentrations

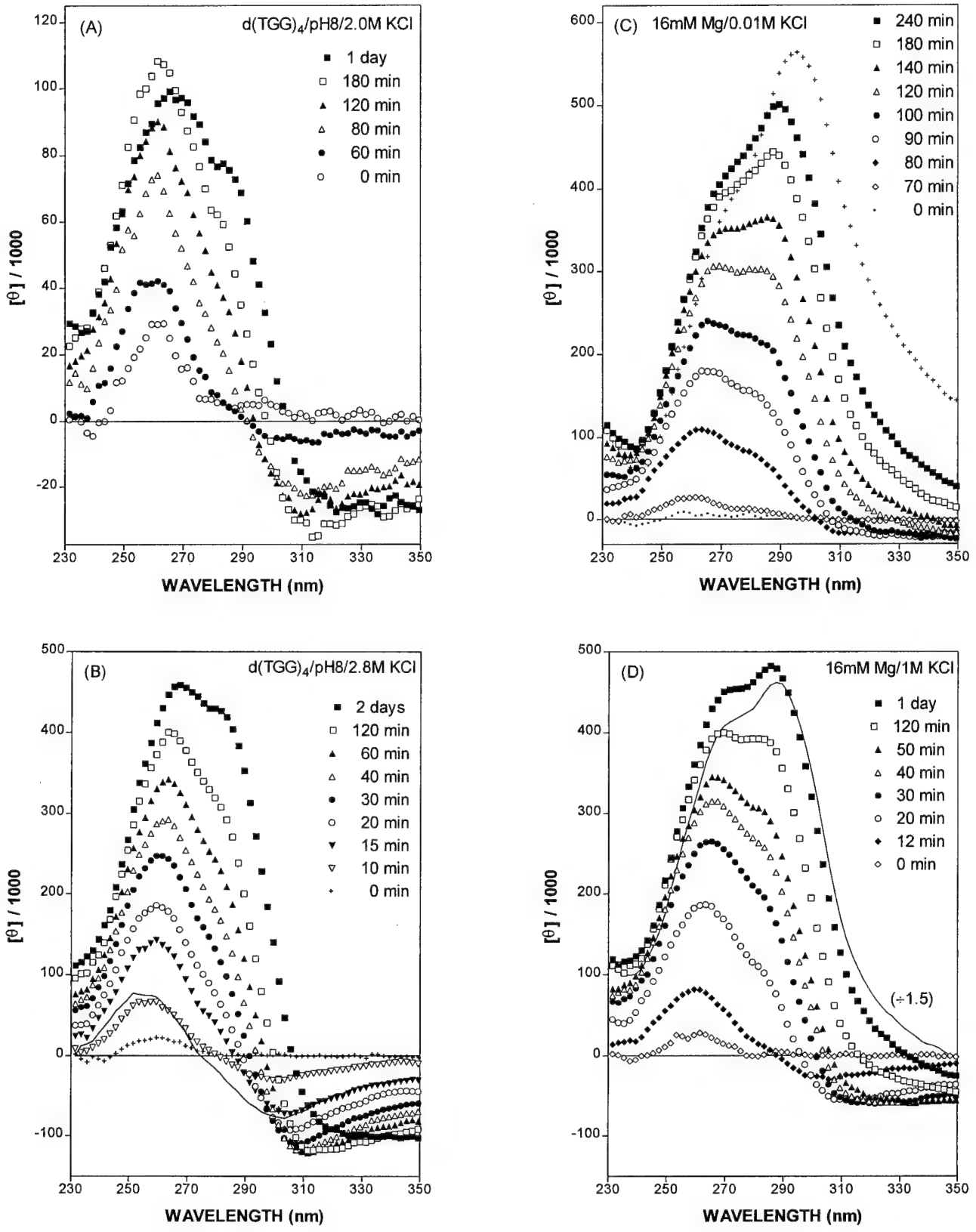

FIGURE 3 Comparison of time-dependent CD spectra for 40 μM d(TGG)$_4$ at pH 8 under various solution conditions. (*A*) In the the presence of 2.0 M KCl. (*B*) In the presence of 2.8 M KCl. The solid curve is that of the postmelt spectrum after a few days. (*C*) In the presence of 16 mM $MgCl_2$ and 0.01 M KCl. The (+) curve is the spectrum after a few days. (*D*) In the presence of 16 mM $MgCl_2$ and 1.0 M KCl. The solid curve is that of postmelt spectrum after a few days (with 1.5-fold reduction in intensity to fit into the scale).

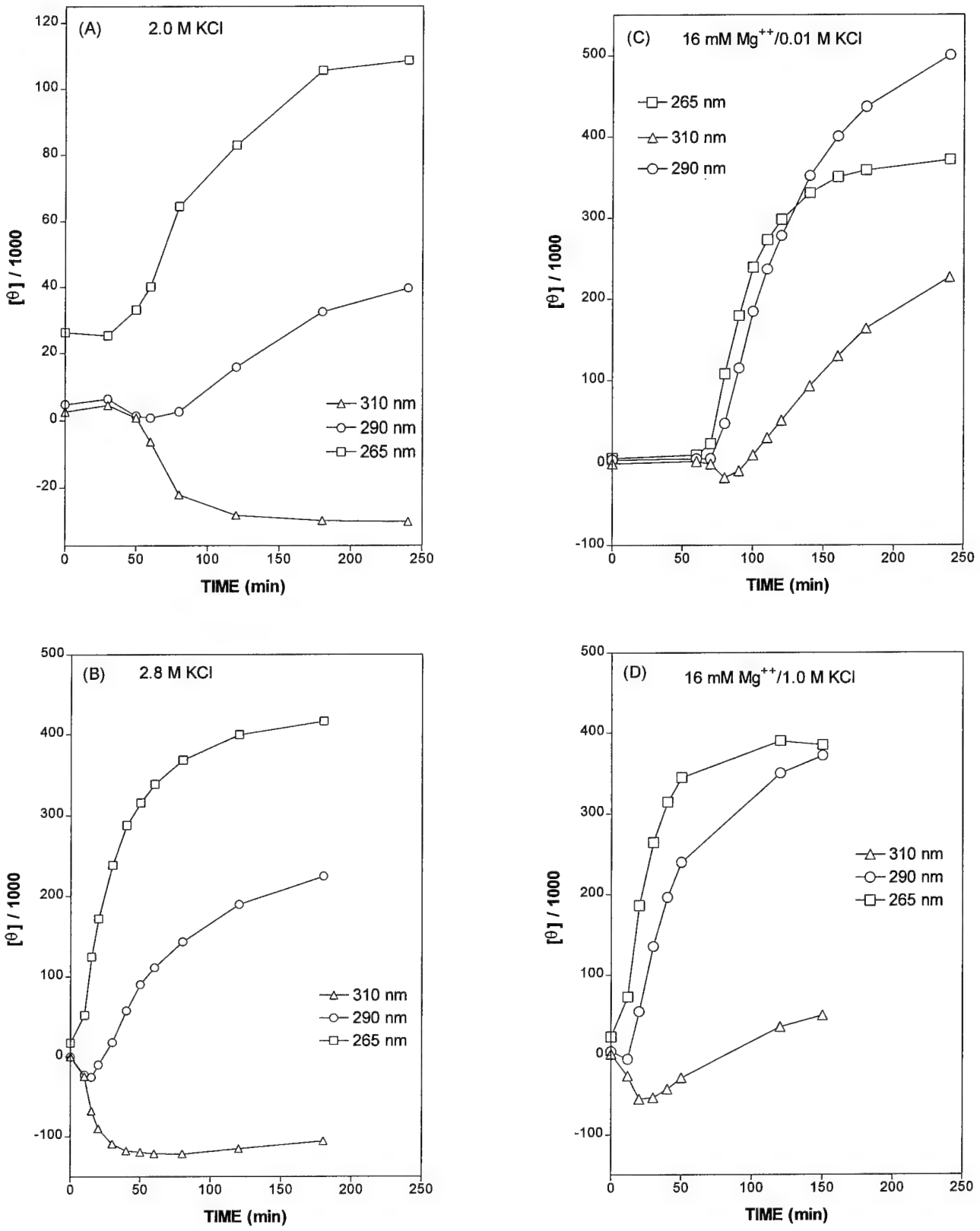

FIGURE 4 Comparison of aggregation kinetic profiles at 20°C via ellipticity monitoring at 310, 290, and 265 nm for 40 μM d(TGG)$_4$ under various solution conditions. (*A*) In the presence of 2.0 M KCl. (*B*) In the presence of 2.8 M KCl. (*C*) In the presence of 16 mM $MgCl_2$ and 0.01 M KCl. (*D*) In the presence of 16 mM $MgCl_2$ and 1.0 M KCl.

of these two ions, and their cooling profiles exhibit gross hystereses. Although the aggregates formed by 2 M KCl alone melt around 55°C, the presence of 16 mM Mg^{2+} increases the melting temperature to ~90°C, with some aggregates remaining unmelted even at 95°C. The interplay of these two ions in the aggregation process appears to be specific, because the replacement of K^+ by Na^+ or the replacement of Mg^{2+} by other divalent cations does not appear to lead to the observed self-assembly phenomenon. However, synergistic effects have been observed with Sr^{2+} and Mg^{2+}.

The observed synergism exhibited by K^+ and Mg^{2+} is consistent with reports by Dai et al. (1995) and Marotta et al. (1996) that oligomers of the form $C_4T_4G_4T_{1-4}G_4$ and $G_xT_2G_y$ self-assemble into multistranded species of high molecular weight in the presence of 100 mM K^+ plus 20 mM Mg^{2+}, but not in the presence of 100 mM K^+, 20 mM Mg^{2+}, or 100 mM Na^+ alone. In contrast to our observations on $d(CGG)_4$ and $d(TGG)_4$, however, their systems do not appear to exhibit ψ-CD spectral characteristics.

In view of the facilitation of this process by the divalent cation Mg^{2+}, it is possible the oligomer forms parallel-stranded homoduplexes in solutions that (aided by the higher concentration and optimal size of K^+ that fits into quadruplex cages) subsequently form in- and/or out-of-register quadruplexes (see Fig. 5). Axial extension of the out-of-register quadruplexes could result if repeated quadruplex formation occurred with sticky ends forming G-wires (Marsh and Henderson, 1994; Dai et al., 1995), whereas those of in-register quadruplexes could result from vertical head-to-tail stacking. In addition, lateral expansion may be achieved by interquadruplex associations via phosphate-Mg^{2+} bond formation. The role of Mg^{2+} in the self-assembly process may be 1) to facilitate the initial homoduplex and subsequent tetraplex formation for axial extension via phosphate charge neutralization and 2) to bridge interquadruplex phosphate groups for lateral expansion, as a consequence of the strong affinity of this divalent cation for phosphates.

The speculated stepwise formation of the self-assembled structure is consistent with the observations of autocatalytic-type kinetics, because each product provides further reaction sites analogous to the products of chain branching polymerization, and with observations of the gross hystereses exhibited by the melting profiles of the aggregates, a consequence of the slow formation kinetics of the aggregates.

The notion of the initial formation of parallel-stranded homoduplexes appears to be supported by a recent study of Suda et al. (1995) on oligonucleotides consisting of a double-helical stretch followed by a single-stranded 3′-terminal overhang of nine GGA sequence repeats. Clever gel electrophoretic experiments led to the conclusion that the $d(GGA)_9$ segment dimerizes in a parallel orientation via G·G base pairings. It was also noted that the parallel homoduplex formation of some of their oligomers and oligonucleotides containing d(GA) repeats (Rippe et al., 1992) was

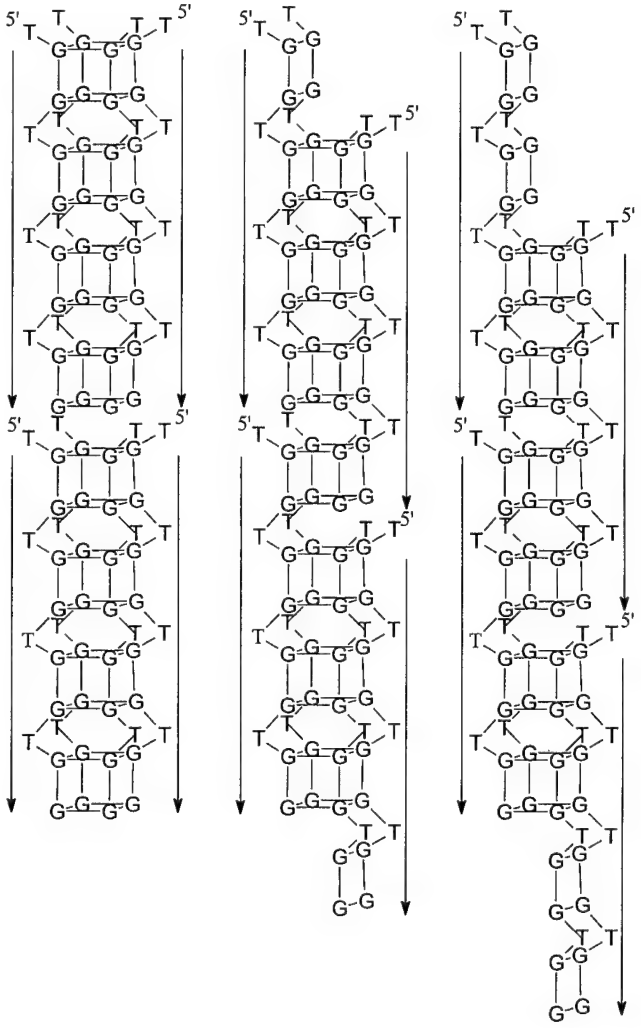

FIGURE 5 Schematic drawings of some possible means of axial extension via in- and out-of-register K^+-driven quadruplex formation (the indicated contiguous G-quartets and looped-out thymidines are purely speculative). For simplicity, only eight strands of $d(TGG)_4$ are shown in the illustration. Lateral expansion via Mg^{2+}-mediated interquadruplex associations (through P-Mg^{2+}-P interactions) is not shown. K^+ ions sandwiched between each pair of G-tetrads are also not shown.

greatly facilitated by Mg^{2+}. Thus considerable ease in aggregate formation should be expected for the AGG trinucleotide repeats, as is indeed borne out by our preliminary studies with $d(AGG)_4$.

The suggested formation of parallel G-quadruplexes before the onset of aggregation is supported by the initial appearance of a characteristic positive 265-nm CD maximum (Balagurumoorthy et al., 1992; Chen, 1992; Hardin et al., 1991) and an earlier observation of Lee (1990) indicating the formation of parallel tetraplex in polyd(GGA). The requirement of molar K^+ for the assembly of $d(CGG)_4$ and $d(TGG)_4$ oligomers and the failure of Na^+ to induce a similar phenomenon under the same conditions also supports the mechanism of initial quadruplex formation of parallel orientation. It is known that Na^+ is too small, but K^+ is the right size for forming a stable octa-coordinated

complex with two G-quartets. Recent Raman studies by Miura et al. (1995) on the quadruplex formation of d(TTTTGGGG)$_4$ further led to the finding that both Na^+ and K^+ facilitate an antiparallel foldback quadruplex at low concentrations but a parallel quadruplex at higher concentrations, with K^+ being more effective in inducing the parallel association. The need for K^+ and a terminal G in the formation of higher ordered structures had been reported by Sen and Gilbert (1992) and Lu et al. (1992). Sen and Gilbert (1992) have shown that oligomers containing a single multiguanine motif at their 3′ or 5′ end, with a guanine as the terminal base, can form higher order products. Methylation protection experiments suggest a nested head-to-tail superstructure containing tetraplexes bonded front-to-back via G quartets formed by out-of-register guanines.

Our speculated mechnism is consistent with the finding that at pH 8, $d(TGG)_4$ aggregates more readily than $d(CGG)_4$ under the same conditions. In contrast, aggregation of $d(CGG)_4$ is facilitated by acidic conditions (Chen, 1995). The presence of cytosines in $d(CGG)_4$ may have trapped this oligomer in conformations that utilize G · C base pairings, such as dimeric duplex or monomeric hairpins, so as to reduce the existence of single-stranded conformers for ease of quadruplex formation. Thus our earlier observed acid-facilitation of aggregate formation in $d(CGG)_4$ may partly be the consequence of the destabilization of these trapped conformers resulting from weakened G · C base pairs due to base protonation of cytidine, and partly the consequence of the facilitation of parallel duplex and/or quadruplex formation via $C \cdot C^+$ base pairings (Hardin et al., 1992, 1993).

We suggest that synergistic effects of K^+ and Mg^{2+} are the consequence of complementary roles played by these two cations, the ability to facilitate the parallel quadruplex formation by the former and binding of phosphate by the latter. The inability of Mg^{2+} to induce aggregation in the absence of K^+ supports the important role of parallel quadruplex formation in the supramolecular self-assembly in $d(TGG)_4$. Thus our rudimentary observation of the ability of Sr^{2+} to synergistically affect aggregation with Mg^{2+} is consistent with the fact that Sr^{2+} has also been shown to facilitate parallel quadruplex formation (Chantot and Guschlbauer, 1969; Chen, 1992).

In their study on the lyotropic liquid crystal formation of four-stranded aggregates of oligodeoxyguanylates, Bonazzi et al. (1991) measured concentration-dependent CD of d(GpG). The spectrum at the maximum concentration compatible with the isotropic solution exhibits a positive double-humped feature, which upon comparison with that of the four-stranded helix of poly(G) or poly(dG), led them to conclude that the d(GpG) aggregates exhibit the right-handed chirality. Except for the much enhanced intensities, CD spectra exhibited by our $d(TGG)_4$ aggregates are very similar. Thus it is reasonable to infer that the superhelical chirality in our system is also right-handed. This inference is consistent with the mostly positive ψ-CD observed in our system, as Maestre and Reich (1980) had established such a sign correlation with the twist sense of the intermolecular organization of the DNA molecules. Our observations of negative ψ-CD tails in some solutions, however, also suggest the existence of more than one chiral structural form in these aggregates and may partly be responsible for the failure to observe large ψ-CD formations in some of our earlier solutions under somewhat different conditions.

The important role played by Mg^{2+} in the formation of G-quadruplex polymers has been noted by Protozanova and Macgregor (1996), who recently investigated the self-assembly of $d(A_{15}G_{15})$ on native and denaturing electrophoretic gels. The complexes consist of integer numbers of strands ranging from one to more than nine monomers. The relative concentration of the various complexes is determined by the solvent conditions. The complexes are quite stable and are resistant to standard denaturation conditions. Mg^{2+} at fairly low concentration leads to the formation of polymers, whereas the presence of the monovalent cations stabilizes lower-molecular-weight complexes consisting of two to six strands of $d(A_{15}G_{15})$. A model of higher order complexes formed by this oligomer consists of two distinct structural regions, a stem made up of G-tetrads and single-stranded adenosine arms projecting radially from the stem. These polymers are termed "frayed wires," in contrast to the G-wires described by Marsh and Henderson (1994).

To gain further insight into the self-assembly processes of XGG trinucleotide repeats, systematic studies on $d(CGG)_n$, $d(TGG)_n$, $d(AGG)_n$, and some related oligomers are currently being carried out in our laboratory under various solution conditions. It should be noted in passing that our rudimentary measurements indicate that d(GGTGGTGGTGG) exhibits a more facile aggregate-forming ability than $d(TGG)_4$, supporting the crucial role played by terminal guanosines, and $d(TTGG)_4$ failed to exhibit ψ-CD formation or 320-nm absorbance increase in the presence of 2 M KCl and 16 mM Mg^{2+}.

I thank Mary Ann Asson-Batres for her careful reading of the manuscript.

This work was supported by Army Medical Research grant DAMD17-94-J-4474.

REFERENCES

Balagurumoorthy, P., S. K. Brahmachari, D. Mohanty, M. Bansal, and V. Sasisekharan. 1992. Hairpin and parallel quartet structures for telomeric sequences. *Nucleic Acids Res.* 20:4061–4067.

Bonazzi, S., M. Capobianco, M. M. De Morais, A. Garbesi, G. Gottarelli, P. Mariani, M. G. P. Bossi, G. P. Spada, and L. Tondelli. 1991. Four-stranded aggregates of oligodeoxyguanylates forming lyotropic liquid crystals: a study by circular dichroism, optical microscopy, and X-ray diffraction. *J. Am. Chem. Soc.* 113:5809–5816.

Chantot, J. F., and W. Guschlbauer. 1969. Physicochemical properties of nucleosides 3. Gel formation by 8-bromoguanosine. *FEBS Lett.* 4:173–176.

Chen, F.-M. 1992. Sr^{2+} facilitates intermolecular G-quadruplex formation of telomeric sequences. *Biochemistry.* 31:3769–3776.

Chen, F.-M. 1995. Acid-facilitated supramolecular assembly of G-quadruplexes in $d(CGG)_4$. *J. Biol. Chem.* 270:23090–23096.

Dai, T.-Y., S. P. Marotta, and R. D. Sheardy. 1995. Self-assembly of DNA oligomers into high molecular weight species. *Biochemistry.* 34: 3655–3662.

Fasman, G. D., editor. 1975. CRC Handbook of Biochemistry and Molecular Biology, Vol. I, 3rd Ed. CRC Press, Boca Raton, FL. 589.

Fry, M., and L. A. Loeb. 1994. The fragile X syndrome $d(CGG)_n$ nucleotide repeats form a stable tetrahelical structure. *Proc. Natl. Acad. Sci. USA.* 91:4950–4954.

Guo, Q., M. Lu, and N. R. Kallenbach. 1993. Effect of thymine tract length on the structure and stability of model telomeric sequences. *Biochemistry.* 32:3596–3603.

Hardin, C. C., M. Corregan, B. A. Brown, II, and L. N. Frederick. 1993. Cytosine-cytosine$^+$ base pairing stabilizes DNA quadruplexes and cytosine methylation greatly enhances the effect. *Biochemistry.* 32: 5870–5880.

Hardin, C. C., E. Henderson, T. Watson, and J. K. Prosser. 1991. Monovalent cation induced structural transitions in telomeric DNAs: G-DNA folding intermediates. *Biochemistry.* 30:4460–4472.

Hardin, C. C., T. Watson, M. Corregan, and C. Bailey. 1992. Cation-dependent transition between the quadruplex and Watson-Crick hairpin form of $d(CGCG_3GCG)$. *Biochemistry.* 31:833–841.

Lee, J. S. 1990. The stability of polypurine tetraplexes in the presence of mono- and divalent cations. *Nucleic Acids Res.* 18:6057–6060.

Lu, M., Q. Guo, and N. R. Kallenbach. 1992. Structure and stability of sodium and potassium complexes of dT_4G_4 and dT_4G_4T. *Biochemistry.* 31:2455–2459.

Maestre, M. F., and C. Reich. 1980. Contribution of light scattering to the circular dichroism of deoxyribonucleic acid films, deoxyribonucleic acid-polylysine complexes, and deoxyribonucleic acid particles in ethanolic buffers. *Biochemistry.* 19:5214–5223.

Marotta, S. P., P. A. Tamburri, and R. D. Sheardy. 1996. Sequence and environmental effects on the self-assembly of DNA oligomers possessing $G_xT_2G_y$ segments. *Biochemistry.* 35:10484–10492.

Marsh, T. C., and E. Henderson. 1994. G-wires: self-assembly of a telomeric oligonucleotide, d(GGGGTTGGGG), into large superstructures. *Biochemistry.* 33:10718–10724.

Marsh, T. C., J. Vesenka, and E. Henderson. 1995. A new DNA nanostructure, the G-wire, imaged by scanning probe microscopy. *Nucleic Acids Res.* 23:696–700.

Miura, T., J. M. Benevides, and G. J. Thomas, Jr. 1995. A phase diagram for sodium and potassium ion control of polymorphism in telomeric DNA. *J. Mol. Biol.* 234:1171–1183.

Protozanova, E., and R. B. Macgregor, Jr. 1996. Frayed wires: a thermally stable form of DNA with two distinct structural domains. *Biochemistry.* 35:16638–16645.

Reich, C., M. F. Maestre, S. Edmondson, and D. M. Gray. 1980. Circular dichroism and fluorescence-detected circular dichroism of deoxyribonucleic acid and poly[d(A-C)·d(G-T)] in ethanolic solutions: a new method for estimating circular intensity differential scattering. *Biochemistry.* 19:5208–5213.

Rippe, K., V. Fritsch, E. Westhof, and T. M. Jovin. 1992. Parallel-stranded DNA, potential intervention of a stable double-helical structure in recombination. *EMBO J.* 11:3777–3786.

Sen, D., and W. Gilbert. 1992. Novel DNA superstructures formed by telomere-like oligomers. *Biochemistry.* 31:65–70.

Shin, Y. A., and G. L. Eichhorn. 1984. Formation of $\psi(+)$ and $\psi(-)$ DNA. *Biopolymers.* 23:325–335.

Suda, T., Y. Mishima, H. Asakura, and R. Kominami. 1995. Formation of a parallel-stranded DNA homoduplex by d(GGA) repeat oligonucleotides. *Nucleic Acids Res.* 23:3771–3777.

Actinomycin D Binds Strongly and Dissociates Slowly at the dGpdC Site with Flanking T/T Mismatches

Chengdi Liu and Fu-Ming Chen

Department of Chemistry, Tennessee State University, Nashville, Tennessee 37209-1561

Biochemistry®

Reprinted from
Volume 35, Number 50, Pages 16346–16353

Actinomycin D Binds Strongly and Dissociates Slowly at the dGpdC Site with Flanking T/T Mismatches†

Chengdi Liu and Fu-Ming Chen*

Department of Chemistry, Tennessee State University, Nashville, Tennessee 37209-1561

Received May 2, 1996; Revised Manuscript Received August 12, 1996®

ABSTRACT: Comparative electrophoretic, thermal denaturation, and spectroscopic studies with dodecamers of the form d(ATTA-XGCX-TAAT) and their self-complementary counterparts suggest that actinomycin D (ACTD) binds strongly to a 5′GC3′ site with flanking T/T mismatches and moderately to that with C/C mismatches but weakly to those with other G/G or A/A mismatches. The relative binding order is found to be T/T > C/C > G/G > A/A. The ACTD binding affinity for the GC site with T/T mismatches is comparable to the strong binding of self-complementary -XGCY- sequences. Both the ACTD association and dissociation kinetics at the GC site with flanking T/T mismatches require two-exponential fits. The slow component of the association rates is slower than those of the self-complementary sequences, whereas that of the dissociation is only slightly faster than that of the -TGCA- sequence. Interestingly, the slow component of dissociation is decidedly slower than those of -AGCT- and -CGCG- sites and is more than an order of magnitude slower than those with C/C, G/G, and A/A mismatches. These kinetic results are further corroborated by fluorescence measurements using 7-amino-ACTD, a fluorescent analog of ACTD. In addition, fluorescence and absorbance spectral characteristics indicate that the binding mode at the GC site with flanking T/T mismatches resembles those of strong-binding self-complementary -XGCY- sites which are known to be intercalative in nature. The observed slow ACTD dissociation at the T/T-mismatched site suggests that the minor-groove environment near the T/T-mismatched pairs provides favorable interactions with the pentapeptide rings of the drug, whereas the others, especially those of bulkier purine/purine mismatches, result in less favorable interactions.

Actinomycin D (ACTD) is an antitumor antibiotic that contains a 2-aminophenoxazin-3-one chromophore and two cyclic pentapeptide lactones. Its DNA binding mode and base sequence specificity have been well characterized by X-ray crystallography (Sobell & Jain, 1972; Takusagawa et al., 1982; Kamitori & Takusagawa, 1992), footprinting (Lane et al., 1983; Scamrov & Beabealashvilli, 1983; Van Dyke & Dervan, 1983; Van Dyke et al., 1983; Fox & Waring, 1984; White & Phillips, 1989; Rehfuss et al., 1990; Goodisman et al., 1992; Goodisman & Dabrowiak, 1992), hydrodynamic (Muller & Crothers, 1968), and spectroscopic (Krugh, 1972; Patel, 1974; Krugh et al., 1977; Brown et al., 1984; Scott et al., 1988a,b; Zhou et al., 1989; Brown et al., 1994) measurements. The most recent crystallographic study with $d(GAAGCTTC)_2$ has largely confirmed the earlier proposed intercalative model and provided additional structural details (Kamitori & Takusagawa, 1994). The complex is formed by the phenoxazinone chromophore intercalating into the 5′GC3′ sequence from the minor groove, with the two cyclic pentapeptide rings resting on both sides of the minor groove and covering four base pairs of DNA. Four threonine−guanine hydrogen bonds and two additional hydrogen bonds between the N2 amino group of phenoxazone and the DNA backbone are formed. The preference of this drug for the 5′GpC3′ step is, thus, the consequence of these threonine−guanine hydrogen-bond formations. These essential drug−DNA hydrogen bonds are protected by the cyclic pentapeptides, which effectively shield them from solvent exposure. The size of the four-base-paired binding site suggests that the binding characteristics of ACTD to the GC site may be affected by the adjacent flanking base pairs. Indeed, studies with self-complementary as well as non-self-complementary -XGCY-containing decamers (Chen, 1988, 1992) have revealed that the binding affinity and dissociation kinetics of this drug are greatly affected by the nature of X and Y bases. For example, ACTD binds strongly to and dissociates very slowly from the -TGCA- site, whereas it binds weakly and dissociates very rapidly from the -GGCC- sequence. Similar adjacent base-pair effects had also been observed by others (Aivasashvilli & Beabealashvilli, 1983; Rill et al., 1989). In addition to the observed GC sequence preference, there have been other reports to indicate that this drug can also bind to some non-GpC sites (Snyder et al., 1989; Waterloh & Fox, 1992; Bailey & Graves, 1993). Of particular interest are the observations of ACTD binding to some single-stranded DNA (Wadkins & Jovin, 1991) and of strong ACTD binding and slow dissociation from the -TGGGT- duplex site (Rill et al., 1989; Bailey, S. A., et al., 1994).

DNA base-pair mismatches can sometimes serve as initiators or intermediates in a mutagenic pathway, and they may be introduced during replication (Modrich, 1987), recombination (Akiyama et al., 1989), or other chemical events. These sites can also serve as preferential targets for drugs or carcinogens. Thus, the effects of base-pair mismatches on DNA structures (Hunter, 1992) and their ligand interactions are of considerable interest, as they may have

† Research Supported by USPHS Grant CA-42682 and Army Medical Research Grant DAMD17-94-J-4474.

* Corresponding author.

® Abstract published in *Advance ACS Abstracts,* December 1, 1996.

S0006-2960(96)01060-4 CCC: $12.00

relevance in DNA repair, transcription, replication, and activation of damaged genes. A logical extension of our earlier studies on the adjacent base-pair effects on the ACTD binding to a GC site would be to investigate the effects of the flanking base mismatches on the affinity and kinetic behaviors of this preferred GpC sequence. This report describes results of such studies but focuses only on ACTD binding and kinetic investigations on GC sites flanked by homobase mismatches. Comparative studies using dodecamers containing self-complementary -XGCY- and non-self-complementary -XGCX- sequences were carried out to accomplish our objectives.

MATERIALS AND METHODS

Synthetic oligonucleotides were purchased from Research Genetics, Huntsville, AL, and used without further purification. These oligomers were purified by the vendor via reverse-phase oligonucleotide purification cartridges and exhibited single-band electrophoretic mobilities in denaturating PAGE with stated purities of ≥95%. All experiments were carried out in 10 mM HEPPS [*N*-(2-hydroxyethyl)-piperazine-*N*′-propanesulfonic acid] buffer solutions of pH 8 containing 0.1 M NaCl and 1 mM $MgCl_2$. Concentrations of these oligomers (per nucleotide) were determined by measuring the absorbances at 260 nm after melting, with use of extinction coefficients obtained via nearest-neighbor approximation using mono- and dinucleotide values tabulated in Fasman (1975). The extinction coefficients used for drug concentration determination are 24 500 M^{-1} cm^{-1} at 440 nm for ACTD and 23 600 M^{-1} cm^{-1} at 528 nm for 7-amino-ACTD. Absorption spectra were measured with a Cary 1E spectrophotometric system. Thermal denaturation experiments were carried out with 1-cm semimicro cells by monitoring absorbances at 275 nm. A heating rate of 0.5 °C/min was maintained by the temperature controller accessory. Spectral titrations were carried out at 20 °C and absorbance changes at 427 and 480 nm were used to obtain Scatchard plots. Fluorescence measurements were made with an SLM 48000S system. Fluorescence kinetic measurements were made by monitoring either 650 or 600 nm for the association and 600 nm for the 1% SDS- (sodium dodecyl sulfate-) induced dissociation with 560-nm excitation and using a stirrer accessory. Absorbance kinetic measurements were made by using a stirrer accessory with 427- and 453-nm monitorings for the ACTD association and SDS-induced dissociation, respectively. Kinetic rate parameters were extracted using a nonlinear least-squares fit program of Micromath (Salt Lake City, Utah).

CD (circular dichroic) spectra were measured with a Jasco J-500A recording spectropolarimeter using water-jacketed cylindrical cells of 1-cm path length. CD kinetic measurements were made by monitoring ellipticity changes at 293 nm for both association and dissociation. Electrophoretic measurements were made on a Pharmacia Phast System using 20% polyacrylamide native gels at 200 V with appropriate pre- and postloading run times at different temperatures. PhastGel buffer strips containing 0.25 M Tris, pH 8.8, were used and the gels were developed by silver staining.

RESULTS

Rationale for the Choice of Oligomers. Dodecamers of the form d(ATTA-XGCX-TAAT), where X = A, T, G, or C, were chosen for this study. Except for the X base, this sequence is self-complementary and contains a single GC site at the center. Thus, several conformations can be envisioned to exist in solutions: a single-stranded form (Ia); a monomeric hairpin consisting of a 4-base-paired stem and a 4-base loop (I); a dimeric form with duplex side arms and a central 5′GC3′ duplex step flanked by X/X mismatches (II); a dimeric form with duplex side arms and a 4-base bulge in the central region (IIa); a dimeric form with a central GC duplex step attached to four single-stranded side arms (IIb); and higher multimeric species such as a cruciformlike tetramer having two ATTA/TAAT and two ATTAXGCX/XGCXTAAT duplex arms. The hairpin form I should predominate in the monomeric conformations, whereas duplex form II is expected to be more stable than forms IIa and IIb in the dimeric species. Furthermore, the presence of base mismatches will significantly destabilize the dimeric duplex conformations and thus favor hairpin formation near room temperatures. The hairpin form would, however, place the GC sequence at the loop region with only A•T base pairings in the duplex stem. Its ACTD binding affinity would, consequently, be expected to greatly diminish. Despite the anticipated multiconformational states and the dominant presence of hairpin conformations in solutions, it follows that if ACTD binds strongly to a duplex GC sequence with flanking base mismatches, it may further shift the equilibrium to favor the dimeric duplex for additional binding and further conformational shifts to result in a predominance of drug complexation with dimeric duplexes. Comparative studies of these oligomers will, consequently, yield the relative binding order of these mismatched sequences, and parallel studies with the corresponding self-complementary dodecamers containing the -XGCY- sequences will provide comparison with the known strong binding sites. The additional rationale for studying the self-complementary dodecamers is to provide further evidence on the effect of adjacent base pairs on the ACTD binding characteristics at the GC site, as revealed by our earlier studies with decamers of the form d(ATA-XGCY-TAT) (Chen, 1988, 1992).

Absorbance Spectral Evidence of Strong ACTD Binding for GpC with T/T Mismatches. DNA binding to ACTD results in the depression and enhancement of absorbance intensities at the 427- and 480-nm regions, respectively. Thus, a qualitative ranking of relative ACTD binding affinities of different sequences can be achieved by simply comparing the absorbance intensity alterations near these regions at the same [nucleotide]/[drug] (P/D) ratio. The absorption difference spectra of 5 μM ACTD in the presence (P/D = 20) and in the absence of DNA are compared in Figure 1 for the self-complementary (panel A) and mismatched (panel B) dodecamers. Consistent with our earlier findings with decamers (Chen, 1988), ACTD's affinity for the -GGCC- site is considerably weaker than for the other three self-complementary -XGCY- sequences, which exhibit very similar intensity alterations (panel A). Interestingly, the absorbance changes induced by ACTD binding to the dodecamer containing T/T mismatches are sizable and are in fact comparable to the self-complementary counterparts in terms of magnitude as well as spectral characteristics. Comparison among the mismatched dodecamers (Figure 1B) further suggests a qualitative ranking of binding order to be T/T > C/C > G/G > A/A for the flanking mismatched pairs.

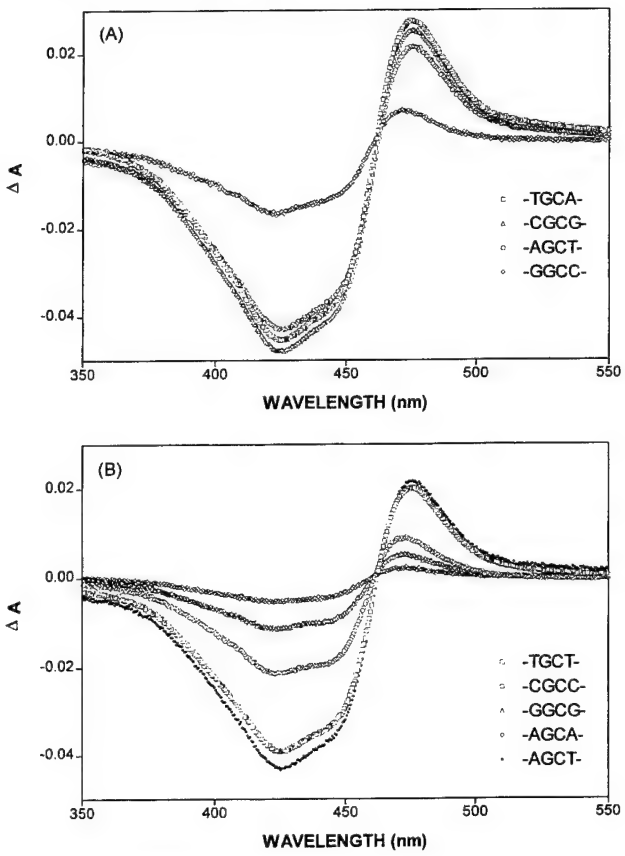

FIGURE 1: Comparison of absorption difference spectra (ACTD/DNA − ACTD) at 20 °C for solutions containing 5 μM ACTD in the absence (P/D = 0) and in the presence (P/D = 20) of self-complementary dodecamers of the form d(ATTA-XGCY-TAAT) (panel A) and mismatched dodecamers of the form d(ATTA-XGCX-TAAT) (panel B, with -AGCT- added for comparison). Spectral measurements were made in HEPPS buffer, pH 8/0.1 M NaCl, using cuvettes of 1-cm path length.

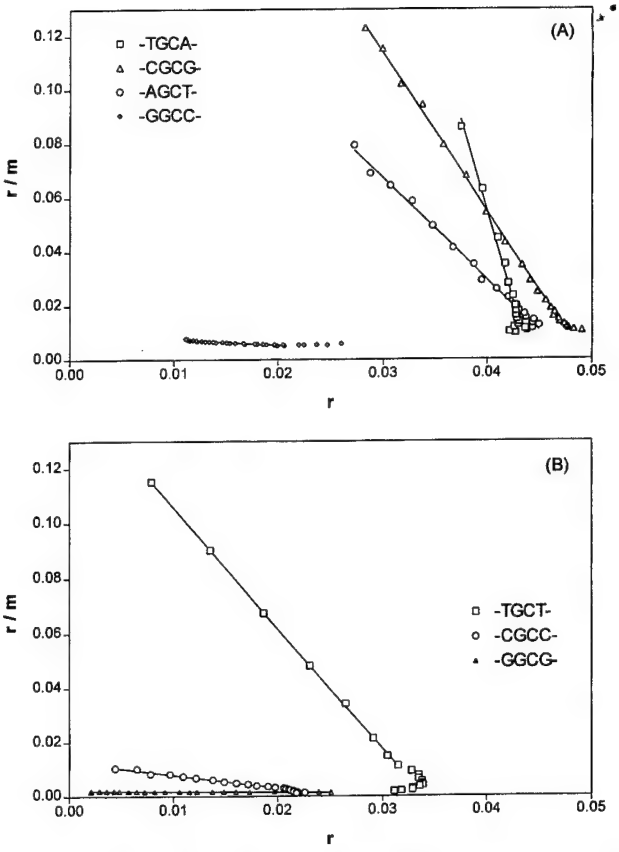

FIGURE 2: Comparison of Scatchard plots for self-complementary (panel A) and mismatched (panel B) dodecamers at 20 °C. Absorbance differences between 427 and 480 nm were employed to construct the binding isotherms. Solid lines are those of linear least-squares fits on the linear portions of the data points using the simple Scatchard equation $r/m = K_a(n - r)$, where r is the ratio of bound drug to DNA base concentrations, n is the saturation binding density, K_a is the apparent association constant, and m is the free drug concentration. Titrations in panel A were carried out by adding aliquots of DNA stock to an ACTD solution to result in nearly constant ACTD concentrations (4−5 μM) and P/D values ranging from 1 to 55 or less. Titrations in panel B were made via adding aliquots of ACTD stock to a DNA solution to result in nearly constant nucleotide concentrations (95−100 μM) and P/D values ranging from 5 to 230. Experiments were carried out in pH 8 buffer solutions containing 0.1 M NaCl and using a stirrer accessory with 1-cm cells.

Scatchard Plots. To obtain more quantitative binding parameters, absorbance spectral titrations were carried out in which aliquots of DNA stock were progressively added to an ACTD solution. The titration data at fixed wavelengths were converted to Scatchard plots (Figure 2A) for the self-complementary dodecamers. It is apparent that the plots are approximately linear, with -GGCC- exhibiting much weaker binding (~0.2 μM^{-1}) than the other three sequences (4−13 μM^{-1}) (see Table 1). In contrast, the plots for the mismatched dodecamers (not shown) exhibit unusual curvatures as if the initial low P/D data points were emanating from the origin and subsequently revert to "normal" linear plots at higher P/D. These curvatures are likely the consequence of the chosen mode of titration in which the initial additions of DNA result in much lower DNA concentrations that are less conducive to duplex formation for these mismatched oligomers even in the presence of ACTD. This situation continues with each titration point until a critical DNA concentration is reached where the duplex formation is now more favorable and the Scatchard plot appears to behave in a normal manner.

To circumvent such effects, an alternative mode of titration was employed in which aliquots of ACTD solution were progressively added to a concentrated DNA solution to result in nearly constant DNA concentrations during the course of spectral titration. The Scatchard plots for the mismatched dodecamers with use of this method are shown in Figure 2B and the binding parameters extracted via linear least-squares fits are summarized in Table 1. It is apparent that

Table 1: Comparison of Melting and ACTD Binding Parameters for Dodecamers[a]

oligomer	K (μM^{-1})	n/duplex	t_m^o (°C)	t_m (°C)
d(ATTA-TGCA-TAAT)	13.1	1.1	34.0	46.8
d(ATTA-AGCT-TAAT)	3.8	1.1	35.5	41.5
d(ATTA-CGCG-TAAT)	5.9	1.2	42.5	53.0
d(ATTA-GGCC-TAAT)	~0.2		39.4	44.8
d(ATTA-AGCA-TAAT)	0.05 (0.037)		<10	
d(ATTA-TGCT-TAAT)	4.4 (5.1)	0.8	<10	31.0
d(ATTA-GGCG-TAAT)	0.024 (0.094)		<10	<20
d(ATTA-CGCC-TAAT)	0.49 (0.29)	0.6	<10	23.3

[a] t_m^o is the estimated dimeric duplex melting temperature of 40 μM DNA (nucleotide) via 275-nm monitoring in pH 8 buffer containing 0.1 M NaCl. t_m is the melting temperature of 40 μM DNA (nucleotide) in the presence of 5 μM ACTD. Values in parentheses are those obtained via model fitting (eqs 1−3) to the experimental binding isotherms in which titrations were carried out by progressively adding aliquots of DNA stock into an ACTD solution.

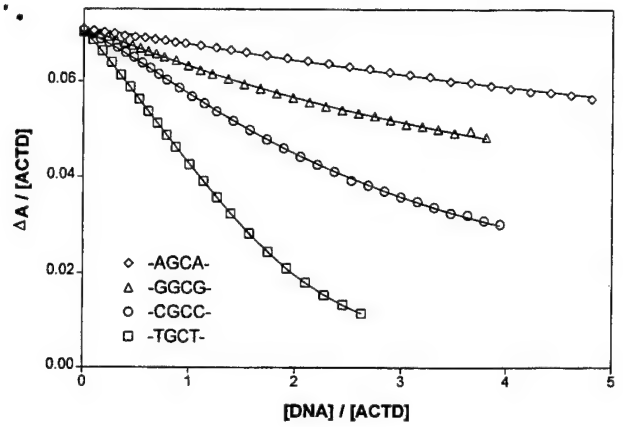

FIGURE 3: Comparison of experimental equilibrium binding isotherms with the fitted curves (solid curves) using the model presented in the text for the mismatched dodecamers of the form d(ATTA-XGCX-TAAT) at 20 °C. Experimental conditions and the titration procedures are similar to those of Figure 2A in which aliquots of DNA stock were progressively added to a 5 μM ACTD solution. ΔA corresponds to the absorbance difference of 427 and 480 nm, whereas [ACTD] is expressed in micromolar.

the ACTD binding affinity of the T/T-mismatched oligomer of 4.4 μM^{-1}, as revealed by the slope, is comparable to the strong-binding self-complementary sequences and is seen to be somewhat weaker than -TGCA- but slightly stronger than -AGCT-. In contrast to the extracted binding densities of around 0.046 (or 1.1 drug molecule/duplex) for the self-complementary sequences, the T/T-mismatched dodecamer extrapolated to approximately 0.034 (or 0.8 drug molecule/duplex). The lower binding densities of less than 1 drug molecule/duplex as exhibited by the mismatched oligomers are consistent with the significant presence of weak or non-binding hairpin and other conformations in these mismatched oligomers.

Fitting the Binding Isotherms with a Binding Model. To investigate the possibility of extracting binding constants for those isotherms which exhibit unusually curved Scatchard plots in the nearly constant [ACTD] mode of titration, the following simple model was assumed: the monomeric hairpin (L) is in dynamic equilibrium with the dimeric duplex (L_2), but only the dimeric duplex binds with the drug (S) to form a 1:1 drug to DNA complex (L_2S):

$$2\,L \overset{K_L}{\Longleftrightarrow} L_2 \quad \text{and} \quad L_2 + S \overset{K_1}{\Longleftrightarrow} L_2S$$

By means of equations for the mass balances of DNA (in strand) and ACTD, the following equations can be derived:

$$2(S_t - S)(1 + K_1S) + [K_1S\,(S_t - S)/K_L]^{1/2} - L_tK_1S = 0 \quad (1)$$

$$L_2 = (S_t - S)/K_1S \quad (2)$$

$$A = \epsilon_S S + \epsilon_1 S K_1 L_2 \quad (3)$$

where ϵ_S and ϵ_1 are the extinction coefficients of the free and bound drugs and S_t and L_t are the total drug and DNA strand concentrations, respectively. For simplicity, brackets were not used to represent concentrations. Nonlinear least-squares fits of the experimental binding isotherms with these equations are excellent and can be seen in Figure 3. The apparent good fit at the low P/D region where the Scatchard plots exhibit unusual curvature is particularly gratifying. The extracted binding constants are also included in Table 1 for comparison. The plausibility of the assumed model and the validity of the titration data are further strengthened by the extracted binding constants being in reasonable agreement with those obtained via Scatchard plots employing an alternative mode of titration as well as the binding orders established via the absorbance difference spectra.

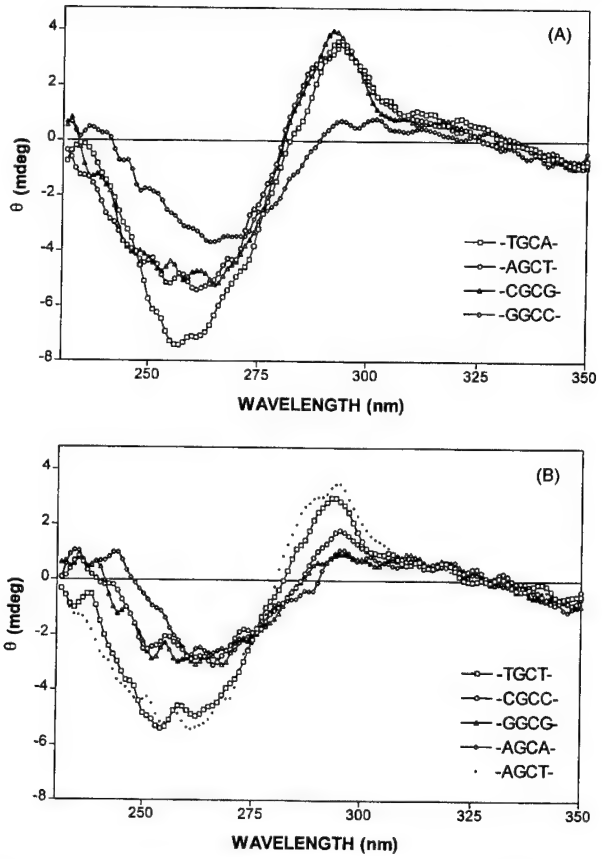

FIGURE 4: Comparison of CD difference spectra (ACTD/DNA - DNA) of 5 μM ACTD in 40 μM of self-complementary dodecamers of the form d(ATTA-XGCY-TAAT) (panel A) and mismatched dodecamers of the form d(ATTA-XGCX-TAAT) (panel B, with -AGCT- added for comparison). Measurements were made with 1-cm water-jacketed cylindrical cells at room temperatures.

CD Spectral Evidence of ACTD Binding. The effect of ACTD binding to a DNA duplex on the CD spectral characteristics is to induce sizable positive and negative CD intensities at the 293- and 255-nm regions, respectively. Thus, qualitative ACTD binding affinities for these oligomers can also be obtained via difference CD (ACTD/DNA − DNA) spectral comparison. The CD difference spectra of the dodecamers are compared in Figure 4. Except for -GGCC-, the three self-complementary sequences induce sizable and similar CD near 293 nm (panel A). In contrast, the dodecamer with T/T mismatches exhibits a larger CD difference spectrum than those of the other mismatched oligomers (panel B, with -AGCT- added for comparison) and is comparable to those of the self-complementary counterparts. The CD results are, thus, consistent with the relative binding order established via absorbance measurements.

ACTD Dissociates Slowly from d(ATTA-TGCT-TAAT). The representative non-stopped-flow-measurable dissociation kinetic traces are shown in Figure 5 and the results of least-squares fits are summarized in Table 2. It is immediately

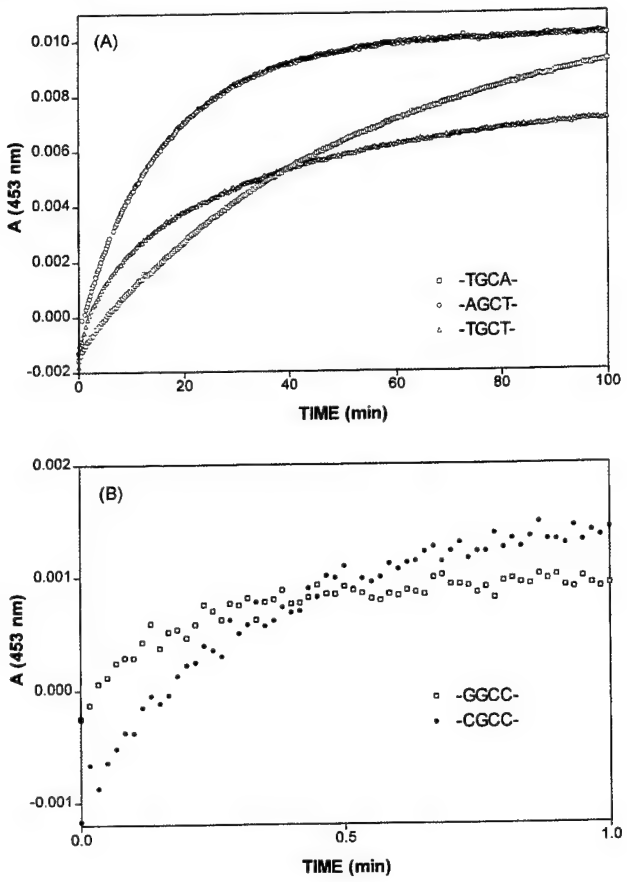

FIGURE 5: Representative 1% SDS-induced ACTD dissociation kinetic traces at 20 °C. (Panel A) Comparison of d(ATTA-TGCT-TAAT) (△) with self-complementary d(ATTA-TGCA-TAAT) (□) and d(ATTA-AGCT-TAAT) (○). (Panel B) Comparison of d(ATTA-GGCC-TAAT) (□) and d(ATTA-CGCC-TAAT) (●). Drug dissociation was initiated by adding an appropriate amount of 20% SDS solution to an ACTD (5μM) / DNA (40 μM) mixture. Kinetic traces were obtained via 453-nm monitoring in a 1-cm cell with use of a stirrer accessory.

Table 2: Comparison of Non-Stopped-Flow-Measurable ACTD Association and Dissociation Kinetics for Selected Dodecamers at 20 °C

oligomer	k_a (min^{-1})	k_d (min^{-1})
d(ATTA-TGCA-TAAT)	2.4	0.019
d(ATTA-AGCT-TAAT)	1.0	0.062
d(ATTA-CGCG-TAAT)	2.3	0.081
d(ATTA-GGCC-TAAT)		4.1
d(ATTA-AGCA-TAAT)	2.9	2.2
d(ATTA-TGCT-TAAT)[a]	1.3; 0.26 (48%)	0.20; 0.023 (68%)
d(ATTA-GGCG-TAAT)		1.9
d(ATTA-CGCC-TAAT)	4.8	2.2

[a] Values obtained via two-exponential fit, with the percent contribution only indicated for the slower component.

apparent (panel A) that the ACTD dissociation kinetic trace of the T/T-mismatched site is comparable to those of the self-complementary sequences but requires a two-exponential fit. Interestingly, its slower component (k = 0.023 min^{-1}) is only slightly faster than that of the -TGCA- site (0.019 min^{-1}) but is significantly slower than those of the -AGCT- (0.062 min^{-1}) and -CGCG- (0.081 min^{-1}) sequences (see Table 2). Furthermore, the ACTD dissociation rate from the GC site with flanking T/T mismatches is seen to be about 2 orders of magnitude slower than those of the other mismatches and that of -GGCC- (compare panels A and B; note the scale changes). It is also interesting to note that the association kinetics of ACTD to the dodecamer with T/T mismatches require a double-exponential fit. The slow component (0.26 min^{-1}) is significantly slower than the strong-binding self-complementary oligomers which can reasonably be approximated by single-exponential kinetics (1.0−2.4 min^{-1}) (see Table 2).

Effects of ACTD Binding on the Melting Temperatures of Oligomers. Thermal denaturation profiles with 275-nm monitoring for 40 μM DNA solutions in the absence and in the presence of ACTD were measured to investigate the effect of ACTD binding on the thermal stabilities of these oligomers. The results are included in Table 1. Due to the multiconformational states and the destabilization of the dimeric duplex resulting from the presence of base mismatches, these oligomers exhibit broad and diffuse melting profiles (not shown). The melting temperatures of the dimeric duplexes in 40 μM nucleotide solutions were estimated to be below 10 °C, from measurements with higher DNA concentrations. However, in the presence of 5 μM ACTD, the melting profile for the T/T-mismatched dodecamer exhibits a highly cooperative transition near 31 °C and the melting temperatures of the C/C and G/G mismatches have increased to about 23 and <20 °C, respectively. No apparent alteration on the melting profile was observed for the A/A-mismatched oligomer. These are to be compared with the melting temperatures of the strong-binding self-complementary dodecamers, which range from 34 to 43 °C, and the ACTD-induced melting temperature increases of 8−13 °C. The UV melting results of the DNA−ACTD complexes have also been corroborated by denaturation experiments via monitoring absorbance changes at 427 nm for the drug release (results not shown). Thus, the melting results also support the relative binding order established via spectral measurements.

Comparison with the Fluorescence Results of 7-Amino-actinomycin D. Although ACTD is only slightly fluorescent, its 7-amino derivative is strongly so. The amino group substitution does not greatly alter the intercalative binding mode of this derivative. It is, thus, of interest to corroborate the ACTD results with those of this derivative via fluorescence measurements. The fluorescence emission difference spectra with 560-nm excitation for the strong-binding self-complementary -XGCY-containing dodecamers exhibit a strong emission maximum near 650 nm (Figure 6A), suggesting fluorescence enhancements around this wavelength region when 7-AM-ACTD binds to these DNA. The much weaker binding of the -GGCC- sequence is again apparent via its negligible intensity enhancement. The fluorescence intensity induced by binding to the GC sequence with T/T mismatches (panel B) is seen to be comparable to that of the strong-binding self-complementary -XGCY- sequences. Interestingly, the intensity induced by binding to the site with flanking C/C mismatches is comparable to that of the self-complementary -CGCG- sequence. In contrast, the intensities for dodecamers with G/G mismatches are considerably smaller but are larger than those with A/A mismatches and -GGCC- sequence. The nearly identical spectral characteristics support the notion that the mode of binding at the GC site with flanking T/T mismatches is very similar to those of the strong-binding self-complementary -XGCY- sequences.

Kinetic measurements were also made by exciting the molecules with 560-nm light and monitoring emission at 650

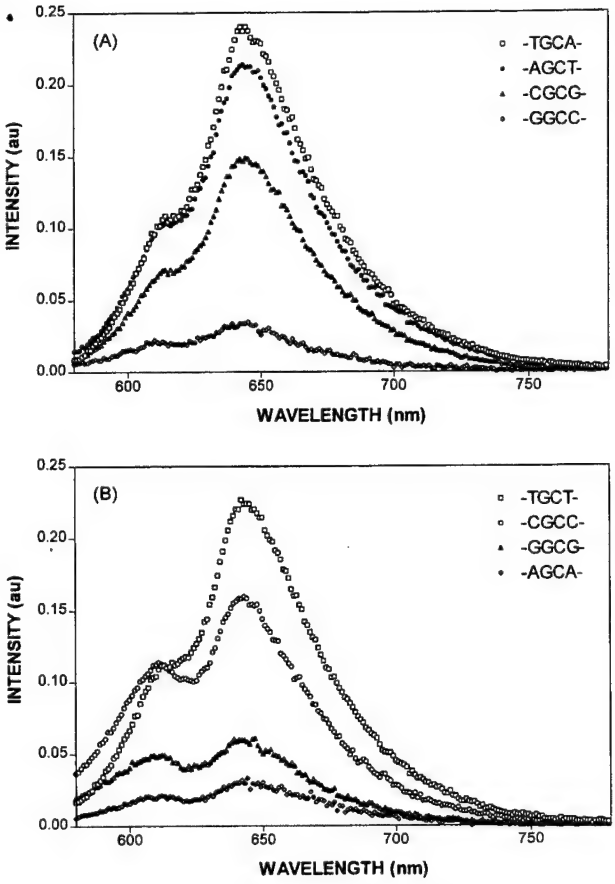

FIGURE 6: Comparison of fluorescence difference emission spectra (not corrected) at 20 °C of 1.5 μM 7-AM-ACTD in the presence of self-complementary dodecamers of the form d(ATTA-XGCY-TAAT) (panel A) and mismatched dodecamers of the form d(ATTA-XGCX-TAAT) (panel B). The spectra were obtained via 4-nm emission slit-width with 560-nm excitation and DNA concentrations of 40 μM.

Table 3: Comparison of 7-AM-ACTD Association and Dissociation Kinetics at 20 °C via Fluorescence Monitoring

oligomer	k_a (min^{-1})	k_d (min^{-1})
d(ATTA-TGCA-TAAT)	0.16	0.0031
d(ATTA-AGCT-TAAT)	0.12	0.011
d(ATTA-CGCG-TAAT)	0.22	0.014
d(ATTA-GGCC-TAAT)	5.8	1.5
d(ATTA-AGCA-TAAT)		6.0
d(ATTA-TGCT-TAAT)[a]	0.86; 0.16 (46%)	0.14; 0.022 (78%)
d(ATTA-GGCG-TAAT)		1.9
d(ATTA-CGCC-TAAT)	3.7	3.9

[a] Values obtained via two-exponential fit, with the percent contribution only indicated for the slower component.

nm for the association and at 600 nm for the SDS-induced dissociation of ACTD. Results of single- or double- (for the T/T-mismatched oligomer) exponential fits on these data are compared in Table 3. These results support our absorbance measurements indicating that the dodecamer with T/T mismatches flanking a GC sequence exhibits a much slower dissociation rate than those with C/C and other mismatches. It is worth noting that both the association and dissociation kinetics of 7-AM-ACTD in self-complementary oligomer solutions are considerably slower (some are almost an order of magnitude slower) than those of the parent ACTD but are not greatly different for the mismatched oligomers (compare Tables 2 and 3). This resulted in comparable association rates and much slower dissociation rates for

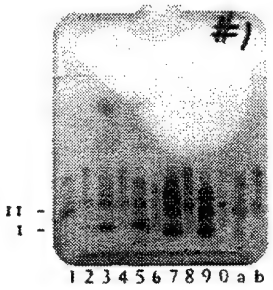

FIGURE 7: Comparison of electrophoretic mobility patterns of dodecamers at 4 °C in the absence (odd-numbered lanes and lane a) and in the presence (even-numbered lanes and lane b) of ACTD. Shown are d(ATTA-TGCA-TAAT) (lanes 1 and 2), d(ATTA-TGCT-TAAT) (lanes 3 and 4), d(ATTA-CGCC-TAAT) (lanes 5 and 6), d(AAAA-TGCT-TTTT) (lanes 7 and 8), d(AAAA-CGCC-TTTT) (lanes 9 and 0), and d(AAAA-TGCA-TTTT) (lanes a and b). [ACTD] = 0.17 mM and [DNA] was approximately 0.8 mM in nucleotides.

7-AM-ACTD at the -TGCA- sequence when compared to those at the T/T-mismatched site, contrary to the faster association rate and comparable dissociation rate observed for the parent ACTD.

Studies with d(AAAA-XGCX-TTTT). To see if the above results are peculiar to our chosen sequences of d(ATTA-XGCX-TAAT), studies were also made with dodecamers of the form d(AAAA-XGCX-TTTT) in which the terminal sequences have been altered. The results (not shown) confirm the strong binding and unusually slow dissociation of ACTD at the GC sequence with T/T flanking mismatches as well as weak binding at sequences with G/G and A/A mismatches. However, the observation of a significantly higher ACTD affinity and slower dissociation (still an order of magnitude faster than the T/T-mismatched oligomer) of d(AAAA-CGCC-TTTT) as compared to d(ATTA-CGCC-TAAT) manifests interesting sequence-dependent effects.

Electrophoretic Mobility Patterns of Oligomers and Their Drug Complexes. To further support the interpretation of our spectral results, electrophoretic measurements were made with dodecamers in the presence and in the absence of ACTD. Figure 7 compares the electrophoretic mobility patterns of selective oligomers at 4 °C. The multiconformational states of these oligomers are clearly evidenced by the presence of multiband and smearing features. The two self-complementary dodecamers d(ATTA-TGCA-TAAT) (lane 1) and d(AAAA-TGCA-TTTT) (lane a) are dominated by bands designated as II which can reasonably be assigned as those of dimeric duplex form. A slight retardation of this band is seen in the presence of ACTD (compare lanes 1 vs 2 and lanes a vs b), suggesting the formation of a complex with the dimeric duplex and the drug. Consistent with the dominant presence of hairpin species, all dodecamers with mismatches (lanes 3, 5, 7, and 9) exhibit prominent presence of electrophoretic bands designated as I which are considerably faster than those of the self-complementary counterparts. Despite the predominance of the hairpin form, the presence of ACTD resulted in the disappearance of band I and the appearance of retarded bands, which are nearly identical to those of the dimeric duplex−ACTD complexes of the self-complementary counterparts, for the T/T-mismatched oligomers (compare lanes 3 vs 4 and lanes 7 vs 8). Consistent with their weak ACTD binding affinities, oligomers containing G/G and A/A mismatches do not exhibit such retardations (results not shown). It is also interesting to note that whereas

d(ATTA-CGCC-TAAT) exhibits only intensity diminution of band I without the prominent appearance of the retarded dimeric duplex−ACTD complex band in the presence of ACTD (compare lanes 5 and 6), d(AAAA-CGCC-TTTT) induces retardation (compare lanes 9 and 0) that is very similar to that of T/T mismatches. This is consistent with the spectral results indicating that d(AAAA-CGCC-TTTT) exhibits stronger ACTD affinity than that of d(ATTA-CGCC-TAAT). These results support the notion of drug-induced allosteric conversion from hairpin to dimeric duplex and suggest that the binding affinities for the pyrimidine (pyr/pyr) mismatches are considerably higher than those with purine (pur/pur) mismatches.

It should be pointed out that possible impurities of 5% or less in our samples will not show up in our gel results. It is also interesting to note in passing that in addition to the prominent presence of the hairpin (I) and dimeric duplex (II) bands, a considerably slower moving band is apparent for each oligomer. The ACTD-induced retardation of its electrophoretic mobility is also clearly evident. It is reasonable to associate this band with that of the aforementioned tetrameric cruciform in which two of the side-arm duplexes contain GC sites. Indeed, the intensity of its retarded band is in concert with that of the corresponding ACTD-retarded band II of dimeric duplex, suggesting binding to the duplex side arms. It thus appears that despite the multiconformational states of the mismatched oligomers in solutions, our ACTD binding results largely reflect the relative ACTD binding affinities of -XGCX- in the duplex states.

DISCUSSION

Comparative electrophoretic, thermal denaturation, and spectroscopic studies with dodecamers of the form d(ATTA-XGCX-TAAT) and the corresponding self-complementary counterparts suggest that despite the dominance of hairpin conformations in solutions for mismatched oligomers, ACTD binds strongly to the GC sequence with flanking T/T mismatches and moderately to that with C/C mismatches but weakly to those of other homo-base mismatches. The relative binding order is found to be T/T > C/C > G/G > A/A. Spectral titrations indicate that the binding affinity of the T/T-mismatched dodecamer is comparable to or even stronger than the corresponding self-complementary -XGCY- sequences. However, the dodecamer with T/T mismatches exhibits surprisingly slow ACTD dissociation kinetics, with a rate more than an order of magnitude slower than those of oligomers with other mismatches but comparable to those of the -TGCA- and somewhat slower than the -AGCT- and -CGCG-containing sequences. The slow dissociation kinetic behaviors exhibited by this T/T-mismatched oligomer are corroborated by fluorescence measurements using 7-amino-ACTD, a fluorescent analog of ACTD. Fluorescence and absorbance spectral characteristics further indicate that the binding mode of the GC site with flanking T/T mismatches resembles those of the strong self-complementary -XGCY-containing sequences, which are known to be intercalative in nature.

The slow ACTD dissociation rate exhibited by the dodecamer containing T/T mismatches is rather unexpected, especially since it is comparable to that of the slow-dissociating -TGCA-containing dodecamer. One would have anticipated that the dimeric duplex destabilization caused by the presence of mismatched bases would have resulted in a very rapid drug dissociation. Thus, the observation of slow dissociation kinetics suggest that the T/T mismatches flanking the duplex 5′GC3′ site provide very favorable minor-groove environments (likely the consequence of its hydrophobicity and base size) for interactions with the pentapeptide rings of ACTD. In this connection, it may also be interesting to note that the site with C/C mismatches also exhibits significant ACTD affinity, whereas dodecamers with pur/pur mismatches exhibit unfavorable ACTD affinities. It thus appears that the bulkier purine bases result in a more distorted minor-groove environment, with the consequence of unfavorable interactions with the pentapeptide rings.

The unusual curvatures in the Scatchard plots exhibited by the mismatched dodecamers are also worth mentioning. This behavior may be understood by using the model presented in which the monomeric hairpin and dimeric duplex conformations are in dynamic equilibrium and ACTD only binds to the dimeric form. It can be shown that the Scatchard equation is now modified to $r/m = K_a (n - nL/L_t - r)$, where r, m, and n were defined in the legend of Figure 2 and L is the monomeric hairpin concentration. As L/L_t approaches unity (hairpin predominates), the equation reduces to a to a linear dependence of r/m vs r passing through the origin. On the other hand if L/L_t approaches zero (dimeric duplex predominates), the equation reduces to a regular Scatchard plot with the saturation binding density extrapolating to n. Thus, the exhibited unusual curvatures, with the appearance of data points emanating from the origin, can be seen as the consequence of the fact that the initial titration points correspond to dilute DNA concentrations, where monomeric hairpin conformations predominate, but later titration points eventually revert to "normal" Scatchard plots at higher DNA concentrations.

As noted earlier, the ACTD association kinetic trace for the dodecamer containing T/T mismatches requires a two-exponential fit with a significant contribution from a slow component which is considerably slower than those exhibited by the self-complementary sequences. The presence of this slow contribution and a multirate kinetic process may be the consequence of ACTD-induced allosteric conversion from the hairpin to the dimeric duplex form in drug binding.

The association as well as dissociation kinetics of 7-AM-ACTD are considerably slower than those of ACTD for the self-complementary sequences. This is consistent with the intercalative binding mode and the steric hindrance due to the presence of the amino group at the 7-position of ACTD. Such kinetic differentials between ACTD and 7-AM-ACTD are much less pronounced in the mismatched oligomers. This difference in kinetic behavior exhibited by the self-complementary vs mismatched sequences may likely be attributed to much lower duplex stabilities of the mismatched dimeric species and their drug complexes so that the hindrance presented by the 7-amino group becomes less critical.

Although the focus of this study is on the GC sequence with flanking homo-base mismatches, our results on the self-complementary dodecamers containing -XGCY- sequences are also of some interest. The dodecamer results are in general agreement with similar studies using decamers of the form d(ATA-XGCY-TAT) (Chen, 1988). The relative ACTD binding affinities are found to be -TGCA- > -CGCG- > -AGCT- >> -GGCC-, whereas the rate of ACTD

dissociation increases in the order -TGCA- < -AGCT- < -CGCG- << -GGCC-, with -TGCA- exhibiting the slowest dissociation kinetics. The fact that ACTD binds slightly more strongly to -CGCG- than to -AGCT- yet dissociates somewhat faster from the former suggests that the 2-amino group of guanine, which resides at the minor groove, may be one of the culprits of unfavorable interactions with the pentapeptide rings of the drug.

REFERENCES

Aivasashvilli, V. A,, & Beabealashvilli, R. S. (1983) *FEBS Lett. 160*, 124−128.

Akiyama, M., Maki, H., Sekiguchi, M., & Horiuchi, T. (1989) *Proc. Natl. Acad. Sci. U.S.A. 86,* 3949−3952.

Bailey, C., Graves, D. E., Ridge, G., & Waring, M. J. (1994) *Biochemistry 33,* 8736-8745.

Bailey, S. A., Graves, D. E., & Rill, R. (1994) *Biochemistry 33,* 11493−11500.

Bailey, S. A., Graves, D. E., Rill, R., & Marsch, G. (1993) *Biochemistry 32,* 5881−5887.

Brown, S. C., Mullis, K., Levenson, C., & Shafer, R. H. (1984) *Biochemistry 23,* 403−408.

Brown, D. R., Kurz, M., Kearns, D. R., & Hsu, V. L. (1994) *Biochemistry 33,* 651−664.

Chen, F.-M. (1988) *Biochemistry 27,* 6393−6397.

Chen, F.-M. (1992) *Biochemistry 31,* 6223−6228.

Chu, W., Shinomiya, M., Kamitori, K., Kamitori, S., Carlson, R. G., Weaver, R. F., & Takusagawa, F. (1994) *J. Am. Chem. Soc. 116*, 7971−7982.

Fasman, G. D., Ed. (1975) *CRC Handbook of Biochemistry and Molecular Biology*, 3rd ed., Vol. I, p 589, Chemical Rubber Company Press, Inc., Cleveland, OH.

Fletcher, M. C., & Fox, K. R. (1993) *Nucleic Acids Res. 21*, 1339−1344.

Fox, K. R., & Waring, M. J. (1984) *Nucleic Acids Res. 12*, 9271−9285.

Goodisman, J., & Dabrowiak, J. C. (1992) *Biochemistry 31,* 1058−1064.

Goodisman, J., Rehfuss, R., Ward, B., & Dabrowiak, J. C. (1992) *Biochemistry 31*, 1046−1058.

Hunter, W. (1992) *Methods in Enzymol. 211*, 221−231.

Kamitori, S., & Takusagawa, F. (1992) *J. Mol. Biol. 225*, 445−456.

Kamitori, S., & Takusagawa, F. (1994) *J. Am. Chem. Soc. 116*, 4154−4165.

Krugh, T. R. (1972) *Proc. Natl. Acad. Sci. U.S.A. 69*, 1911−1914.

Krugh, T. R., Mooberry, E. S., & Chiao, Y.-C. C. (1977) *Biochemistry 16,* 740−755.

Lane, M. J., Dabrowiak, J. C., & Vouurrnakis, J. N. (1983) *Proc. Natl. Acad. Sci. U.S.A. 80,* 3260−3264.

Liu, X., Chen, H., & Patel, D. J. (1991) *J. Biomol. NMR 1*, 323−347.

Modrich, P. (1987) *Annu. Rev. Biochem. 56,* 435−466.

Muller, W., & Crothers, D. M. (1968) *J. Mol. Biol. 35*, 251−290.

Patel, D. J. (1974) *Biochemistry 13*, 2396−2402.

Rehfuss, R., Goodisman, J., & Dabrowiak, J. C. (1990) *Biochemistry 29,* 777−781.

Rill, R. L., Marsch, G. A., & Graves, D. E. (1989) *J. Biomol. Struct. Dyn. 7*, 591−605.

Scamrov, A. V., & Beabealashvilli, R. Sh. (1983) *FEBS Lett. 164,* 97−101.

Scott, E. V., Jones, R. L., Banville, D. L., Zon, G., Marzilli, L. G., & Wilson, W. D. (1988) *Biochemistry 27*, 915−923.

Snyder, J. G., Hartman, N. G., D'Estantoit, B. L., Kennard, O., Remeta, D. P., & Breslauer, K. J. (1989) *Proc. Natl. Acad. Sci. U.S.A. 86,* 3968−3972.

Sobell, H. M., & Jain, S. C. (1972) *J. Mol. Biol. 68,* 21−34.

Takusagawa, F., Dabrow, M., Neidle, S., & Berman, H. M. (1982) *Nature 296,* 466-469.

Van Dyke, M. W., & Dervan, P. B. (1983) *Nucleic Acids Res. 11*, 5555−5567.

Van Dyke, M. W., Hertzberg, R. P., & Dervan, P. B. (1983) *Proc. Natl. Acad. Sci. U.S.A. 79*, 5470−5474.

Wadkins, R. M., & Jovin, T. M. (1991) *Biochemistry 30,* 9469−9478.

Waterloh, K., & Fox, K. R. (1992) *Biochim. Biophys. Acta 1131,* 300−306.

White, R. J., & Phillips, D. R. (1989) *Biochemistry 28,* 6259−6269.

Zhou, N., James, T. L., & Shafer, R. H. (1989) *Biochemistry 28,* 5231−5239.

BI961060D

Biochemistry

Is the Strong Actinomycin D Binding of d(5′CGTCGACG3′) the Consequence of End-Stacking?

Fu-Ming Chen and Chengdi Liu

Department of Chemistry, Tennessee State University, Nashville, Tennessee 37209-1561

Reprinted from
BIOCHEMISTRY, Volume 35, Number 22, Pages 7283–7291

Is the Strong Actinomycin D Binding of d(5′CGTCGACG3′) the Consequence of End-Stacking?†

Fu-Ming Chen* and Chengdi Liu

Department of Chemistry, Tennessee State University, Nashville, Tennessee 37209-1561

Received December 11, 1995; Revised Manuscript Received March 21, 1996®

ABSTRACT: It has been reported that ACTD binds strongly and cooperatively to a non-GC containing self-complementary octamer d(CGTCGACG) with a 2:1 drug to duplex ratio (Synder et al., 1989). If one views the classic intercalative preference of ACTD for the 5′GpC3′ sequence to be the drug favoring the 3′-side of dG, the possibility exists that the drug molecules may in fact stack on the G·C base pairs at both ends of this oligomeric duplex. To investigate this possibility, d(CGTCGACG) and several related oligomers resulting from replacing the terminal base(s) or appending with dT and/or dA are used in a comparative study employing equilibrium titration, thermal denaturation, kinetic, and various spectral measurements. Absorbance titrations at 20 °C confirm the strong and highly cooperative nature of ACTD binding to this octamer. The stoichiometric association constants for the binding of the first and second drugs were found to be 1×10^5 and 3.2×10^7 M^{-1}, respectively. The base replacements of dG and dC at the respective ends resulted in a much weaker ACTD binding affinity, the loss of binding cooperativity, and much faster association and dissociation kinetics. These are consistent with the inability of the drug to stack on the 3′-side of dG due to base replacements. Appending the end(s) with dA and/or dT resulted in some diminution of binding affinity and cooperativity, appearance of slower association kinetic components, and unusually strong 7-amino-ACTD fluorescence enhancement for oligomers with dA or dT attached to dG at the 3′-terminal. To further support our postulate, studies were also made with d(CGACGTCG), which is related to the parent octamer by inverting the A·T pairs. It was found that, despite the altered internal sequence, this oligomer exhibits cooperative ACTD binding and kinetic characteristics very similar to those of the parent octamer, consistent with its ability to end-stack on the 3′-side of dG.

Actinomycin D (ACTD) is a chromopeptide antibiotic which consists of a 2-aminophenoxazin-3-one chromophore and two identical cyclic pentapeptide side chains. It has been well established that this drug prefers duplex DNA and binds via intercalation of the planar chromophore (Muller & Crothers, 1968; Waring, 1970; Sobell & Jain, 1972), preferably at the GpC sequence, with the two pentapeptide rings resting on the minor groove. X-ray studies (Sobell et al., 1971; Kamitori & Takusagawa, 1992) have clearly shown that its duplex and GpC sequence preference is the consequence of the ability of the carbonyl oxygens and the NH groups of the L-threonine residues to form hydrogen bonds with the 2-amino group and the N(3) of guanines on both sides of the intercalated drug. However, there have been recent reports to indicate that ACTD can also bind strongly to some non-GC sequences (Synder, et al., 1989; Rill et al., 1989; Bailey et al., 1994) as well as to some single-stranded DNA (Wadkins & Jovin; 1991). In particular, calorimetric studies by Synder et al. (1989) had led to the conclusion that ACTD binds cooperatively to the octamer d(5′CGTCGACG3′) with a binding constant higher than 10^7 M^{-1} and a 2:1 drug to duplex ratio. It is important to understand the nature of such a strong binding and to delineate the origin of its high cooperativity. Since it has been suggested by Snyder et al. (1989) that the mode of ACTD binding to d(CGTCGACG) is distinct from its classic mode of binding to GpC sequence, it will be of value to see if this is in fact the case. The possibility that the cooperative and strong ACTD binding of this oligomer is a consequence of the drug molecules stacking at the ends of the DNA duplex is hereby investigated. The basis for such a speculation stems from the fact that if one is to view the classic preferred ACTD intercalative site as G3′p5′C, then it follows that the drug favors stacking and hydrogen bonding at a G·C base pair on the 3′-side of dG. To elucidate the possibility of ACTD stacking at the duplex ends of d(CGTCGACG), comparative binding, melting, and kinetic studies were carried out with oligomers of the form d(XGTCGACY), in which X = A, T, G, or C, and d(X-CGTCGACG), d(CGTCGACG-Y), and d(X-CGTCGACG-Y) in which X is A or T, with Y being complementary to X. It is reasoned that if end-stacking of ACTD on the 3′-side of dG is the culprit, the replacement of the terminal dG by another base and a concomitant complementary replacement at the other end will lead to a considerable reduction in the ACTD binding affinity. In contrast, minimal alteration in binding characteristics should result if it is due to the internal sequence binding. Such a rationale should be particularly valid for the base-added oligomers, where the entire 8 base-paired duplex is now intact with only a dangling base or a base pair being appended to each end. On the other hand, significant effects on the binding behaviors will be expected for these oligomers

† Research Supported by USPHS Grant CA-42682 and Army Medical Research Grant DAMD17-94-J-4474.

* Corresponding author, Dr. Fu-Ming Chen at the Department of Chemistry, Tennessee State University, Nashville, TN 37209-1561. Tel: (615) 963-5325; FAX: (615) 963-5434; E-Mail: chenf@acad.tnstate.edu.

® Abstract published in *Advance ACS Abstracts,* May 1, 1996.

S0006-2960(95)02907-2 CCC: $12.00

if the end-stacking mechanism is operative. Additional studies were also made with d(CGACGTCG), which is related to the parent octamer by inverting the A·T base pairs without altering the terminal bases and should thus retain its end-stacking abilities. The results of these experiments and their significance are presented and discussed in this report.

MATERIALS AND METHODS

Oligonucleotides were purchased from Integrated DNA Technologies, Coralville, IA and used without further purification. Concentrations of these oligomers (per nucleotide) were determined by measuring the absorbances at 260 nm after melting, with use of extinction coefficients obtained via nearest-neighbor approximation using mono- and dinucleotide values tabulated by Fasman (1975). The extinction coefficients used for drug concentration determination are 24 500 M^{-1} cm^{-1} at 440 nm for ACTD and 23 600 M^{-1} cm^{-1} at 528 nm for 7-amino-ACTD. All experiments were carried out in 10 mM HEPPS (N-(2-hydroxyethyl)piperazine-*N*′-propanesulfonic acid) buffer solutions of pH 8 containing 0.1 M NaCl. Absorption spectra were measured with a Cary 1E spectrophotometric system. Absorbance changes at 427 and 480 nm were used to obtain Scatchard plots. Thermal denaturation experiments were carried out with 1-cm semimicro cells by monitoring absorbances at 275 or 427 nm. A heating rate of 0.5 °C/min was maintained by the temperature controller accessory. Melting temperatures were determined via differential melting plots.

Circular dichroic (CD) spectra were measured at room temperature with a Jasco J-500A recording spectropolarimeter using water-jacketed cylindrical cells of 1-cm path length. Fluorescence measurements were made with an SLM48000S system. Stopped-flow kinetic measurements were made with an Olis RSM-1000 rapid scan spectrophotometer. Nonlinear least-squares fits on the kinetic data and binding isotherms were carried out with the MINSQ program of Micromath (Salt Lake City, UT).

RESULTS

Equilibrium Binding Titrations. (A) Qualitative Binding Order. Spectral measurements indicate that the binding of DNA to ACTD results in an absorbance increase and decrease at the 480 and 427 nm spectral regions of the drug, respectively. Thus, a comparison of absorbance difference spectra at a given P/D ratio, where P and D are nucleotide and drug concentrations, respectively, can provide qualitative ACTD binding orders for these oligomers. Representative absorbance difference spectra at P/D = 10 are compared in Figure 1 for these oligomers. It is apparent that the qualitative ACTD binding order for the d(XGTCGACY) series (panel A) is as follows: d(CGTCGACG) > d(GGTCGACC) > d(TGTCGACA) ≥ d(AGTCGACT). On the other hand, the order for the oligomers containing terminally-added base(s) of dA and/or dT (panel B) is found to be the following: d(CGTCGACG) > d(CGTCGACG-T) ≥ d(A-CGTCGACG) > d(CGTCGACG-A) ≥ d(T-CGTCGACG) ≅ d(A-CGTCGACG-T) > d(T-CGTCGACG-A). It is apparent that the replacement and blocking of the 5′-end of dC and/or 3′-end of dG had considerably diminished the

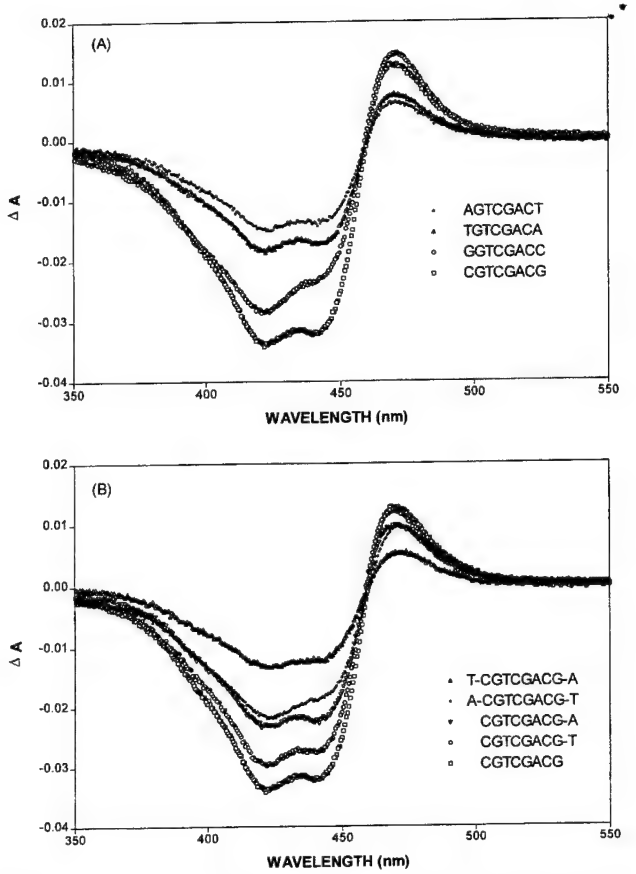

FIGURE 1: Absorbance difference spectra (ACTD/DNA − ACTD) for P/D = 10 at 20 °C. (A) Comparison for octamers of the form d(XGTCGACY). (B) Representative plots for oligomers formed by adding dA and/or dT to the terminal(s) of d(CGTCGACG). The difference spectra for oligomers with dA and dT attached to the dC of the 5′-terminal are somewhat smaller than the corresponding oligomers with dT and dA attached to the dG of the 3′-terminal, respectively, and are thus not shown.

oligomer's ability to bind ACTD. In addition, the binding affinities are strongly dependent on the nature and the location of the replacing/blocking base(s). The moderate ACTD binding to d(GGTCGACC) most likely is the consequence of binding to the GG/CC sequence.

(B) Scatchard Plots. To obtain more quantitative binding parameters, results of spectral titrations were converted to binding isotherms. Scatchard plots were constructed using absorbance differences between 427 and 480 nm, and the representative plots are shown in Figure 2. It is apparent that the plot for d(CGTCGACG) is decidedly curved and its binding parameters cannot be obtained via linear least-squares fits. It is also clear that the oligomers with the terminal base replacements had significantly diminished binding affinities, as evidenced by the much reduced slopes (panel A). Their binding constants were estimated from linear least-squares fits, and their values are included in Table 1. Effects due to the terminal addition with A and/or T base(s) can be seen in panel B, where representative plots are compared with the parent octamer. Although the weaker binding plots appear to be linear, the stronger binding ones are decidedly curved. Thus, a more straightforward approach was taken by directly fitting the experimental binding isotherms with a binding model.

(C) Fitting the Binding Isotherms with a Binding Model. If ACTD were to bind via end-stacking, two binding sites

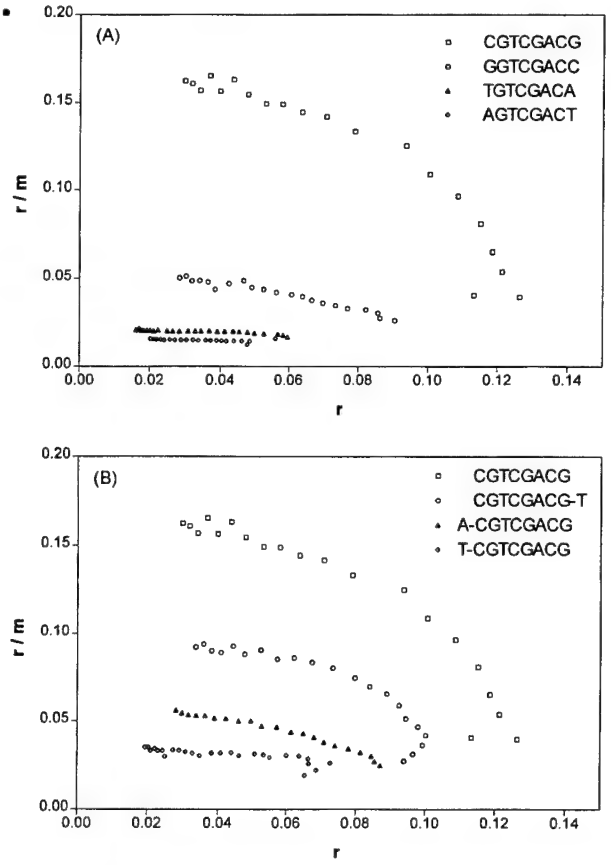

FIGURE 2: Scatchard plots derived from absorbance titrations at 20 °C. (A) Comparison of the d(XGTCGACY) oligomers. (B) Representative plots for oligomers with dA and/or dT added to either or both ends of the parent octamer d(CGTCGACG). Absorbance difference between 427 and 480 nm has been used to construct the plots. [Bound drug]/[DNA, nucleotide] is designated by *r*, and *m* represents the free drug concentration.

are available. Thus, the following binding model was assumed:

$$S + L_2 \overset{K_1}{\rightleftharpoons} SL_2 \qquad S + SL_2 \overset{K_2}{\rightleftharpoons} S_2L_2$$

where S and L_2 represent the drug and oligomeric duplex, respectively. With use of mass balance equations of the DNA and drug concentrations, the following equations can be derived:

$$K_1K_2S^3 + [K_1K_2(L_t - S_t) + K_1]S^2 + [K_1(0.5L_t - S_t) + 1]S - S_t = 0 \quad (1)$$

$$L_2 = (L_t - S_t + S)/(2 + K_1S) \quad (2)$$

$$\Delta A = [\epsilon_S + \epsilon_1K_1L_2(1 + 2K_2S)]S \quad (3)$$

where ΔA is the observed absorbance difference between 427 and 480 nm. ϵ_S and ϵ_1 are extinction coefficients of the free and bound drugs, respectively. L_t and S_t are the respective total DNA oligomeric (in strand) and drug concentrations. These equations were used to extract binding parameters via nonlinear least-squares fits on the experimentally observed data. As can be seen in Figure 3, excellent fits are obtained for most of the binding isotherms, and the extracted binding parameters from these fits are included in Table 1 for comparison. Of particular interest are the values

Table 1: Summary of Binding and Melting Parameters[a]

DNA Oligomer	K_a (μM^{-1})	K_1 (μM^{-1})	K_2 (μM^{-1})	$T_m°$ (°C)	ΔT_m (°C)
CGACGTCG	-	0.08	35.6	42	21
AGTCGACT	< 0.1	-	-	36	6
TGTCGACA	< 0.1	-	-	34	9
GGTCGACC	0.38	-	-	40	6
CGTCGACG	-	0.11	31.5	45	20
A-CGTCGACG	-	0.87	0.80	49	14
CGTCGACG-T	-	0.70	4.16	45	18
A-CGTCGACG-T	-	0.56	0.15	52	14
T-CGTCGACG	-	0.22	0.94	47	13
CGTCGACG-A	-	0.03	7.96	45	16
T-CGTCGACG-A	-	0.03	0.96	50	11

[a] K_a is the binding constant estimated via linear least-squares fit of the Scatchard plot. K_1 and K_2 are stoichiometric association constants for binding one and two molecules, respectively. The values are extracted via nonlinear least-squares fit using eqs 1−3 in the text. $T_m°$ is the melting temperature of 40 μM (nucleotide) oligomeric solution, and ΔT_m is the melting temperature increase in the presence of 7 μM ACTD.

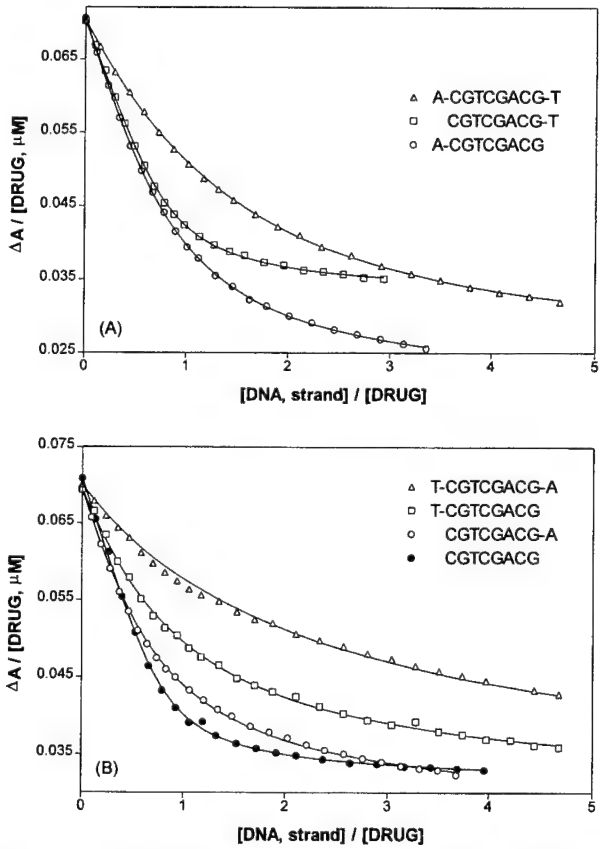

FIGURE 3: Comparison of the experimental binding isotherms at 20 °C and the theoretically fitted curves (connected lines) using the binding model and eqs 1−3 as described in the text. Panel A: Plots for oligomers of the form (A)-CGTCGACG-(T). Panel B: For oligomers of the form (T)-CGTCGACG-(A) and the parent octamer.

found for d(CGTCGACG) of 1×10^5 and 3.2×10^7 M^{-1} for the binding constants K_1 and K_2, respectively. The highly cooperative nature of ACTD binding to this octamer is confirmed by $K_2 \gg K_1$ in which binding of the second drug

is much stronger than that of the first. Although a good nonlinear least-squares fit does not guarantee the correctness of the model, the finding of a highly cooperative binding for the parent octamer and the considerably reduced binding affinities and cooperativities for the terminally replaced or base-added oligomers suggest the plausibility of the assumed model. It is interesting to note that significant binding affinity and cooperativity are retained in d(CGTCGACG-T) and d(CGTCGACG-A) (see Table 1).

It should be pointed out that K_1 and K_2 in the above model are stoichiometric rather than microscopic binding constants. They are, however, related and in the special case of two identical binding sites can be shown (Connors, 1987) to be:

$$K_1 = 2k_{11} \quad \text{and} \quad K_2 = wK_1/4$$

where k_{11} is the microscopic binding constant for the formation of 1:1 drug to duplex complex and w is the interaction (or cooperativity) parameter which measures the extent of interaction between the two sites in a 2:1 complex formation.

Thermal Denaturation Measurements. The extent of melting temperature increases upon drug binding can also provide information on the drug binding affinity of a DNA. Melting temperatures of the oligomers and the increases upon ACTD binding are also included in Table 1 for comparison. It is apparent that the pattern of melting temperature increases is in general agreement with that of binding affinities. For example, the ACTD-induced melting temperature increase is about 20 °C for d(CGTCGACG), whereas it is less than 10 °C for any of the terminally replaced oligomer, in agreement with their much reduced binding affinities. In addition, the base-added oligomers exhibit somewhat smaller melting temperature increases than that of the parent octamer. Consistent with the retention of significant binding affinity and cooperativity, a dT or dA addition to the 3′-end of dG resulted in the largest drug-induced duplex stability among the derived oligomers.

Stopped-Flow Kinetic Measurements via Absorbance Monitoring. (A) Association Kinetics. Association kinetic measurements were made by mixing equal volumes of 8 μM ACTD and 100 μM (nucleotide) DNA in a stopped-flow rapid-scanning instrument. Representative kinetic profiles with 428-nm absorbance monitoring are shown in Figure 4, and the results of 1- or 2-exponential fit along with their total absorbance changes are compared in Table 2. As can be seen from Figure 4A, the two oligomers with terminal A·T base pair replacement exhibit small absorbance changes and fast association kinetics with characteristic times of around 0.25 s at 20 °C. Despite an observed significant total absorbance change, the oligomer d(GGTCGACC) exhibits even faster association kinetics, with a measured slowest association characteristic time of around 0.04 s. In contrast, nearly 50% of the absorbance changes were measurable by the stopped-flow technique for d(CGTCGACG), with the bulk of the measured changes exhibiting the slow characteristic association time of around 14 s. Interestingly, oligomers with bases added to both ends exhibit significantly smaller total absorbance changes and slower association kinetics than those of oligomers with a dangling base, which in turn are slower than the parent octamer. It should also be noted that the two oligomers with respective dangling dT and dA added to the 3′-end of dG exhibit the largest

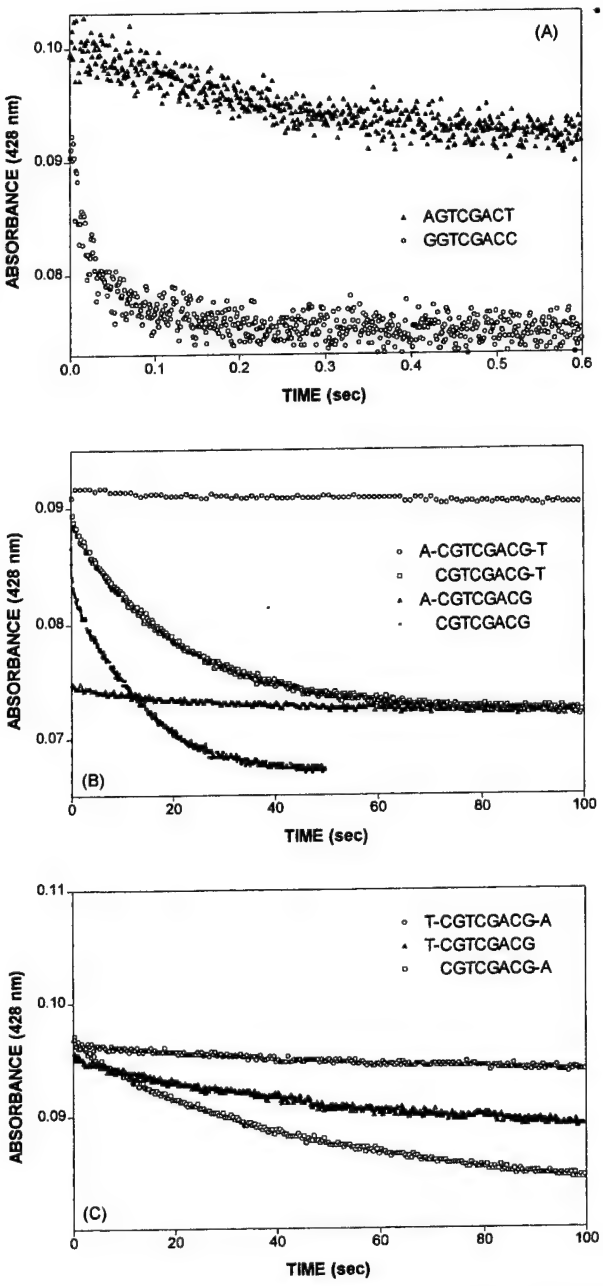

FIGURE 4: Typical ACTD association kinetic profiles with 428-nm absorbance monitoring at 20 °C. Panel A: GGTCGACC (○) and TGTCGACA ≅ AGTCGACT (△). Panel B: Comparison of CGTCGACG and oligomers of the form (A)-CGTCGACG-(T). Panel C: Oligomers of the form (T)-CGTCGACG-(A).

absorbance changes for the slow association component (see panels B and C) and the magnitudes of the total absorbance changes ΔA_t (see Table 2) are in general agreement with the qualitative binding orders established in the earlier section.

(B) Dissociation Kinetics. SDS-induced ACTD dissociation kinetics were also measured at 20 °C. The results indicate that, in the d(XGTCGACY) series, only the parent octamer d(CGTCGACG) exhibits a slow enough dissociation kinetics to be measured by the stopped-flow technique to yield a characteristic dissociation time of 0.8 s. Except for d(CGTCGACG-T), the considerably smaller binding-induced total absorbance changes of the base-added oligomers prevented us from obtaining meaningful dissociation kinetic profiles. Nevertheless, a dissociation time of about 1.3 s is

Table 2: Summary of Association Kinetic Parameters of ACTD at 20 °C[a]

DNA Oligomer	τ_f (s)	% (fast)	τ_s (s)	% (slow)	ΔA_t
CGACGTCG	0.22 ± 0.03	6.1	10.3 ± 0.2	36.5	0.0386
AGTCGACT	0.26 ± 0.02	62.8			0.0156
TGTCGACA	0.24 ± 0.01	69.4			0.0170
GGTCGACC	0.04 ± 0.003	42.1			0.0335
CGTCGACG	0.14 ± 0.02	4.8	14.1 ± 0.4	42.4	0.0397
A-CGTCGACG	0.17 ± 0.03	8.2	52.6 ± 5.5	7.0	0.0348
CGTCGACG-T	0.15 ± 0.01	6.7	34.5 ± 1.2	50.8	0.0341
A-CGTCGACG-T	0.15 ± 0.03	21.1	222 ± 30	14.9	0.0178
T-CGTCGACG	0.20 ± 0.02	20.3	55.5 ± 3.1	37.7	0.0175
CGTCGACG-A	0.16 ± 0.01	17.3	50.0 ± 2.5	55.9	0.0238
T-CGTCGACG-A	0.15 ± 0.01	34.8	109 ± 2	24.9	0.0140

[a] τ_f and τ_s are the fast and slow components of the 428-nm association kinetic trace as extracted via 1- or 2-exponential fit. ΔA_t is the total absorbance change.

obtained for the base-added oligomer d(CGTCGACG-T), which is slower than that of the parent octamer.

(C) Circular Dichroic Spectral Characteristics. Binding of ACTD to DNA induces a characteristic positive and negative CD maxima near 293 and 270 nm, respectively. Thus, the extent of induced CD intensity at these wavelengths can be used to provide qualitative binding information. Representative CD difference spectra (drug/DNA − DNA) are compared in Figure 5. Consistent with the absorbance results, d(CGTCGACG) exhibits the largest CD intensity enhancement at 293 nm. Much weaker CD intensities were induced at this wavelength for the end-base-replaced oligomers (panel A). The distinctly different induced CD spectral characteristics can also clearly be seen. The progressive reduction of the 293-nm CD intensity on the base-added oligomers are also apparent (panels B and C). Thus, the CD measurements are in general agreement with the binding order established earlier via absorbance titrations. CD spectral measurements in the 520−320 nm region were also made to indicate weak broad positive maxima near 460 nm (not shown), in agreement with the work of Snyder et al. (1989).

Fluorescence Spectral Enhancement of 7-Amino-ACTD. (A) Emission Spectral Characteristics. In contrast to ACTD, its 7-amino derivative is highly fluorescent. Despite the presence of an amino group at the 7 position, its DNA binding mode has been shown to be similar to that of ACTD (Chiao et al., 1979). Thus, this compound was used for the fluorescence binding studies. Binding of 7-AM-ACTD to an oligomeric duplex containing a GpC sequence usually results in a strongly enhanced fluorescence emission spectrum exhibiting a maximum at 650 nm and a shoulder near 610 nm. Fluorescence intensity enhancement patterns for 7-AM-ACTD upon binding to d(CGTCGACG) and the related oligomers are compared in Figure 6 as difference spectra (drug/DNA − drug). It is immediately apparent that,

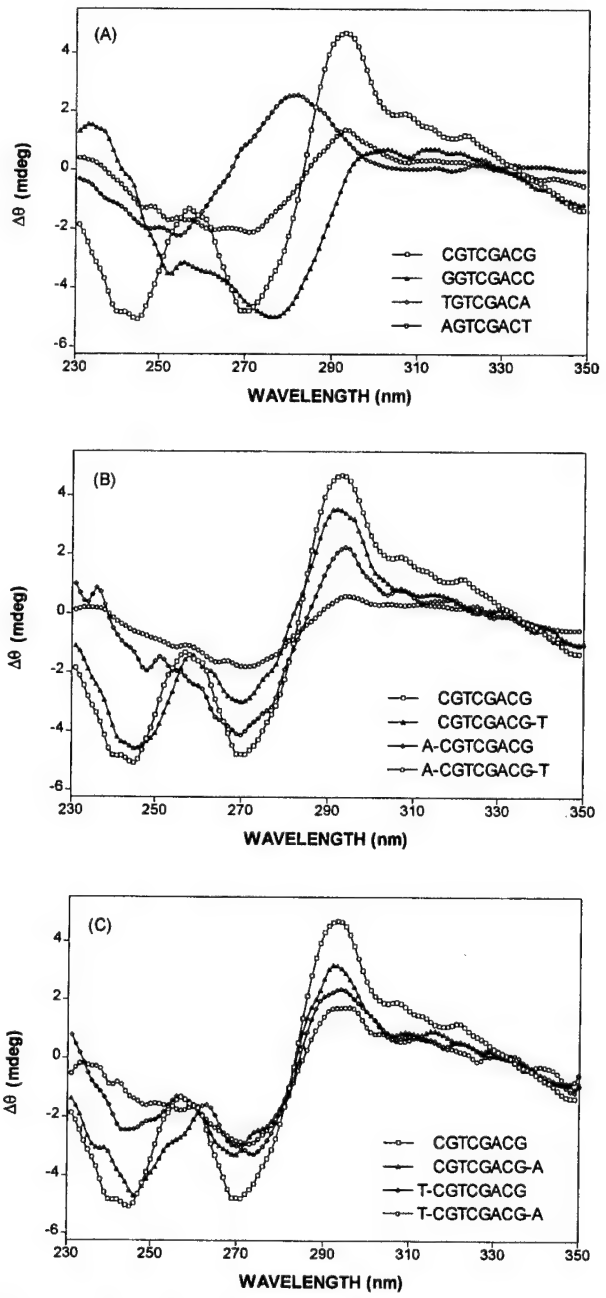

FIGURE 5: Comparison of difference CD spectra at room temperature for 5 μM ACTD in 40 μM/base of oligonucleotide solutions with the contributions due to DNA subtracted. Panel A: Octamers of the form XGTCGACY. Panel B: Oligomers of the form (A)-CGTCGACG-(T). Panel C: Oligomers of the form (T)-CGTCGACG-(A).

in contrast to the GpC containing oligomers, d(CGTCGACG) and the base-added oligomers induced a much stronger fluorescence enhancement at 610 nm than at 650 nm. This results in a double-humped spectral pattern, with the intensity of the former now being larger than that of the latter. Panel A compares the effect of adding dA to the 5′-terminal and/or dT to the 3′-terminal of the parent octamer on the fluorescence spectral patterns of 7-AM-ACTD. Consistent with its weaker ACTD binding, d(A-CGTCGACG) induces a smaller fluorescence intensity enhancement than that of d(CGTCGACG). In contrast, a dramatic intensity enhancement much more than the parent octamer is induced by d(CGTCGACG-T), and despite its considerably weaker binding affinity, d(A-CGTCGACG-T) induces nearly identi-

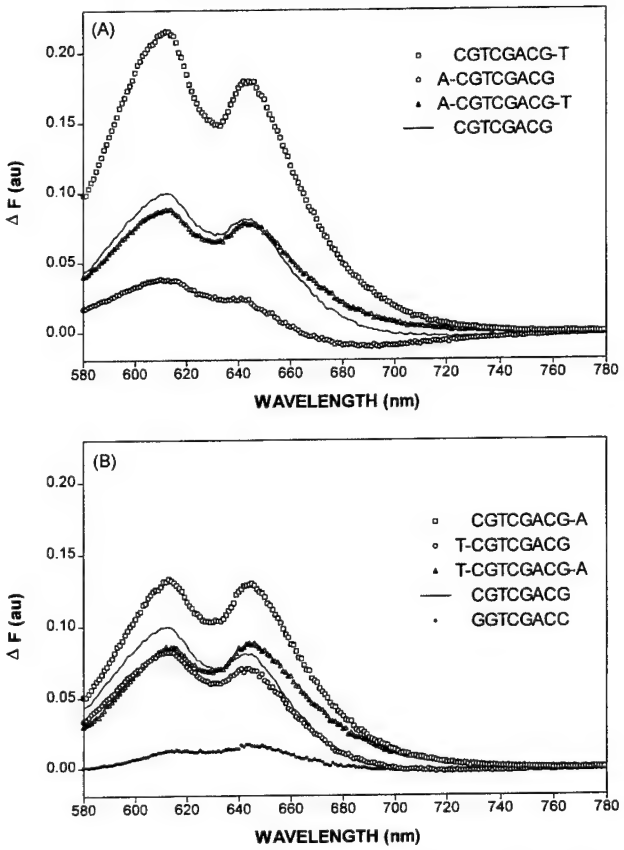

FIGURE 6: DNA-induced fluorescence emission spectral characteristics of 2 μM 7-amino-ACTD at 20 °C. Panel A: Comparison of the parent octamer and oligomers of the form (A)-CGTCGACG-(T). Panel B: Comparison with oligomers of the form (T)-CGTCGACG-(A) and GGTCGACC.

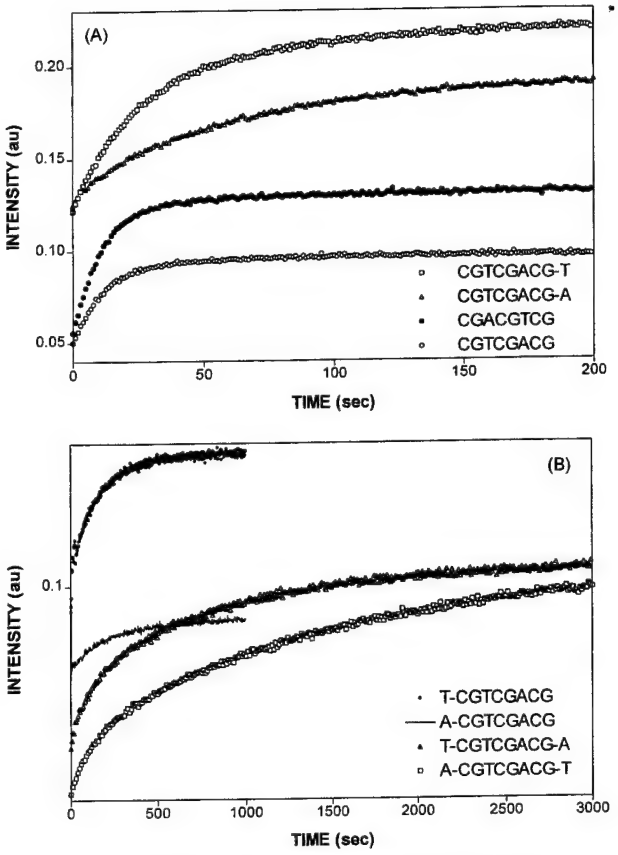

FIGURE 7: Association kinetic profiles of 7-AM-ACTD at 20 °C via fluorescence monitoring at 610 nm. Excitation wavelength is at 550 nm. Panel A: Comparison of d(CGTCGACG) and d(CGACGTCG) vs d(CGTCGACG-X), where X = A or T. Panel B: Comparison of d(X-CGTCGACG) and d(X-CGTCGACG-Y), where X = A or T and Y is complementary to X.

cal intensity enhancement as that of the parent octamer (panel A). Similarly, d(CGTCGACG-A) induces a stronger fluorescence intensity enhancement than its parent octamer, but the effect is not as dramatic as that of dT attachment (see panel B). Also, despite their weaker binding affinities, d(T-CGTCGACG) and d(T-CGTCGACG-A) induced nearly identical fluorescence enhancements as that of the parent octamer. As for the end-base-replaced octamers, significantly weaker fluorescence enhancements than the parent octamer were observed (see also panel B).

(B) Fluorescence Kinetic Measurements. In contrast to the small absorbance changes for some of the base-added oligomers, those of the corresponding fluorescence changes are quite considerable even for the oligomers with bases added to both ends. Thus, the slow component of the association kinetics, which was barely discernible via absorbance monitoring, can now be seen clearly in the fluorescence monitoring. The association kinetic profiles at 20 °C for the base-added oligomers are shown in Figure 7. It is immediately apparent that the association kinetics for the base-added oligomers are considerably slower than those of the parent octamer. In particular, the decamers with terminal A·T base pairs exhibit more than an order of magnitude slower kinetics than the parent octamer. The nonlinear least-squares fitted kinetic parameters with 1- or 2-exponential equation are summarized in Table 3.

SDS-induced dissociation kinetics were also measured. These non-stopped-flow measurable dissociation kinetic profiles can be adequately fitted with single exponential decays, and the extracted parameters were also included in Table 3 for comparison. It is apparent that the rates of dissociation for the base-added oligomers are considerably slower than that of the parent octamer. Also, the rates of dissociation show strong dependence on the nature and the location of the attached base(s).

Studies with d(CGACGTCG). To further support our thesis on end-stacking, studies were also made with d(CGACGTCG) which is related to the parent octamer by inverting the A·T base pairs without altering the terminal bases. This oligomer is expected to bind well to ACTD if end-stacking is the culprit. Indeed, the following are found: (1) that ACTD binds strongly to this oligomer with high cooperativity, as indicated by the considerable curvature of its Scatchard plot (not shown) and the respective values of 1×10^5 and 3.6×10^7 M^{-1} for K_1 and K_2 (see Table 1) obtained via nonlinear least-squares fit on its binding isotherm using the described binding model; (2) that the ACTD-induced CD exhibits a sizable positive intensity near 293 nm as well as 460 nm; (3) that the melting temperature increase upon drug binding is around 21 °C; and (4) that the characteristic association and SDS-induced dissociation times were estimated to be 10 and 0.6 s, respectively. Furthermore, this oligomer induces strong fluorescence intensity enhancement, exhibiting a 600-nm maximum (not shown). All these characteristics are very similar to those of the parent octamer d(CGTCGACG).

Table 3: Summary of Fluorescence Kinetic Parameters of 7-AM-ACTD at 20 °C[a]

DNA Oligomer	τ_1 (s)	% (1)	τ_2 (s)	% (2)	τ_d (s)
CGACGTCG	12.7 ± 0.2	62			~1
AGTCGACT					
TGTCGACA					
GGTCGACC					
CGTCGACG	13.7 ± 0.2	57			~1
A-CGTCGACG	232 ± 5	~100			15.5 ± 1.4
CGTCGACG-T	32.8 ± 0.4	67			3.3 ± 0.1
A-CGTCGACG-T	169 ± 6	18	1640 ± 19	51	7.1 ± 0.5
T-CGTCGACG	150 ± 2	65			19.1 ± 1.2
CGTCGACG-A	59.2 ± 0.4	58			25.6 ± 1.3
T-CGTCGACG-A	119 ± 6	20	813 ± 13	42	16.9 ± 1.2

[a] τ_1 and τ_2 are characteristic association times, and τ_d is the characteristic SDS-induced dissociation time.

DISCUSSION

Consistent with previous calorimetric studies of Synder et al. (1989), our equilibrium binding titrations indicate that d(CGTCGACG) binds strongly to ACTD and exhibits very high cooperativity to result in a 2:1 drug to DNA complex. Nonlinear least-squares fits of the experimental binding isotherms with a binding model yielded stoichiometric binding constants of 1×10^5 and 3.2×10^7 M^{-1} for the 1- and 2-drug binding processes, respectively. In support of our postulate that the strong ACTD binding of this octamer is the consequence of ACTD stacking on the 3′-side of dG at the terminal G·C base pairs, the replacement of G at the 3′-terminal by A, T, or C and the complementary base at the other end resulted in more than an order of magnitude reduction in the binding affinities, the loss of binding cooperativity, the considerably smaller ACTD-induced melting temperature increases, and the much faster drug−DNA association as well as dissociation kinetics. The weak binding of d(AGTCGACT), d(TGTCGACA), and even d(GGTCGACC) which contains as many G·C base pairs as in the parent octamer may partly be due to the decreased duplex stability, as indicated by their lower melting temperatures (see Table 1). However, the most likely reason for these observations is the absence of dG at the 3′-terminal in these oligomers for the ACTD end-stacking.

To further support our thesis on end-stacking, studies were also made with oligomers by appending dA or dT to the 5′- and/or 3′-ends, the rationale being that, by adding a dT or dA to the terminal(s) without altering the 8-base self-complementary internal sequence, minimal effect on the binding affinity will be expected if binding occurs at the internal sequences. On the other hand, significant alteration on the binding characteristics should occur if end-stacking to the G·C base pairs is the culprit. The results indicate that, in contrast to their parent octamer, these oligomers exhibit significantly weaker ACTD binding affinities with considerably reduced cooperativity as more bases are added. In addition, association kinetic measurements indicate that each end-base-added oligomer exhibits a slow association component which is significantly slower than that of the parent octamer. In particular, the oligomeric duplexes with A·T base pairs at both ends exhibit considerably weaker binding and slower association kinetics than the corresponding duplexes with a dangling A or T at the end. These results are consistent with the drug molecules stacking at the duplex ends. Interestingly, both the binding and kinetic characteristics are strongly dependent on the nature and the location of the added bases. For example, the (A)-CGTCGACG-(T) series of oligomers exhibit somewhat higher binding affinities than the corresponding (T)-CGTCGACG-(A) counterparts. Significant ACTD binding affinity and cooperativity are retained when dA or dT is added to the 3′-end of dG, whereas weaker binding and cooperativity are apparent for oligomers with dA or dT attached to the 5′-end of dC.

Despite the fact that the extent of fluorescence enhancements of 7-amino-ACTD do not exactly correlate well with the binding order of oligomers studied, the fluorescence results appear to provide the most convincing evidence that the binding of ACTD to d(CGTCGACG) occurs at the duplex termini rather than at the internal sequences. If the binding were to occur at the internal sequences, a dangling base at either end of a duplex is not expected to have a significant influence on the fluorescence spectral characteristics of the bound drug. Yet, our results clearly indicate that when the dangling dA or dT is attached to the dG of the 3′-terminal, dramatic fluorescence enhancement is observed. In contrast, weak or moderate enhancement is seen when the dangling base is attached to dC at the 5′-terminal.

The large fluorescence intensity enhancements for the base-appended oligomers provided us with the opportunity to study the SDS-induced dissociation kinetic behaviors of the drug, which was not possible with the absorbance monitoring. In addition to confirming the expected slower dissociation rates for the base-added oligomers than their parent octamer, these kinetic results provided us with a powerful argument for the end-stacking mechanism. For example, characteristic times for the dissociation of 7-AM-ACTD from d(CGTCGACG), d(CGTCGACG-T), and d(CGTCGACG-A) are about 1, 3.3, and 26 s, respectively. One would be hard pressed to explain how a dangling A base can induce a 30-fold decrease in the drug's off rate, if the binding were at the internal sequences rather than at the ends. Also, how can a change in the dangling base from A to T result in a rate change of nearly 10-fold? These results can, however, be more easily explained in terms of the drug interacting at the terminal G·C base pairs. The strong fluorescence enhancement is likely the consequence of the drug's experiencing a more hydrophobic environment via wrapping around of the dG-attached dangling A or T base to stack on the benzenoid portion of the phenoxazone ring of ACTD. Such an interpretation is consistent with the observation and interpretation on the splitting of the H7 and H8 NMR proton signals during the ACTD titrations with dinucleotide pdG-dT or pdG-dA (Krugh & Neely, 1973). It is further supported by the earlier fluorescence studies of 7-AM-ACTD (Modest & Sengupta, 1974; Chiao, et al., 1979) indicating that binding of dAMP enhances the fluorescence intensity near 600 nm. The extent of such interactions should be dependent on the nature of the base, with base A expected

to provide stronger stacking interactions than base T.

Another piece of evidence implicating stacking at dG comes from the positive sign of the CD band at 460 nm. Binding of ACTD to DNA usually results in a negative intensity in this region except for binding to the mononucleotide pdG (Homer, 1969; Brown & Shafer, 1987). The unusual feature of the positive CD intensity at this wavelength observed for ACTD binding to d(CGTCGACG) was pointed out earlier by Synder et al. (1989). It is also interesting to note that the long wavelength CD band of 7-AM-ACTD reverts from negative with intercalative binding of dinucleotide pdG-dC to positive with stacking interactions of pdC-dG (Chiao et al., 1979). Thus, the observation of a positive 460-nm CD band is consistent with ACTD stacking to dG at the duplex ends.

Additional corroborating evidence supporting the notion of ACTD stacking on the 3′-side of dG at the terminal G·C base pairs comes from the study with the octamer d(CGACGTCG). This octamer is related to the parent octamer by inverting the A·T pairs without disturbing the C and G at the respective 5′- and 3′-ends. It was found that this octamer exhibits a strong ACTD binding affinity with high cooperativity, a large ACTD-induced melting temperature increase, a significant fluorescence intensity enhancement of 7-AM-ACTD near 600 nm, a positive CD band around 460 nm for the bound ACTD, and relatively slow association as well as dissociation kinetics. These characteristics are very similar to those of the parent d(CGTCGACG) and are consistent with its ability to accommodate ACTD at the duplex ends.

Our results suggest that the binding constant (K_1) for the initial ACTD stacking at one of the termini is around 1×10^5 M^{-1}. This value is more than an order of magnitude higher than binding to the mononucleotide pdG (Krugh & Neely, 1973), but about an order of magnitude lower than intercalation at the GpC sequence of a duplex DNA. The stronger affinity compared to the mononucleotide is most certainly due to the ability of the oligomer to interact with one of the drug's pentapeptide rings. The weaker binding, compared to the intercalation at the duplex GpC site, is likely the consequence of the facts that (1) end-stacking only results in the formation of half the number of hydrogen bonds as that of intercalation at the duplex GpC site, (2) only one of the two pentapeptide rings can be anchored at the minor groove, and (3) the fraying of the duplex ends may somewhat hamper the initial ACTD binding. No ready explanation, however, is at hand to account for the origin of the observed highly cooperative binding of the second drug ($K_2 = 3.2 \times 10^7$ M^{-1}). Somehow the binding of the first drug results in more favorable stacking, hydrogen-bonding, groove−pentapeptide ring interactions for the second drug.

It should be noted that Snyder et al. (1989) have also studied d(CGTACG) and d(CATCGATG). They found the binding constants to be 3.3×10^5 and 7.1×10^5 M^{-1}, respectively. Weaker binding affinities were also found for d(CTAGATCTAG) and d(CGTTAACG), with corresponding binding constants of $<7.4 \times 10^4$ and $<3.1 \times 10^4$ M^{-1}, respectively. Since end-stackings can occur with these oligomers, their weaker ACTD bindings thus suggest strong sequence as well as length dependence on the proposed cooperative binding. To further investigate the length-dependent binding characteristics, studies were also made with d(CGTXCGX′ACG), d(CGTCGXX′CGACG), and d(CGXCGYCGY′CGX′CG), where X or Y is either A or T while X′ and Y′ are complementary to X and Y, respectively. The results indicate that these oligomers with longer lengths exhibit ACTD binding constants on the order of 10^5 M^{-1} with no evidence of cooperativity.

The above two-step process of binding may also account for the observed much slower association kinetics exhibited by d(CGTCGACG) and d(CGACGTCG) than the other XGTCGACY octamers studied. The weak bindings of the other XGTCGACY octamers most likely occur at the internal sequences. The slower dissociation kinetics exhibited by the parent octamer may be attributed to hydrogen bonding with the stacked guanines and minor groove interactions with one of the two pentapeptide rings. These interactions are similar to those observed for intercalative binding at the GpC site. The observation of an association or dissociation process slower than that of the parent octamer for each of the (X)-CGTCGACG-(Y) series of oligomers is consistent with the varying degrees of interference by the dangling bases or A·T base pairs.

An alternative model which seems plausible in light of our data is that binding occurs to the termini of the oligomers in a hairpin, rather than duplex, conformation. If the hairpin conformation is preferred by ACTD, then the drug will drive the equilibrium to the hairpin with an associated energy cost. Such a scenario could explain positive cooperativity, since the cost of shifting the equilibrium (melting the duplex) is paid only when ACTD binds to the first oligomer of the associated duplex. Binding to the second oligomer is "free". The difference between K_2 and K_1 would then be a measure of the relative free energies of the duplex and hairpin. This free energy difference would be sequence-dependent, which might explain why some oligomers with 3′-G residues exhibit cooperative binding, and others do not. To test the possible strong ACTD binding to the hairpin termini, spectral titrations were made with d(CGGTTCCG) and d(CGTTTTCG) which favor hairpin conformations. The results, however, indicate only moderate binding strengths ($\sim 10^5$ M^{-1}) for these oligomers. Comparison of the gel electrophoretic patterns of these oligomers as well as d(CGTCGACG) in the absence and in the presence of ACTD also failed to show evidence of gel retardation due to drug binding to hairpin (results not shown).

If ACTD were indeed stacking at the termini of dimeric duplex ends, there exist the possibilities that a drug-induced self-association of oligonucleotides can occur to form higher aggregates via ACTD dimerization or via ACTD sandwiching between two stacked duplexes (Lancelot & Thuong, 1986) to simulate a preferred classic GC site. Contribution from the former scenario probably will not be significant since the dimerization constant of ACTD in aqueous solution is roughly 10^3 M^{-1} (Crothers et al., 1968). Although attempts were made to observe such possible aggregate formation, no evidence of ladder-like gel patterns with progressively slower moving bands was observed in our gel experiments.

ACKNOWLEDGMENT

We thank Q. Johnson for her careful reading of the manuscript.

REFERENCES

Bailey, S. A., Graves, D. E., & Rill, R. (1994) *Biochemistry 33*, 11493−11500.

Chiao, Y.-C. C., Rao, G., Hook, J. W., III, & Krugh, T. R. (1979) *Biopolymers 18*, 1749−1762.

Connors, K. A. (1987) *Binding Constants*, pp 50−51, John Wiley & Sons, New York, NY.

Crothers, D. M., Sabol, S. L., Ratner, D. I., & Muller, W. (1968) *Biochemistry 7*, 1817−1823.

Fasman, G. D., Ed. (1975) *CRC Handbook of Biochemistry and Molecular Biology*, 3rd ed., Vol. I, p 589, CRC Press, Cleveland, OH.

Homer, R. B. (1969) *Arch. Biochem. Biophys. 129*, 405−407.

Kamitori, S., & Takusagawa, F. (1992) *J. Mol. Biol. 225*, 445−456.

Krugh, T. R. (1972) *Proc. Natl. Acad. Sci. U.S.A. 69*, 1911−1914.

Krugh, T. R., & Neely, J. W. (1973) *Biochemistry 12*, 4418−4425.

Lancelot, G., & Thuong, N. T. (1986) *Biochemistry 25*, 5357−5363.

Modest, E. J., & Sengupta, S. K. (1974) *Cancer Chemother. Rep. 58*, 35−48.

Muller, W., & Crothers, D. M. (1968) *J. Mol. Biol. 35*, 251−290.

Rill, R. L., Marsch, G. A., & Graves, D. E. (1989) *J. Biomol. Struct. Dyn. 7*, 591−604.

Snyder, J. G., Hartman, N. G., D'Estantoit, B. L., Kennard, O., Remeta, D. P., & Breslauer, K. J. (1989) *Proc. Natl. Acad. Sci. U.S.A. 86*, 3968−3972.

Sobell, H. M., & Jain, S. C. (1972) *J. Mol. Biol. 68*, 21−34.

Wadkins, R. M., & Jovin, T. M. (1991) *Biochemistry 30*, 9469−9478.

Waring, M. (1970) *J. Mol. Biol. 54*, 247−279.

BI952907T

THE JOURNAL OF BIOLOGICAL CHEMISTRY
Vol. 270, No. 39, Issue of September 29, pp. 23090–23096, 1995

Printed in U.S.A.

Acid-facilitated Supramolecular Assembly of G-quadruplexes in $d(CGG)_4$*

(Received for publication, April 14, 1995, and in revised form, July 20, 1995)

Fu-Ming Chen

From the Department of Chemistry, Tennessee State University, Nashville, Tennessee 37209-1561

Molar $[K^+]$ induces aggregate formation in $d(CGG)_4$, as evidenced by absorbance, circular dichroic (CD), and gel measurements. The kinetics of this transformation are extremely slow at pH 8 but are found to be greatly facilitated in acidic conditions. Kinetic profiles via absorbance or CD monitoring at single wavelength resemble those of autocatalytic reacting systems with characteristic induction periods. More than 0.8 M KCl is needed to observe the onset of aggregation at 20 °C and pH 5.4 within the time span of 1 day. Time-dependent CD spectral characteristics indicate the formation of parallel G-tetraplexes prior to the onset of aggregation. Despite the evidence of K^+-induced parallel G-quadruplex and higher molecular weight complex formation, both $d(TGG)_4$ and $d(CGG)_4T$ fail to exhibit the observed phenomenon, thus strongly implicating the crucial roles played by the terminal G and base protonation of cytosines. A plausible mechanism for the formation of a novel self-assembled structure is speculated. Aided by the C^+·C base pair formation, parallel quadruplexes are initially formed and subsequently converted to quadruplexes with contiguous G-tetrads and looped-out cytosines due to high $[K^+]$. These quadruplexes then vertically stack as well as horizontally expand via inter-quadruplex C^+·C base pairing to result in dendrimer-type self-assembled super structures.

Fragile X syndrome is the most common cause of inherited mental retardation (1). Individuals affected by this disorder have an X chromosome in which the tip of its long arm is attached by only a slender thread of DNA. A gene designated as FMR-1 contains about 60 or fewer tandem repeats of CGG trinucleotide sequence in normal individuals. Healthy carriers of this disease may have as many as 200 tandem copies. In sick individuals, however, the tandem repeat region is dramatically larger (2). Recently, amplifications of trinucleotide repeats have also been shown to be associated with several other disorders, including Kennedy and Huntington diseases (3). Although the mechanism of this unusual trinucleotide amplification is still unknown, it would not be surprising if there were structural bases for such remarkable amplifications.

Guanine is unique among the four DNA bases by virtue of its four hydrogen bonding sites being strategically distributed in such a way that four G bases can readily form 8 hydrogen bonds to result in a cyclic base-quartet (see Fig. 1). Thus, a DNA sequence with a stretch of G bases can form a four-stranded helical structure called G-quadruplex which is of current intense interest. This interest has been further stimulated by the possible relevance of such structures in the recombinational events at the immunoglobulin switching regions as well as in telomeric functions (4).

Telomeres are specialized DNA-protein complexes comprising the chromosomal termini and are essential for the stability and integrity of chromsomes. The telomeric DNA consists of a simple tandemly repeated sequence characterized by clusters of G residues in one strand with a 3′ overhang of 12–16 nucleotides in length (5). Effects of monovalent cations on the G-quadruplex structural formation of telomeric DNA sequences have been extensively studied in recent years (see reviews in Refs. 6–9). Evidence suggests that due to its optimal size, K^+ is much more effective in stabilizing G-quadruplex formation. The ion is found to be sandwiched between two G-tetrads to form an octa-coordination complex with the carbonyl groups of guanines. It was also found that for a contiguous guanine oligomer, the parallel strand orientation is thermodynamically more favorable than the anti-parallel orientation in the G-quadruplex formation (4, 10). A G-quadruplex with parallel strand orientation is further characterized by a strong positive CD band near 265 nm (11–13).

Cytosine is also unusual in that it can form three hydrogen bonds with its protonated counterpart (see also Fig. 1). A tract of C bases can, thus, form a parallel duplex via C^+·C base pairing in acidic solutions. The ability of oligomers containing contiguous guanines to form quadruplex G-DNA and the recent findings indicating that cytosine base protonation can facilitate such a quadruplex formation (14, 15) suggest that a physicochemical study on oligomers containing CGG repeats will be of considerable value.

This report describes the observation of an interesting K^+-induced CD intensity enhancement and aggregate formation of dodecamer $d(CGG)_4$ and proposes a plausible mechanism for the formation of super molecular assemblies of G-quadruplexes via C^+·C base pairing.

MATERIALS AND METHODS

Oligonucleotides were purchased from Integrated DNA Technologies, Coralville, IA and used without further purification. Experiments were carried out in either 10 mM HEPPS[1] buffer solutions of pH 8 containing 0.1 M NaCl and 1 mM $MgCl_2$, or 10 mM sodium citrate buffer of pH 5.4 containing 0.1 M NaCl and 1 mM EDTA. Concentrations of these oligomers (per nucleotide) were determined by measuring the absorbances at 260 nm after melting, with use of extinction coefficients obtained via nearest-neighbor approximation using mono- and dinucleotide values tabulated by Fasman (16). Absorption spectra were measured with a Cary 1E spectrophotometric system. Thermal denaturation experiments were carried out with 1-cm semimicro cells by monitoring absorbances at various wavelengths. A heating rate of 0.5 °C/min was maintained by the temperature controller accessory. Absorbance kinetic measurements were made with a stirrer accessory.

* This work was supported by United States Public Health Service Grant CA-42682, Army Medical Research Grant DAMD17-94-J-4474, and a subproject of Minority Biomedical Research Support Grant S06GM0892. The costs of publication of this article were defrayed in part by the payment of page charges. This article must therefore be hereby marked "*advertisement*" in accordance with 18 U.S.C. Section 1734 solely to indicate this fact.

[1] The abbreviations used are: HEPPS, *N*′-2-hydroxyethylpiperazine-*N*′-propanesulfonic acid.

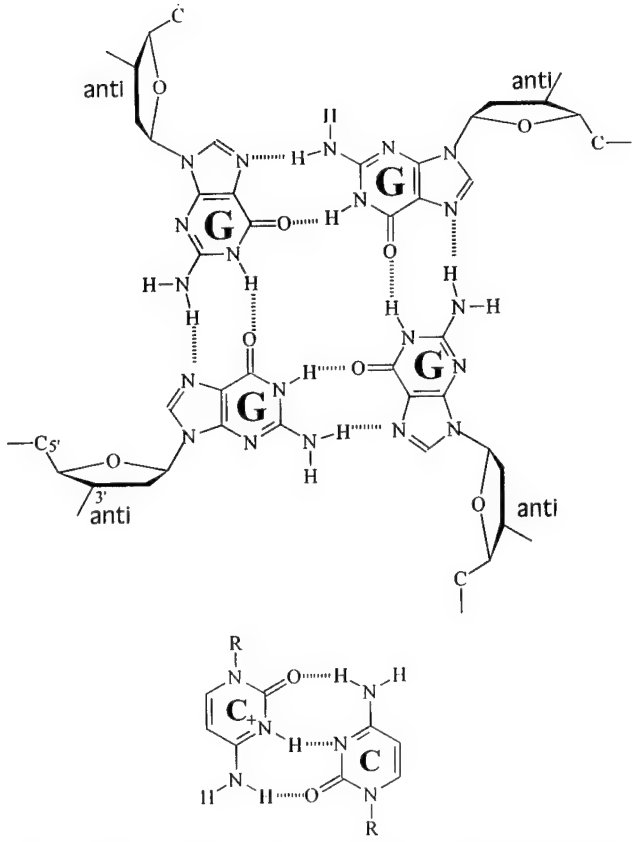

FIG. 1. *Upper panel*, schematic representation of base pair formation in G-quartet of parallel strand orientations. *Lower panel*, C^+·C base pairing scheme.

CD (circular dichroic) spectra were measured with a Jasco J-500A recording spectropolarimeter using water-jacketed cylindrical cells of 2-cm pathlength. CD kinetic measurements were made by monitoring ellipticity changes at appropriate wavelengths. Electrophoretic measurements were made on a Pharmacia Phast System using 20% polyacrylamide native gels at 200 V with appropriate pre- and post-loading run times at different temperatures. PhastGel buffer strips containing 0.25 M Tris of pH 8.8 were used, and the gels were developed by silver staining.

RESULTS

Multi-conformational States of d(CGG)$_4$ in Solutions—Although dodecamer d(CGGCGGCGGCGG) is not entirely self-complementary, some monomeric and dimeric conformations involving conventional Watson-Crick base pairings are possible (see Scheme 1). Thus, the single-stranded form (I) can coexist with dimeric duplex conformations (II and III) having 8 G·C base pairs with 4 or 3 G·G mismatches and with hairpin conformations (IV and V) having duplex stems of 3 G·C base pairs with 4- or 3-base loop. In addition, the presence of a large number of guanine bases may also result in possible triplex or quadruplex DNA conformations (not shown). Indeed, the multi-conformational state of this oligomer in a pH 8 buffer containing 0.1 M NaCl is reflected by a very weak and diffuse CD spectrum, a non-monophasic melting profile, and a multi-band electrophoretic pattern with smear background (see below).

5'C-G-G-C-G-G-C-G-G-C-G-G3' 5'C-G-G-C-G-G-C-G-G-C-G-G3'
3'G-G-C-G-G-C-G-G-C-G-G-C5' 3'G-G-C-G-G-C-G-G-C-G-G-C5'
II III

5'C-G-G-C-G-G-C-G-G-C-G-G3'
I

5'C-G-G-C-G-G
3'G-G-C-G-G-C
IV

5'C-G-G-C-G \
G
3'G-G-C-G-G-C /
V

SCHEME I

CD Enhancement and Spectral Characteristics of the K^+-induced Aggregation—A CD intensity enhancement of nearly 2 orders of magnitude is observed upon additions of molar concentration of KCl to a d(CGG)$_4$ solution of pH 8, resulting in a positive maximum near 290 nm, a shoulder around 265 nm, and a large tail extending well beyond 350 nm. A very slight turbidity is also discernible in such a solution. An intense CD with extended long wavelength tail had previously been coined as Ψ-type CD (17, 18) and is usually associated with aggregate formation. The kinetics of this enhancement process, however, are extremely slow at pH 8 and take about 10 days to reach equilibrium in the presence of 2 M KCl at room temperature (Fig. 2*A*). In fact, no appreciable CD intensity changes were apparent within the first 2 h of KCl addition. Interestingly, molar quantity of NaCl failed to induce a similar enhancement.

In contrast to pH 8, addition of molar concentration of KCl to an acidic d(CGG)$_4$ solution results in immediately noticeable CD intensity changes. The initial CD spectral alteration after the addition of 1 M KCl to a d(CGG)$_4$ solution of pH 5.4 is shown in Fig. 2*B*. Of interest is the initial development of a maximum at 265 nm. Subsequent intensity enhancement slowly changes to a Ψ-type spectrum with a maximum near 300 nm.

In addition to acidity, it was also found that the kinetics of aggregation can further be accelerated by a slight increase in temperature and/or melting and cooling the oligomer in the presence of molar $[K^+]$ (see below). Taking advantage of these facts, the large K^+-induced CD intensity enhancement can be observed in a reasonably short time. Fig. 2*C* shows the time-dependent CD spectral characteristics of a post-melt d(CGG)$_4$ solution in pH 5.4/2 M KCl buffer at 40 °C. As is apparent, significant intensity enhancement is already evident at 10 min after cooling the solution back from 95 °C to 40 °C. More dramatic spectral enhancements occur during the next 20 min to result in Ψ-type CD characteristics with a maximum near 300 nm and large intensities well beyond 350 nm. The equilibrium is seen to be approached in slightly over 1 h. Notice the gradual red shift of the long wavelength maximum as time progresses and the presence of a CD maximum at 265 nm prior to the onset of Ψ-type CD spectra.

Kinetics of Aggregate Formation Resemble Those of Autocatalytic Systems—The kinetics of aggregate formation were investigated by monitoring CD intensity enhancements at several wavelengths. Fig. 3*A* shows the time-dependent CD intensity changes at 263 nm for d(CGG)$_4$ of pH 5.4 at three different temperatures with 2 M KCl additions. Although aggregates are barely formed at 20 °C after 2 h, the multiphasic nature of the kinetics are clearly evident at higher temperatures. At 40 °C, for example, the initial slow CD intensity enhancement is overtaken by a much greater intensity increase due to aggregation around 30 min, which eventually levels off and commences a slight decrease near 100 min, consequence of the progressive spectral red shift (see Fig. 2*C*). At 30 °C, both the initial enhancement and the aggregation process are significantly slower so that no leveling effect is apparent even after 2 h.

Kinetic profiles for the K^+-induced aggregation of d(CGG)$_4$ at 40 °C in pH 5.4 and 8 via respective 300 and 290 nm mon-

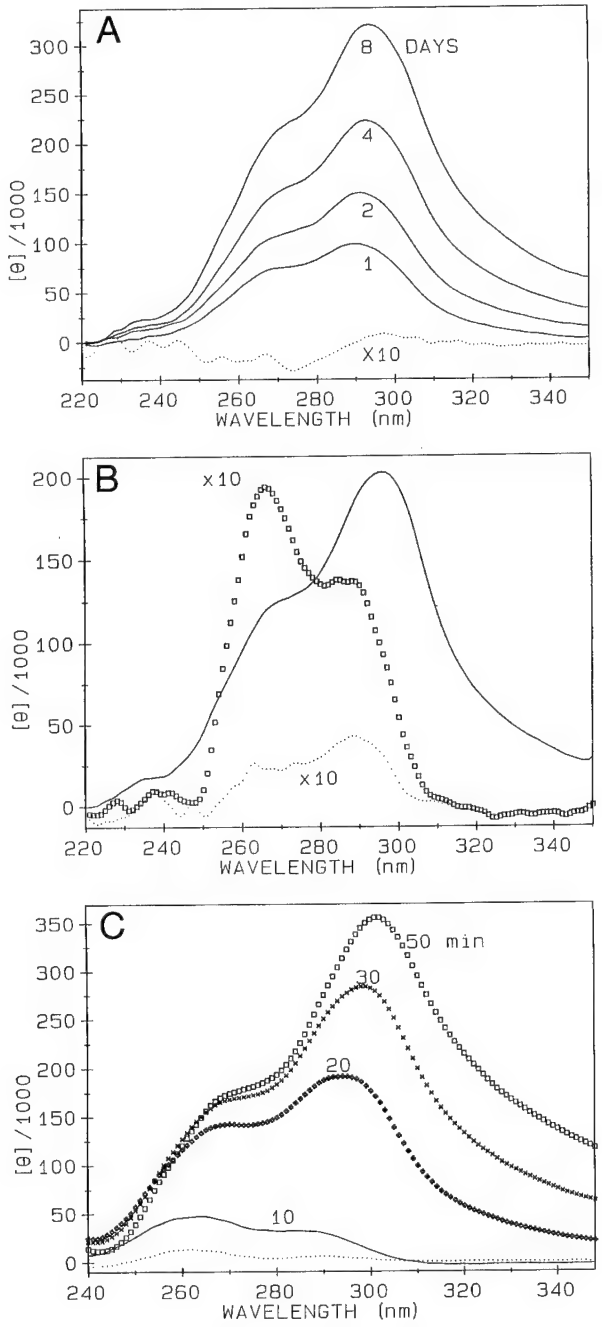

FIG. 2. *A*, *top panel*, CD spectra before (*dotted curve* with 10-fold amplification) and at 1, 2, 4, and 8 days after the addition of 2 M KCl to a 40 μM (per nucleotide) $d(CGG)_4$ solution in pH 8/0.1 M NaCl buffer. Each spectrum was measured at room temperature after rigorous manual shaking of the solution. *B*, *middle panel*, CD spectra of 40 μM $d(CGG)_4$ solution in acidic buffer of pH 5.4/0.1 M NaCl before (*dotted curve*) and after 40 min (*squares*) and 1 week (*solid curve*) of 1 M KCl addition. *C*, *bottom panel*, time-dependent CD spectra of 40 μM $d(CGG)_4$ solution of pH 5.4/2 M KCl after cooling the solution from 95 °C to 40 °C. Immediately (*dots*), 10 (*solid curve*), 20 (+), 30 (×), and 50 (*squares*) min after 40 °C is reached.

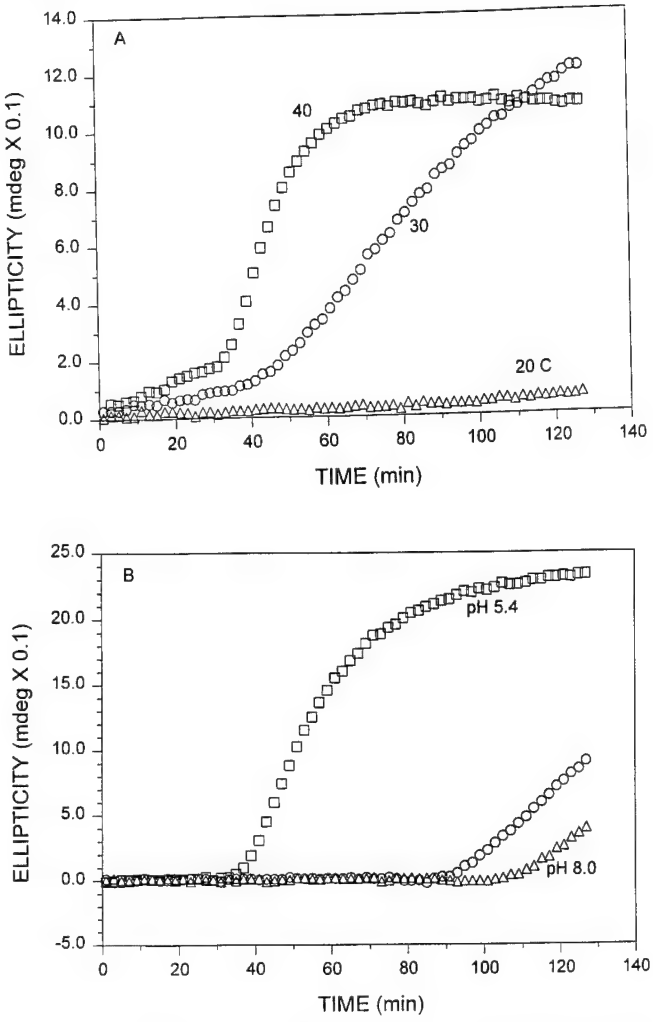

FIG. 3. *A*, CD kinetic traces of pH 5.4 $d(CGG)_4$ solution with 263 nm ellipticity monitoring at 20 °C (*triangles*), 30 °C (*circles*), and 40 °C (*squares*). *B*, time-dependent CD intensity enhancements at 40 °C via 300 nm (pH 5.4, *squares*) and 290 nm (pH 8, *triangles*) monitoring. The process was initiated by adding solid KCl to a 40 μM nucleotide solution of appropriate temperature to result in 2 M salt concentration. Less than 10 s is needed to dissolve the added solid via rigorous manual shaking. Cooling curve from 95 °C to 40 °C for the pH 8 solution in the presence of 2 M KCl (*circles*) is also included for comparison, with $t = 0$ corresponding to 95 °C.

itoring are compared in Fig. 3*B*. Despite the absence of initial slow phase intensity enhancement at these wavelengths, the onset of aggregation for the acidic solution commences near 30 min, in agreement with the 263 nm monitoring. In contrast, the pH 8 solution exhibits the first sign of aggregation only after about 2 h. These kinetic patterns resemble those of autocatalytic reacting systems, exhibiting characteristic induction periods and subsequent rapid rate accelerations (19). Facilitation of aggregate reformation via prior melting in the presence of KCl is also included for comparison with a pH 8 solution (see the following section).

Melting of DNA and Cooling in the Presence of Molar $[K^+]$ Facilitates the Kinetics of Aggregate Formation—Melting of aggregates was also investigated by CD monitoring at 300 nm to yield a melting temperature of approximately 65 °C in pH 5.4/2 M KCl. Interestingly, melting of DNA in the presence of molar concentration of KCl appears to facilitate the reformation of aggregates upon cooling. Time-dependent ellipticity changes at 300 nm were monitored when $d(CGG)_4$ solutions of pH 5.4/2 M KCl were first melted and cooled back from 95 °C to three different temperatures (not shown). The onsets of aggregation are seen to be rather abrupt and occur on or before 30 min. In view of the fact that about 20 min are needed to cool the solutions from 95 °C to 40 °C, it is apparent that the kinetics of aggregate formation have been significantly accelerated. This is dramatically illustrated for the 20 °C cooling, as considerable aggregation has already occurred by the time it reached this temperature. This is to be contrasted with the lack of apparent aggregate formation after 2 h of adding KCl directly (see Fig. 3*A*). The corresponding pH 8 solution after melting and cooling

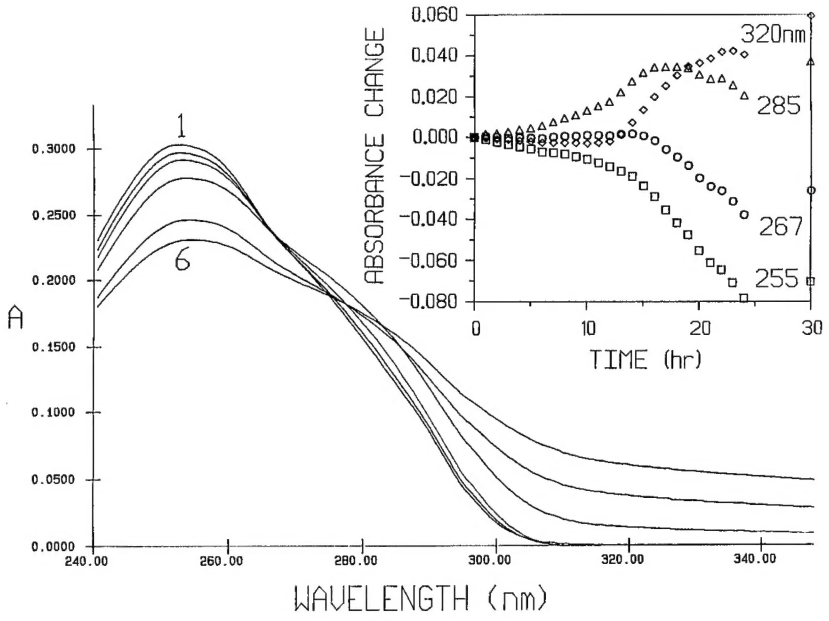

FIG. 4. **Representative absorption spectra at 20 °C of 40 μM d(CGG)$_4$ in pH 5.4 buffer at: 0 (*1*), 5 (*2*), 10 (*3*), 15 (*4*), and 20 (*5*) h after the addition of 1 M KCl.** *Curve 6* corresponds to that of 30 h and after rigorous manual shaking. *Inset*, time-dependent absorbance changes at 255 (*squares*), 267 (*circles*), 285 (*triangles*), and 320 nm (*diamonds*).

to 30 °C exhibits negligible intensity enhancement in 2 h, confirming the much slower kinetics in non-acidic solutions.

K^+-induced Aggregate Formation as Evidenced by Absorption Spectral Measurements—Time-dependent absorption spectral measurements also provide evidence of aggregate formation, as typified by a pH 5.4 solution of d(CGG)$_4$ with 1 M KCl induction at 20 °C (Fig. 4). Initial spectral changes consist of absorbance increases around 285 nm and decreases near 255 nm with an isosbestic point at 267 nm. Beyond 10 h, aggregate formation becomes progressively more important, as evidenced by the prominent presence of a long wavelength tail. This is seen more clearly by comparing the time-dependent absorbance changes at four different wavelengths, as shown in the *inset*. The multiphasic nature of the process is quite evident in the 285 nm plot, in which an initial slow intensity increase is followed by a more rapid enhancement and then a decrease (due to the slow sedimentation of aggregates). The absorbance changes at 255 nm exhibit a slight progressive decrease initially and then a more rapid decrease starting around 13 h. In contrast, no discernible absorbance changes are evident for the initial 15 h when one monitors at the isosbestic wavelength of 267 nm. The aggregate formation starting near 13 h is further supported by the significant absorbance increases at 320 nm, where a regular DNA solution exhibits negligible absorbance. The slow sedimentation of aggregates is also evidenced by the observed larger absorbances for all four wavelengths after shaking at 30 h. Similar results were observed with solutions containing higher KCl concentrations except the kinetics of aggregate formation become somewhat more rapid.

Minimum [K^+] Required for the d(CGG)$_4$ Aggregation—Effects of K^+ concentration on the aggregate formation of d(CGG)$_4$ at 20 °C were investigated by similar time-dependent absorbance measurements. Spectra were taken for d(CGG)$_4$ solutions containing KCl concentrations ranging from 0.4 to 1.2 M at 1-h intervals for 24 h and thereafter at 24-h intervals for 3 days. Absorbances at 320 nm were then plotted *versus* time, and the results (not shown) indicate that in the time span of 24 h, only solutions containing 1.0 and 1.2 M KCl exhibit significant absorbance increases at 320 nm, signifying the onset of aggregation at 14 and 9 h, respectively, after the salt additions. Although there is a discernible absorbance increase after 3 days for the 0.8 M KCl solution, these results suggest that at 40 μM nucleotide concentration, greater than 0.8 M KCl is needed to observe aggregation within the time span of 1 day.

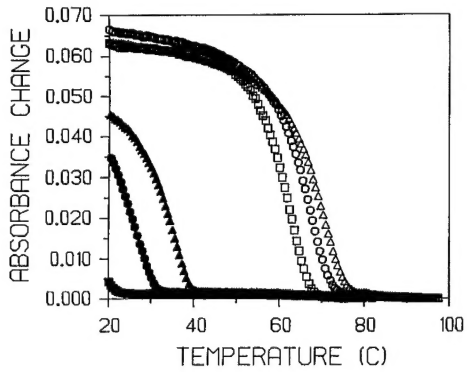

FIG. 5. **Comparison of melting profiles for 40 μM d(CGG)$_4$ solutions of pH 5.4 containing 1.4 (*squares*), 1.8 (*circles*), and 2.2 M (*triangles*) KCl with heating (*open symbols*) and cooling (*solid symbols*).**

[K^+]-dependent Melting Profiles of Aggregates—Melting profiles of aggregates were also obtained by absorbance monitoring at 320 nm. Consistent with the CD results, the aggregates in a pH 5.4/2 M KCl solution melt near 65 °C but exhibit a gross hysteresis. The apparent hysteresis exhibited by the cooling profile testifies to the slow kinetics of this self-assembly process. To investigate the [K^+] dependence on the stability of aggregates, melting measurements were made with solutions containing various KCl concentrations and the results are shown in Fig. 5 for the 1.4, 1.8, and 2.2 M KCl solutions. The enhanced stability of aggregates at higher [K^+] can be more clearly seen via cooling hysteresis. In particular, the onset of reaggregation for the 1.4 M KCl solution does not occur until approaching 20 °C.

Absence of ψ-type CD in d(TGG)$_4$ or d(CGG)$_4$T Solutions—To ascertain the role played by cytosines in the observed aggregate formation of d(CGG)$_4$, similar experiments were carried out with d(TGG)$_4$. Additions of 2 M KCl to a 40 μM d(TGG)$_4$ solution of either pH 8 or 5.4 failed to induce ψ-type CD characteristics after 4 days. Instead, the only significant CD intensity enhancement was observed near 265 nm. No appreciable CD spectral changes were evident with the addition of molar quantities of NaCl. Similarly, aside from the presence of a large CD

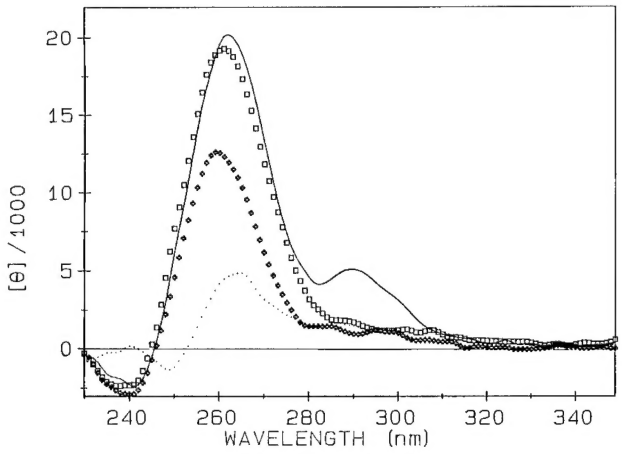

FIG. 6. **Comparisons of CD spectra of 40 μM nucleotide solutions of pH 5.4 for $d(TGG)_4$ in the absence (+) and in the presence (*squares*) of 2 M KCl for 4 days and for $d(CGG)_4T$ before (*dotted curve*) and after 4 days of 2 M KCl addition (*solid curve*).**

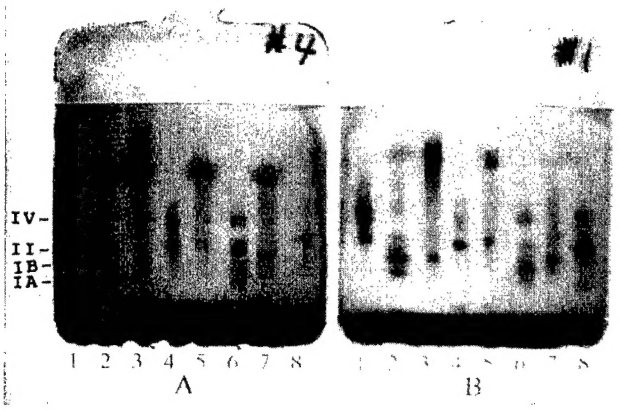

FIG. 7. **Comparison of gel electrophoretic mobility patterns at 4 °C (*A*) and 14 °C (*B*) for $d(CGG)_4$, $d(TGG)_4$, and $d(CGG)_4T$ of pH 5.4 in the absence (*lanes 2, 4,* and *6,* respectively) and in the presence of 2 M KCl (*lanes 3, 5,* and *7,* respectively).** Dodecamer d(TGGGGGGGGGGT) (*lane 1*) of pH 5.4/2 M KCl and self-complementary dodecamer d(CCGCCGCGGCGG) (*lane 8*) of pH 8/0.1 M NaCl in the presence (*A*) and in the absence (*B*) of 2 M KCl are included to serve as references. Measurements were made after 3 months of KCl additions.

maximum at 265 nm and a shoulder near 290 nm, no aggregation was observed for an acidic $d(CGG)_4T$ solution in the presence of 2 M KCl. These spectral features are compared in Fig. 6.

Gel Electrophoretic Mobility Patterns—Electrophoretic mobility patterns of $d(CGG)_4$, $d(TGG)_4$, and $d(CGG)_4T$ in the absence and in the presence of 2 M KCl along with a G-rich dodecamer and a self-complementary oligomer of the same size are compared in Fig. 7. As expected, the self-complementary dodecamer d(CCGCCGCGGCGG) at 14 °C (*panel B, lane 8*) is dominated by the dimeric duplex form, but a faster moving band of apparent hairpin conformation is also barely discernible. Band locations for the dimeric duplex and the monomeric hairpin form of a dodecamer, designated as II and IA, respectively, have also been established by other oligomers that are capable of forming such conformations (results not shown). The electrophoretic pattern of dodecamer d(TGGGGGGGGGGT) (*lane 1* of *A* and *B*) in 2 M KCl is seen to consist of a band with a mobility similar to that of the dimeric duplex reference and a considerably slower band of somewhat higher intensity (designated as band IV). The slower moving band can reasonable be attributed to the G-quadruplex structure, in view of the ability of K^+ to facilitate the formation of such a conformation in oligomers containing a stretch of contiguous guanines. Consistent with the multi-conformational state of $d(CGG)_4$, a complex gel mobility pattern is apparent in 0.1 M NaCl (*lane 2*). At 4 °C (*panel A*), bands corresponding to monomeric hairpin (IA), single strand (IB), and dimeric duplex (II) conformations as well as a slow moving blob can be discerned. Aside from conforming with the dodecameric reference, the assignment of II as the dimeric duplex band is further supported by the 14 °C mobility pattern (*panel B, lane 2*) where the intensity reduction of this band is clearly apparent. This is consistent with the destabilizing effect of G·G mismatches (see Scheme 1) and the lower thermal stability of the dimeric duplex as compared to the monomeric hairpin. Three diffuse bands moving slower than band II are also discernible in this lane, which can reasonably be attributed to complexes with molecularities of 4, 8, and >16, respectively. In the presence of 2 M KCl (*panel A, lane 3*), however, a striking appearance of a much slower moving tail with concomitant diminution of the faster moving bands is clearly evident. The prominent presence of a much slower moving smear of molecularities estimated to be higher than 16 is consistent with the aggregate formation of polydispersive nature for $d(CGG)_4$ in 2 M KCl.The effect of 2 M KCl on $d(TGG)_4$ and $d(CGG)_4T$ is the appearance of slow moving smears capped with bands having molecularities near 16 but without the much slower trailing tails (compare *lanes 4 versus 5* and *6 versus 7*). The presence of K^+-induced slow moving smears for these two oligomers most likely is the consequence of vertical stackings of G-quadruplexes (20, 21) and/or G-wire type of structural formation (38).

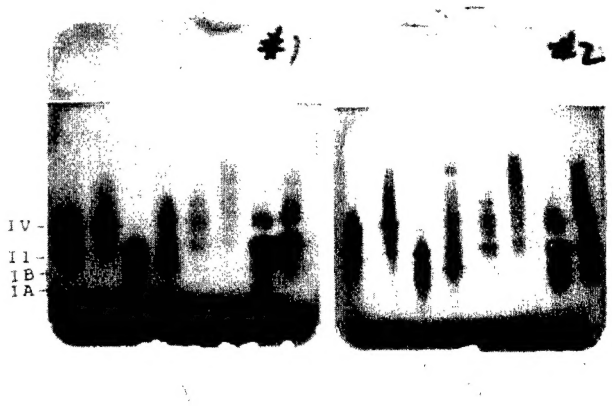

FIG. 8. **Comparison of gel electrophoretic mobility patterns after 1 (*panel A*) and 6 (*panel B*) days of 2 M KCl additions for d(TGGGGGGGGGGT), $d(CGG)_4$, $d(TGG)_4$, and $d(CGG)_4T$ of pH 5.4 at 4 °C in the absence (*lanes 1, 3, 5,* and *7,* respectively) and in the presence of 2 M KCl (*lanes 2, 4, 6,* and *8,* respectively).**

It is instructive to follow the progression of gel electrophoretic mobility patterns during the course of aggregate formation. Fig. 8 compares the gel patterns at 4 °C after 1 (*panel A*) and 6 (*panel B*) days of 2 M KCl additions (*even-numbered lanes*) to solutions of d(TGGGGGGGGGGT) (*lane 1*), $d(CGG)_4$ (*lane 3*), $d(TGG)_4$ (*lane 5*), and $d(CGG)_4T$ (*lane 7*). It is evident that the prominent presence of slow moving tails is already apparent for all oligomers after 1 day of KCl additions but becomes more so after 6 days. Of particular interest is the observation that for $d(CGG)_4$ (lane 4) the quadruplex conformation (band IV) is predominantly induced after day 1 (*panel A*) but complexes with molecularities higher than 16 become apparent after day 6 (*panel B*), as indicated by the appearance of a much slower band with a accompanied trailing tail. This, however, is accomplished via concomitant intensity reduction of band IV, suggesting that the quadruplex formation precedes the higher molecular weight aggregation.

DISCUSSION

Although G-quadruplex formation in oligomers containing a large number of guanine is to be expected, the large K^+-induced CD intensity enhancement of $d(CGG)_4$ is somewhat surprising. The kinetic facilitation of such a process in acidic solutions and the absence of ψ-type CD characteristics in $d(TGG)_4$ suggest a crucial role played by cytosines in this oligomer, likely via the C^+·C base pair formation. The presence of a terminal G appears to be also important, since $d(CGG)_4T$ does not aggregate in molar KCl solutions. Thus, the ability of $d(CGG)_4$ to form ψ-type aggregates appears to be the consequence of the simultaneous presence of C bases and a terminal G in the strand.

As stated earlier, a G-quadruplex with parallel strand orientation is characterized by a strong positive CD band at 265 nm (11–13). The observations that $d(TGG)_4$ or $d(CGG)_4T$ in the presence of molar concentration of KCl exhibits a strong positive CD maximum at 265 nm (see Fig. 6) and that an initial intensity enhancement near this wavelength was also observed for $d(CGG)_4$ prior to the onset of ψ-type CD appearance (see Figs. 2*B* and 3*A*) strongly support the notion that aggregate formation in $d(CGG)_4$ is preceded by parallel G-quadruplex formation. This is further strengthened by the time-dependent gel mobility measurements of $d(CGG)_4$ on the effect of 2 M KCl, which indicate an initial prominent presence of quadruplex band that subsequently diminishes as the much slower moving tail becomes progressively more important (Fig. 8). Such speculation appears to be consistent with observations by others, indicating that the presence of cytosines (15) or high monocation concentration (22) facilitates the parallel G-quadruplex formation and the most recent report on the observation of stable tetraplex formation of oligomers with CGG repeats in 0.2 M KCl, especially those with 5-methylated cytosines (23).

C^+·C base pairing had been shown to result in a greatly enhanced positive CD at wavelengths above 280 nm (24, 25) and to form parallel duplexes (26, 27). CD spectral studies on poly(dC-dT) even led to the proposal that this polynucleotide forms a structure consisting of a core of $C{\cdot}C^+$ base pairs and individually looped-out thymidyl residues in acidic solutions (28–30). Furthermore, self-assembly via branching of parallel C^+·C duplex formation has recently been proposed (31). These observations, thus argue strongly for the involvement of C^+·C base pairing in the observed phenomenon in $d(CGG)_4$.

DNA oligomers containing guanine clusters and a terminal guanine are known to generate, in addition to tetramers, higher order products via quadruplex stacking in the presence of K^+ (20, 21). Since both $d(TGG)_4$ and $d(CGG)_4$ contain terminal G at the 3′-end, formation of these higher order products are possible. Although the absence of K^+-induced ψ-type CD in $d(TGG)_4$ suggests that the remarkable CD intensity enhancement observed in $d(CGG)_4$ is not due to the sole presence of these higher order products, they may play important roles in furthering the observed aggregate formation. Indeed, the inability of oligomer $d(CGG)_4T$ to exhibit ψ-type CD suggests that the mere presence of C bases is not sufficient and testifies to the important role played by terminal G in the aggregation process, possibly via vertical end stacking.

Based on these spectral observations, a mechanism of self-assembly may be envisioned. Aided by the C^+·C base pair formation, parallel quadruplexes are initially formed. Driven by favorable K^+ complexation and purine stacking interactions, they further convert to quadruplexes with contiguous G-tetrads and looped-out cytosines (see Fig. 9). These quadruplexes can expand vertically via stacking and horizontally via inter-quadruplex C^+·C base pairing to link with additional quadruplexes and the process continues to result in dendrimer-

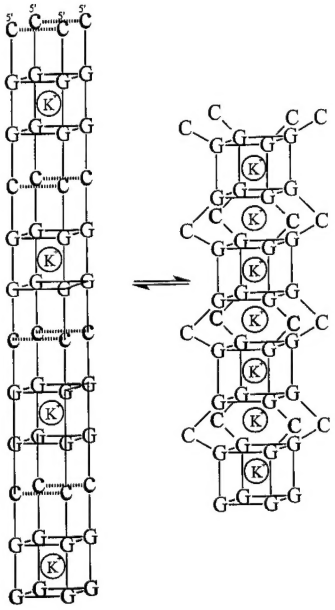

FIG. 9. **Schematic representation of the K^+-driven formation of quadruplexes with contiguous G-quartets and looped-out cytosines.**

type self-assembled super structures. The structures formed by branching covalent connections have been termed dendrimers (Ref. 32 and references therein). The proposed self-assembly structures of G-quadruplexes can thus be regarded as G-DNA dendrimers with the novel feature of branching via vertical stacking of G-quartets and lateral expansion via C^+·C base pairing rather than covalent formation. The role of C^+·C base pairing in the proposed model is, thus, two-fold: to facilitate the initial G-quadruplex formation via parallel dimeric duplex formation and subsequent inter-quadruplex association via looped out cytosine base pairing.

Interestingly, chemical probing by Kohwi *et al.* (33) has revealed that under physiological salt and pH conditions, Zn^{2+} or Co^{2+} ions induce AGC repeats to adopt a novel non-B DNA structure where all cytosines but no adenine residues in either strand become unpaired. Looping-out of thymidines has also been speculated in the G-DNA structural studies on d(TGT-GGGTGTGTGTGGG) (34). These results lend further credence to our proposed looping out of cytosines for inter-quadruplex C^+·C base pairing. The fact that poly(dC) was shown to form a self-complex via C^+·C base pair formation with a pK_a of 7.4 at 0.05 M NaCl (35) further suggests that such a process is not impossible at pH 8 and accounts for its extremely slow kinetics. Unfortunately, such slow kinetics have prevented us from carrying out a detailed pH titration.

The fact that the observed kinetic behaviors exhibit characteristics of autocatalytic reactions with induction periods (19) gives additional support to the proposed mechanism, as each product provides further stacking and cytosine binding sites analogous to that of chain branching polymerization. The failure of concentrated Na^+ to induce similar phenomenon is also consistent with the proposed model, as this ion is too small to form a stable octa-coordinated complex with two G-quartets. The facilitation of aggregate formation via melting in the presence of molar $[K^+]$ most likely is the consequence of freeing the kinetically or thermodynamcally trapped conformers for ready participation in the parallel quaruplex formation upon cooling.

Although the proposed mechanism seems plausible, other possibilities cannot be ruled out, such as: extensive concatemers stabilized by stacking and protonation, some geometrical arrangements with crossover of strands, formation of linked

G-quadruplexes and C-tetraplexes (i-DNAs) (36, 37) via interdigitation of inter G-quadruplex C^+·C duplexes to result in a network of linked G-tetraplexes with alternating tetraplex polarities. Most recently, Marsh and Henderson (38) observed the self-assembly of a telomeric oligonucleotide d(GGGGTTGGGG) into a superstructure, which they termed "G-wire." This structure is formed by slipped tetraplex association to result in a long vertical extension consisting of parallel G-4 DNA domains punctuated by T nodes (see also Ref. 43). A model incorporating lateral extension via inter-G-wire C^+·C base pairing would not be inconsistent with our observed aggregation phenomenon in $d(CGG)_4$.

The observed molar K^+-induced aggregation phenomenon is the more remarkable when it is realized that in optical measurements one is dealing with rather dilute solutions of μM strand concentrations. Thus, facilitation of inter-quadruplex assembly via C^+·C base pair formation is eminently reasonable. However, the role of H^+ may not simply be the base protonation but also the neutralization of phosphate groups to reduce the interchain repulsive effect (39). It is also of interest to note that the gel formed by 8-bromoguanosine exhibits a strong positive CD maximum near 290 nm and a shoulder around 265 nm but without the presence of extended long wavelength tail (40). The x-ray structural determination of this gel had indicated a right-handed helical formation of tetraplex (41). The gross similarity with the observed ψ-type CD characteristics in this report suggests that the quadruplexes of $d(CGG)_4$ most likely are also of right-handed helical form.

In their studies on the contribution of light scattering to the CD of DNA films with twisted structures, DNA-polylysine complexes, and condensed DNA aggregates, Maestre and Reich (42) showed that ψ-type CD spectra are a manifestation of superorganization of the DNA in these films, particles, and aggregates. The sense of twist or superhelix can be determined from the sign of the CD bands. A right-handed helix gives positive CD signals and *vice versa*. The periodicity is given by the Bragg law. The CD tail would be a property of the size of the particle since it is caused by birefringence dispersion. Thus, a $\psi(+)$ CD maximum near 300 nm in our aggregates would suggest a right-handed helical periodicity on the order of 1500 Å. However, the elucidation of structural details of the aggregates must await the availability of other techniques. It is interesting to note in passing that the observed progressive red-shift of the ψ-CD maximum (see Fig. 2*C*) is consistent with the formation of progressively larger complexes during the aggregation process.

Although this report has focused only on $d(CGG)_4$, similar results have also been found with $d(CGG)_2$, $d(CGG)_3$, and other cytosine-containing sequences. In addition, Sr^{2+}, which has been shown to facilitate parallel G-quadruplex formation (12, 40), is also found to be capable of inducing self-assembly of oligomers with CGG repeats.

Note Added in Proof—A study with $d(CGG)_{15}$ (Mitas, M., Yu, A., Dill, J., & Haworth, I. S. (1995) *Biochemistry*, in press) has indicated that this oligomer exists predominantly in the hairpin confirmations at $[K^+] \leq 0.75$ M. This, however, does not alter our interpretation on the observed aggregation phenomena induced by $[K^+] \geq 1$ M.

Acknowledgments—I thank C. Liu for running the gel and D. Dunson, T. Krugh, and M. Stone for helpful comments on the manuscript.

REFERENCES

1. Hirst, M. C., Knight, S. J. L., Bell, M. V., Super, M. & Davies, K. E. (1992) *Clin. Sci. (Lond.)* **83,** 255–264
2. Rennie, J. (1993) *Sci. Am.* **266,** 126–127
3. Sutherland, G. R. & Richards, R. I. (1994) *Am. Sci.* **82,** 157–163
4. Sen, D. & Gilbert, W. (1988) *Nature* **334,** 364–366
5. Blackburn, E. H. (1990) *J. Biol. Chem.* **265,** 5919–5921
6. Guschlbauer, W., Chantot, J.-F. & Thiele, D. (1990) *J. Biomol. Struct. & Dyn.* **8,** 491–511
7. Sundquist, W. I. (1991) *Nucleic Acids Mol. Biol.* **5,** 1–24
8. Sen, D. & Gilbert, W. (1991) *Curr. Opin. Struct. Biol.* **1,** 435–438
9. Williamson, J. R. (1994) *Annu. Rev. Biophys. Biomol. Struct.* **23,** 703–730
10. Lu, M., Guo, Q. & Kallenbach, N. R. (1993) *Biochemistry* **32,** 598–601
11. Hardin, C. C., Henderson, E. R., Watson, T. & Prosser, J. K. (1991) *Biochemistry* **30,** 4460–4472
12. Chen, F.-M. (1992) *Biochemistry* **31,** 3769–3776
13. Balagurumoorthy, P., Brahmachari, S. K., Mohanty, D., Bansal, M. & Sasisekharan, V. (1992) *Nucleic Acids Res.* **20,** 4061–4067
14. Hardin, C. C., Watson, T., Corregan, M. & Bailey, C. (1992) *Biochemistry* **31,** 833–841
15. Hardin, C. C., Corregan, M., Brown, B. A., II & Frederick, L. N. (1993) *Biochemistry* **32,** 5870–5880
16. Fasman, G. D. (ed) (1975) *CRC Handbook of Biochemistry and Molecular Biology*, 3rd Ed., Vol. I, p. 589, CRC Press, Cleveland, OH
17. Jordan, C. F., Lerman, L. S. & Venable, J. H. (1972) *Nat. New Biol.* **236,** 70–76
18. Shin, Y. A. & Eichhorn, G. L. (1984) *Biopolymers* **23,** 325–335
19. Boudart, M. (1991) *Kinetics of Chemical Processes*, pp. 124–127, Butterworth-Heinemann, Stoneham, MA
20. Sen, D. & Gilbert, W. (1992) *Biochemistry* **31,** 65–70
21. Lu, M., Guo, Q. & Kallenbach, N. R. (1992) *Biochemistry* **31,** 2455–2459
22. Miura, T. & Thomas, G. J., Jr. (1994) *Biochemistry* **33,** 7848–7856
23. Fry, M. & Loeb, L. A. (1994) *Proc. Natl. Acad. Sci. U. S. A.* **91,** 4950–4954
24. Gray, D. M. & Bollum, F. J. (1974) *Biopolymers* **13,** 2087–2102
25. Marck, C., Thiele, D., Schneider, C. & Guschlbauer, W. (1978) *Nucleic Acids Res.* **5,** 1979–1996
26. Robbinson, H., Van Der Marel, G., Van Boom, J. H. & Wang, A. H-J. (1992) *Biochemistry* **31,** 10510–10517
27. Pilch, D. S. & Shafer, R. H. (1993) *J. Am. Chem. Soc.* **115,** 2565–2571
28. Gray, D. M., Vaughan, M., Ratliff, R. L. & Hayes, F. N. (1980) *Nucleic Acids Res.* **8,** 3695–3707
29. Brown, D. M., Gray, D. M., Patrick, M. H. & Ratliff, R. L. (1985) *Biochemistry* **24,** 1676–1683
30. Sarma, M. H., Gupta, G. & Sarma, R. H. (1986) *FEBS Lett.* **205,** 223–229
31. Edwards, E. L., Patrick, M. H., Ratliff, R. L. & Gray, D. M. (1990) *Biochemistry* **29,** 828–836
32. Hudson, R. H. E. & Damha, M. J. (1993) *J. Am. Chem. Soc.* **115,** 2119–2124
33. Kohwi, Y., Wang, H. & Kohwi-Shigematsu, T. (1993) *Nucleic Acids Res.* **21,** 5651–5655
34. Venczel, E. A. & Sen, D. (1993) *Biochemistry* **32,** 6220–6228
35. Inman, R. B. (1964) *J. Mol. Biol.* **9,** 624–637
36. Gehring, K., Leroy, J.-L. & Gueron, M. (1993) *Nature* **363,** 561–565
37. Leroy, J.-L., Gehring, K., Kettani, A. & Gueron, M. (1993) *Biochemistry* **32,** 6019–6031
38. Marsh, T. C. & Henderson, E. (1994) *Biochemistry* **33,** 10718–10724
39. Chantot, J. F. & Guschlbauer, W. (1972) *Jerus. Symp. Quant. Chem. Biochem.* **IV,** 205–216
40. Chantot, J. F. & Guschlbauer, W. (1969) *FEBS Lett.* **4,** 173–176
41. Tougard, P., Chantot, J. F. & Guschlbauer, W. (1973) *Biochim. Biophys. Acta* **308,** 9–16
42. Maestre, M. F. & Reich, C. (1980) *Biochemistry* **19,** 5214–5223
43. Dai, T.-Y., Marotta, S. P. & Sheardy, R. D. (1995) *Biochemistry* **34,** 3655–3662